

**MECHANISM OF SYNAPTOTAGMIN ACTION IN
NEUROTRANSMITTER RELEASE**

APPROVED BY SUPERVISORY COMMITTEE

Jose Rizo-Rey, Ph.D., Advisor

Kevin Gardner, Ph.D., Committee Chair

Rama Ranganathan, M.D., Ph.D.

Ege Kavalali, Ph.D.

Joseph Albanesi, Ph.D.

To my loved ones

**MECHANISM OF SYNAPTOTAGMIN ACTION IN
NEUROTRANSMITTER RELEASE**

by

DEMET ARAÇ-ÖZKAN

DISSERTATION

Presented to the Faculty of the Graduate School of Biomedical Sciences

The University of Texas Southwestern Medical Center at Dallas

In Partial Fulfillment of the Requirements

For the Degree of

DOCTOR OF PHILOSOPHY

The University of Texas Southwestern Medical Center at Dallas

Dallas, Texas

November, 2005

Copyright

by

DEMET ARAÇ-ÖZKAN, 2005

All Rights Reserved

MECHANISM OF SYNAPTOTAGMIN ACTION IN NEUROTRANSMITTER RELEASE

Publication No. _____

Demet Araç-Özkan, Ph.D.

The University of Texas Southwestern Medical Center at Dallas, 2005

Jose Rizo-Rey, Ph.D.

Neurotransmitter release occurs by fusion of the synaptic vesicle membrane with the plasma membrane. Formation of a highly stable complex, known as the SNARE (soluble NSF-attachment protein receptors) complex, brings the two membranes close in space. SNARE complex formation is required but probably not sufficient for fusion to occur. An increase in the local Ca^{2+} concentration at the synaptic terminal rapidly triggers neurotransmitter release. The mechanism of Ca^{2+} action is still unknown. Synaptotagmin 1, a brain-specific vesicular transmembrane protein, is the Ca^{2+} sensor in neurons. It has two

cytoplasmic C₂ domains (C₂A and C₂B) that bind Ca²⁺. Both C₂ domains interact with negatively charged phospholipids in a Ca²⁺ dependent manner. The interaction of synaptotagmin 1 with the SNARE complex is also reported. We investigated whether the interaction of synaptotagmin 1 with membranes or with the SNARE complex is critical for membrane fusion.

A new method to detect protein-protein interactions by 1D NMR spectroscopy was developed. Either the ¹³C signal of the SNARE complex or synaptotagmin 1 was monitored to perform competition experiments between SNAREs and lipid vesicles for binding to synaptotagmin 1. In the presence of both lipids and the SNARE complex, synaptotagmin 1 binds to lipids but cannot bind to the SNARE complex. This result suggests that Ca²⁺-dependent membrane binding is the primary activity of synaptotagmin 1.

We investigated the mechanism of Ca²⁺-dependent phospholipid binding to synaptotagmin 1 C₂ domains. A combination of crosslinking and FRET experiments showed that synaptotagmin 1 does not oligomerize upon Ca²⁺-dependent binding to phospholipid vesicles. Intriguingly, it binds to two membranes simultaneously and brings them into close proximity as visualized by cryo-EM experiments. We showed that the isolated C₂B domain is sufficient to induce close membrane proximity. Mutational analysis suggested that the abundance of basic residues around the C₂B surface, which generates a highly positive electrostatic potential together with the bound Ca²⁺ ions, is essential for this activity. We suggest that the ability of the C₂B domain to bring membranes into close proximity can explain why the C₂B domain has a more critical function in vivo than the C₂A domain.

Acknowledgements

First, I would like to thank my dissertation advisor, Jose Rizo-Rey. During the last five years, it has been a very pleasant experience to pursue science with him. He has been an exceptional mentor for me and dramatically contributed to my education by providing his time, consideration and expertise, generously. I had the chance to learn how to be a good scientist by observing his enthusiasm and passion for science, and scientific objectivity to give the right decisions. Jose has been a great scientist and a great person, at the same time. He has always been supportive, kind and friendly at all occasions. My scientific improvement could never be the same without his mentorship.

I also would like to thank all the members of the Rizo-Rey lab, for creating such a nice and friendly lab environment. They have been extremely generous with any kind of help I needed during the last five years. Josep Ubach has supervised me during my rotation and provided me invaluable information about how to work with synaptotagmin. Irina Dulubova has been a great friend and also provided good scientific advice and help. We have shared related projects and had very fruitful and fun discussions/chats with Xiaocheng Chen, who has always been very friendly to me. Tara Murphy provided excellent help with the development of a new method. Xuelian Luo, Lun Lu, Han Dai, Irina Huryeva, Oleg Guryev, Rong Guan, Tim Craig and Minghua Wen created a friendly lab atmosphere by their kind and supportive attitudes. These people have been excellent friends who have volunteered to

help me about all scientific and non-scientific matters (including free rides, cold medicine, advice on formal clothing etc.).

I thank my dissertation committee members Drs. Kevin Gardner, Rama Ranganathan, Ege Kavalali, Joseph Albanesi and our long-term collaborator Dr. Thomas Sudhof for useful discussion and constructive suggestions. I also thank my family and Engin Özkan for their support and encouragement.

TABLE OF CONTENTS

Committee Signatures	I
Dedication	II
Title Page	III
Abstract	V
Acknowledgements	VII
Table of Contents	IX
Prior Publications	XV
List of Figures	XVII
List of Tables	XXII
List of Definitions	XXIII
Chapter 1 General Introduction	1
1.1 Signal Transduction in Neurons	1
1.1.1 The Neuron	1
1.1.2 Action Potential	4
1.1.3 Synaptic Vesicle Cycle	6
1.1.4 Comparison of constitutive membrane fusion with synaptic vesicle fusion ...	8
1.1.5 Calcium Dependence of Neurotransmitter Release	9
1.1.6 Membrane Fusion	11
1.2 Proteins involved in membrane Fusion.....	14
1.2.1 SNARE proteins	14
1.2.2 Synaptotagmin 1	20

1.2.3	SM proteins	20
1.2.4	Munc13/ Rim	21
1.2.5	Rab Proteins	23
1.2.6	Complexins	23
1.3	Synaptotagmin 1	24
1.3.1	Synaptotagmin 1 as a Calcium Sensor.....	25
1.3.2	C ₂ domain Structure	26
1.3.3	Interaction with negatively charged phospholipid membranes	33
1.3.4	Interaction with SNARE proteins	35
1.3.5	Self-association of synaptotagmin 1 to form oligomers	38
1.3.6	Functional studies to reveal synaptotagmin 1 action	39
1.3.7	Synaptotagmin Isoforms and Localization	43
Chapter 2 Characterization of Different SNARE Complexes : Interaction of Synaptotagmin with SNAREs.....		45
2.1	Introduction	45
2.2	Results	46
2.2.1	Detection of different SNARE complexes by monitoring the syntaxin crosspeaks	46
2.2.2	Detection of different SNARE complexes by monitoring the SNAP25C crosspeaks	55
2.2.3	The C ₂ AB domain of synaptotagmin 1 interacts with the SNARE complex	58
2.3	Discussion	60

2.4 Materials and Methods	62
2.4.1 Expression and purification of proteins	62
2.4.2 NMR sample preparation	64
2.4.3 NMR spectroscopy	65
Chapter 3 A New Method to Detect Protein-Protein Interactions by 1D NMR: Analysis of Synaptotagmin 1 Interactions	66
3.1 Introduction	66
3.2 Results	67
3.2.1 The basis for the SMR method	67
3.2.2 SMR method	73
3.2.3 Testing the validity of SMR method	76
3.2.4 SMRC method	79
3.2.5 The requirement for a new method to study synaptotagmin 1 function	84
3.2.6 Application of SMRC method to study synaptotagmin 1 function	86
3.3 Discussion	93
3.4 Materials and Methods.....	97
3.4.1 Protein expression and purification	97
3.4.2 Preparation of lipid vesicles	98
3.4.3 Sample preparation	99
3.4.4 NMR spectroscopy	99
Chapter 4 Interaction of Synaptotagmin 1 with Phospholipid Membranes	101
4.1 Preliminary results for the basis of chapter 4	101

4.2	Introduction.....	104
4.3	Results	106
4.3.1	C ₂ A and C ₂ B domains act independent of each other	106
4.3.1.1	NMR spectroscopy	106
4.3.1.2	Insertion of Ca ²⁺ -binding loops into the membranes	110
4.3.2	Lipid binding mode of synaptotagmin 1 suggests multiple sites of the C ₂ B domain is involved in lipid binding	116
4.3.3	Synaptotagmin 1 is monomeric in solution and on the membranes	128
4.3.3.1	Negative Staining Electron Microscopy	131
4.3.3.2	Crosslinking experiments.....	137
4.3.3.3	FRET experiments	142
4.3.4	Synaptotagmin 1 clusters membrane vesicles and brings membranes in close proximity	149
4.3.4.1	Ca ²⁺ -dependent synaptotagmin 1 binding induces vesicle clustering	151
4.3.4.2	Vesicle clustering is visualized by Cryo-Electron microscopy	160
4.3.4.3	Mass density of synaptotagmin 1 is visualized between the clustered vesicles	165
4.3.4.4	Synaptotagmin 1 brings two membranes into close proximity	169
4.4	Discussion	173
4.5	Materials and Methods	182
4.5.1	Expression and Purification of proteins	182
4.5.2	Preparation of lipid vesicles	182

4.5.3	Labeling proteins with fluorescent dyes	182
4.5.4	Fluorescence experiments	184
4.5.5	Crosslinking Experiments	185
4.5.6	Negative staining electron microscopy	186
4.5.7	Cryo electron microscopy	187
4.5.8	Dynamic Light Scattering	188
4.5.9	NMR Spectroscopy	189
Chapter 5 Three-Dimensional Structure of the rSly1 N-terminal Domain: A Conformational		
Change Induced by Binding to Syntaxin 5		190
5.1	Introduction	190
5.1.1	A SNARE protein: Syntaxin	190
5.1.2	SM Proteins	191
5.1.3	Interactions of SM Proteins with Syntaxins	194
5.2	Results	197
5.2.1	Secondary structure determination of isolated and peptide bound rSly1N .	197
5.2.2	Peptide-induced chemical shift changes in rSly1N	200
5.2.3	Three dimensional structure of the isolated rSly1N	204
5.2.4	Peptide induced conformational changes in rSly1N	204
5.2.5	Syx5-induced conformational changes are conserved in the Sly1 family ..	215
5.3	Discussion	220
5.4	Materials and Methods	223
5.4.1	Protein expression and Purification	223

5.4.2	NMR Spectroscopy	223
5.4.3	Structure Calculations	224
5.4.3.1	Backbone Assignments	224
5.4.3.2	Side Chain Assignments	225
5.4.3.3	NOE Assignments and Structure Calculation.....	226
5.4.4	Sequence Analysis	227
	References	229

PRIOR PUBLICATIONS

L. Li, OH. Shin, JS. Rhee, D. Arac, J. Rizo, TC. Sudhof, C. Rosenmund. Phosphatidylinositolphosphates are co-activators of Ca^{2+} -binding by synaptotagmin 1: Functional asymmetry of synaptotagmin 1 C₂-domains. (*In preparation*)

AD. Ferguson, VM. Labunskyy, DE. Fomenko, D. Arac, Y. Chelliah, CA. Amezcua, J. Rizo, VN. Gladyshev, J. Deisenhofer. NMR structures of the selenoproteins Sep15 and SelM reveal redox activity of a new thioredoxin-like family. (*J Biol Chem., in press.*)

D. Arac, X. Chen, HA. Khant, J. Ubach, SJ. Ludtke, M. Kikkawa, A.E. Johnson, W. Chiu, TC. Südhof and J. Rizo. Close Membrane-Membrane Proximity Induced by Ca^{2+} -dependent Multivalent Binding of Synaptotagmin 1 to Phospholipids. (*Nat Struct Mol Biol, in press*)

X. Chen, D. Arac, TM. Wang, C. Gilpin, J. Rizo. Lysophospholipids inhibit SNARE-mediated lipid mixing. (*Biophysical J. in press*)

D. Arac, I. Dulubova, J. Pei, I. Huryeva, NV. Grishin, J. Rizo. Three-dimensional structure of the rSly1 N-terminal domain reveals a conformational change induced by binding to syntaxin 5. *J Mol Biol.* 346(2):589-601, 2005.

N. Jarousse, J. D. Wilson, D. Arac, J. Rizo, and R. B. Kelly. Endocytosis of synaptotagmin 1 is mediated by a novel, tryptophan-containing motif. *Traffic* 4 (7):468-478, 2003.

D. Arac, T. Murphy, and J. Rizo. Facile detection of protein-protein interactions by one-dimensional NMR spectroscopy. *Biochemistry* 42 (10):2774-2780, 2003.

I. Dulubova, T. Yamaguchi, D. Arac, H. M. Li, I. Huryeva, S. W. Min, J. Rizo, and T. C. Sudhof. Convergence and divergence in the mechanism of SNARE binding by Sec1/Munc18-like proteins. *Proc Natl Acad Sci U S A* 100 (1):32-37, 2003.

W. Antonin, I. Dulubova, D. Arac, S. Pabst, J. Plitzner, J. Rizo, and R. Jahn. The N-terminal domains of syntaxin 7 and vti1b form three-helix bundles that differ in their ability to regulate SNARE complex assembly. *J Biol Chem.* 277 (39):36449-36456, 2002.

X. Chen, D. R. Tomchick, E. Kovrigin, D. Arac, M. Machius, T. C. Sudhof, and J. Rizo. Three-dimensional structure of the complexin/SNARE complex. *Neuron* 33 (3):397-409, 2002.

I. Fernandez*, D. Arac*, J. Ubach*, S. H. Gerber, O. H. Shin, Y. Gao, R. G. W. Anderson, T. C. Sudhof, and J. Rizo. Three-dimensional structure of the synaptotagmin 1 C2B-domain: Synaptotagmin 1 as a phospholipid binding machine. *Neuron* 32 (6):1057-1069, 2001.

*These authors contributed equally.

J. Ubach, Y. Lao, I. Fernandez, D. Arac, T. C. Sudhof, and J. Rizo. The C2B domain of synaptotagmin I is a Ca^{2+} -binding module. *Biochemistry* 40 (20):5854-5860, 2001.

V. Kulik, M. Weyand, R. Seidel, D. Nicks, D. Arac, M. F. Dunn, and I. Schlichting. On the role of alpha Thr183 in the allosteric regulation and catalytic mechanism of tryptophan synthase. *J Mol Biol.* 324 (4):677-690, 2002.

M. Hafezparast, S. Ball, S. J. Nicholson, A. Witherden, D. Arac, N. Broadway, D. Saggerson, E. Cooper, M. Naase, S. Gokhale, P. Quant, C. Lascelles, C. Nickols, C. S. Baker, J. Peters, J. E. Martin, and E.M.C. Fisher. A new mouse mutant, skijumper. *Mammalian Genome* 13 (7):359-364, 2002.

A. S. Witherden, M. Hafezparast, S. J. Nicholson, A. Ahmad-Annuar, N. Bermingham, D. Arac, J. Rankin, M. Iravani, S. Ball, J. Peters, J. E. Martin, D. Huntley, H. Hummerich, M. Sergot, and E.M.C. Fisher. An integrated genetic, radiation hybrid, physical and transcription map of a region of distal mouse chromosome 12, including an imprinted locus and the 'Legs at odd angles' (Loa) mutation. *Gene* 283 (1-2):71-82, 2002.

LIST OF FIGURES

Figure 1.1	Neurons have axons and dendrites and communicate via synapses	2
Figure 1.2	The life cycle of synaptic vesicles at the active zone	7
Figure 1.3	The transition states of the stalk model of membrane fusion	13
Figure 1.4	Structures and schematic representations of neuronal SNARE proteins	15
Figure 1.5	SNARE complex brings the membranes into close proximity	16
Figure 1.6	The available structural information of synaptotagmin 1	28
Figure 1.7	The Ca ²⁺ -binding loops of synaptotagmin 1 C ₂ A and C ₂ B domains	30
Figure 2.1	TROSY-HSQC spectrum of monomeric syntaxin	48
Figure 2.2	TROSY-HSQC spectrum of the mixture of monomeric and oligomeric syntaxin	50
Figure 2.3	TROSY-HSQC spectrum of the syntaxin/SNAP25N complex	51
Figure 2.4	TROSY-HSQC spectrum of the syntaxin/SNAP25 complex	52
Figure 2.5	Glycine regions of the TROSY-HSQC spectra of the ² H, ¹⁵ N-labeled syntaxin in different complexes	54
Figure 2.6	TROSY-HSQC spectrum of the SNARE complex	56
Figure 2.7	TROSY-HSQC spectrum of monomeric SNAP25C	57
Figure 2.8	TROSY-HSQC spectrum of the syntaxin/SNAP25N complex	59
Figure 2.9	TROSY-HSQC spectrum of synaptotagmin 1 C2AB domain	61
Figure 3.1	SMR intensities of sample proteins and protein complexes	71
Figure 3.2	Scheme summarizing the SMR method for detecting protein-protein interactions	74

Figure 3.3 Testing the validity of the SMR method with a well-studied protein-protein interaction	77
Figure 3.4 Scheme summarizing the SMRC method for detecting protein-protein interactions	80
Figure 3.5 Application of the SMRC method to measure dissociation constants	83
Figure 3.6 Application of the SMRC method to study the interactions of synaptotagmin	87
Figure 3.7 Application of the SMRC method to study the interactions of the SNARE complex	91
Figure 3.8 Monitoring SMRC intensity at sub-micromolar protein concentrations	96
Figure 4.1 C ₂ B domain binds to negatively charged vesicles in a Ca ²⁺ -dependent manner	103
Figure 4.2 The synaptotagmin 1 C ₂ domains are flexibly linked	108
Figure 4.3 Relative membrane insertions of Ca ²⁺ binding loops of C ₂ A, C ₂ B and C ₂ AB domains	113
Figure 4.4 HSQC spectrum of ¹⁵ N-C277S-C ₂ AB	118
Figure 4.5 The positions of the cysteine mutations on the surface of the C ₂ B domain ...	121
Figure 4.6 Reaction of a thiol with an alkyl halide	122
Figure 4.7 Relative NBD fluorescence increases of C ₂ B surface mutants within C ₂ AB domain	124
Figure 4.8 Ca ²⁺ -dependent oligomerization of Synaptotagmin 1 C ₂ AB domain on the lipid membranes observed by negative staining EM	129

Figure 4.9 Negative staining electron microscopy images of synaptotagmin 1 bound to lipid vesicles	132
Figure 4.10 Single molecule reconstruction of synaptotagmin 1 oligomers	133
Figure 4.11 Negative staining electron microscopy images of distorted lipid vesicles ...	135
Figure 4.12 Negative staining EM images and single molecule reconstruction of GroEL	136
Figure 4.13 Photo-initiated protein cross-linking reaction of tris-bipyridylruthenium(II)	139
Figure 4.14 Crosslinking experiments of synaptotagmin 1 C ₂ AB domain using tris-bipyridylruthenium(II) as a crosslinking reagent.....	141
Figure 4.15 Schematic illustration of the binding of monomeric and oligomeric proteins on the vesicle surface	144
Figure 4.16 FRET efficiency between NBD-labeled and Rho-labeled C ₂ AB fragments upon binding to vesicles	147
Figure 4.17 Comparison of FRET efficiency between NBD and Rho labeled proteins at different lipid concentrations	150
Figure 4.18 The increase in the size of lipid vesicles upon Ca ²⁺ -dependent C ₂ AB binding ..	152
Figure 4.19 The positions of the mutations on the surface of the C ₂ B domain	157
Figure 4.20 Diagrams summarizing the vesicle clustering ability of different synaptotagmin mutants	159
Figure 4.21 Negatively charged lipid vesicles imaged by cryo-EM	163

Figure 4.22 Formation of vesicle clusters in the presence of synaptotagmin 1 and Ca^{2+} imaged by cryo-EM	164
Figure 4.23 Observation of the mass density between the vesicles at moderate defocus values	166
Figure 4.24 Representative images from cryo-EM tomography of lipid vesicles at different tilt angles	168
Figure 4.25 Tomographic 3D reconstruction of a vesicle cluster	170
Figure 4.26 Histogram summarizing the measured distances between the vesicle clusters	172
Figure 4.27 Hypothetical model of synaptotagmin action in neurotransmitter release ...	177
Figure 5.1 Three dimensional structures of SM proteins demonstrate the different modes of SM protein/syntaxin interactions	192
Figure 5.2 The N-terminal domain of rSly1 binds to the N-terminal Syntaxin 5 peptide	198
Figure 5.3 The secondary structure elements of the isolated and Syx5 peptide bound N- terminal domain of rSly1	199
Figure 5.4 Binding of Syntaxin 5 peptide induces changes in the NOE patterns of rSly1N	201
Figure 5.5 Three-dimensional NMR structure of the N-terminal domain of rat Sly1	205
Figure 5.6 Conformational change of rSly1N structure upon binding to syntaxin 5	208
Figure 5.7 Peptide-binding induced changes in the hydrophobic packing between helix 5 and strand 5	211

Figure 5.8 The register of strand 5 shifts with respect to strand 4 upon binding of Syntaxin 5 to rSly1N	214
Figure 5.9 Multiple sequence alignment of the helix 5-strand 5 region of SM proteins .	217
Figure 5.10 An evolutionary tree of SM proteins	219

LIST OF TABLES

Table 4.1	List of single cysteine mutations on the C ₂ A, C ₂ B and C ₂ AB domains	111
Table 4.2	List of C ₂ B surface residue mutations within the C ₂ AB domain	120
Table 4.3	List of synaptotagmin 1 proteins used in DLS experiments	155
Table 5.1	Structural statistics of the 20 lowest energy structures of the N-terminal domain of rSly1N	206

LIST OF DEFINITIONS

1D, 2D, 3D	one, two and three-dimensional
BoNT	botulinum neurotoxin
BSA	bovine serum albumin
CCD	charged coupled device
CD	circular dichroism
<i>C.elegans</i>	<i>Caenorhabditis elegans</i>
CNS	crystallography and NMR system
DLS	Dynamic light scattering)
DOPS	1,2-dioleoyl phosphatidylserine
DTT	dithiothreitol
<i>E.coil</i>	<i>Escherichia coli</i>
EDTA	ethylene diamine tetraacetic acid
EGTA	ethylene glycol-bis (β -aminoethyl ether)-tetraacetic acid
EM	electron microscopy
EPR	electron paramagnetic resonance
FRET	fluorescence resonance energy transfer
GST	glutathione-S-transferase
H/D exchange	hydrogen-deuterium exchange
HEPES	N-(2-hydroxyethyl) piperazine-N'-ethanesulphonic acid
HSQC	heteronuclear single quantum coherence
IPTG	isopropyl β -D-thiogalactopyranoside
KD	dissociation-constant

KDa	kilodalton
LB	luria broth
LUV	large unilamellar vesicles
NBD	<i>N,N'</i> -dimethyl- <i>N</i> - (iodoacetyl)- <i>N'</i> -(7-nitrobenz-2- oxa-1,3-diazol-4-yl)ethylenediamine
Ni-NTA	nickel-nitrilotriacetic acid
NMR	nuclear magnetic resonance
NOE	nuclear Overhauser effect
NOESY	nuclear Overhauser effect spectroscopy
OD	optical density
PAGE	polyacrylamide gel electrophoresis
PBS	phosphate buffered saline
PC	phosphatidylcholine
PE	phosphatidylethanolamine
POPC	1-palmitoyl, 2-oleoyl phosphatidylcholine
ppm	part per million
PS	phosphatidylserine
Rho	tetramethylrhodamine-5-iodoacetamide dihydroiodide
rmsd	root mean square deviation (Å)
SDS	sodium dodecylsulfate
SMR	the strongest methyl resonance
SMRC	the strongest methyl resonance ¹³ C-labeled
SNAP	soluble NSF attachment protein

SNAP-25	synaptosome-associated protein of 25 kDa
SNARE	SNAP receptor
SNAP25C	the C-terminal SNARE motif of SNAP-25
SNAP25N	the N-terminal SNARE motif of SNAP-25
Syb2	rat synaptobrevin 2 (29-93)
SyxS	rat syntaxin 1A (191-253)
TeNT	tetanus neurotoxin
TOCSY	total correlation spectroscopy
TRIS tris	(hydroxymethyl) aminomethane
TROSY	transverse-relaxation optimized spectroscopy
t-SNARE	target membrane SNARE
UV	ultra-violet
v-SNARE	vesicle SNARE

CHAPTER 1

GENERAL INTRODUCTION

1.1 Signal Transduction in Neurons

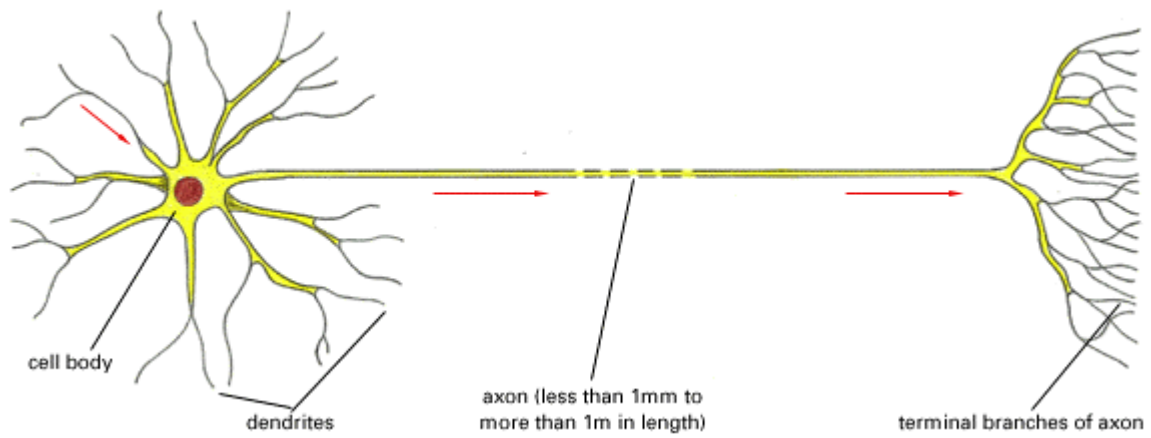
The brain is the primary center to receive and interpret sensory impulses, transmit information and regulate bodily activities. It is also the basis for thought, memory, emotion and consciousness. In the brain, specialized cells, called neurons, receive, conduct and transmit the signal to control all these processes.

1.1.1 The Neuron

No other cell type has attracted as much attention or caused as much controversy as the nerve cell, the neuron. The reason for this is some unique properties of the neurons like the establishment of the full neuronal population in an organism shortly after birth, the inability of mature neurons to divide and an average death rate of 20,000 neurons per day in humans.

Neurons are highly specialized cells with very distinct shapes. The stereotypical image of a neuron is a star-like cell body with broad dendrites emerging from one pole and a fine axon emerging from the other pole as reported by Purkinje who first described the nerve cell in 1839 (Figure 1.1A). The asymmetric shape of the neurons helps to form a unidirectional network where the information can flow from the source to the center of the nervous system to be processed. The signal is received by the dendrites of the nerve cell and is passed to the axon to be sent to the succeeding neuron. The extent of the

A



B

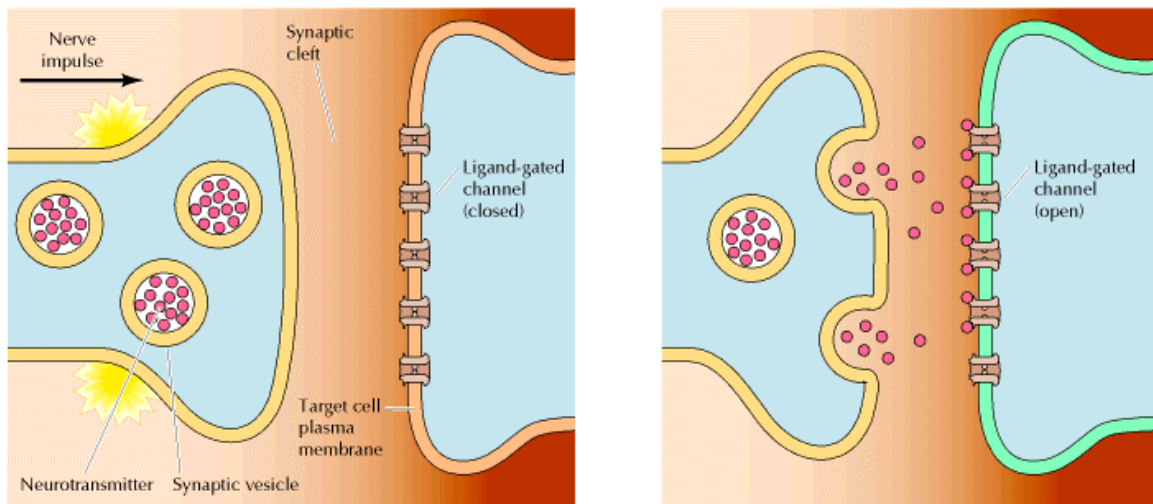


Figure 1.1 Neurons have axons and dendrites and communicate via synapses

(A) The dendrites and the axons of a nerve cell are shown. The action potential moves down from the cell body of the presynaptic cell to the axon terminal where it arrives at a synapse.

(B) Signaling by neurotransmitter release at the synapse is shown. The arrival of the action potential at the synapse causes the fusion of the synaptic vesicles with the plasma membrane and the release of neurotransmitters that bind to the receptors in the postsynaptic cell. (Molecular Biology of the Cell, Watson; The Cell A Molecular Approach, Cooper)

branching in the dendrites is an indication of the functional importance of the neuron as large dendritic trees represent that a single neuron has many connections with the other cells. The axon, emerging from the cell body as a single thin thread, can be as long as 5 meters in some organisms and stays unbranched until it reaches its target. To increase its efficiency as a conducting unit, it is frequently covered by myelin, a spirally wrapped membrane. The diameter of an axon can be as small as a micrometer in certain nerves of the human brain and as large as a millimeter in the giant fiber of the squid.

The signal received by a neuron is passed to the following cell through a specialized cell-cell junction called the synapse (Figure 1.1B). Synapses transmit the signal in only one direction, from the axon terminal of the presynaptic cell to the dendrites of the postsynaptic cell. Both axons and dendrites branch extensively at the synapses to maximize the interaction surface. At the highly specialized active zones, the proteins that form the machinery for transduction of the neural signal are localized. The arrival of an action potential at the active zone opens the Ca^{2+} channels, which triggers the fusion of the vesicles full of neurotransmitters with the plasma membrane and releases the neurotransmitters into the synaptic cleft between the neurons to be received by the postsynaptic cell. Neurotransmitters are small signaling molecules that are secreted from the presynaptic cell to relay the synaptic signal to the postsynaptic cell. The reception of the neurotransmitters by the receptors on the postsynaptic cell passes the signal to the postsynaptic cell in the vertebrate brain.

1.1.2 Action Potential

The concentrations of Na^+ and K^+ ions inside and outside of the neuron cell are not equal. ATP-dependent Na^+ - K^+ pumps on the cell membrane actively transport Na^+ out of and K^+ into the cells. This energy requiring process maintains the intracellular Na^+ concentration 10 fold lower and K^+ concentration 20 fold higher than the extracellular concentrations. Under these conditions, the osmotic balance across the cell membrane is maintained and the negatively charged molecules are properly balanced by the positively charged K^+ and Na^+ ions. However, K^+ ions tend to leave the cell through the K^+ leak channels, driven by its concentration gradient. A membrane potential arises because of the difference in the electrical charge on the two sides of the membrane, due to a slight excess of positive K^+ ions outside of the cell. The equilibrium condition where there is no net flow of ions across the cell membrane defines the resting membrane potential and is expressed by the Nernst equation.

When a neuron is at the resting state, the electric potential across the membranes is approximately -70 mV. If the membrane potential is reduced by a threshold of 15 mV to -55 mV, an action potential forms. An action potential is a series of sudden changes in the electric potential, across the plasma membrane and is 100-110 mV in amplitude (HODGKIN, 1964; HUXLEY, 1964; Katz and Miledi, 1968). The membrane potential reaches to 40 mV during the action potential. This depolarization of the membrane is followed by a rapid repolarization, returning the membrane potential to the resting value in about 1 ms (Jessell and Kandel, 1993). The sequential opening and closing of the voltage gated Na^+ and K^+ channels along the axon in a direction from the cell body to the axon terminal carries the action potential to the tip of the axon. The arrival of the action potential at the axon terminal opens voltage-gated Ca^{2+} channels at the synapse and

causes a sudden increase in intracellular Ca^{2+} concentration up to 200-300 μM (Llinas *et al.*, 1992; Llinas *et al.*, 1995). The increase in the intracellular Ca^{2+} concentration triggers the fusion of synaptic vesicles with the plasma membrane.

1.1.3 Synaptic Vesicle Cycle

Synaptic vesicles are independent functional organelles that contain neurotransmitters. Fusion of the synaptic vesicle membrane with the plasma membrane to release its contents into the synaptic cleft is an essential step for transmission of the signal. In the nerve terminal, synaptic vesicles undergo a life cycle which consists of many steps as shown in Fig 1.2 (Sudhof, 1995; Sudhof, 2004). Synaptic vesicles are first filled with neurotransmitters by active transport and are translocated to the active zone to attach to the synaptic plasma membrane, a process known as docking. The vesicles prepare for fusion by going through a priming step, which probably involves the formation of a complex between the vesicle and plasma membrane proteins as well as some cytoplasmic proteins. Upon arrival of an action potential, Ca^{2+} influx through the voltage-gated Ca^{2+} channels triggers membrane fusion and empties the synaptic vesicles. After the empty synaptic vesicles are coated with clathrin and other proteins required for endocytosis, they bud from the plasma membrane back into the cytoplasm. The clathrin coat is removed and the vesicles are acidified to return to the endosome where they are freshly regenerated. Two steps in this cycle can be slightly different: 1) Upon fusion, the fusion pore may close quickly by a rapid endocytosis (kiss and run) mechanism so that the vesicles will not be emptied. 2)

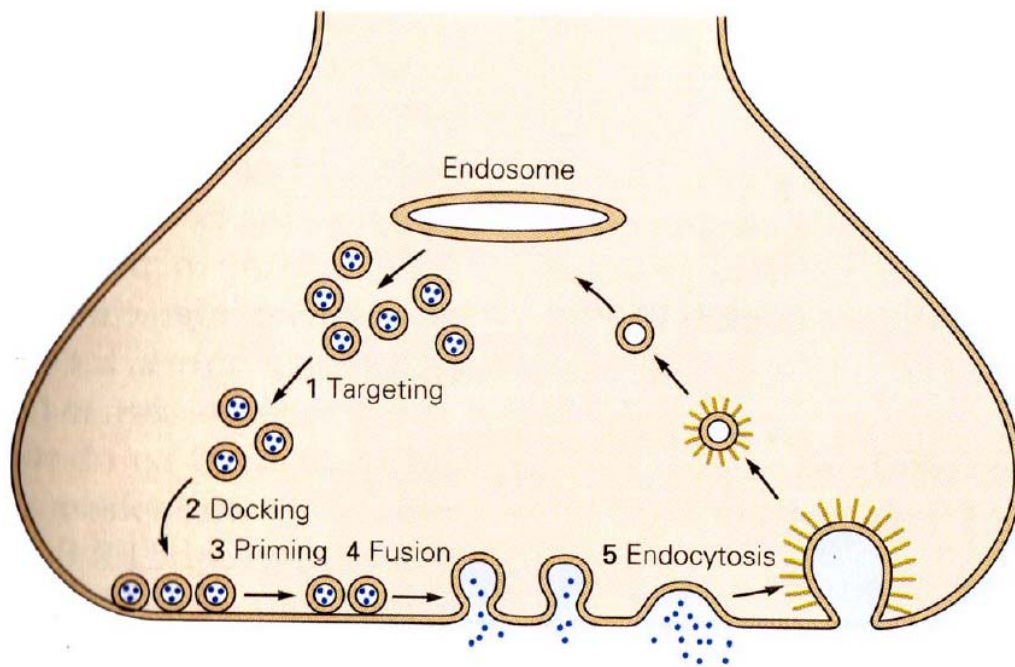


Figure 1.2 The life cycle of synaptic vesicles at the active zone

After the vesicles are filled with neurotransmitters, the vesicles are targeted, docked and primed to the plasma membrane. The increase in the intracellular Ca^{2+} concentration causes fusion of the synaptic vesicle with the plasma membrane and release of neurotransmitters into the synaptic cleft. The vesicles are endocytosed by a clathrin-mediated mechanism. Circles, dots and bars represent synaptic vesicles, neurotransmitters and clathrin molecules, respectively.

Endocytosed vesicles can be refilled with neurotransmitters directly, without fusing with the endosomal membrane.

The number of proteins known to be involved in the synaptic vesicle cycle is in the order of a hundred and it is possible that many remain undiscovered. The entire cycle takes about 1 min (Betz and Bewick, 1992; Ryan *et al.*, 1993). Exocytosis takes less than 1 ms, endocytosis occurs in 5 sec, and the remaining 55 sec is used for recycling of the vesicle.

1.1.4 Comparison of constitutive membrane fusion with synaptic vesicle fusion

Membrane fusion occurs in organisms from yeast to humans and in a variety of organelles including endoplasmic reticulum, lysosome, golgi complex, endosome, vacuole, synaptic vesicle and plasma membrane (Ferro-Novick and Jahn, 1994; Bennett and Scheller, 1994). The mechanism of membrane fusion in all these cases is similar. Most types of membrane fusion are constitutive. However, the special case of neurotransmitter release in the synapse creates unique requirements. In the synapse, a localized and rapid signal that can be repeated at high frequency and regulated by time is required. Thus membrane fusion between synaptic vesicles and the plasma membrane has two unique features: 1) It is tightly regulated by Ca^{2+} so that there will not be any significant fusion in the absence of Ca^{2+} and an increase in the local Ca^{2+} concentration will dramatically increase the probability of release. 2) It has a very fast response time and occurs with a delay of less than 1 ms after the arrival of the action potential. This sophisticated mechanism in the synaptic vesicle fusion is maintained by a basic

machinery that is homologous to the one used for constitutive membrane fusion, but has additional components specialized for its tight regulatory requirements.

1.1.5 Calcium Dependence of Neurotransmitter Release

In late 1960s, Katz and Miledi performed a set of experiments on the squid synapse and the vertebrate neuromuscular junction that led them to the calcium hypothesis (Katz *et al.*, 1968). This hypothesis stated that Ca^{2+} influx into the cell is required for neurotransmitter release and Ca^{2+} has to be present almost exactly when the action potential arrives at the presynaptic terminal. Further support for the calcium hypothesis came from Miledi when he showed that direct injection of Ca^{2+} into the presynaptic terminal of the squid synapse led to transmitter release (Miledi, 1973). In 1967, Dodge and Rahamimoff proposed that neurotransmitter release is dependent upon the fourth power of the Ca^{2+} concentration in the extracellular bath which means that four Ca^{2+} ions act in a cooperative manner to cause release (Dodge, Jr. and Rahamimoff, 1967). It was concluded that Ca^{2+} binds to some critical site at the presynaptic terminal in order for transmitter release to occur.

The free intracellular Ca^{2+} concentration of a resting nerve cell is about 100-200 nM, 10000-fold lower than the outside Ca^{2+} concentration (2.5-5 mM). Neurotransmitter release is tightly coupled to the increase in intracellular Ca^{2+} concentration that is caused by the arrival of a nerve impulse. The classical view is that the probability of vesicle fusion increases within less than 0.2 msec after Ca^{2+} influx and returns to lower levels within 1 msec (Barrett and Stevens, 1972). However, it has been shown that this kinetics holds only at room temperature and response to action potential is even faster at

physiological temperatures. Optical measurements of voltage and currents simultaneously from pre- and postsynaptic neurons showed that postsynaptic responses begin 150 μsec after the arrival of an action potential and there is only 60 μsec between Ca^{2+} influx and membrane fusion (Sabatini and Regehr, 1999). The speed and precision of Ca^{2+} regulation is the major difference of synaptic neurotransmitter release from other membrane trafficking processes.

It is generally assumed that fast neurotransmitter release is triggered by elevations in intracellular Ca^{2+} concentration to at least 100 μM near the sites of vesicle fusion. However, studies on synapses from central nervous system showed that step-like elevations to only 10 μM Ca^{2+} induce fast neurotransmitter release and depletes around 80% of the pool of available vesicles in less than 3 msec (Schneggenburger and Neher, 2000). Measurements of calcium sensitivity of glutamate release in rat brainstem synapses concluded that a rise in Ca^{2+} concentration to 1 μM evokes release while an increase to >30 μM depletes the available vesicle pool in less than 0.5 msec. (Bollmann *et al.*, 2000). A comparison with action potential-evoked release suggested that a brief increase of calcium to ~ 10 μM would be sufficient to reproduce the physiological release pattern.

This mechanism requires a Ca^{2+} sensor, which will sense the increase in Ca^{2+} concentration and act immediately to help fuse the two membranes. As the physiological Ca^{2+} concentration required for neurotransmitter release is ~ 10 μM and the timescale of neurotransmitter release is less than milliseconds, the Ca^{2+} sensor in the synapse should be very fast and have a Ca^{2+} affinity of about 10 μM .

1.1.6 Membrane Fusion

Biological membrane fusion is a local-point event that occurs extremely rapidly and is tightly regulated so that only the appropriate membranes will fuse with each other. The time and place of fusion is controlled by proteins that are responsible for recognizing and bringing the fusion partners together. These proteins determine the initiation of membrane fusion. However, the real fusion event requires the merger of two membranes and the reorganization of the membrane lipids into curved intermediates. For this reason, lipids are central players in membrane fusion.

A small area of the lipid bilayers is required to be closer than 3 nm for fusion to occur (Helm and Israelachvili, 1993). A repulsive hydration force arises from water that is tightly bound to the lipid headgroups. This force pushes the membranes away. The membrane interior can be exposed more when there are defects in the membranes and these cause an increase in the hydrophobic interactions of the hydrophobic carbon chains of the membranes. Extreme membrane curvature, local changes in membrane lipid composition and insertion/de-insertion of hydrophobic peptides into the membranes can cause disorder in membrane lipid packing and thus can be helpful to overcome the energy required for fusion (White, 1992;Bentz, 2000).

The willingness of a membrane to fuse is primarily determined by the membrane lipid composition (Chernomordik, 1996). At the same temperature and electrolyte composition, different lipids form different phases. It is suggested that specific lipid species may play an active role in the local destabilization and fusion of membranes (Chernomordik, 1996).

It is unlikely that a fusion pore can be formed from two lamellar bilayers in a single catastrophic rearrangement of hundreds of lipid molecules since the required activation energy is extremely large (Siegel, 1993). It is more likely that fusion occurs via formation of different intermediate structures with continuous lipid/water interfaces. In the stalk model of fusion, a thin layer of water separates the membranes before fusion. Van der Waals attraction, electric repulsion of charged lipids and hydration repulsion act on the membrane bilayers. Although the membranes are parallel on average, they exert bending fluctuations towards each other. The first intermediate is a stalk, which is a structure that makes the facing monolayers of the two membranes continuous (Figure 1.3). The cylindrically symmetric stalk expands radially and forms a trans monolayer contact (TMC) bilayer, which consists of distal monolayers of fusing membranes (Figure 1.3). The final stage of the fusion process is achieved by the formation of a pore in the contact bilayer.

Although the stalk model identifies stalks and TMCs as the lowest energy intermediates of fusion, their energies calculated by the model are still large. This suggests that either the current model is not a good representation of the real fusion event or other factors, such as proteins, are helping lipid molecules to reduce the energy barriers. Proteins might be catalyzing membrane fusion by making local changes in the lipid properties, by physically bringing the membranes together or by inserting/deinserting into the membranes to cause disruption in the lipid packaging of membranes.

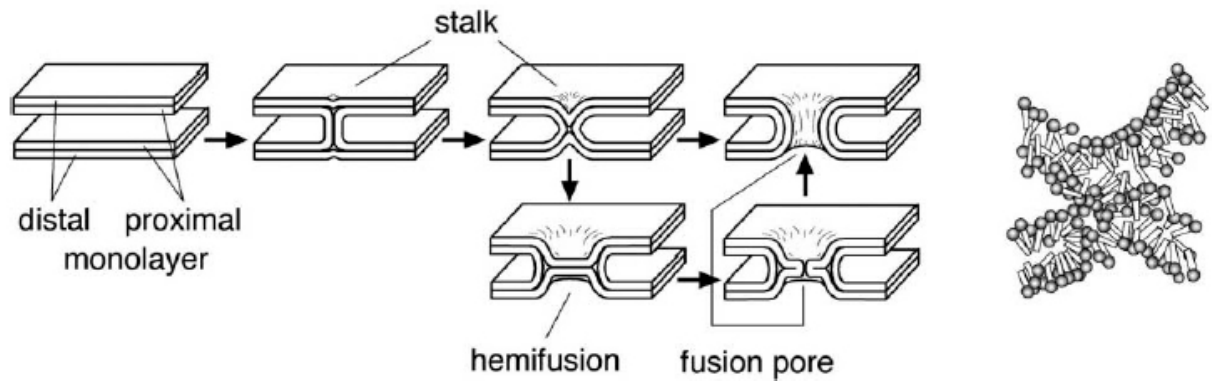


Figure 1.3 The transition states of the stalk model of membrane fusion

Two membrane bilayers are schematized. The stalk model of membrane fusion describes the membranes as smooth and bendable sheets that contain random curvatures. The stalk is formed when the proximal but not the distal leaflets form a continuous layer. Transbilayer contact occurs when the distal bilayers contact with each other. The fusion pore forms when both proximal and distal leaflets become continuous. A snapshot of a nonbilayer intermediate derived from a simulation of membrane fusion is shown on the right. (Jahn *et al.*, 2003)

1.2 Proteins involved in membrane fusion

1.2.1 SNARE proteins

A major role in exocytosis is played by a superfamily of proteins known as the SNARE (Soluble NSF-attachment Protein Receptor) proteins. The SNARE proteins share a homologous domain of ~60 residues which is referred to as the SNARE motif (Terrian and White, 1997; Weimbs *et al.*, 1998). SNARE superfamily can be classified into t-SNAREs (for SNAREs localized to the target membrane) and v-SNAREs (for SNAREs localized to the vesicle membrane) on the basis of their localization. The t-SNAREs are further divided into syntaxin and SNAP25 families whereas v-SNAREs contain synaptobrevin homologues.

The syntaxins and the synaptobrevins contain a single SNARE motif that is preceded by variable N-terminal sequences and is followed by a C-terminal transmembrane region (Weimbs *et al.*, 1997). The α -helical N-terminal domain of neuronal syntaxin 1a interacts with the SM protein Munc18. The N-terminal domain is involved in the regulation of syntaxin function by helping to switch between closed and open conformations upon Munc18 binding (Fernandez *et al.*, 1998; Dulubova *et al.*, 1999). Other SNAREs might not have the same pattern. For instance, SNAP25 family members do not have a transmembrane domain but contain two SNARE motifs that are separated by a cysteine-rich sequence. The cysteines are palmitoylated and attach SNAP25 to the plasma membrane (Hess *et al.*, 1992) (Figure 1.4).

In the synapse, the SNARE proteins synaptobrevin 2, syntaxin 1 and SNAP25 assemble into a very stable α -helical coiled coil complex with a 1:1:1 stoichiometry (Jahn and Sudhof, 1999) (Figure 1.5). This complex is named the SNARE or core

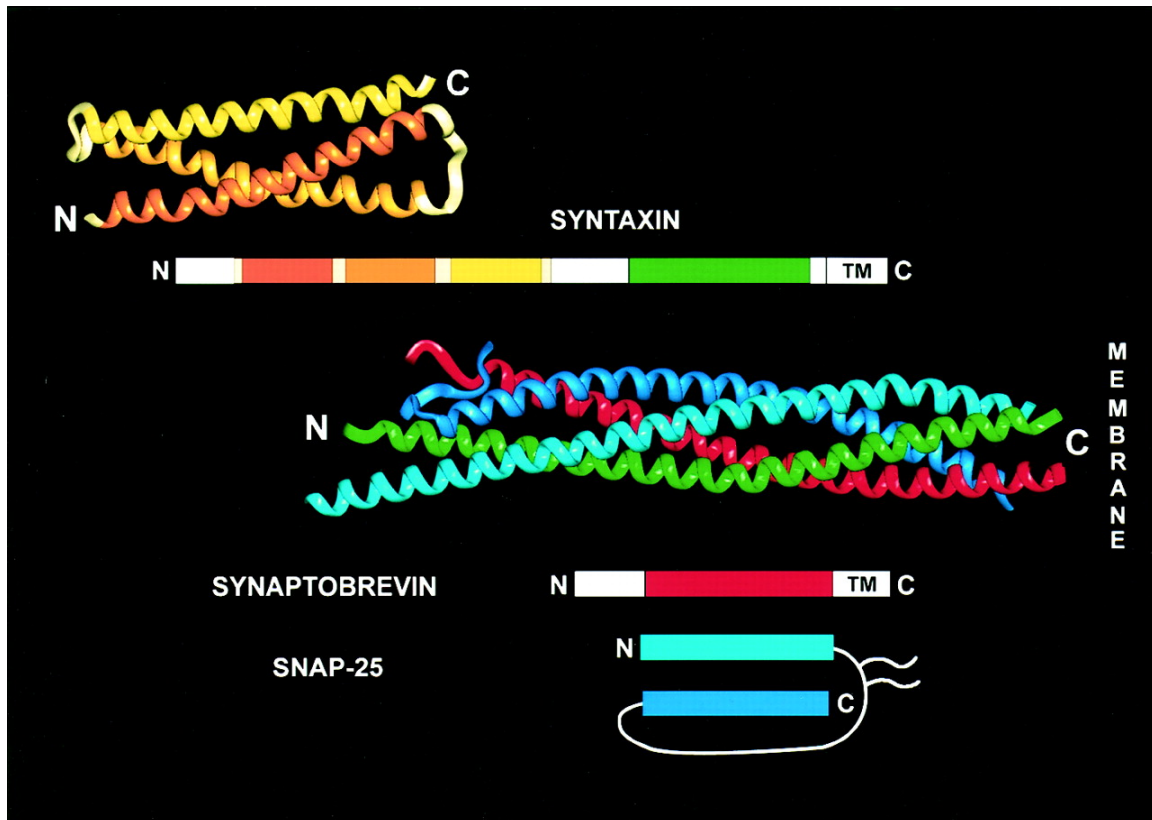


Figure 1.4 Structures and schematic representations of neuronal SNARE proteins
 The ribbon diagram of the structures of the N-terminal H_{abc} domain of syntaxin 1A and the SNARE complex are shown. The linear arrangement of the domains of SNARE proteins is schematized. The SNARE motifs of syntaxin, synaptobrevin and SNAP25 are colored as green, red and blue, respectively. N and C termini and the transmembrane domains are indicated as N, C and TM, respectively. Four SNARE motifs align in a parallel manner to form the SNARE complex with their C-termini close to the membranes. (Jahn *et al.*, 1999)

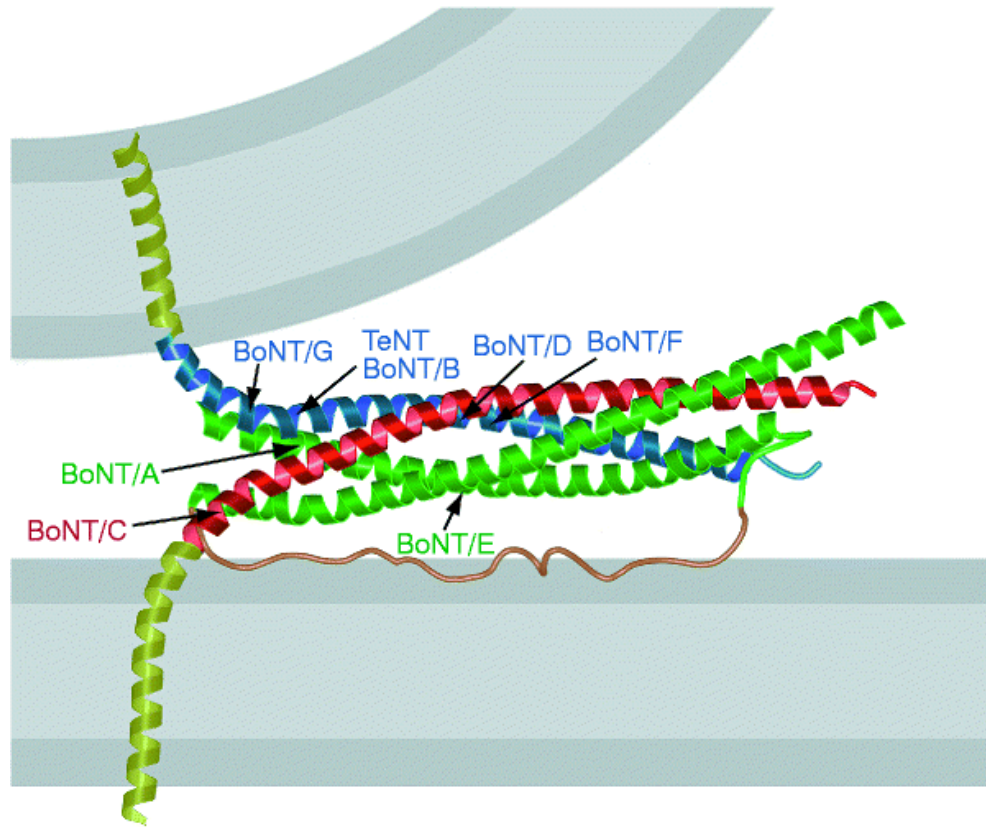


Figure 1.5 The SNARE complex brings the membranes into close proximity

Hypothetical model of the SNARE complex showing that the membranes come into close proximity when the SNARE complex is formed. The crystal structure of the neuronal SNARE complex is extended to include the transmembrane domains of syntaxin 1A and synaptobrevin II and the loop connecting the SNARE motifs of SNAP25. The transmembrane regions are represented as helices. The loop region of SNAP25 is represented as unstructured polypeptide chain. The cleavage sites of neurotoxins are also indicated. (Sutton et al., 1998) (syntaxin:red, synaptobrevin: blue, SNAP25: green, transmembrane regions: yellow, SNAP25 loop: orange)

complex. Site-directed mutagenesis and limited proteolysis (Hayashi *et al.*, 1994; Hayashi *et al.*, 1995; Poirier *et al.*, 1998a) revealed that the SNARE proteins bind to each other via their SNARE motifs. Four SNARE motifs (one from synaptobrevin, one from syntaxin and two from SNAP25) contribute to the SNARE complex. Electron microscopy, FRET, CD spectroscopy and site-specific labeling showed that the core complex is composed of a helical bundle formed in a parallel fashion where the transmembrane regions emerge from the C-terminal end of the bundle (Hanson *et al.*, 1997; Lin and Scheller, 1997; Fasshauer *et al.*, 1997b; Fasshauer *et al.*, 1998; Poirier *et al.*, 1998a). The SNARE motifs are unstructured in isolation but form helices upon SNARE complex formation (Fasshauer *et al.*, 1998; Poirier *et al.*, 1998b; Dulubova *et al.*, 1999).

The SNARE complex, shown to be heat and SDS resistant *in vitro* (Hayashi *et al.*, 1994; Fasshauer *et al.*, 1997b), overcomes the repulsive force between the two membranes and brings them close in space. Because the SNARE motifs of syntaxin and synaptobrevin are adjacent to their transmembrane regions, which are anchored to the plasma and vesicle membranes, the formation of core complex in a parallel orientation brings the opposing membranes in close proximity. According to the zipper model of SNARE-mediated fusion (Hanson *et al.*, 1997; Lin *et al.*, 1997), the SNARE proteins associate from the N to C-terminus as the synaptic vesicle and presynaptic membranes approach each other. The importance of the SNARE complex formation in membrane fusion has been discovered by the observation that botulinum and tetanus neurotoxins inhibit neurotransmitter release by proteolytic cleavage of the SNARE proteins (Schiavo *et al.*, 1992; Link *et al.*, 1992; Blasi *et al.*, 1993a; Blasi *et al.*, 1993b) (Figure 1.5). The proteolytic cleavage occurs at sites near the C terminus of the core complex. The effect of

neurotoxins is thus maximized by cleaving the core complex at the vicinity of the membranes.

The crystal structure of the neuronal SNARE complex (Sutton *et al.*, 1998) shows that it consists of a four-helix coiled-coil structure with a length of 12 nm and confirms that all chains are aligned in parallel (Figure 1.5). The interactions in the core of the bundle are mostly hydrophobic except for an ionic layer formed in the center of the four-helical bundle. This layer contains one arginine residue from synaptobrevin and three glutamine residues from each of the other SNARE motifs and is suggested to help core complex to zip correctly during assembly. The interior residues of the SNAREs are more conserved than the surface residues and the polar layer is conserved all over the SNARE family. The strict conservation of arginine and glutamine residues led to another classification of SNAREs as the Q-SNAREs and the R-SNAREs. The crystal structure of a mammalian endosomal SNARE complex has very similar properties to that of the neuronal SNARE complex in spite of low sequence homology (Antonin *et al.*, 2002). Although the interior residues of the neuronal core complex are mostly hydrophobic, the surface residues are highly charged. Syntaxin 1a and both SNARE motifs of SNAP25 are negatively charged whereas synaptobrevin 2 is positively charged.

The formation of the core complex was proposed to cause membrane fusion by using the energy released upon formation of this highly stable helix bundle to overcome the energy barrier for fusion (Hanson *et al.*, 1997; Lin *et al.*, 1997). Reconstitution experiments with synaptobrevin and syntaxin/SNAP25 incorporated into separate lipid vesicles suggested that SNAREs constitute the minimal machinery for membrane fusion (Weber *et al.*, 1998). However, only lipid mixing at very slow rates was demonstrated by

these experiments implying that physiological membrane fusion probably cannot be observed under these conditions. Many other studies indicate that SNAREs are important but not sufficient for membrane fusion. Genetic experiments supported the role of SNAREs for membrane fusion but suggested a catalytic rather than an essential role for SNAREs. In synaptobrevin knockout mice Ca^{2+} -triggered release is 100-fold less but 10% of spontaneous miniature release events (minis) and reduced hypertonic sucrose-induced release remains (Schoch *et al.*, 2001). In the SNAP25 knockout mice, Ca^{2+} -triggered release is abolished but the frequency of minis is increased (Washbourne *et al.*, 2002). Similarly, deletion of syntaxin in *Drosophila* abolishes evoked neurotransmitter release while maintaining the minis (Schulze *et al.*, 1995; Broadie *et al.*, 1995). These data suggest that SNAREs act as catalysts and facilitate membrane fusion rather than being the minimal fusion machinery.

In the SNARE hypothesis of fusion, recognition between v-SNAREs and t-SNAREs is proposed to mediate vesicle docking and targeting specificity (Sollner *et al.*, 1993b; Rothman, 1994). SNAREs have biologically specific functions but their specificity may arise from surface or hydrophobic interior residues of the SNARE motifs as well as other regions of the SNARE proteins. Reconstitution experiments using different combinations of yeast SNAREs suggested that membrane traffic specificity is largely encoded by the SNAREs (McNew *et al.*, 2000; Paumet *et al.*, 2001; Parlati *et al.*, 2002). Although numerous studies show that SNAREs determine specificity, the extent of specificity contributed by the SNAREs is under debate. The facts that membrane fusion occurs only at the active zones in spite of the presence of syntaxin 1 and SNAP25 throughout the plasma membrane (Garcia *et al.*, 1995) and that the synaptic vesicles

target different compartments while recycling during their life span (Pelham, 1999) indicate the requirement for other factors in the maintenance of membrane fusion specificity. In addition, experiments with *Drosophila* mutants show that SNAREs are not required for docking vesicles to the active zone (Broadie *et al.*, 1995). Also, the observation that clostridial toxins interfere with the fusion event but not with the recognition of synaptic vesicles and the active zones (Sudhof *et al.*, 1993) suggest that other factors are also involved in determining the specificity of membrane fusion.

1.2.2 Synaptotagmin 1

In the brain, the Ca^{2+} sensor for the fast component of neurotransmitter release is most likely synaptotagmin 1 (Perin *et al.*, 1990; Brose *et al.*, 1992a; Fernandez-Chacon *et al.*, 2001). Synaptotagmin 1 is a synaptic vesicle membrane protein and has two cytoplasmic C_2 domains (C_2A and C_2B) that bind Ca^{2+} . Detailed information about synaptotagmin 1 is given in Section 1.3.

1.2.3 SM proteins

Sec1/Munc18 (SM) proteins are 60-70 KDa cytosolic proteins and are required for all types of intracellular traffic, similar to SNAREs. Mutations in SM proteins completely block membrane fusion (Ossig *et al.*, 1991; Hosono *et al.*, 1992; Schekman, 1992; Harrison *et al.*, 1994). The absolute requirement of the neuronal SM protein, munc18-1, for neurotransmitter release was demonstrated by the total lack of Ca^{2+} -evoked release, minis or fusion triggered by hypertonic sucrose or α -latrotoxin in munc18-1 knockout mice (Verhage *et al.*, 2000). Studies indicate that munc18-1 might

function after SNARE complex formation (Verhage *et al.*, 2000; Grote *et al.*, 2000; Wang *et al.*, 2002) but the precise role of SM proteins in fusion is still unclear.

The interaction of neuronal syntaxin 1a with munc18-1 has been demonstrated to be important for neurotransmitter release (Hata *et al.*, 1993; Wu *et al.*, 1998; Wu *et al.*, 1999; Verhage *et al.*, 2000; Voets *et al.*, 2001). Syntaxin 1a has an N-terminal domain which is an autonomously folded three helix bundle called the H_{abc}-domain (Fernandez *et al.*, 1998). In isolated syntaxin 1a, the H_{abc} domain folds back onto the SNARE motif of the syntaxin 1a forming a closed conformation. Syntaxin, which is incorporated into the SNARE complex, is in an open conformation and the H_{abc}-domain does not interact with the SNARE motif. Munc18-1 binds to the closed conformation and competes with core complex formation (Dulubova *et al.*, 1999; Yang *et al.*, 2000). Thus Munc18-1 is suggested to have an inhibitory role on fusion.

SM proteins tightly interact with the syntaxins. However, the mode of this interaction is not conserved as both the binding site of SM proteins to the syntaxins and the required region in the syntaxin for SM protein binding is variable. More information about SM proteins and syntaxin/SM protein interactions is given in section 5.1.

1.2.4 Munc13/ Rim

The interaction of munc18 with the closed form of syntaxin is inhibitory for the formation of the core complex. The syntaxin/munc18 complex should be disassembled in order to form the core complex and prepare for membrane fusion. Two large proteins at the active zone of neurons, unc13/munc13 and RIM (Rab3-interacting protein), are suggested to mediate the disassembly of syntaxin/munc18 complex to enable the switch

of syntaxin from closed to open conformation preparing it for core complex formation. *C. elegans* unc13 (Maruyama and Brenner, 1991) and the mammalian munc13s (Brose *et al.*, 1995) are involved in priming the synaptic vesicles in the plasma membrane. (Augustin *et al.*, 1999). Mutations of unc13 in *C. elegans* (Richmond *et al.*, 1999), *Drosophila* (Aravamudan *et al.*, 1999) and double knockout of munc13-1 and 2 in mice (Rosenmund *et al.*, 2002) completely block neurotransmitter release, indicating the critical role of unc13/munc13s. Mutations of RIM in *C. elegans* also cause a severe decrease in release probably due to a defect in synaptic vesicle priming (Koushika *et al.*, 2001). Deletion of a RIM isoform in mice decreases the release probability (Schoch *et al.*, 2002).

A study detected an interaction between munc13-1 and the amino terminal of syntaxin 1 and showed that munc13 displaces syntaxin from the munc18 suggesting a direct role for munc13 in the dissociation of syntaxin/munc18 complex (Betz *et al.*, 1997). Another study suggests that munc13 binds to munc18 to release syntaxin (Sassa *et al.*, 1999). A mutant syntaxin which has a constitutively open form and thus is unable to interact with munc18 (Dulubova *et al.*, 1999) was shown to almost completely rescue neurotransmitter release in *C. elegans* with an Unc13 mutation whereas wild type syntaxin was unable to rescue release (Richmond *et al.*, 2001). This showed that the open form of syntaxin bypasses the requirement for Unc13 in vesicle priming suggesting that unc13 is involved in releasing syntaxin from the syntaxin/munc18 complex. Similar results were observed in *C. elegans* RIM mutant. These observations can be explained by a model in which the syntaxin/munc18 complex maintains the off-state of release by inhibiting each other whereas RIM and Munc13 are required to dissociate the complex

for the on-state. The restricted localization of Munc13 and RIM to the active zone ensures that neurotransmitter release occurs only at the right place.

1.2.5 Rab Proteins

Rab/Ypt GTPases are proteins that shuttle between a GDP bound soluble inactive state and a GTP, membrane bound active state. In most fusion events, active Rabs on the donor membranes either bind to effectors to recruit them or bind to proteins and lipids on the acceptor membrane to tether the two membranes together. The high number of Rab isoforms (11 in yeast and 60 in mammals) localized at specific intracellular compartments contributes to the specificity of fusion (Pereira-Leal and Seabra, 2001).

Rab3 is the most abundant Rab protein on the synaptic vesicles. The Rab3A,B,C,D quadruple knockout mice demonstrate that Rab3 is not itself essential for synaptic membrane traffic but functions to modulate the basic release machinery (Schluter *et al.*, 2004). In the active zone, Rim acts as an effector for Rab3. Although the deletion of Rim or Rab3 does not alter the vesicle attachment, it has dramatic effects on Ca^{2+} -triggered exocytosis, suggesting that binding of Rab3 to Rim is required for the regulation of synaptic vesicle activation in the active zone (Dobrunz and Garner, 2002). Rab3 and Rim act as the central components to nucleate large, biochemically insoluble protein complexes that are involved in synaptic vesicle fusion.

1.2.6 Complexins

Complexin 1 and 2 are evolutionarily conserved, 16-17 kDa proteins that are highly enriched in the brain and co-localize with the neuronal SNAREs (McMahon *et al.*,

1995;Takahashi *et al.*, 1995;Ishizuka *et al.*, 1995). Complexins bind to the neuronal SNARE complex in a Ca^{2+} -independent manner (McMahon *et al.*, 1995;Pabst *et al.*, 2002). Complexin knockout mice showed that complexins are critical for the Ca^{2+} -dependent neurotransmitter release but not for hypertonic sucrose triggered release, indicating a late role in the Ca^{2+} -evoked exocytosis for complexins (Reim *et al.*, 2001). Injection of a peptide that interferes with complexin/SNARE complex interaction into the squid giant synapse also indicated similar conclusions (Tokumaru *et al.*, 2001).

The crystal structure of the complexin-1/SNARE complex showed that complexin adopts an α -helical conformation to bind to the SNARE complex in an antiparallel fashion between the syntaxin and synaptobrevin, interface and does not cause any changes in the SNARE complex structure (Chen *et al.*, 2002). Numerous salt bridges, hydrogen bonds and hydrophobic interactions between complexin and the SNARE complex stabilize the interface between syntaxin and synaptobrevin as observed by deuterium exchange experiments (Chen *et al.*, 2002). This observation led to a model in which priming occurs in two stages. The SNARE complex starts forming in the first stage bringing the membranes in close proximity. However, full core complex formation occurs only after binding of complexin to the SNARE complex to stabilize it. Sealing the interface between the syntaxin and synaptobrevin –the two SNARE motifs at opposing membranes- helps to overcome the strong repulsive forces between the membranes and prepares the vesicle for fusion for the Ca^{2+} -triggered exocytosis.

1.3 Synaptotagmin 1

1.3.1 Synaptotagmin 1 as a Calcium Sensor

Synaptotagmin 1 was first discovered as p65 by using a monoclonal antibody that was raised to interact with synaptic plasma membranes but the antibody was found to bind to a synaptic vesicle protein (Matthew *et al.*, 1981). Biochemical studies indicate that synaptotagmin 1 is a highly conserved brain-specific transmembrane protein abundant on the synaptic vesicle membrane (Perin *et al.*, 1990; Perin *et al.*, 1991a; Perin *et al.*, 1991b). It has two C₂ domains, which bind to Ca²⁺. Because of these properties synaptotagmin 1 was suggested as the most likely candidate for being the Ca²⁺ sensor in neurons. Gene disruption studies in *C. elegans* and *Drosophila* demonstrated the importance of synaptotagmin 1 in neurotransmitter release (Nonet *et al.*, 1993; Littleton *et al.*, 1993; Littleton *et al.*, 1994; DiAntonio and Schwarz, 1994). Electrophysiological studies of the synaptotagmin 1 knockout mice showed that it is selectively required for fast Ca²⁺-dependent neurotransmitter release (Geppert *et al.*, 1994). Neurotransmitter release in wild type neurons is observed in a fast phase, which corresponds to 80% of the release, followed by a slow phase. The observation that the synchronous, fast component of Ca²⁺-dependent neurotransmitter release is severely decreased in the synaptotagmin 1 knock-out mouse, whereas asynchronous, slow release is unaffected demonstrated that synaptotagmin 1 function is required for Ca²⁺ triggering of neurotransmitter release (Geppert *et al.*, 1994). However, the actual low affinity Ca²⁺ sensor in the synapse was not clear until it was shown that a knock-in mouse with a point mutation in synaptotagmin 1 (R233Q in rat) that causes a twofold decrease in overall Ca²⁺ affinity without inducing structural changes, has also decreased Ca²⁺ sensitivity of

neurotransmitter release twofold (Fernandez-Chacon *et al.*, 2001). R233 is a positively charged residue located close to the Ca^{2+} binding aspartate residues of the C₂A domain. Although it is not essential, it contributes to the Ca^{2+} dependent membrane binding ability of the double C₂AB domain. This finding strongly suggests that Ca^{2+} binding to synaptotagmin 1 participates in triggering neurotransmitter release at the synapse. However, the action of other Ca^{2+} sensors is also possible.

In a recent study, membrane fusion of reconstituted vesicles was reported to be strongly stimulated with synaptotagmin 1 in a Ca^{2+} -dependent manner (Tucker *et al.*, 2004). This observation suggested that SNAREs and synaptotagmin 1 form the minimal machinery for membrane fusion although reconstitution methods to mimic membrane fusion in vitro are evaluated with skepticism.

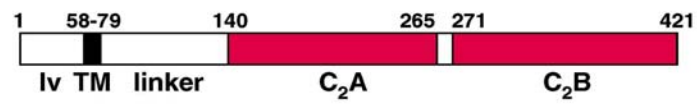
1.3.2 C₂ domain structure

C₂ domains are autonomously folded protein modules of approximately 130 residues. These domains were first defined in protein kinase C and later were identified in more than 50 proteins, most of which participate in signal transduction and membrane traffic (Kikkawa *et al.*, 1989; Brose *et al.*, 1995; Rizo and Sudhof, 1998a). The most common properties of the C₂ domains are Ca^{2+} and phospholipid binding, although not all C₂ domains share these characteristics. The C₂ domains from synaptotagmin 1, PKCs and perforin bind to negatively charged phospholipids, whereas the cPLA₂ C₂ domain only interacts with neutral lipids (Davletov and Sudhof, 1993; Li *et al.*, 1995; Shao *et al.*, 1996; Uellner *et al.*, 1997; Nalefski *et al.*, 1998).

Synaptotagmin 1 is an intrinsic membrane protein and has a conserved structure within vertebrates and invertebrates (Perin *et al.*, 1990). It has a short intravesicular amino terminus that is N-glycosylated and a single transmembrane region followed by two C₂ domains (named as C₂A and C₂B) that are connected to each other by a short linker (Figure 1.6A). The C₂ domains form most of the cytoplasmic region and mediate Ca²⁺-dependent and Ca²⁺-independent interactions with target molecules that may regulate membrane fusion.

The three-dimensional structures of both C₂A and C₂B domains of synaptotagmin 1 have been solved (Sutton *et al.*, 1995b; Shao *et al.*, 1998; Sutton *et al.*, 1999; Fernandez *et al.*, 2001). Both C₂ domains are formed by a compact eight-stranded β -sandwich composed of two antiparallel β -sheets that are extensively hydrogen bonded (Figure 1.6B). The β -sandwich core is very similar in various C₂ domains and probably serves as a scaffold. Whereas C₂A domain does not contain any α -helices, C₂B domain is 20 residues longer than C₂A and contains two α -helices, one at the C-terminus and the other at the bottom face between strands 7 and 8. Variable loops emerge from the top and bottom faces of the β -sandwich. The three loops (named loops 1, 2 and 3) on the top of the synaptotagmin 1 C₂ domains bind to Ca²⁺ ions. The C₂A domain can bind three Ca²⁺ ions coordinated by five aspartate side chains, one serine side chain and three backbone carbonyl groups (Shao *et al.*, 1996; Ubach *et al.*, 1998) (Figure 1.7). The Ca²⁺-binding loops of C₂B domain are very similar to the C₂A domain and coordinate two Ca²⁺ ions by five conserved aspartates. Mutation of one of the aspartate residues in loop 1 (D178 in C₂A, D309 in C₂B in rat), which coordinates the first Ca²⁺, strongly abolishes the Ca²⁺-binding to the C₂ domains. Mutations in other aspartate residues in loop 3 (D238 in

A



B

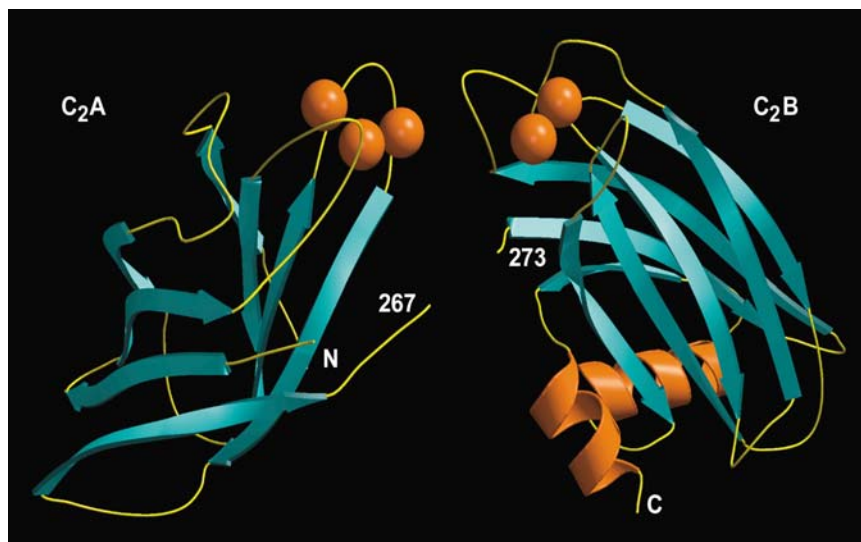


Figure 1.6 The available structural information of synaptotagmin 1

(A) Domain structure of synaptotagmin 1. C₂A and C₂B domains are colored in red and the transmembrane region is indicated as TM. The residue numbers of the domain boundaries are labeled.

(B) The NMR structures of C₂A and C₂B domains of synaptotagmin 1 are shown as ribbon diagrams (PDB accession codes 1BYN and 1K5W). Helices are colored in orange and the strands are colored in cyan. Ca²⁺ ions are represented with orange spheres. The two C₂ domains are oriented with their Ca²⁺-binding sites in close proximity. (Fernandez *et al.*, 2001)

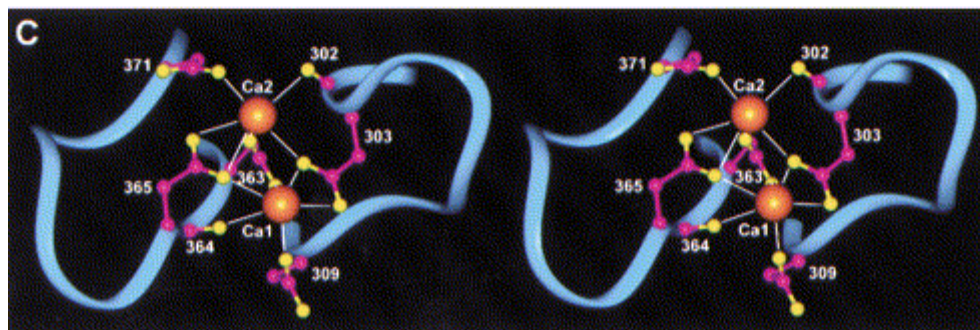
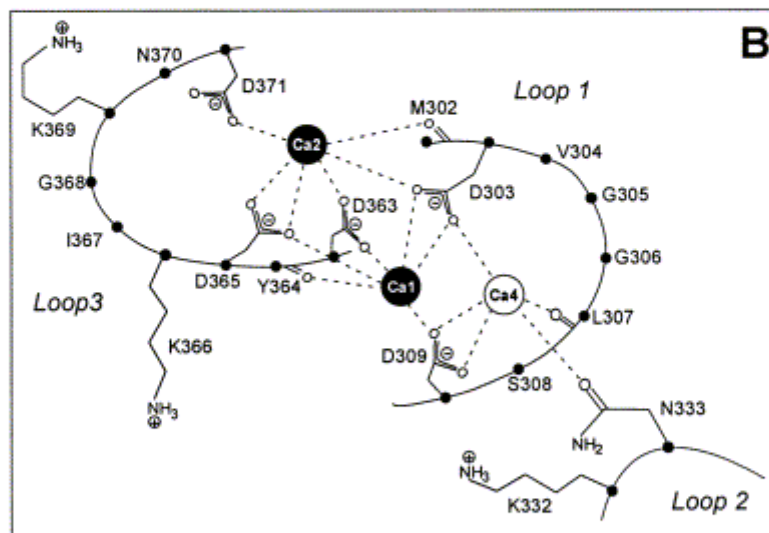
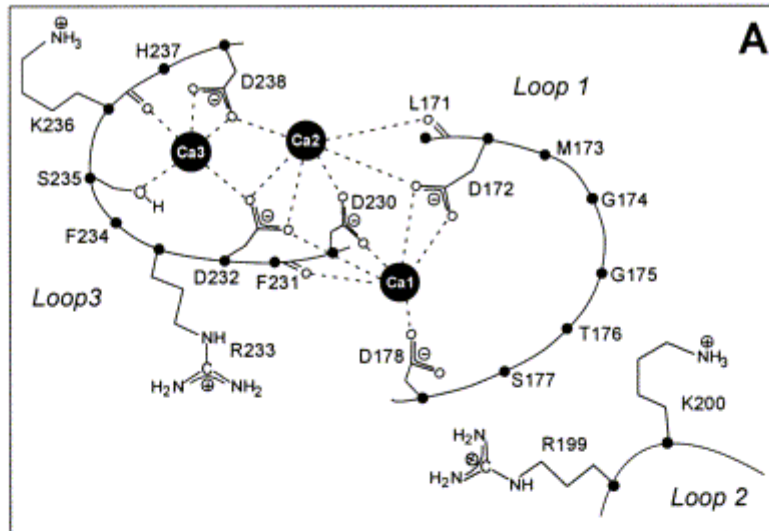


Figure 1.7 The Ca^{2+} -binding loops of synaptotagmin 1 C₂A and C₂B domains

Diagrams summarizing the three Ca^{2+} -binding sites of the C₂A domain (A) and the two Ca^{2+} -binding sites of the C₂B domain (B) and their ligands are shown. Solid spheres represent the Ca^{2+} ions coordinated by the loop residues. No Ca^{2+} binding was detected to the potential Ca^{2+} -binding site in the C₂B domain (indicated as Ca4, hollow circle) by NMR data. The Ca^{2+} -binding loops and the loop residues are labeled. (C) A stereodiagram of the Ca^{2+} -binding loops of the C₂B domain is shown. The backbone is represented with a blue ribbon and the Ca^{2+} ions are represented as orange spheres. The Ca^{2+} -binding residues are shown in ball-and-stick models with oxygen atoms in yellow and carbon atoms in magenta. (Fernandez *et al.*, 2001)

C₂A, D371 in C₂B), which coordinate the second Ca²⁺, have less severe effects on Ca²⁺ binding, indicating that binding of the first Ca²⁺ stabilizes the structure and facilitates Ca²⁺-binding to other sites (Ubach *et al.*, 1998; Fernandez *et al.*, 2001).

As the coordination spheres of the bound Ca²⁺ ions on the C₂ domains of synaptotagmin 1 are incomplete, the intrinsic Ca²⁺ affinities of these sites measured by 1H-15N HSQC Ca²⁺ titrations are weak (K_d of 54 μM, 530 μM and > 10 mM for sites Ca1, Ca2 and Ca3, respectively in C₂A) (Ubach *et al.*, 1998; Fernandez-Chacon *et al.*, 2001). The apparent Ca²⁺ affinity of the synaptotagmin 1 C₂ domains increases dramatically upon binding to phospholipid membranes because phospholipids provide additional coordination sites for the Ca²⁺ ions (Zhang *et al.*, 1998; Fernandez-Chacon *et al.*, 2001).

Binding of Ca²⁺ does not cause any conformational change in either C₂ domain but induces a dramatic switch in the electrostatic potential that mediates the Ca²⁺-dependent interactions (Shao *et al.*, 1997; Shao *et al.*, 1998; Ubach *et al.*, 1998; Fernandez *et al.*, 1998). The binding of positively charged Ca²⁺ ions changes the charge in the Ca²⁺-binding region from negative to positive. Both Ca²⁺-binding sites are surrounded by positively charged residues, which are known to be important for various interactions. These basic residues circle the Ca²⁺-binding site and contribute to the binding of synaptotagmin 1 to its negatively charged targets.

A second and important difference between C₂A and C₂B domain structures, other than the additional two α-helices in the C₂B domain, is the highly conserved polybasic region of C₂B at the side of the β-sandwich. Although C₂A also has some positively charged residues in the same region, the presence of consecutive lysines in C₂B makes

this region very basic. This region of C₂B was reported to be involved in many interactions (AP2, Ca²⁺ channels, inositol polyphosphates, synaptotagmin 1 self association) and binds to negatively charged contaminants (Fukuda *et al.*, 1994; Zhang *et al.*, 1994a; Sheng *et al.*, 1997; Chapman *et al.*, 1998b; Ubach *et al.*, 2001).

1.3.3 Interaction with negatively charged phospholipid membranes

Phospholipid binding was the first Ca²⁺-dependent activity of synaptotagmin 1 that was discovered (Brose *et al.*, 1992b). Although, it is now clear that both C₂ domains of synaptotagmin 1 bind to negatively charged phospholipids in a Ca²⁺-dependent manner, initially only the C₂A domain was assigned for membrane-binding activity (Davletov *et al.*, 1993). The Ca²⁺-dependence of phospholipid binding is highly cooperative and C₂ domains have apparent Ca²⁺ affinity of 5-10 μ M, much higher than the intrinsic Ca²⁺ affinities in the absence of phospholipids (Davletov *et al.*, 1993; Fernandez-Chacon *et al.*, 2001; Fernandez *et al.*, 2001).

The apparent Ca²⁺-affinity of synaptotagmin 1 in the presence of phospholipids corresponds well to the Ca²⁺ concentration required for neurotransmitter release, suggesting that Ca²⁺ binding to synaptotagmin 1 may regulate exocytosis *in vivo* (Davis *et al.*, 1999; Schneggenburger *et al.*, 2000; Bollmann *et al.*, 2000). The synaptotagmin 1 C₂A domain has a very fast kinetics of binding/unbinding to lipids (Davis *et al.*, 1999) probably because of the lack of a time consuming conformational change in the C₂A domain upon binding to Ca²⁺ but the requirement for only an electrostatic switch. This property is also supportive for the action of synaptotagmin 1 in fast neurotransmitter release, which takes place in less than 1 msec *in vivo*.

The top loops of the synaptotagmin 1 C₂A domain are suggested to bind to negatively charged phospholipid headgroups in a Ca²⁺-dependent manner by a combination of 1) electrostatic interactions 2) hydrophobic forces and 3) Ca²⁺ coordination by phospholipid headgroups (Zhang *et al.*, 1998). The requirement for negatively charged phospholipids and the Ca²⁺ dependence of the binding indicates that electrostatic interactions are the determining force for membrane binding of synaptotagmin 1. Mutations of the acidic residues involved in Ca²⁺ binding or basic residues around the Ca²⁺ binding loops disrupt phospholipid binding and demonstrate the importance of electrostatic interactions (Zhang *et al.*, 1998). In addition, two hydrophobic residues at the tips of loop 1 and loop 3 (M173, F234 in C₂A and V304, I367 in C₂B) are exposed and available for interaction with the hydrophobic core of the lipid bilayer. Fluorescence experiments and mutational analysis confirmed that these residues insert into the lipids and contribute to the binding via hydrophobic forces (Chapman and Davis, 1998a; Davis *et al.*, 1999; Gerber *et al.*, 2002). Coordination of Ca²⁺ by the phospholipids creates an additional contribution as has been demonstrated by the crystallographic studies with the PKC α C₂ domain, which showed that phospholipid headgroups complete the coordination spheres of the Ca²⁺ ions as the aspartate residues in the top loops of C₂ domains cannot provide enough number of coordination sites for Ca²⁺ (Verdaguer *et al.*, 1999). In the presence of Ca²⁺ and phospholipids, the C₂A domain forms a ternary complex in which Ca²⁺ is simultaneously ligated by the top loops of the C₂A domain and by phospholipid headgroups. Ca²⁺ ions and the positively charged residues that surround the Ca²⁺-binding sites in C₂A bind phospholipids to provide the required positive charge and change the negative charge of the aspartate residues in the loops to create a positive

patch which can bind to negatively charged residues. The binding mode of C₂A and C₂B domains on the lipids analyzed by EPR experiments supports the presence of the mentioned forces on the lipid/synaptotagmin 1 interactions (Frazier *et al.*, 2003;Rufener *et al.*, 2005).

Early studies using GST-pulldown experiments suggested that the C₂B domain does not bind to lipid membranes (Schiavo *et al.*, 1996;Sugita *et al.*, 1996;Chapman *et al.*, 1996;Bai *et al.*, 2000). These results were very surprising because the similar structural features of the Ca²⁺ binding loops of the C₂A and C₂B domains would predict lipid binding activity for the C₂B domain, too. Later, the presence of acidic bacterial contaminants bound to the polybasic region of the C₂B domain was discovered and an extensive purification protocol to produce contaminant-free C₂B was reported (Ubach *et al.*, 2001). FRET experiments done using highly purified C₂B domain revealed that the C₂B domain binds to negatively charged phospholipids in a Ca²⁺-dependent manner similar to the C₂A domain (Fernandez *et al.*, 2001). This result suggested that the two C₂ domains of synaptotagmin 1 have a common activity and can cooperate to bind to lipids. Thus, the unaffected neurotransmitter release in knock-in mice carrying a mutation that disrupts Ca²⁺-dependent lipid binding to the C₂A domain was explained as it was clear that C₂B can bind lipids and cooperate with the C₂A domain (Fernandez-Chacon *et al.*, 2002). The binding of both C₂ domains to phospholipids in the double C₂AB domain has been shown to cause a higher Ca²⁺ affinity than the individual C₂ domains.

1.3.4 Interaction with SNARE proteins

It is widely proposed that synaptotagmin 1 and SNAREs, two of the major players in membrane fusion, should interact with each other to couple the Ca^{2+} sensing with membrane fusion and trigger neurotransmitter release.

Synaptotagmin 1 has been observed to interact with the plasma membrane protein syntaxin in many studies (Bennett *et al.*, 1992; Yoshida *et al.*, 1992; Li *et al.*, 1995; Chapman *et al.*, 1995). Syntaxin deletion mutants suggest that the minimal domain required for Ca^{2+} -dependent binding of synaptotagmin 1 to syntaxin was localized to amino acids 220-266 of the syntaxin C terminus (Kee and Scheller, 1996). This domain overlaps with the SNARE motif of syntaxin. NMR experiments showed that the C₂A domain binds to syntaxin through the region surrounding the Ca^{2+} -binding sites of C₂A, indicating the importance of the electrostatic switch from negative to positive upon binding to Ca^{2+} (Shao *et al.*, 1997). Since syntaxin is highly acidic, the electrostatic potential of the C₂A domain plays a critical role in mediating the Ca^{2+} -dependent interaction of synaptotagmin 1 with syntaxin.

The interaction between syntaxin and synaptotagmin 1 is particularly interesting, first because syntaxin is a member of the SNARE complex which has been proposed to mediate most types of membrane fusion; second because syntaxin is one of the specific targets for clostridial neurotoxins which are known to block neurotransmitter release (Blasi *et al.*, 1993b); third because the mode of binding is Ca^{2+} dependent (Li *et al.*, 1995). Half maximal binding of the isolated C₂A domain to syntaxin occurs at concentrations of $>200 \mu\text{M}$ Ca^{2+} , higher than the intrinsic Ca^{2+} affinity of the C₂A domain and the Ca^{2+} concentrations required for synaptic vesicle exocytosis.

In spite of many studies where interaction of synaptotagmin 1 with syntaxin is observed, there is other work which actually suggests that the interaction of syntaxin with synaptotagmin 1 is indirect and the C terminus of SNAP25 is essential for Ca^{2+} dependent binding of synaptotagmin 1 to SNARE complexes (Gerona *et al.*, 2000). It is suggested that syntaxin can bind to synaptotagmin 1 only in the presence of SNAP25 via its interaction with SNAP25, but SNAP25 is able to bind synaptotagmin 1 even in the absence of syntaxin.

The interaction of synaptotagmin 1 with SNAP25 was reported in another study, where it was suggested that a Ca^{2+} -independent interaction of synaptotagmin 1 with SNAP25 can help the vesicles dock even if the cells are treated with neurotoxins which cleave synaptobrevin and syntaxin. A short region in the C terminus of SNAP25 was suggested to be essential for late post-docking steps and to mediate membrane fusion via an interaction with the Ca^{2+} sensor (Banerjee *et al.*, 1996).

Many additional studies have described the Ca^{2+} -dependent and Ca^{2+} -independent interactions between the C₂A, C₂B or C₂AB domains of synaptotagmin 1 and syntaxin, SNAP25, syntaxin/SNAP25 complex or the SNARE complex (Sollner *et al.*, 1993a; Schiavo *et al.*, 1997; Sheng *et al.*, 1997; Matos *et al.*, 2000; Earles *et al.*, 2001; Zhang *et al.*, 2002; Chieriegatti *et al.*, 2002; Shin *et al.*, 2003; Rickman and Davletov, 2003; Rickman *et al.*, 2004; Bai *et al.*, 2004). The observation of these inconsistent data in the literature is probably a result of nonspecific electrostatic interactions of the highly charged synaptotagmin 1 and SNARE proteins with each other under different experimental conditions.

Several observations suggest a role of the SNARE complex in a Ca^{2+} -dependent step of exocytosis (Banerjee *et al.*, 1996; Sorensen *et al.*, 2002). Mutations in two sites on the surface of the core complex formed by SNAP25 and synaptobrevin residues interfere with Ca^{2+} triggering of exocytosis in chromaffin cells (Sorensen *et al.*, 2002). However, these mutations were shown to severely impair SNARE complex assembly suggesting that SNAREs do not act directly as Ca^{2+} receptors but couple tightly to Ca^{2+} sensing during release (Chen *et al.*, 2005b). Several other studies indicate that Ca^{2+} -dependent binding of synaptotagmin 1 to syntaxin may not be important for release (Matos *et al.*, 2000; Sugita and Sudhof, 2000). There is also evidence that Ca^{2+} causes synaptotagmin 1 to dissociate from syntaxin in synaptosomes (Leveque *et al.*, 2000). In summary, the results about the SNARE/synaptotagmin 1 interactions are not conclusive and it is still not clear if the SNARE complex is a target of synaptotagmin 1 for the Ca^{2+} -triggered neurotransmitter release. In Chapter 2, we have focused on analyzing the interaction of different SNARE proteins/complexes with synaptotagmin 1.

1.3.5 Self-association of synaptotagmin 1 to form oligomers

Many synaptotagmin 1 isomers have been reported to bind to each other to form homooligomers or heterooligomers (Chapman *et al.*, 1998b; Osborne *et al.*, 1999; Thomas *et al.*, 1999; Fukuda and Mikoshiba, 2000). The oligomerization was reported to occur in Ca^{2+} -dependent or Ca^{2+} -independent manners in different studies. The Ca^{2+} -dependent self association of synaptotagmin 1 was mapped to the polybasic region in the C₂B domain as mutating the lysine residues in this region to neutralize the charge inhibits synaptotagmin 1 oligomerization (Chapman *et al.*, 1998b; Desai *et al.*, 2000; Littleton *et*

al., 2001). Earlier studies had shown that injection of a peptide from the lysine rich polybasic region of the C₂B domain of synaptotagmin 1 blocks a late step in vesicle fusion and inhibits neurotransmitter release (Bommert *et al.*, 1993). This observation strengthened the idea that self oligomerization of synaptotagmin 1 via the polybasic region in the C₂B domain is critical for release.

However, NMR experiments performed using highly purified C₂B domain revealed that the C₂B domain does not oligomerize even at millimolar protein concentrations in solution (Ubach *et al.*, 2001). The use of improperly purified C₂B with negatively charged contaminants bound to its polybasic region was shown to have caused the false positive oligomerization results. Later, it was suggested that although well-purified C₂B is monomeric in solution, synaptotagmin 1 C₂AB domain oligomerizes into heptameric ring-like structures upon binding to negatively charged monolayer lipids as observed by negative staining electron microscopy (Wu *et al.*, 2003). Mutation of two lysine residues in the polybasic region of C₂B (KK326/327AA) was shown to abolish oligomerization while it does not affect the lipid binding ability of C₂AB. We have focused our studies on the oligomerization of C₂AB on lipid membranes as explained in Chapter 4.

1.3.6 Functional studies to reveal synaptotagmin 1 action

The characterization of Ca²⁺-dependent and Ca²⁺-independent interactions of synaptotagmin 1 has allowed the design of single point mutations to disrupt interactions and monitor its effect on neurotransmitter release using genetic and electrophysiological experiments performed on neurons.

A study where knock-in mice were produced with either D232N or D238N point mutations revealed that disrupting the Ca^{2+} binding to the C_2A domain and abolishing the Ca^{2+} dependent phospholipids binding activity of the isolated C_2A domain has no major effect on neurotransmitter release in vivo (Fernandez-Chacon *et al.*, 2002). However, double C_2AB domains isolated from mutant mouse brains were shown to have no change in the ability of Ca^{2+} -dependent phospholipid binding. This result can be explained by the presence of a functional C_2B domain which can preserve the PL binding activity of synaptotagmin 1 even without help from a C_2A domain and maintain the neurotransmitter release in vivo (Fernandez *et al.*, 2001).

Other studies were done in *Drosophila* by introducing mutations that disable the Ca^{2+} -binding ability of C_2A or C_2B domains. These experiments produced surprising results. Introduction of synaptotagmin 1 with a Ca^{2+} coordinating D mutation (D178N in rat) into synaptotagmin 1-null mutants can rescue the transmission, although recombinant C_2A domain with the same mutation was shown to be unable to bind syntaxin or phospholipids (Robinson *et al.*, 2002). However, full rescue was not observed, in correlation with the observation that the mutation partially disrupts the phospholipid binding of the C_2AB domain. Intriguingly, mutating aspartates involved in Ca^{2+} coordination (D363 and D365 in rat) in the C_2B domain decreased neurotransmitter release by more than 95% (Mackler *et al.*, 2002). The decrease in neurotransmitter release is in correlation with the severe disruption of the C_2AB domain binding to phospholipids. Although these point mutations have similar effects on individual C_2A and C_2B domains, such as abolishing Ca^{2+} binding and phospholipid binding activities, the effect of mutations in vivo are very different. These results show that Ca^{2+} -binding to

the C₂B domain is essential for neurotransmitter release but Ca²⁺-binding to the C₂A domain is not. It is difficult to explain this asymmetry in the in vivo activities of these two similar domains. Now that the essentiality of C₂B domain for membrane fusion is clear, it is a major question what structural feature and what activity of C₂B maintains its function. Although the Ca²⁺ binding loops and the core β -sandwich structure of both domains bear no structural differences, the C₂B domain has two additional α -helices at the bottom face and a more polybasic region different from the C₂A domain (Fernandez *et al.*, 2001). The involvement of a unique structural feature of C₂B domain in an activity specific to C₂B can be the reason for this discrepancy of phenotypes in vivo. Unraveling the activity responsible for this difference will help to understand the mechanism of neurotransmitter release.

Many studies have focused on clarifying which interaction of synaptotagmin 1 is more important for the Ca²⁺-dependent action of this protein in the last step of membrane fusion. Interactions of synaptotagmin 1 with membranes or with the SNARE complex are believed to be the most essential ones as SNAREs and membranes are the major players in the fusion event. Although there is a continuous debate on this subject, many studies indicate that phospholipid binding is the most physiologically relevant activity of synaptotagmin 1. This idea is supported by the strong correlation between the apparent Ca²⁺ affinity of synaptotagmin 1 C₂ domains in lipid binding and the ability to inhibit secretion in PC12 cells, whereas SNARE binding exhibited no clear correlation (Shin *et al.*, 2002). It is suggested that defects in the recycling and Ca²⁺-dependent oligomerization of synaptotagmin 1 cannot account for the severe decrease in synaptic transmission in *Drosophila* carrying a Ca²⁺ binding mutation on the C₂B domain

(Mackler *et al.*, 2002). However, decreased Ca^{2+} -dependent lipid binding may account for this effect as lower lipid binding was observed for the mutant C₂AB domain. Another study was done to differentiate the involvement of phospholipid binding or SNARE binding activities of synaptotagmin 1 in the fast component of neurotransmitter release by using Sr^{2+} , a Ca^{2+} agonist which can trigger release less efficiently (Shin *et al.*, 2003). The fact that Sr^{2+} is able to mediate interaction of synaptotagmin 1 C₂B domain with phospholipids but not with the SNARE complex, suggests that synaptotagmin 1/SNARE interactions are not required for fast neurotransmitter release. This study also indicates the essential role of the C₂B domain of synaptotagmin 1 in release rather than the C₂A domain.

Our results explained in Chapter 3 also contribute to the idea that interaction of synaptotagmin 1 with the membranes is more important than SNARE interaction (Arac *et al.*, 2003). Competition experiments where the interactions of synaptotagmin 1 C₂AB fragment were monitored in the presence of both lipid membranes and SNARE complex showed that when both targets are available, synaptotagmin 1 prefers to bind to the lipid membranes rather than the SNARE complex. These two interactions are incompatible and cannot occur simultaneously. The preferential binding of synaptotagmin 1 to phospholipid membranes indicates that membrane binding might be the essential interaction of synaptotagmin 1 in vivo, where all targets will be available for binding in the active zone.

To test whether the increase in the hydrophobicity of Ca^{2+} -binding loops will increase neurotransmitter release, three tryptophans were introduced into the Ca^{2+} -binding loops of C₂A or C₂B domains (Rhee *et al.*, 2005). The enhanced hydrophobicity

in the loops increased the apparent sensitivity of Ca^{2+} -triggered release and both C₂A and C₂B domains contributed to the effect in an additive manner. The fact that increased hydrophobicity of a protein is likely to enhance protein/membrane interactions and to decrease protein-protein interactions indicates that the increase in neurotransmitter release is a result of favored synaptotagmin 1/membrane interactions rather than favored synaptotagmin 1/ SNARE interactions, and points out the importance of synaptotagmin 1/ membrane interactions in fusion.

Knock in mice with point mutations in either the polybasic region of C₂B domain (KK326/7AA) or the positively charged residues around the Ca^{2+} -binding loops of C₂A domain (R233) nicely demonstrated the correlation between a two-fold decrease in the apparent Ca^{2+} affinity of the C₂AB domain in vitro with a two-fold decrease in the Ca^{2+} sensitivity of neurotransmitter release in vivo (Fernandez-Chacon *et al.*, 2001; Li *et al.*, 2005). These experiments strongly indicate that synaptotagmin 1 is the major Ca^{2+} sensor in neurons and also suggest that phospholipid binding activity is the physiologically relevant interaction of synaptotagmin 1. Although Ca^{2+} -dependent phospholipid binding is essential, data demonstrating the discrepancy in the behavior of the C₂A and C₂B domains in vivo indicates the presence of a modified Ca^{2+} -dependent phospholipid binding activity of synaptotagmin 1.

1.3.7 Synaptotagmin Isoforms and Localization

Synaptotagmin 1 is an abundant synaptic vesicle and secretory granule protein that is expressed in neurons and endocrine cells and is involved in Ca^{2+} -triggered exocytosis. Synaptotagmins are not found in yeast, suggesting that they are not a part of

the basic fusion machinery. Synaptotagmins 1 and 2 are highly homologous but differentially distributed synaptic vesicle proteins. Synaptotagmin 1 is primarily expressed in the forebrain while synaptotagmin 2 is in the brain stem and spinal cord. (Ullrich *et al.*, 1994). However, at least 11 other synaptotagmin isoforms are present in the mammalian brain. After synaptotagmin 1 and 2, synaptotagmin 3 and 7 are the most abundant. Different than synaptotagmin 1 and 2, synaptotagmin 3 and 7 are uniformly co-distributed throughout the brain and are localized to the plasma membrane instead of the synaptic vesicles (Butz *et al.*, 1999; Sugita *et al.*, 2001).

All synaptotagmin isoforms are expressed in the brain. However, synaptotagmins I-V and IX-XI are primarily expressed in brain whereas synaptotagmins VI-VIII are primarily expressed in non-neuronal tissues such as heart, kidney and intestine.

Although C₂ domains of different synaptotagmin isoforms are structurally similar, they may vary in terms of their abilities to bind Ca²⁺ or to bind phospholipids. For example the C₂B domain of rat synaptotagmin 4 does not bind to Ca²⁺ in spite of extensive similarity of its Ca²⁺ binding loops to the synaptotagmin C₂ domains. On the other hand, the C₂B domain of fly synaptotagmin 4 is capable of binding to Ca²⁺ (Dai *et al.*, 2004). The reason why there are so many isoforms of synaptotagmin with different activities and localizations and their roles in membrane fusion is still unclear.

CHAPTER 2

CHARACTERIZATION OF DIFFERENT SNARE COMPLEXES: INTERACTION OF SYNAPTOTAGMIN 1 WITH SNARES

2.1 *Introduction*

The SNARE motifs of syntaxin, synaptobrevin and SNAP25 are reported to assemble in a variety of combinations to form different SNARE complexes. Two t-SNARE proteins, syntaxin and SNAP25, are observed to form a complex with a 2:1 ratio. The syntaxin/SNAP25 complex is composed of two identical SNARE motifs of syntaxin and the N-terminal and C-terminal SNARE motifs of SNAP25. This complex assembles into a parallel four-helix bundle similar to the full SNARE complex (Fasshauer *et al.*, 1997a; Margittai *et al.*, 2001; Xiao *et al.*, 2001). It was suggested that a complex composed of t-SNAREs might act as an intermediate in the pathway to full SNARE complex formation. In spite of the structural similarity to the full SNARE complex, the middle region of the syntaxin/SNAP25 complex is observed to be more flexible. Such flexibility may facilitate interactions between synaptobrevin and the syntaxin/SNAP25 complex.

On the other hand, syntaxin and the N-terminal SNARE motif of SNAP25 (SNAP25N) are sufficient to form an independent 1:1 complex, which has higher stability than the syntaxin/SNAP25 complex (Fasshauer *et al.*, 1997a). The rate of syntaxin/SNAP25N complex assembly is slow but once the complex is formed, it is

kinetically restricted from forming other SNARE complexes. The crystal structure of the syntaxin/SNAP25N complex consists of a parallel, four-stranded coiled-coil including two copies each of syntaxin and SNAP25N (Misura *et al.*, 2001).

The isolated SNARE motifs of the SNAP25 and synaptobrevin were observed unstructured in solution. However, upon formation of different SNARE complexes, the α -helicity increases dramatically and the SNARE motifs assemble into parallel four helix bundles (Fasshauer *et al.*, 1997a). More than one copy of the same SNARE motif can be incorporated into the complex in order to substitute for missing SNAREs and form a helical structure similar to the full SNARE complex. At high concentrations, isolated syntaxin was also observed to form homooligomeric helical bundles. At least some of the syntaxin molecules in the oligomer were reported to align in a parallel conformation in an EPR study (Margittai *et al.*, 2001).

We used NMR spectroscopy to characterize and identify different SNARE complexes. We aimed to study the interaction of synaptotagmin 1 with these complexes in the presence and absence of Ca^{2+} . Our experiments yielded a set of data, which can be used as a reference in future experiments to detect the presence of different SNARE complexes in a sample. However, the interaction of synaptotagmin 1 with the SNARE complex could not be characterized due to the lack of a specific, stoichiometric SNARE complex/synaptotagmin 1 complex.

2.2 Results

2.2.1 Detection of different SNARE complexes by monitoring the syntaxin crosspeaks

The ^1H - ^{15}N HSQC spectrum of a protein can be used as the fingerprint of a protein. An amide group of each non-proline residue has a corresponding crosspeak in an HSQC spectrum. The chemical shift values of amide nitrogens and amide hydrogens are very sensitive to their immediate environment. Hence, a slight change in their surroundings can easily be detected by monitoring the HSQC spectra of a protein. For example, the residues at the binding site of a protein can easily be assigned using this method as the crosspeaks corresponding to the binding site residues will change upon interaction with the protein's binding partner.

We made use of the environment-sensitive nature of protein amide groups to characterize different SNARE complexes. To decrease the broadening of the signals upon complex formation, we expressed the protein in D_2O and replaced all hydrogens with deuterium. ^2H , ^{15}N -labeled syntaxin was mixed with unlabeled SNARE motifs to produce different SNARE complexes. The comparison of the ^1H - ^{15}N HSQC spectrum of the isolated ^2H , ^{15}N -labeled syntaxin with the ^1H - ^{15}N HSQC spectrum of the ^2H , ^{15}N -labeled syntaxin incorporated into SNARE complexes yielded a useful set of data to distinguish between different SNARE complexes.

The ^1H - ^{15}N TROSY-HSQC spectrum of ^2H , ^{15}N -labeled syntaxin at pH 7.4 is shown in Figure 2.1. The low chemical shift dispersion indicates that syntaxin is unstructured as expected. A single set of signals suggests that syntaxin is monomeric. There is a single glycine residue in the syntaxin sequence. Since glycine residues appear in the upper region of an HSQC spectrum, we could easily identify the crosspeak corresponding to the single glycine and used it to follow the different states of syntaxin.

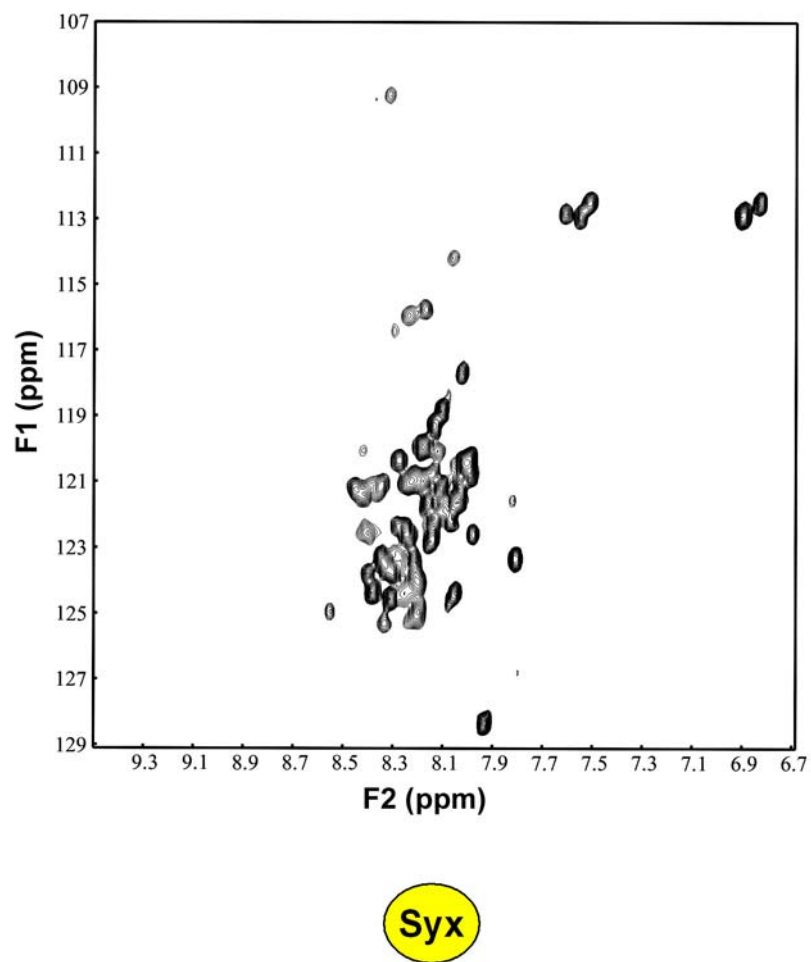


Figure 2.1 TROSY-HSQC spectrum of the monomeric syntaxin

^1H - ^{15}N TROSY-HSQC spectrum of 170 μM ^2H , ^{15}N -labeled syntaxin in 20 mM Tris (pH 7.4), 100 mM NaCl buffer is shown. The yellow circle represents the monomeric syntaxin.

Decreasing the pH to 6.4 induces the formation of oligomeric structures. In addition to the crosspeaks of the monomeric syntaxin, a second set of crosspeaks is observed for each residue. Two sets of crosspeaks correspond to the monomeric and oligomeric syntaxins (Figure 2.2) co-existing in solution. The large chemical shift dispersion of the oligomer crosspeaks indicates that syntaxin is structured within the oligomer. All syntaxin molecules in the oligomer experience identical conditions resulting in a single set of crosspeaks for the oligomer.

The syntaxin/SNAP25N complex is formed by mixing the $^2\text{H}, ^{15}\text{N}$ -labeled syntaxin with the unlabeled N-terminal SNARE motif of SNAP25 (SNAP25N) in 1:1 ratio at pH 6.4. The resulting $^1\text{H}-^{15}\text{N}$ TROSY-HSQC spectrum has two sets of crosspeaks, one corresponding to monomeric syntaxin and the other corresponding to the syntaxin/SNAP25N complex (Figure 2.3). The high chemical shift dispersion and the presence of a single set of peaks corresponding to the complex is in agreement with the parallel four helix bundle including two syntaxin and two SNAP25N molecules (Margittai *et al.*, 2001). The formation of the complex and also possible aggregation cause signal broadening as a result of increased molecular size.

Addition of the C-terminal domain of SNAP25 (SNAP25C) onto the preformed syntaxin/SNAP25N complex did not cause any changes in the HSQC spectrum indicating that syntaxin/SNAP25N complex is a kinetic trap. The syntaxin/SNAP25 complex including two syntaxins, one SNAP25N and one SNAP25C can be formed only when all three components are mixed simultaneously to prevent the formation of the kinetically trapped binary complex. The $^1\text{H}-^{15}\text{N}$ TROSY-HSQC spectrum of the syntaxin/SNAP25 complex (Figure 2.4) shows two sets of $^2\text{H}, ^{15}\text{N}$ -labeled syntaxin signals both

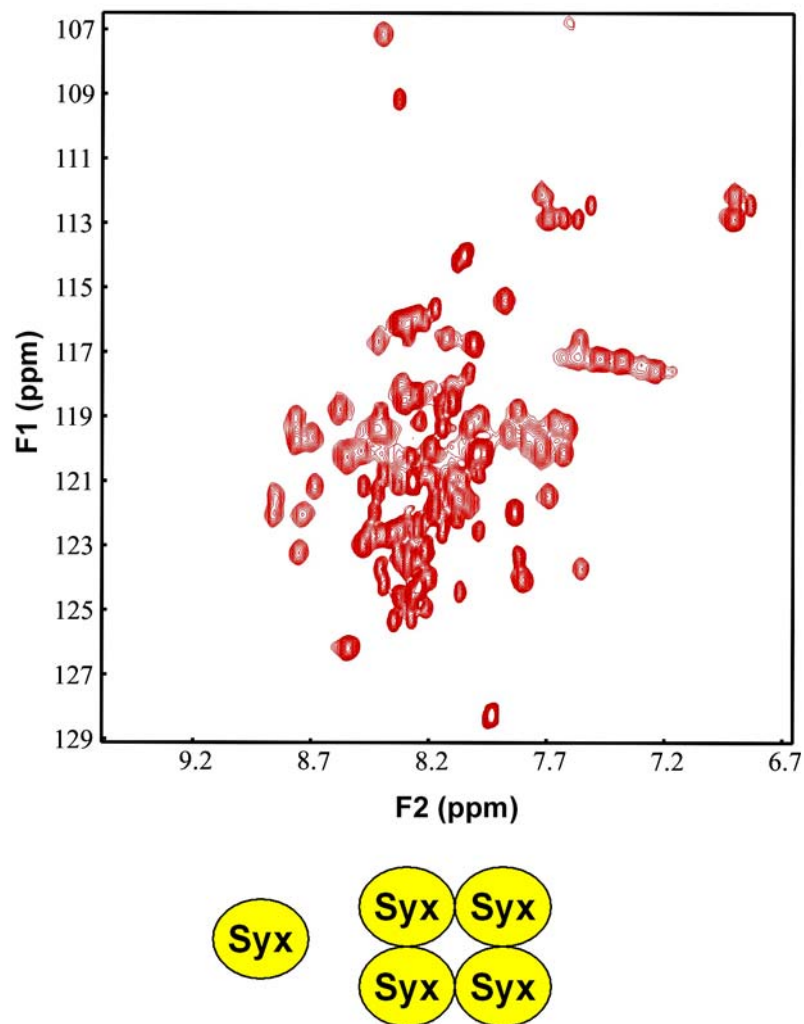


Figure 2.2 TROSY-HSQC spectrum of the mixture of monomeric and oligomeric syntaxin.

^1H - ^{15}N TROSY-HSQC spectrum of 170 μM ^2H , ^{15}N -labeled syntaxin in 20 mM MES (pH 6.4), 130 mM NaCl buffer is shown. The yellow circles represent the monomeric and oligomeric syntaxin.

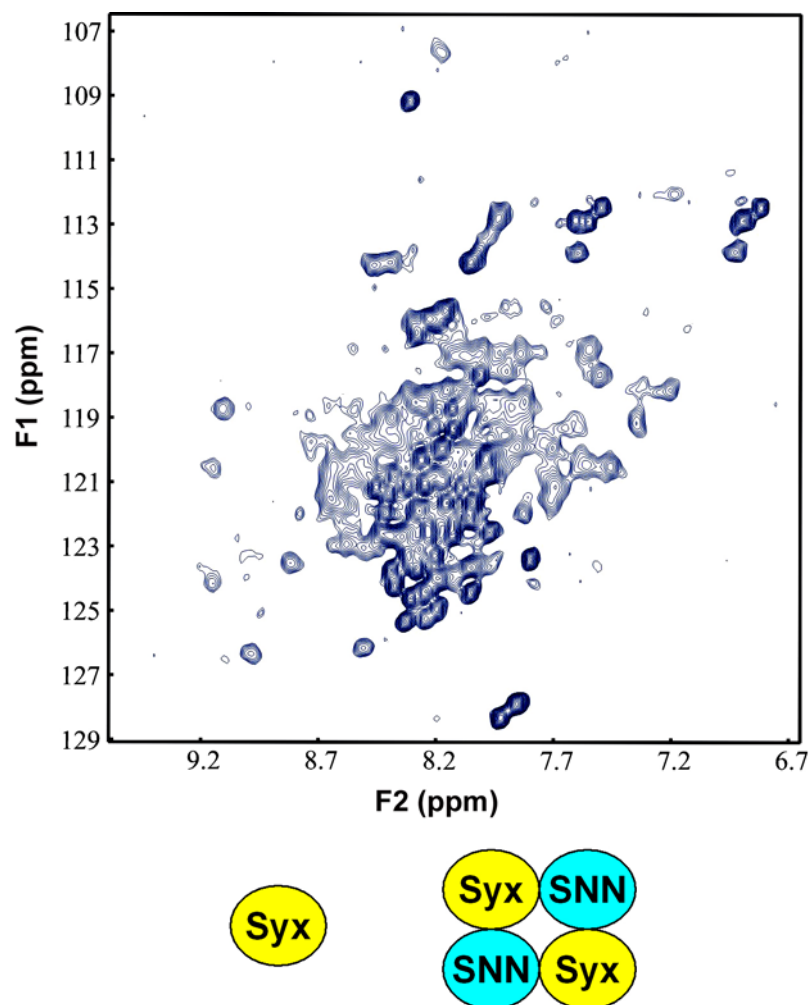


Figure 2.3 TROSY-HSQC spectrum of the syntaxin/SNAP25N complex

^1H - ^{15}N TROSY-HSQC spectrum of 56 μM ^2H , ^{15}N -labeled syntaxin and unlabeled SNAP25N mixed with 1:1 ratio in 20 mM MES (pH 6.4), 130 mM NaCl buffer is shown. The yellow and blue circles represent syntaxin and SNAP25N, respectively. The sample is a mixture of monomeric syntaxin and syntaxin/SNAP25 complex. The syntaxin/SNAP25 complex is schematized from the top view.

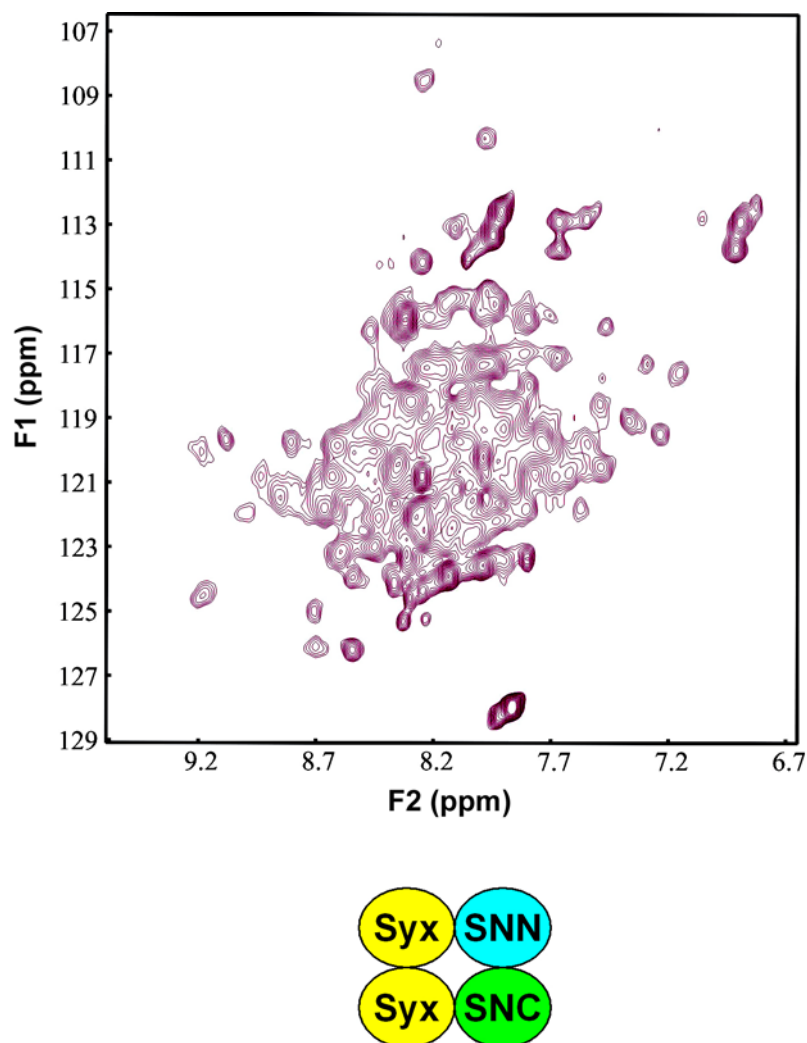


Figure 2.4 TROSY-HSQC spectrum of the syntaxin/SNAP25 complex

^1H - ^{15}N TROSY-HSQC spectrum of 200 μM ^2H , ^{15}N -labeled syntaxin, unlabeled SNAP25N and unlabeled SNAP25C mixed with 2:1:1 ratio in 20 mM MES (pH 6.4), 130 mM NaCl buffer is shown. The yellow, blue and green circles represent syntaxin, SNAP25N and SNAP25C, respectively. The syntaxin/SNAP25 complex is schematized from the top view.

corresponding to the syntaxin/SNAP25 complex. The signals of the monomeric syntaxin are not observed, indicating that this complex is formed more efficiently than the syntaxin/SNAP25N complex. The presence of two sets of signals shows that there are two syntaxin molecules in the syntaxin/SNAP25 complex, experiencing different environments, because one is closer to SNAP25N and the other is closer to SNAP25C. These observations are in agreement with the previously reported results suggesting that syntaxin and SNAP25 form a parallel four-helix bundle including two syntaxin, one SNAP25N and one SNAP25C SNARE motif.

The formation of different SNARE complexes can be easily observed by monitoring the single glycine residue in syntaxin. Figure 2.5 shows the superimposed and expanded glycine region in the HSQC spectra of the isolated syntaxin (red), the syntaxin/SNAP25N complex (blue) and the syntaxin/ SNAP25 complex (magenta). The isolated syntaxin has two glycine crosspeaks corresponding to the monomeric and oligomeric conformations. The crosspeak of the monomer is indicated by an arrow. The syntaxin/SNAP25N complex sample is a mixture of the monomeric syntaxin and the complex, yielding two glycine peaks, one of which overlaps with the monomeric syntaxin crosspeak. On the other hand, two glycine crosspeaks are observed for the syntaxin/SNAP25 complex, as well. However, none of the peaks overlaps with the monomeric syntaxin crosspeak, indicating the lack of any isolated syntaxin in the sample. Instead, both peaks arise from the syntaxin/SNAP25 complex as the two syntaxin molecules within the complex have distinct structural environments, yielding two different signals.

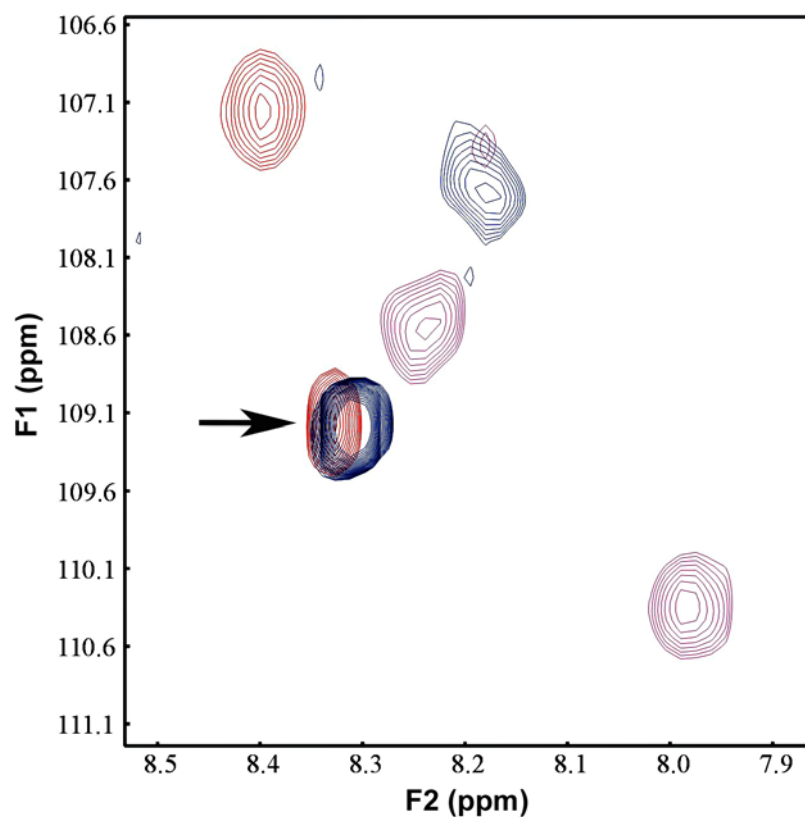


Figure 2.5 Glycine regions of the TROSY-HSQC spectra of the ^2H , ^{15}N -labeled syntaxin in different complexes.

Superimposition of the glycine region of the ^1H - ^{15}N TROSY-HSQC spectra of ^2H , ^{15}N -labeled syntaxin in oligomeric form (red), in complex with SNAP25N (blue), and in complex with SNAP25N and SNAP25C (magenta) is shown. Arrow indicates the monomeric syntaxin crosspeak.

The full SNARE complex was formed by mixing ^2H , ^{15}N -labeled syntaxin and unlabeled SNAP25N, SNAP25C and synaptobrevin. This complex has much higher stability than the others and the rate of complex assembly is faster. The ^1H - ^{15}N TROSY-HSQC spectrum of the SNARE complex is shown in Figure 2.6A. A single set of peaks is observed corresponding to the single syntaxin molecule in the SNARE complex. The addition of the unlabeled C₂AB domain of synaptotagmin 1 on the SNARE complex causes extreme broadening and disappearance of most of the peaks. The addition of the C₂AB domain in the presence of Ca^{2+} results in a similar spectrum (Figure 2.6B). The dramatic broadening of the signal indicates that synaptotagmin 1 (33 KDa) and the SNARE complex (33 KDa) either interacts with a stoichiometry different than 1:1 or they interact nonspecifically because a 1:1 complex, which would be 66 KDa, is expected to result in much less broadening. Addition of synaptotagmin 1 and Ca^{2+} on other SNARE complexes yielded similar results. Our data show that synaptotagmin 1 interacts with the SNARE complex in the presence and absence of Ca^{2+} . However, it is difficult to conclude whether this interaction is a nonspecific interaction due to high protein concentrations or not.

2.2.2 Detection of different SNARE complexes by monitoring the SNAP25C crosspeaks

The formation of different SNARE complexes can be detected by monitoring the signal of other SNARE motifs, as well. We have expressed and purified ^2H , ^{15}N -labeled SNAP25C to perform similar experiments. Figure 2.7 is the ^1H - ^{15}N TROSY-HSQC spectrum of the isolated SNAP25C in the monomeric conformation. The low chemical

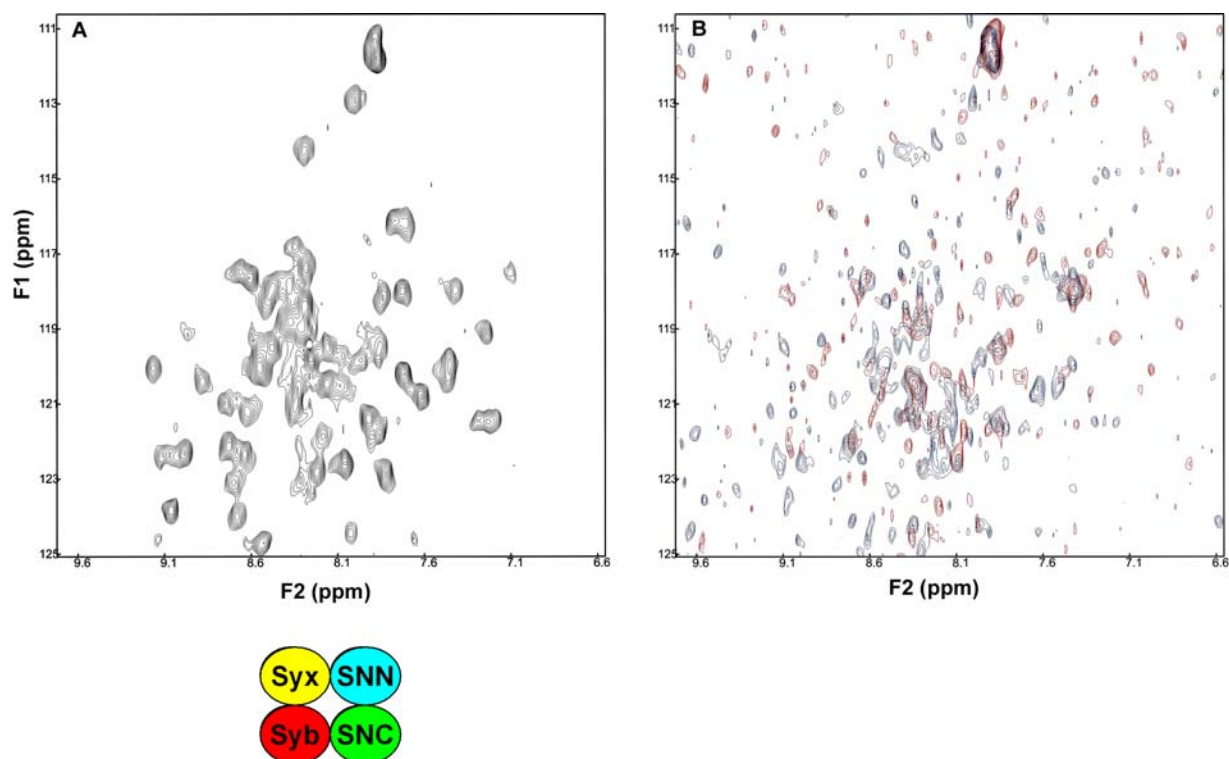


Figure 2.6 TROSY-HSQC spectrum of the SNARE complex

^1H - ^{15}N TROSY-HSQC spectrum of 100 μM SNARE complex, formed by mixing ^2H , ^{15}N -labeled syntaxin, SNAP25N, SNAP25C and synaptobrevin at 1:1:1:1 ratio in 20 mM MES (pH 6.4), 130 mM NaCl buffer, is shown(A). Spectra in the presence of synaptotagmin 1 C₂AB domain (B, red) and synaptotagmin 1 C₂AB domain and Ca^{2+} (B, blue) are also shown. The yellow, blue, green and red circles represent syntaxin, SNAP25N, SNAP25C and synaptobrevin, respectively. The SNARE complex is schematized from the top view.

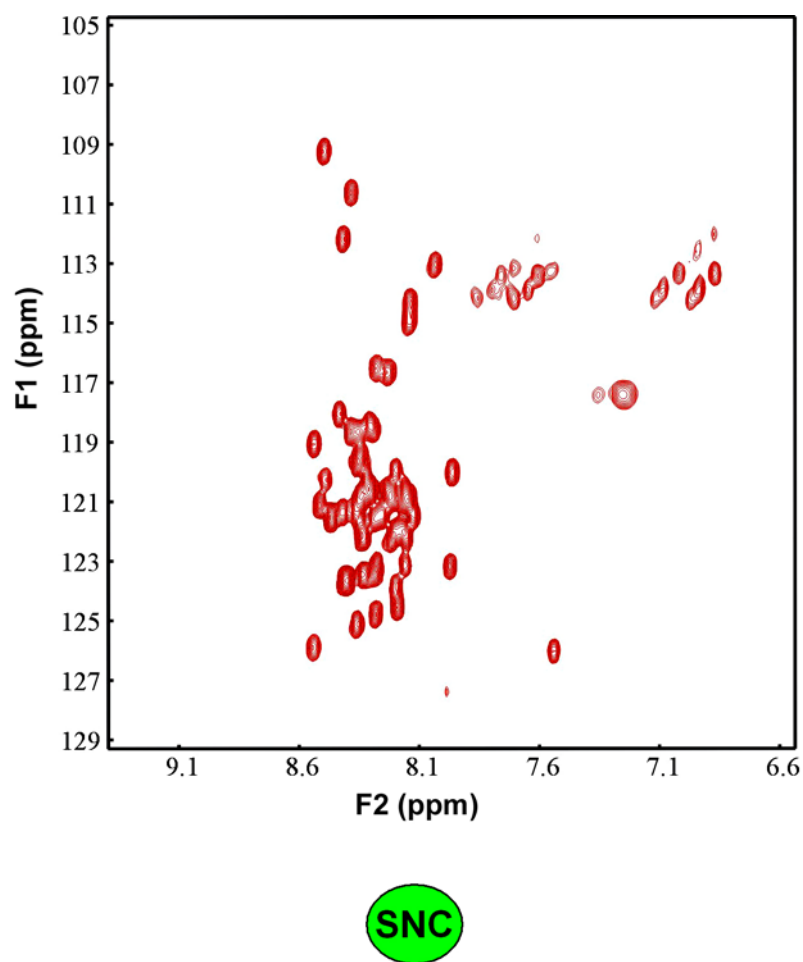


Figure 2.7 TROSY-HSQC spectrum of the monomeric SNAP25C

^1H - ^{15}N TROSY-HSQC spectrum of 200 μM ^2H , ^{15}N -labeled SNAP25C in 20 mM MES (pH 6.4), 130 mM NaCl buffer is shown. The green circle represents the monomeric SNAP25C.

shift dispersion indicates that the protein is unstructured. The three glycine residues in the SNAP25C protein can be observed on the upper left corner of the spectrum.

The syntaxin/SNAP25 complex is formed upon mixing ^2H , ^{15}N -labeled SNAP25C with unlabeled syntaxin and SNAP25N. The HSQC spectrum of the complex contains two sets of signals one corresponding to the monomeric SNAP25C, and the other corresponding to the syntaxin/SNAP25 complex (Figure 2.8). Three additional crosspeaks are observed on the upper region of the spectrum resulting from the incorporation of glycine residues into the complex. Addition of synaptotagmin 1 with or without Ca^{2+} resulted in severe signal broadening.

2.2.3 The C₂AB domain of synaptotagmin 1 interacts with the SNARE complex

Our experiments to study the different SNARE complexes resulted in a set of data, which can be used as a reference to determine the presence of SNARE complexes in any further experiments. However, the extreme signal broadening upon addition of synaptotagmin 1 prevented us from advancing our studies to understand the synaptotagmin 1/SNARE interactions. These experiments were performed at protein concentrations higher than 100 μM , which are necessary for obtaining sufficient quality data on 600 or 500 MHz spectrometers. We suspected that the severe signal broadening might be a result of the formation of nonspecific multimeric complexes at high protein concentrations. Upon the arrival of our 800 MHz NMR spectrometer, we decided to revisit synaptotagmin 1/SNARE interactions using lower protein concentrations. The 800 MHz spectrometer improved the signal-to-noise ratio and dramatically increased the resolution of the spectrum.

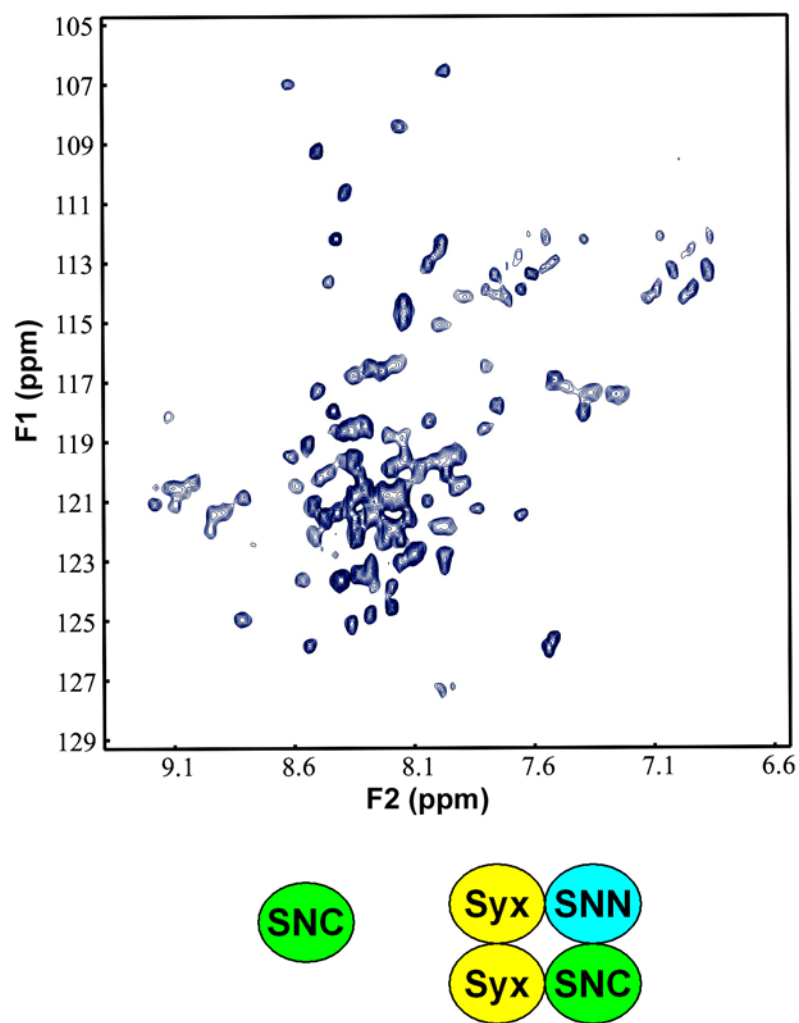


Figure 2.8 TROSY-HSQC spectrum of the syntaxin/SNAP25N complex

^1H - ^{15}N TROSY-HSQC spectrum of 200 μM ^2H , ^{15}N -labeled SNAP25C, syntaxin and SNAP25N mixed with 1:2:1 ratio in 20 mM MES (pH 6.4), 130 mM NaCl buffer is shown. The yellow, blue and green circles represent syntaxin, SNAP25N and SNAP25C, respectively. The syntaxin/SNAP25 complex is schematized from the top view.

We produced the ^2H , ^{15}N -labeled C₂AB domain of synaptotagmin 1 and monitored the change in the crosspeaks upon its interaction with the SNARE complex. The ^1H - ^{15}N TROSY-HSQC spectrum of 25 μM Ca^{2+} -free ^2H , ^{15}N -labeled C₂AB domain of synaptotagmin 1 in the absence (black) and presence (red) of the unlabeled SNARE complex is shown in Figure 2.9. The previous assignments of the C₂A and C₂B domains were used to find out that the resonances of the C₂B domain are substantially more broadened than those of the C₂A domain. This result suggests that synaptotagmin 1 interacts with the SNARE complex via its C₂B domain in a Ca^{2+} -independent manner. Addition of Ca^{2+} to the sample produced a similar spectrum, but the crosspeaks from both C₂ domains were broadened, indicating that both C₂ domains are involved in the Ca^{2+} -dependent interaction of synaptotagmin 1 with the SNARE complex. Addition of unlabeled SNARE complex to the ^2H , ^{15}N -labeled C₂B domain did not cause any changes in the C₂B crosspeaks in the presence or absence of Ca^{2+} , suggesting that C₂A domain is also required for the interaction of synaptotagmin 1 with the SNARE complex.

2.3 Discussion

The interaction of synaptotagmin 1 with the SNARE complex is widely believed to be critical for neurotransmitter release as such an interaction involves two of the major components known to be important for release. In this chapter, we focused on characterization of different SNARE complexes with the aim of studying their interaction with synaptotagmin 1. We accumulated a useful set of data to distinguish different SNARE complexes. However, addition of the synaptotagmin 1 C₂AB domain in the presence or absence of Ca^{2+} to any of these complexes resulted in severe broadening in

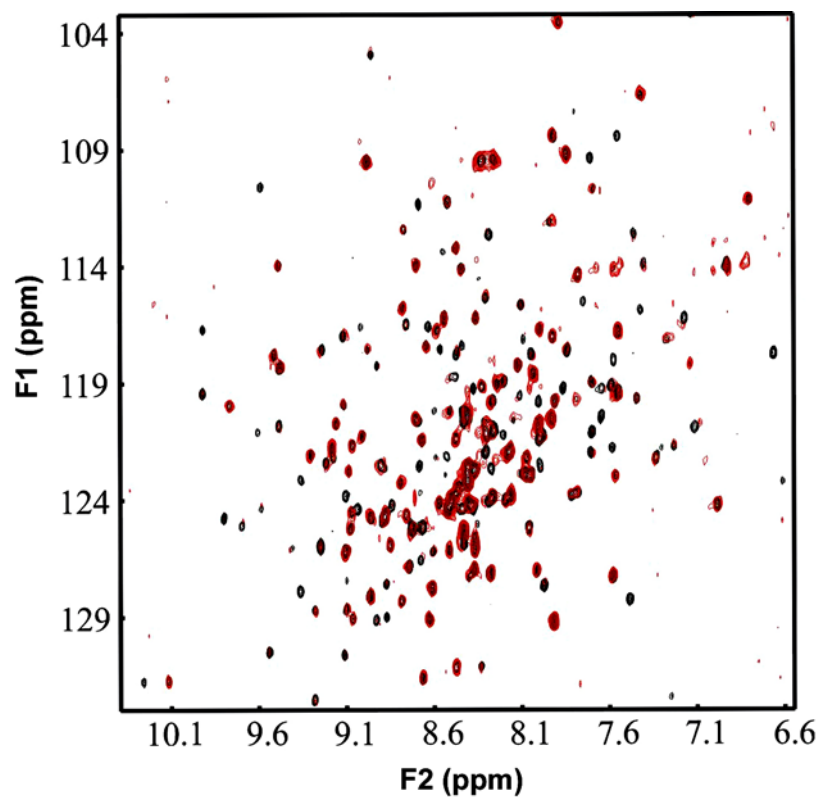


Figure 2.9 TROSY-HSQC spectrum of the synaptotagmin 1 C₂AB domain
¹H-¹⁵N TROSY-HSQC spectrum of 25 μM ²H, ¹⁵N-labeled C2AB in the absence (black) and presence (red) of 30 μM unlabeled SNARE complex in 20 mM D-Hepes (pH 7.2), 100 mM NaCl buffer is shown.

the HSQC spectra. When similar experiments were performed with much lower protein concentrations, broadening was less dramatic. The residues at the binding site of synaptotagmin 1 were determined from the movement of the crosspeaks upon addition of the SNARE complex, but these residues did not converge at a single region. These results suggest that synaptotagmin 1 and SNARE complex nonspecifically interact and form multimeric structures. The increase of protein concentrations and the presence of Ca^{2+} enhance this type of interactions. Also, the lack of a Ca^{2+} -dependent interaction between synaptotagmin 1 and the SNARE complex suggests that synaptotagmin 1 acts via a different mechanism upon Ca^{2+} influx to trigger release. However, we cannot rule out a role for the synaptotagmin 1/SNARE complex interaction in a Ca^{2+} -independent step.

2.4 *Materials and Methods*

2.4.1 Expression and purification of proteins

DNA constructs encoding GST fusion proteins of the SNARE motifs of rat synaptobrevin 2 (residues 29-93), rat syntaxin 1A (191-253), and human SNAP25 (residues 11-82 and 141-203, abbreviated as SNAP25N and SNAP25C, respectively) in the pGEX-KT expression vector were prepared by Evgenii Kovrigin. All SNARE proteins were expressed as GST-fusion proteins in *Escherichia coli* BL21 cells. Cell pellets were resuspended in phosphate buffer saline (PBS) solution containing protease inhibitors. Cells were passed three times through an EmulsiFlex-C5 cell disrupter (Avensis) at 14000 psi and spun at 28000 g for 30 min. Supernatants were incubated with glutathione-sepharose beads. The resin was extensively washed with PBS solution to remove unbound proteins. In the cases of synaptobrevin and SNAP25N, samples were

treated with benzonase (0.25 units/ul, 1 hr incubation at RT) to remove DNA. The resin was then washed with PBS buffer and the GST moiety was cleaved from the proteins by thrombin cleavage (5-7 units/ml, 2 hr incubation at RT). Proteins were eluted with 20 mM sodium phosphate (pH 7.4), 200 mM NaCl, and purified by gel filtration chromatography on a Superdex-75 Hiload 16/60 column (Amersham Pharmacia Biotech.) in the presence of 20 mM NaP (pH 8.0), 150 mM NaCl.

The C₂B domain (residues 271-421) was expressed at 27°C overnight. The cell pellet was resuspended in PBS containing 2 mM DTT and protease inhibitors. Cells were passed three times through an EmulsiFlex-C5 cell disrupter (Avensis) at 14000 psi and spun at 28000 g for 30 min. The supernatant was incubated with glutathione-sepharose beads. The resin was extensively washed with a) PBS, b) 40 mM Tris, 200 mM NaCl pH 8.2 c) 40 mM Tris, 200 mM NaCl pH 8.2 50 mM CaCl₂ solutions, consecutively, and washes were repeated two times. The C₂B domain was cleaved from the GST moiety by thrombin (10 units) in 3 ml of thrombin cleavage buffer (50 mM Tris [pH 8.0], 200 mM NaCl, 2.5 mM CaCl₂, 1 mM DTT) at 25°C for 2 hrs. The protein was eluted from the resin with a solution containing 200 mM sodium phosphate (pH 6.2), 300 mM NaCl and purified by gel filtration chromatography on a Superdex 75 column in 200 mM sodium phosphate (pH 6.2), 300 mM NaCl. After desalting the sample, the protein was further purified with cation exchange chromatography on a SourceS column (Pharmacia) in 50 mM MES (pH 6.2) using a linear gradient from 300 mM to 600 mM NaCl in 8 column volumes.

The C₂AB-fragment (residues 140-421) was expressed at 20°C overnight. The cell pellet was resuspended in a solution containing 40 mM Tris (pH 8.2), 200 mM NaCl,

1% Triton X-100, 2 mM DTT and protease inhibitors. Cells were passed three times through an EmulsiFlex-C5 cell disrupter (Avensin) at 14000 psi and spun at 28000 g for 30 min. The supernatant was incubated with glutathione-sepharose beads. The resin was extensively washed with at least 200 ml of 40 mM Tris (pH 8.2), 200 mM NaCl followed by 200 ml of 40 mM Tris (pH 8.2), 200 mM NaCl, 50 mM CaCl₂, which was repeated two times. The C₂AB-fragment was cleaved from the GST moiety with thrombin (12 units) in 10 ml of thrombin cleavage buffer (50 mM Tris [pH 8.0], 200 mM NaCl, 2.5 mM CaCl₂, 1 mM DTT) at 25°C for 3 hrs. The protein was eluted from the resin with 200 mM sodium phosphate (pH 6.2), 300 mM NaCl buffer and purified by cation exchange chromatography on a SourceS column (Pharmacia) in 50 mM NaAc (pH 6.2), 5 mM CaCl₂ using a linear gradient from 300 mM to 600 mM NaCl in 8 column volumes. UV spectra were acquired on a Hewlett-Packard 8452A spectrophotometer to verify the absence of bacterial contaminants, which absorb at 260 nm. Proteins were stored at -80°C after adding 0.3 mM TCEP to the samples.

2.4.2 NMR sample preparation

Three SNARE complex samples were prepared by mixing: 1) ²H,¹⁵N-labeled syntaxin with unlabeled SNAP25N, SNAP25C and synaptobrevin; 2) ²H,¹⁵N-labeled SNAP25C with unlabeled SNAP25N, syntaxin and synaptobrevin; and 3) four unlabeled SNARE motifs. Other SNARE complexes were prepared as described in the text. The samples were incubated at 4°C overnight or longer for better assembly. The unassembled SNARE motifs were removed by extensive concentration/dilution with a Millipore concentrator (10 KDa cutoff) for the full SNARE complex. The unassembled SNARE

motifs could not be removed from the syntaxin/SNAP25N or syntaxin/SNAP25C complexes due to the low stability of the complexes.

NMR samples containing labeled SNAREs were prepared in 20 mM MES (pH 6.4), 130 mM NaCl unless indicated otherwise. All NMR samples contained 5% D₂O. Deuterated C₂AB and C₂B domains were incubated at 37°C overnight to allow the exchange of amide protons.

2.4.3 NMR spectroscopy

All NMR experiments were performed at 25°C on Varian INOVA500, 600 or 800 spectrometers. ¹H-¹⁵N TROSY-HSQC experiments were acquired with acquisition times between 2 to 24 hours. All NMR data were processed with the program NMRPipe (Delaglio *et al.*, 1995) and analyzed with the program NMRView (Johnson and Blevins, 1994).

CHAPTER 3

A NEW METHOD TO DETECT PROTEIN-PROTEIN INTERACTIONS BY 1D NMR: ANALYSIS OF SYNAPTOTAGMIN 1 INTERACTIONS

Parts of this chapter are adapted from “Facile detection of protein-protein interactions by one-dimensional NMR spectroscopy. Biochemistry 42 (10):2774-2780, 2003” by D. Arac, T. Murphy, and J. Rizo.

3.1 Introduction

Many processes in a cell to sustain its vital activities are maintained by interaction of proteins with other proteins or molecules. These interactions are of particular interest to scientists to unravel the course of different mechanisms in the cells. Numerous biochemical, molecular biological and genetic methods with various advantages and drawbacks have been developed to study protein-protein interactions (Phizicky and Fields, 1995). Comprehensive analyses of protein-protein interactions have been done using two-hybrid assays (Uetz *et al.*, 2000; Ito *et al.*, 2001) and mass spectrometry of tagged protein complexes (Gavin *et al.*, 2002; Ho *et al.*, 2002). However, the reported interactions were supported by only one method and their relevance should be verified by additional methods which study a single interaction at a time (von *et al.*, 2002). Direct protein interactions in living cells were observed by fluorescent resonance energy transfer techniques (Tsien, 1998). However, in vitro methods are needed to verify the validity of one-to-one interactions. Various methods such as ultracentrifugation, chromatography, fluorescence spectroscopy, electrophoresis, isothermal titration calorimetry and methods

based on immobilization of proteins on resins or solid supports have been developed for detecting interactions in vitro (Phizicky *et al.*, 1995). However, some of these methods produce false results because of the use of tags, chemical modifications or fusion proteins, while others can detect interactions only with slow off-rates or require very high amounts of protein. Another drawback is that multicomponent systems cannot be analyzed by most of these methods as they are limited to detecting binary interactions.

After studying synaptotagmin 1/SNARE interactions using ^{15}N -HSQC experiments and observing an interaction which we could not characterize well in spite of all our efforts (Chapter 2), we decided to use other methods to study interaction of synaptotagmin 1 with different SNAREs. We looked for a practical method which will give us reliable results free of artifacts and requires unmodified proteins at low concentrations. We also wanted to do competition experiments between SNAREs and lipid vesicles for binding to synaptotagmin 1. Thus, we needed a method which can be used to study multicomponent systems. However, the inabilities and drawbacks of the existing methods led us to develop a new method which can analyze protein interactions in multicomponent systems using 1D NMR spectroscopy. This method is a simple, general tool for detecting interactions in solution using nanomolar protein concentrations and can complement existing techniques.

3.2 Results

3.2.1 The basis for the SMR method

NMR spectroscopy is a well-developed technique that is currently used for many purposes. Structures of proteins are determined at atomic resolution, binding sites on

proteins of known structure are mapped, dissociation constants are measured and protein dynamics are studied using heteronuclear two-dimensional or three-dimensional NMR spectra (Ikura *et al.*, 1992; Gronenborn and Clore, 1993; Fernandez *et al.*, 1998; Zuiderweg, 2002). Although HSQC experiments are commonly used for detecting protein-protein interactions, these experiments require high protein concentrations (around 100 μ M without cold probes) creating solubility problems and promoting nonspecific interactions.

We have developed a new NMR method that uses 1D NMR spectra of proteins as a general tool to detect protein interactions. The idea that forms the theory of this method is based on two observations: 1) 1D ^1H NMR spectra of a protein sample have higher sensitivity than multidimensional NMR spectra of the same sample because the resonances overlap and increase the signal in 1D NMR whereas they spread in many dimensions to form smaller resonances in multidimensional NMR. This is especially true for the methyl resonances from valine, leucine and isoleucine which overlap in the region corresponding to 0.8-0.9 ppm and form the strongest resonance in 1D NMR spectra of proteins. We have named this resonance as strongest methyl resonance (SMR) and defined the SMR intensity as the height of the SMR signal rather than the area. SMR can be reliably detected at low micromolar and sub-micromolar protein concentrations with a good signal to noise ratio. 2) The SMR intensities of different monomeric proteins at the same concentrations are similar and do not depend on the molecular mass of the protein. This observation was a result of NMR studies of more than 50 proteins with molecular masses in the range of 7 to 100 kDa over many years in our lab.

The independence of the SMR intensity on the molecule size but its dependence on the protein concentration can be explained as follows: The slow tumbling of large molecules causes increased transverse relaxation rates. This effect results in increased line widths and decreased intensities of protein resonances by increasing molecular mass. The decreased intensity of individual resonances almost linearly depends on the molecule size. The decrease in the intensity of resonances is compensated by the increase in the number of leucine, valine and isoleucine residues which also depends linearly on the molecule size. The increase in SMR intensity due to higher number of methyl groups balances the decrease due to resonance broadening by lower tumbling rates, making the final effect of molecule size on the SMR intensity almost insignificant.

The degree of compensation depends on the average amino acid sequence composition of proteins, the dispersion of the methyl resonances and the shape of the molecules etc. In practice, these parameters are similar enough in most proteins to result in a similar SMR intensity for the same protein concentration with a 20-30% error. Unfolded proteins and proteins with unstructured regions are exceptions because their SMR intensity is much sharper and stronger due to the increased internal motility and decreased resonance dispersion. Thus, care should be taken when working with such proteins. In addition, the comparison of SMR intensities should be done under similar conditions as temperature and ionic strength have significant effects on the SMR intensities.

The phenomenon that proteins at the same concentrations have similar SMR intensities can be demonstrated by examples. SMR intensities of 10 μM solutions of the

third BIR domain (BIR3, 14 kDa) of the X-linked inhibitor-of-apoptosis protein (XIAP) (Deveraux and Reed, 1999) (Figure 3.1A) and the cytoplasmic C₂ domains (C₂AB, 33 kDa) of synaptotagmin 1 are compared in Figure 3.1. In spite of their different molecular masses, their SMR intensities are similar.

However, the SMR intensity of proteins that form stable dimers is determined by the dimer concentration rather than the monomer concentration. Figure 3.1C shows the SMR intensity of the dimeric apoptotic protein Smac (20 kDa monomer and 40 kDa dimer) (Du *et al.*, 2000) at a monomer concentration of 10 μ M. The observed SMR intensity is approximately half of that observed for 10 μ M Bir3 and C₂AB as the relevant Smac concentration is the dimer concentration which is 5 μ M.

The same idea can be applied to protein complexes so that the SMR intensity of a stable protein complex corresponds to that of the concentration of the complex and is independent of the size and number of the proteins involved in the complex. In other words, SMR intensity depends on the complex concentration rather than the total protein concentration in the sample. The SMR intensity of neuronal syntaxin 1A-munc18-1 complex (95 kDa) at 10 μ M complex concentration is similar to that of 10 μ M Bir3 and 10 μ M C₂AB (Figure 3.1D). Similarly, Figure 3.1E demonstrates that the SMR intensity of neuronal SNARE complex (33 kDa), composed of four SNARE proteins, at 10 μ M complex concentration is the same as the SMR intensities of 10 μ M monomeric proteins in A and B although the total protein concentration is actually 40 μ M.

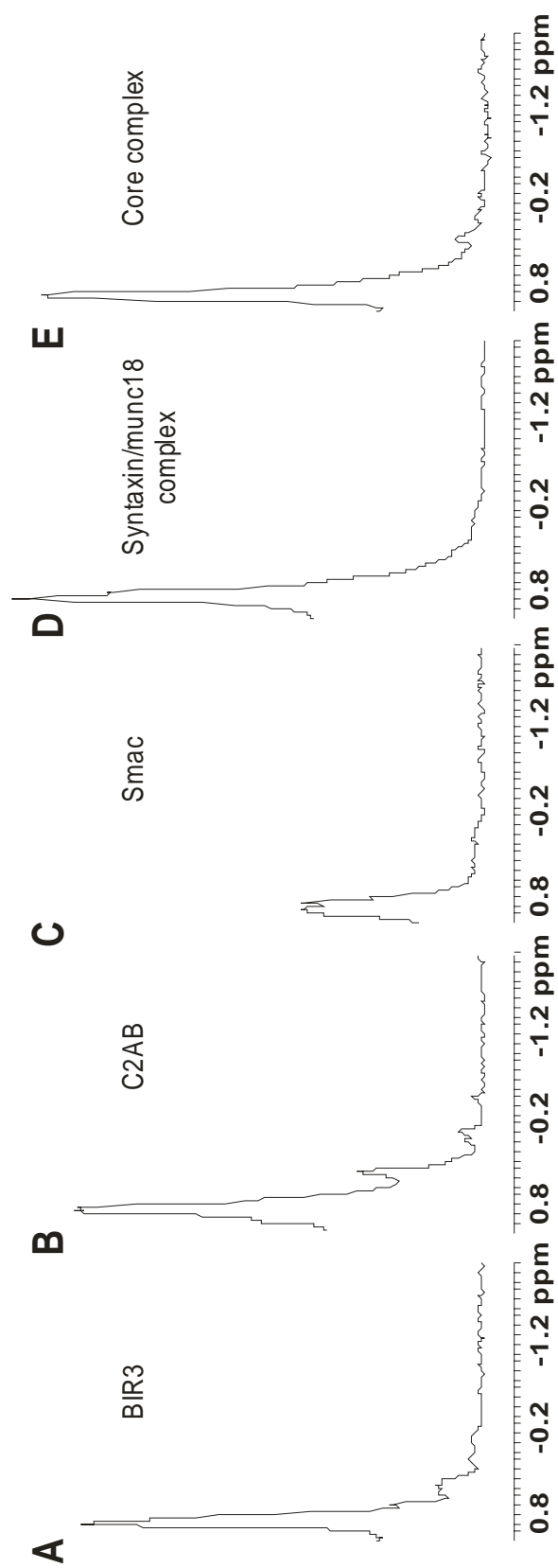


Figure 3.1 SMR intensities of sample proteins and protein complexes

The methyl regions of ^1H NMR spectra are expanded to show the SMR intensities of 10 μM XIAP BIR3 (A), 10 μM synaptotagmin 1 C₂AB (B), 10 μM dimeric Smac (5 μM dimer concentration) (C), 10 μM complex of cytoplasmic region of syntaxin 1A and munc18-1 (D) and 10 μM SNARE complex formed by four SNARE motifs from syntaxin 1A, synaptobrevin and SNAP25 (E). The same vertical scale was used for all spectra and all SMR intensities are comparable to each other. The SMR intensity of most proteins is independent of their molecular weight and depends on the protein concentration. The SMR intensity of protein complexes does not depend on the total protein concentration or the number of the proteins involved in the complex but depends on the complex concentration. All samples were prepared in 20 mM Tris-d11 buffer, 0.5 mM EDTA, 5 % D₂O with pH 7.7 (A and C) or pH7.4 (B,D,E) and 150 mM NaCl (A-C) or 200 mM NaCl (D and E).

3.2.2 SMR method

These observable facts naturally guide the development of a new method to detect protein-protein interactions, which we called the SMR method. The scheme in Figure 3.2 summarizes the SMR method. When two proteins with the same concentration (thus, similar SMR intensities) are mixed, the SMR intensity of the mixture can be monitored and compared with the SMR intensities of individual proteins to find out if the two proteins interact with each other. If the proteins do not interact, the SMR intensities of individual proteins simply add up and the SMR intensity of the mixture corresponds to the intensity resulting after adding the spectra of the two separate proteins (indicated as 0% binding in Figure 3.2). However, if full binding between proteins occurs, the formation of a higher molecular weight complex causes resonance broadening, thus a substantially lower SMR intensity that is similar to the intensity of each protein and 50% of the intensity of the added spectra (indicated as 100% binding in Figure 3.2).

The percent change in SMR intensity upon complex formation depends on the methyl group content of proteins, dispersion of resonances in the NMR spectra and the molecular shape and oligomerization state of individual proteins and the complex. As the molecule's shape affects its tumbling rate, it may increase or decrease the percent change in SMR intensity. The stoichiometry of the protein complex directly affects the SMR intensity as a mixture of proteins in 1:1 ratio will not produce 100% binding and will cause a smaller percent change in SMR intensity. However, this can be used to determine the stoichiometry of the complex by trying to mix proteins in different ratios and find out the ratio that gives the maximum decrease in SMR intensity.

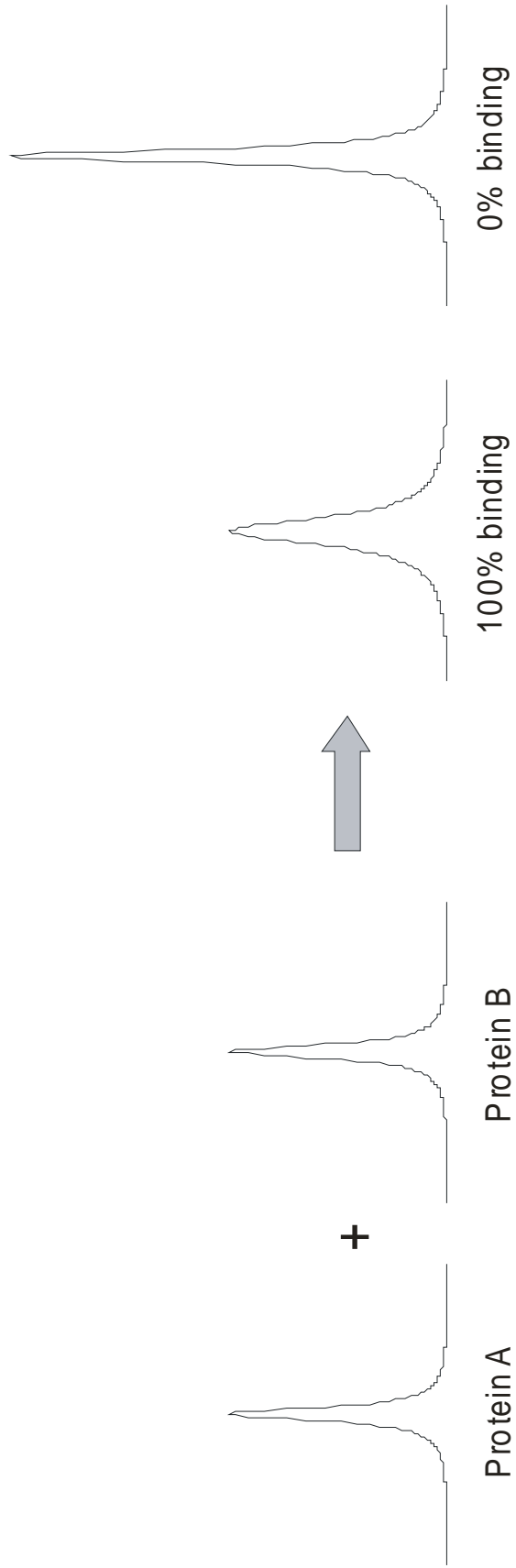


Figure 3.2 Scheme summarizing the SMR method for detecting protein-protein interactions

The SMR signals of 1D ^1H NMR spectra of arbitrary proteins A and B are symbolized on the left and the expected SMR signals for 100% and 0% binding upon mixing proteins are represented on the right. When the proteins are mixed, if there is no binding, the SMR intensities of the individual proteins add up to form a higher intensity SMR with similar linewidth to the individual proteins (0% binding). However, if there is full binding, the SMR intensity is comparable to those of the individual proteins because the SMR increases in linewidth rather than the intensity due to the resonance broadening caused by complex formation. In a real spectrum, the increase in the width might not be obvious as SMR is a combination of many partially overlapping resonances.

If individual proteins contain unstructured regions that become less mobile within the complex, the decrease in SMR intensity upon complex formation will be larger than 50%. However, if unstructured regions remain unstructured, the percent decrease will be less than 50%. In most cases, complex formation causes a substantial decrease in the SMR intensity when compared to the added SMR intensities of individual proteins (at least 20-30% decrease) so that the binding of proteins can be detectable.

3.2.3 Testing the validity of SMR method

The interaction of Smac and BIR3 of XIAP is a well-established protein-protein interaction involved in the regulation of a caspase activity that is in the apoptotic cascade (Du *et al.*, 2000). The structure of the complex between Smac and Bir3 has been solved (Wu *et al.*, 2000;Liu *et al.*, 2000) and a dissociation constant of 0.8 μM has been reported based on a florescence competition assay (Kipp *et al.*, 2002). We have tested the SMR method by using this system and analyzing complex formation between Smac and BIR3. We have acquired the ^1H NMR spectra of samples containing 2 μM BIR3, 2 μM Smac or a mixture of 2 μM BIR3 and 2 μM Smac. The SMR intensity of the mixture was observed to be 40% smaller than that of the added spectra of the two separate proteins (Figure 3.3A). When analogous experiments were done using 5 μM proteins instead of 2 μM , an additional decrease in the SMR signal of the mixture with respect to that of the added spectra was observed, showing higher percentage binding of proteins at higher protein concentrations (Figure 3.3B). No further decrease was observed at higher protein concentrations, indicating that BIR3 and Smac partially interact at 2 μM and the interaction is saturated at 5 μM , as expected for a 0.8 μM dissociation constant.

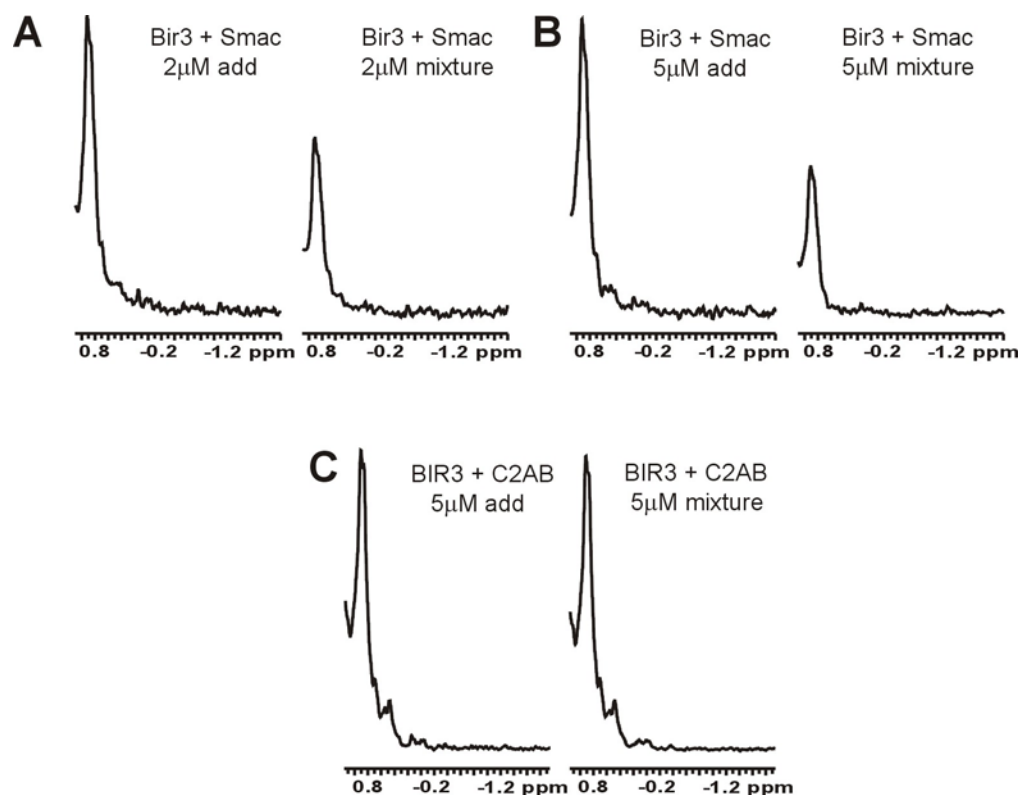


Figure 3.3 Testing the validity of the SMR method with a well-studied protein-protein interaction

Interaction of BIR3 with Smac and C₂AB was used as positive and negative controls to test the SMR method. (A) SMR resulting from the addition of 1D ^1H NMR spectra of 2 μM BIR3 and 2 μM Smac (left) is compared with the SMR of the mixture of 2 μM BIR3 and 2 μM Smac (right). (B) Analogous experiments were repeated using 5 μM protein concentrations. (C) SMR resulting from the addition of 1D ^1H NMR spectra of 5 μM BIR3 and 5 μM C₂AB (left) is compared with the SMR of the mixture of 5 μM BIR3 and 5 μM C₂AB (right). Comparisons were made by using the same vertical scale for plotting the added spectrum and the spectrum of the mixture. Samples were prepared in 20 mM imidazole- d_3 (pH 7.7), 150 mM NaCl, 0.5 mM EDTA, and D₂O was used as solvent.

A negative control experiment was done to observe the SMR intensity of a protein mixture composed of two non-interacting proteins. We have acquired the ^1H NMR spectra of samples containing 5 μM BIR3, 5 μM C₂AB (an unrelated protein that does not interact with BIR3) or a mixture of 5 μM BIR3 and 5 μM C₂AB. The SMR intensity of the mixture was observed to be similar to that of the added spectra of the two separate proteins (Figure 3.3C) showing that BIR3 and C₂AB do not interact. These experiments suggest that SMR is a reliable method to detect protein-protein interactions easily at low micromolar concentrations using very low amounts of protein without the necessity of any tags or modifications on the proteins, which might hinder binding sites or promote unreal interactions.

The SMR method can be used to detect protein-protein interactions at low micromolar protein concentrations. Actually, even lower protein concentrations can be used because of the good signal to noise ratio at 2 μM concentration. This method can also be used for semiquantitative measurement of dissociation constants of interactions. Titrations in which the concentration of both proteins are kept equal to each other and changed simultaneously can indicate the percentage binding at each protein concentration. The protein concentrations should be equal because otherwise the SMR intensity will be dominated by the excess free protein and the binding will not be reliably quantitated. For example, the dissociation constant of BIR3 and Smac can be measured by making a series of experiments where the SMR intensity of the mixture of BIR3 and Smac is monitored at protein concentrations of 0.05, 0.1, 0.2, 0.5, 1, 2, 5, 10 μM and compared with the added spectra of separate proteins. At low protein concentrations, the percent decrease in SMR intensity should be low as the concentration is too low for full

binding. The percent decrease should increase by increasing protein concentration and reach saturation as full binding will be achieved at high protein concentrations. Figure 3.3A and 3B shows the percent decrease at 2 μM and 5 μM . As expected at 5 μM protein concentrations, the decrease in SMR intensity is higher.

3.2.4 SMRC method

The same principles for the SMR method can be applied to create the SMRC method, which involves isotopic labeling of one of the proteins with ^{13}C . In this method, the SMRC signal of the ^{13}C labeled protein is monitored using 1D ^{13}C -edited ^1H NMR spectra so that only the protons that are connected to a ^{13}C atom will be observable. The signals from the unlabeled protein do not contribute to the spectra at all. The scheme in Figure 3.4 summarizes the SMRC method. The SMRC of the ^{13}C -labeled protein is observed by 1D ^{13}C -edited ^1H NMR spectrum but no signal is detected from the unlabeled protein. If the proteins do not interact upon mixing, the SMRC intensity of the ^{13}C -labeled protein remains unaffected (indicated as 0% binding). However, if full binding between proteins occurs, the SMRC intensity of the ^{13}C -labeled protein decreases due to resonance broadening upon binding to the unlabeled protein (indicated as 100% binding). If the molecular masses of the proteins are similar, the SMRC intensity is expected to decrease 50% assuming an approximately linear relationship between molecular mass and line width. If one of the proteins is larger than the other one, the smaller protein should be chosen for ^{13}C -labeling because its resonances will experience a more severe broadening upon binding to the larger protein and the SMRC intensity will decrease more than 50%. However, if the larger protein is ^{13}C -labeled, the interaction

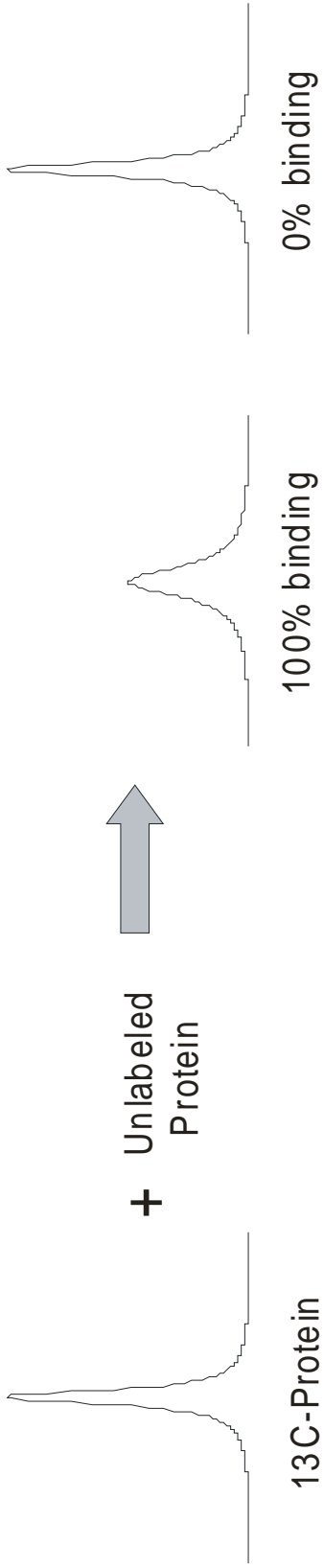


Figure 3.4 Scheme summarizing the SMRC method for detecting protein-protein interactions

The SMRC signal of the ^{13}C -labeled protein is monitored by 1D ^{13}C -edited ^1H NMR spectrum. The unlabeled protein has no detectable signal in the ^{13}C -edited spectrum (left). When the proteins are mixed, the SMRC signal of the ^{13}C -labeled protein is decreased because of the resonance broadening upon binding to the unlabeled protein (100% binding). The decrease in SMRC intensity depends on the ratio of the molecular mass and shape of the proteins. The resonance broadening is more dramatic if the molecular size of the unlabeled protein is larger than the labeled protein. If there is no interaction between the proteins, the SMRC intensity is not affected and is similar to that of the individual ^{13}C -labeled protein (0% binding).

with the smaller protein will cause less resonance broadening and the SMRC intensity will decrease less than 50%.

In practice, quantitative measurements of dissociation constants are more easily done using the SMRC method by labeling one of the proteins with ^{13}C . Figure 3.5A illustrates the application of the SMRC method to detect the interaction between BIR3 and Smac and to measure the dissociation constant of the binding. The BIR3 (14 kDa) protein was labeled with ^{13}C and its SMRC signal was monitored by ^{13}C -edited 1D NMR spectra. Addition of increasing amounts of unlabeled Smac (20 kDa) onto a constant concentration of 3 μM ^{13}C -labeled BIR3 caused progressive decrease in the SMRC intensity of ^{13}C -BIR3. The SMRC intensity changed as a function of Smac concentration and the full titration showed that the decrease in SMRC intensity stopped at high Smac concentrations, indicating that the binding has saturated (Figure 3.5B). The data can be fit to an equation which assumes a simple 1:1 binding model to calculate the dissociation constant. The following equation expresses the SMRC intensity of the ^{13}C -labeled BIR3 as a function of the constant ^{13}C -BIR3 concentration (P_1) and the changing unlabeled Smac concentration (P_2):

$$I = I_F + (I_B - I_F) * (P_1 * P_2 * K_D - \sqrt{(P_1 * P_2 * K_D)^2 - 4 * P_1 * P_2}) / (2 * P_1)$$

where I_F and I_B represent the SMRC intensities of the free and bound ^{13}C -BIR3, respectively and K_D is the dissociation constant. The data in Figure 3.5B was fit to this equation using a constant P_1 value of 3 μM and varying P_2 values up to 20 μM , and the dissociation constant was measured as 0.6 +/- 0.3 μM , which is a very similar value to the previously reported value (0.8 μM) (Kipp *et al.*, 2002).

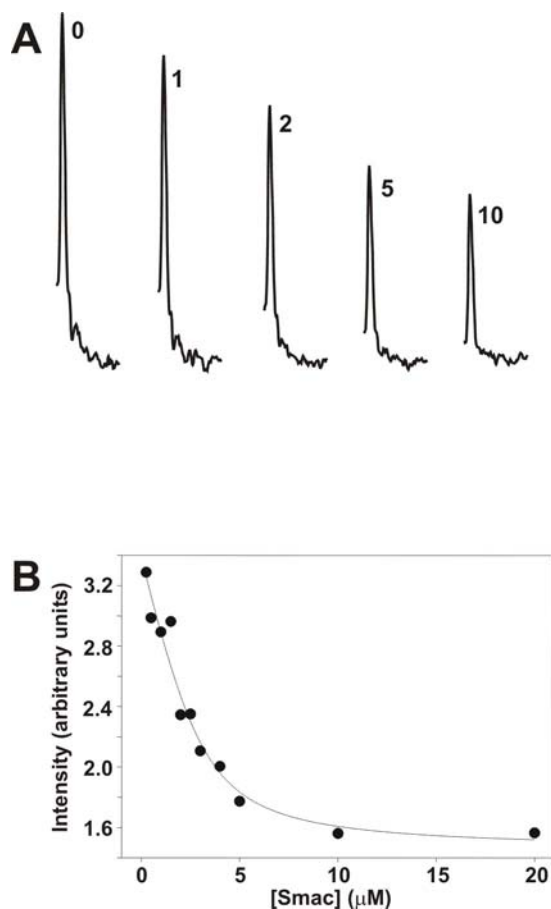


Figure 3.5 Application of the SMRC method to measure dissociation constants

The utilization of the SMRC method to measure dissociation constants is demonstrated for the BIR3-Smac system. (A) The SMRC intensities of a series of 1D ^{13}C -edited ^1H NMR spectra of 3 μM ^{13}C -labeled BIR3 in the presence of increasing amounts of unlabeled Smac are shown. The concentration of Smac (μM) used in each sample is indicated. All spectra were plotted at the same vertical scale. (B) The SMRC intensities observed in (A) were plotted as a function of unlabeled Smac concentration and the data were fit to an equilibrium 1:1 binding model explained in the text. The dissociation constant of the binding was calculated as $0.6 \pm 0.3 \mu\text{M}$. The samples were prepared in 20 mM Tris-d11 (pH 7.7), 150 mM NaCl, 0.5 mM EDTA and 5% D_2O . 10 μM unlabeled bovine serum albumin was added to all samples to avoid binding of Smac to the glass.

The same equation can be used for calculating dissociation constants by the SMR method where both proteins are unlabeled. However, during a titration the concentration of proteins should be kept equal to each other and changed simultaneously for each data point. The signal intensity can be expressed using the above equation but with P_1 being equal to P_2 .

3.2.5 The requirement for a new method to study synaptotagmin 1 function

As summarized in Chapter 2, we previously focused on characterizing the interaction of synaptotagmin 1 with the SNARE complex and its components using NMR spectroscopy. We labeled different SNARE motifs with ^{15}N and formed the SNARE complex or different subcomplexes of SNAREs to run ^1H ^{15}N -HSQC experiments and look for changes in the HSQC peaks upon addition of unlabeled synaptotagmin 1. We also repeated these experiments by labeling synaptotagmin 1 and adding unlabeled SNAREs. These experiments produced inconclusive results as we observed disappearance of HSQC peaks and extreme resonance broadening even in the absence of Ca^{2+} . Most of the experiments were performed using at least 70 μM protein concentrations as this is required for a good signal to noise ratio in an HSQC spectra. We concluded that these protein concentrations are probably too high and produce nonspecific interactions, especially considering that SNARE proteins are highly acidic and synaptotagmin 1 has a polybasic region. We decided to use other methods to analyze the interaction of synaptotagmin 1 with the SNAREs. We searched for a method which is sensitive enough to detect protein-protein interactions at low concentrations so that we can avoid nonspecific interactions caused by high concentration. We also required that

this method should avoid using protein modifications and tags which can produce false positive or negative results.

Synaptotagmin 1 acts as a Ca^{2+} sensor in neurotransmitter release and this role can be associated to the two cytoplasmic C_2 domains. Both C_2 domains bind to negatively charged phospholipids in a Ca^{2+} -dependent manner (Fernandez-Chacon *et al.*, 2001; Fernandez *et al.*, 2001). In addition, it was reported to interact with the SNARE complex (Rizo *et al.*, 1998a; Bennett, 1999; Tucker and Chapman, 2002). Ca^{2+} -dependent binding to phospholipids and/or the SNARE complex is widely believed to be the essential function of synaptotagmin 1 to trigger Ca^{2+} -dependent neurotransmitter release. However, it is unclear whether these two interactions occur simultaneously or compete with each other. The C_2AB region of synaptotagmin 1 was suggested to bind to the SNARE complex and phospholipids simultaneously by co-immunoprecipitation experiments (Davis *et al.*, 1999). GST pulldown assays failed to show quantitative binding of SNARE complex to the synaptotagmin 1 C_2AB domain, whereas ultracentrifugation experiments indicated that the SNARE complex is unable to bind to synaptotagmin 1 in the presence of phospholipids. However, these results might be an outcome of a fast off-rate of synaptotagmin 1/SNARE interaction which is too fast for the time scales of these methods.

As an additional step to characterizing synaptotagmin 1/SNARE interactions, we wanted to do competition experiments between SNAREs and phospholipid membranes for binding to synaptotagmin 1 to determine whether synaptotagmin 1 can bind to SNAREs and membranes simultaneously or it has a preferential binding for one of them. Answering this question is critical for understanding the mechanism of neurotransmitter

release. For this purpose, we needed to use a method that can study multicomponent systems and detect the interaction of two molecules in the presence of other components. The lack of such a method with these properties led us to develop the SMR and SMRC methods and we successfully applied the SMRC method to study the interactions of synaptotagmin 1 with SNAREs and phospholipid membranes.

The SMRC method has the following advantages that make it so useful to fulfill our requirements to study the synaptotagmin 1 interactions: 1) SMRC method can also be used to study multicomponent systems. Labeling each protein one at a time, the SMRC signal can selectively be monitored to determine if the labeled protein is involved in an interaction with the other components. Competition between different targets of a given protein can be observed by determining whether the two targets can bind to the protein simultaneously or one of them prohibits the binding of the other one to the protein. 2) This method can also be used to study interaction of proteins with macromolecules other than proteins such as lipid membranes because the NMR signal of the unlabeled component does not need to be observable. 3) Very low protein concentrations are enough for signal detection. This eliminates the requirement for high amounts of protein and decreases the chances of detecting an unspecific interaction. 4) SMRC method is not limited to detecting interactions with slow off-rates but can detect interactions with fast off-rates, as well.

3.2.6 Application of SMRC method to study synaptotagmin 1 function

We have expressed and purified ^{13}C labeled C₂AB and monitored the SMRC signal of 2 μM ^{13}C -C₂AB using 1D ^{13}C -edited NMR spectra (Figure 3.6A). Similar

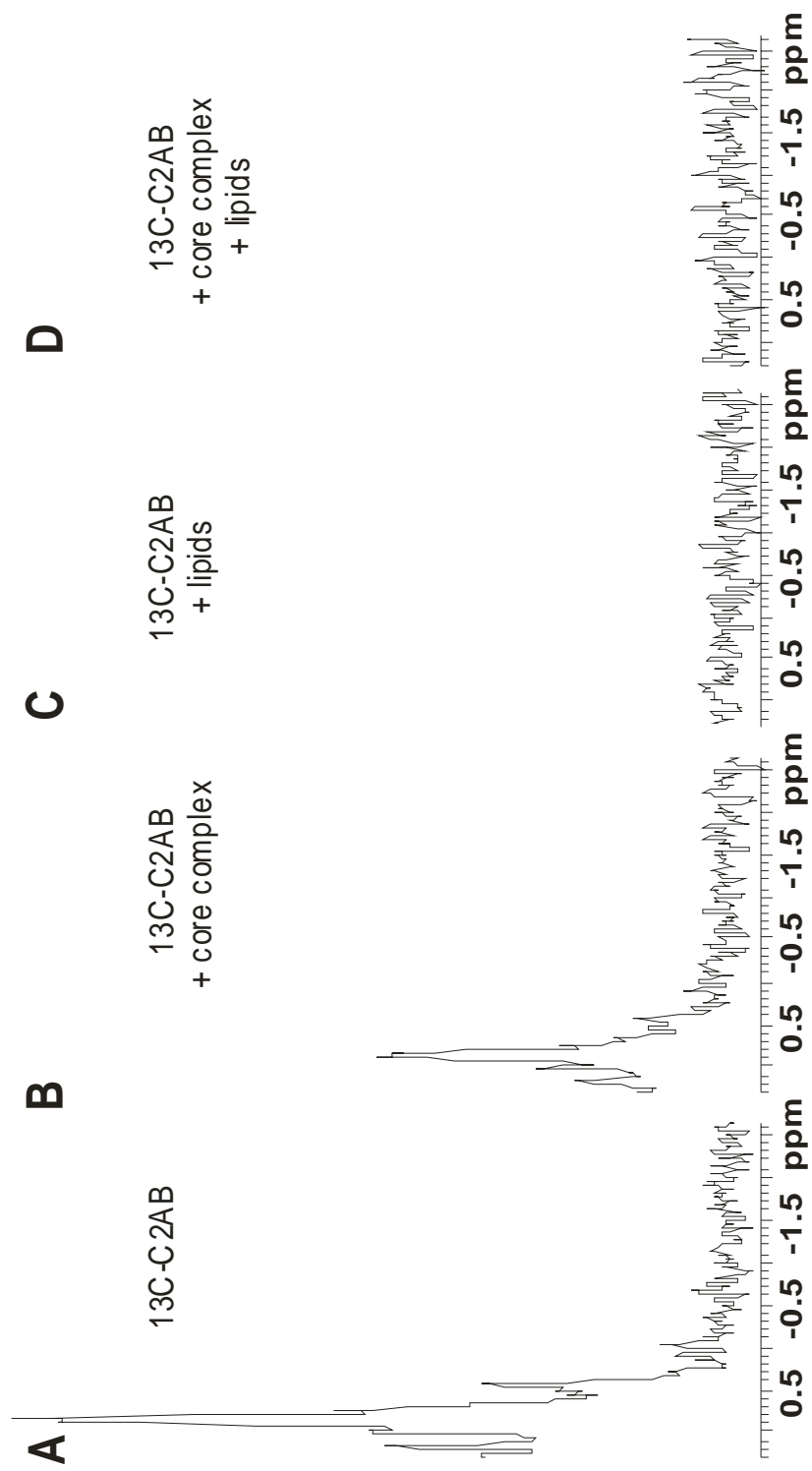


Figure 3.6 Application of the SMRC method to study the interactions of synaptotagmin

The SMRC of 2 μM ^{13}C -labeled C_2AB is monitored in the 1D ^{13}C -edited ^1H NMR spectra in isolation (A) and after addition of 3 μM unlabeled SNARE somplex (B), 0.3 mg/ml lipid vesicles (C), or 3 μM unlabeled SNARE complex and 0.3 mg/ml lipid vesicles (D). Samples were prepared in 20 mM imidazole- d_3 (pH 7.2), 100 mM NaCl, 1mM CaCl_2 , and 5% D_2O . The SMRC intensity of ^{13}C -labeled C_2AB is decreased upon addition of unlabeled SNARE complex, indicating interaction (B). The SMRC is broadened beyond detection upon binding to lipid vesicles due to the large size of the vesicles (C). Addition of both SNARE complex and lipid vesicles on ^{13}C -labeled C_2AB produces a spectra similar to (C), indicating that C_2AB remains bound to lipid vesicles even in the presence of SNARE complex.

SMRC signal was observed in the presence of 1 mM Ca^{2+} . Our control experiments performed in the absence of Ca^{2+} showed no or slight decrease in the SMRC intensity of ^{13}C -C₂AB upon addition of unlabeled SNARE complex, indicating that the SNARE complex and C₂AB does not bind or binds weakly in the absence of Ca^{2+} . This result is consistent with our previous idea that high protein concentrations produce nonspecific synaptotagmin 1/SNARE interactions even in the absence of Ca^{2+} . As we decrease the protein concentration from ~70-100 μM (HSQC) to 2 μM (1D), we observe much less binding in the absence of Ca^{2+} . We decided to perform our binding experiments using protein concentrations around 2 μM as fewer artifacts will be observed under these conditions. We performed all of the following experiments in the presence of 1 mM Ca^{2+} . All observed interactions were Ca^{2+} -dependent and reversible as observed from the spectra acquired after the addition of 1 mM excess EDTA.

Addition of 3 μM unlabeled SNARE complex on 2 μM ^{13}C -C₂AB in the presence of Ca^{2+} caused more than 50% decrease in the SMRC intensity of ^{13}C -C₂AB, indicating an interaction between the SNARE complex and C₂AB (Figure 3.6B). Addition of excess SNARE complex did not cause further decrease in the SMRC intensity, showing that the binding is quantitative and saturated under these conditions. We have repeated these experiments using the Syx:SN1 complex (complex formed by the SNARE motif of syntaxin and the N-terminal SNARE motif of SNAP25) and observed similar results. We conclude that the Syx:SN1 complex is enough for synaptotagmin 1 binding. It is possible that these two SNAREs form the binding site in the SNARE complex for synaptotagmin 1 binding.

We also used the SMRC method to detect the interaction of synaptotagmin 1 with phospholipids. Addition of 0.3 mg/ml large unilamellar phospholipid vesicles (LUVs) onto ^{13}C -C₂AB in the presence of Ca²⁺ resulted in disappearance of the SMRC signal completely (Figure 3.6C). This dramatic decrease in the SMRC intensity is an expected result because the large size of the vesicles (100 nm diameter) causes extreme broadening in the resonances upon binding of vesicles to C₂AB. The SMRC intensity gradually decreased as increasing amounts of lipid vesicles were added and complete disappearance of signals was achieved when 0.3 mg/ml lipid concentration was used. This result indicates quantitative binding of C₂AB to lipids and shows that approximately 2 μM C₂AB saturates the surface area of 0.3 mg/ml lipid vesicles.

Competition experiments were performed by monitoring the SMRC intensity of 2 μM ^{13}C -C₂AB in the presence of both 3 μM unlabeled SNARE complex and 0.3 mg/ml lipid vesicles. The SMRC signal was observed to disappear completely, indicating that C₂AB remains bound to vesicles even in the presence of the SNARE complex (Figure 3.6D). However, these experiments do not reveal whether the SNARE complex, vesicles and C₂AB form a ternary complex or the SNARE complex is excluded from the vesicle/C₂AB complex.

To answer this question, we decided to follow the SMRC signal of the SNARE complex. We labeled all four SNARE motifs of the SNARE complex with ^{13}C . The SMRC signal of 1.5 μM ^{13}C -SNARE complex, monitored by 1D ^{13}C -edited NMR spectra, is shown in Figure 3.7A. Addition of 2 μM unlabeled C₂AB on this sample caused a 33% decrease in the SMRC intensity confirming the interaction (Figure 3.7B). The slightly lower decrease in the SMRC of the SNARE complex upon C₂AB binding

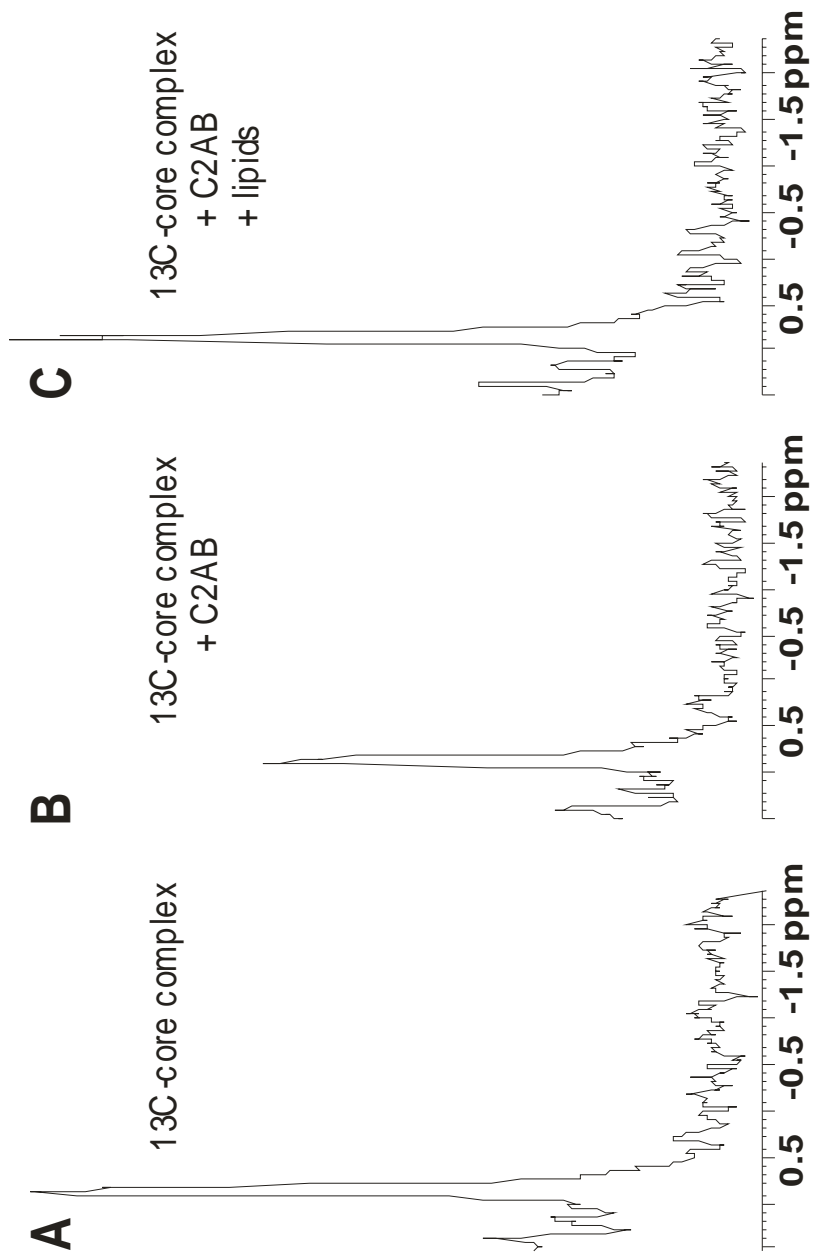


Figure 3.7 Application of the SMRC method to study the interactions of the SNARE complex

The SMRC of 1.5 μM ^{13}C -labeled SNARE complex is monitored in the 1D ^{13}C -edited ^1H NMR spectra in isolation (A) and after addition of 2 μM unlabeled C_2AB (B), or 2 μM unlabeled C_2AB and 0.3 mg/ml lipid vesicles (C). Samples were prepared in 20 mM imidazole- d_3 (pH 7.2), 100 mM NaCl, 1mM CaCl_2 , and 5% D_2O . The SMRC intensity of ^{13}C -labeled SNARE complex is decreased upon addition of unlabeled C_2AB , indicating interaction (B). The SMRC increases back to its original intensity upon addition of both unlabeled C_2AB and lipid vesicles and produces a spectra similar to (A), indicating that when C_2AB is present, the SNARE complex is not bound to lipid vesicles and is free in solution (C).

compared to the decrease in SMRC of C₂AB upon SNARE complex binding in Figure 3.6B is due to the slower correlation time of SNARE complex arising from its elongated shape and because of the contributions from the unstructured tails to the SMRC of SNARE complex. The small amount of unassembled free SNARE motifs remaining in spite of the purification step might also contribute to the lower decrease in the SMRC of SNARE complex.

The critical experiment where both 0.3 mg/ml lipid vesicles and 2 μ M unlabeled C₂AB were added to ¹³C-SNARE complex yielded the same SMRC intensity as that observed for free ¹³C-SNARE complex (Figure 3.7A and C). The full recovery of SMRC intensity indicates that the SNARE complex is not bound to the vesicle/ C₂AB complex but is free in solution. If the SNARE complex had bound to the C₂AB/vesicle complex, the SMRC intensity would have broadened beyond detection and we would observe a spectrum similar to that in Figure 3.6D. These results show that phospholipid binding competes with the SNARE complex binding to the C₂AB domain of synaptotagmin 1, indicating that the preferred target of synaptotagmin 1 in the presence of Ca²⁺ is the lipids. This observation contributes to the widely believed idea that Ca²⁺-dependent phospholipid binding activity is the crucial interaction of synaptotagmin 1 to trigger neurotransmitter release upon Ca²⁺ influx into the presynaptic neuron (Fernandez-Chacon *et al.*, 2001; Fernandez *et al.*, 2001; Shin *et al.*, 2002).

3.3 Discussion

Application of the SMR and SMRC methods to the BIR3/Smac and synaptotagmin 1 systems proved that they are powerful tools to study protein-protein

interactions as well as protein-macromolecule interactions in bicomponent or multicomponent systems. These methods can also be used to determine dissociation constants and complement other existing techniques. One of the major advantages of the SMR and SMRC methods is that they are unlikely to produce false positive results as they are performed in solution with pure proteins that have no tags or chemical modifications. The populations of free and bound states of protein are directly reflected on the spectra. Thus, interactions can be detected whether the off-rate is fast or slow, whereas other techniques such as chromatography can yield false negative results for interactions with fast off-rates. Hence, the SMRC and SMR methods are largely free of artifacts and can unambiguously determine whether two or more proteins are interacting. Titrations can be performed to saturate the binding and determine the stoichiometry of the interactions. In addition, dissociation constants above 0.5 μM can be measured. Standard NMR experiments commonly used in most NMR spectrometers with a ^1H frequency ≥ 400 MHz can be used to perform these experiments easily.

Both recombinant proteins and proteins purified from natural sources can be used for the SMR method, whereas for the SMRC method, one of the proteins should be expressed by recombinant methods and labeled with ^{13}C . Labeling with ^{13}C brings the advantage of being able to work with multicomponent systems as the SMRC intensity of the labeled protein can be selectively monitored independent of how many other proteins or macromolecules are bound to it as the signals of unlabeled components are not observable in ^{13}C -edited spectra. Our experiments involving synaptotagmin 1 C₂AB domain represent a good example of the usefulness of the SMRC method. Many proteins can easily be labeled with ^{13}C in bacteria using minimal media with [$^{13}\text{C}_6$]-glucose as the

only carbon source. Major vendors of isotopically labeled compounds provide different types of ^{13}C -enriched media for expression in bacteria, CHO cells and insect cells. As the amount of protein required for the experiments is 100 to 1000 fold less than that is required for structural studies, the cost of these experiments is moderate.

It is also possible to use ^{15}N labeled proteins to study protein-protein interactions similar to the SMRC method. The only difference is that the amide protons of the protein, which are around 6-8 ppm, are monitored instead of the methyl protons using the first trace of a standard ^1H - ^{15}N HSQC experiment. As the amide protons are more spread in the 1D ^1H NMR spectra, the signal intensity of the amide hydrogens is not as strong as the SMR. This requires use of slightly higher protein concentrations ($\sim 5\ \mu\text{M}$) and longer acquisition times.

The advantage of the SMR and SMRC methods over the 2D NMR techniques is the ability to use micromolar concentrations to study protein-protein interactions. The detection of nonspecific interactions is minimized by the SMR and SMRC methods, and proteins do not suffer from solubility problems due to high protein concentrations. We have obtained spectra even at submicromolar protein concentrations. Figure 3.8 shows the 500 MHz 1D ^{13}C -edited ^1H NMR spectrum of 250 nM ^{13}C -labeled BIR3 acquired at 8 hours acquisition time. The use of higher magnetic fields and cryoprobe technology can shorten the acquisition times and even lower the required protein concentration for application of these methods.

We applied these methods to give an unambiguous answer to an important question in the synaptotagmin 1 system. Determining the physiologically relevant interaction(s) of synaptotagmin 1 is a crucial task to understand the mechanism of

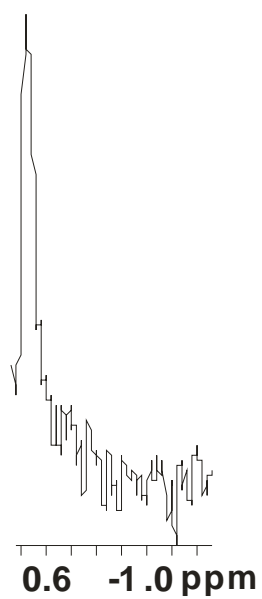


Figure 3.8 Monitoring SMRC intensity at sub-micromolar protein concentrations
 The SMRC of 250 nM ^{13}C -labeled BIR3 monitored by 500 MHz 1D ^{13}C -edited ^1H NMR spectrum with 20000 transients and 8 hours total acquisition time is shown.

synaptotagmin 1 action in triggering Ca^{2+} -dependent neurotransmitter release. However, synaptotagmin 1 has been reported to be involved in many interactions, some of which are probably nonspecific, due to its highly charged surface. Synaptotagmin 1 is strongly believed to mediate its activity via binding to phospholipid membranes and/or the SNARE complex. Contradicting views are present about whether both interactions occur simultaneously or compete with each other. We used the SMRC method to follow the interactions of highly purified proteins and performed competition experiments where stoichiometric ratios of proteins and lipids were used. Monitoring the SMRC intensities of ^{13}C -labeled C_2AB or ^{13}C -labeled SNARE complex revealed that in the presence of both lipid vesicles and SNARE complex, synaptotagmin 1 preferentially binds to lipid vesicles and SNARE complex is excluded from the synaptotagmin 1/lipids complex. These in vitro experiments strongly suggest that the physiologically relevant Ca^{2+} -dependent interaction of synaptotagmin 1 in vivo is membrane binding.

3.4 *Materials and Methods*

3.4.1 Protein expression and purification

The DNA constructs used in the experiments encode XIAP BIR3 (residues 238-358), synaptotagmin 1 C_2AB (residues 140-421), Smac (residues 1-162), cytoplasm region of syntaxin 1A (residues 2-253), SNARE motif of syntaxin 1A (residues 188-259), SNARE motif of synaptobrevin (residues 29-93) and two SNARE motifs of SNAP25 (residues 11-82 and 141-203). BIR3 and Smac were expressed in bacteria with a His6 tag and all others were expressed as GST fusion proteins. The expressed proteins were

isolated by affinity chromatography and further purified by gel filtration or ion exchange chromatography after thrombin cleavage of the GST moiety. The syntaxin 1A –munc18-1 complex was obtained by adding purified syntaxin 1A to GST-munc18-1 cell supernatants followed by affinity chromatography and gel filtration.

Unlabeled and ^{13}C -labeled C₂AB domain of Syt1 and four SNARE motifs of the SNARE complex were expressed and purified as described earlier (Chapter 2 Methods). The SNARE complex was formed by mixing equimolar amounts of the four SNARE motifs and incubated overnight for assembly. The SNARE complex formed by ^{13}C -labeled SNARE proteins was further purified by gel filtration chromatography to remove unassembled SNARE motifs as otherwise their SMRC signal will dramatically contribute to the SMRC of the SNARE complex.

3.4.2 Preparation of lipid vesicles

Negatively charged lipid vesicles (~100 nm diameter) contained 30% brain phosphatidylserine and 70% phosphatidylcholine. Phospholipids dissolved in chloroform were mixed in a glass tube and chloroform was evaporated under N₂ gas flow to completely dry the lipids. The required buffer was added onto the lipids to make a stock of 1 mg/ml. The mixture was vortexed for 3-5 minutes to resuspend the lipids, and was frozen and thawed 3 times on dry ice to hydrate the lipids. Lipid vesicles of homogeneous size were formed by passing the lipid solution through a 0.08 μM filter using a mini-extruder system from Avanti Polar Lipids according to the procedure recommended by the manufacturer. The homogeneity of the sample was achieved after passing the solution

through the filter approximately 15 times. The lipid vesicles were stored at 4 C and used within 1-3 days.

3.4.3 Sample preparation

The NMR samples were prepared using deuterated buffers (Tris-d11 or imidazole-d3) to decrease the intensity of the buffer signals as otherwise the ratio of buffer signal to protein signal is very high and causes difficulty in phasing the 1D spectra. In addition, samples prepared for the demonstration of the SMR method were prepared using D₂O as the solvent to remove the signal of the water.

The SMR method requires careful handling of the sample because any contaminants containing methyl groups will contribute to the SMR signal especially when using sub-micromolar protein concentrations. Another problem when working with low protein concentrations is that some proteins have tendency to bind to the glass and stick to the NMR tube, leading to a decrease in the SMR signal. Using the SMRC method provides solution to both problems, as the methyl groups of the unlabeled contaminants will not be observable. Also, glass-coating reagents can be used to minimize the binding of the protein to the glass and not be detected in 1D ¹³C-edited ¹H NMR spectra. For example, 10 μM bovine serum albumin was added in all samples used for the titration of BIR3 and Smac and in Figure 3.5B and very consistent results were obtained.

3.4.4 NMR spectroscopy

NMR spectra were acquired on Varian INOVA500 or INOVA600 NMR spectrometers with PFG triple-resonance probes at 27 °C. A standard 1D pulse sequence using very low power saturation and watergate (3-9-19) for water suppression was used to acquire ^1H NMR spectra. The FIDs were multiplied with a strong Gaussian function with maximum at 0 ms and half-height at 30 ms to improve the sensitivity before the Fourier transformation. The first increment of a gradient-enhanced ^1H - ^{13}C heteronuclear single quantum coherence (HSQC) was acquired to obtain the 1D ^{13}C -edited ^1H NMR spectra. The SMRC intensity observed in the 1D ^{13}C -edited ^1H NMR spectrum was 85% of the SMR intensity of the same sample observed in 1D ^{13}C -decoupled ^1H NMR spectrum.

The spectra were acquired at 500 MHz or 600 MHz with 1000, 2000 or 3000 transients for total acquisition times of 26, 53 or 79 min, respectively. (1.6 s recycling delay).

CHAPTER 4

INTERACTION OF SYNAPTOTAGMIN 1 WITH PHOSPHOLIPID MEMBRANES

4.1 Preliminary results for the basis of chapter 4

When I started working on my thesis project in 2000, there was very limited information about the second C₂ domain of synaptotagmin 1. Although it was known that the synaptotagmin 1 C₂B domain plays a critical role in Ca²⁺-triggered fusion (Littleton *et al.*, 2001), its structural and biochemical properties were uncertain. It was reported that the C₂B domain binds to the clathrin adaptor protein (AP-2) (Zhang *et al.*, 1994a), Ca²⁺-channels (Sheng *et al.*, 1997), inositol polyphosphates (Fukuda *et al.*, 1994) and others. Several of these interactions were mapped to the highly basic region of the C₂B domain. One of the most surprising results was the observation that the C₂B domain did not exhibit Ca²⁺-dependent binding to negatively charged phospholipids (Schiavo *et al.*, 1996; Bai *et al.*, 2000). Phospholipid binding is the most characteristic property of C₂ domains (Rizo and Sudhof, 1998b). In addition, based on sequence homology, the 3D structure of the C₂B domain was expected to be similar to the structure of the C₂A domain, which binds negatively charged phospholipids in a Ca²⁺-dependent manner. Later, the NMR structure of the C₂B domain demonstrated the similarity in the overall structures of the C₂A and C₂B domains (Fernandez *et al.*, 2001). Thus, the lack of phospholipid binding to the C₂B domain was puzzling.

In our lab, Josep Ubach, realized that the recombinant C₂B protein can contain acidic bacterial contaminants tightly bound to the polybasic region, which may have promoted binding artifacts while hindering relevant interactions (Ubach *et al.*, 2001). A purification method that includes extensive washing with a high salt buffer and gel filtration followed by ion-exchange chromatography was developed. This protocol successfully produced highly pure C₂B domain without any acidic contaminants.

The C₂A domain binds negatively charged phospholipids as a function of Ca²⁺ via the Ca²⁺ binding loops (Davletov *et al.*, 1993; Zhang *et al.*, 1998). To determine whether the highly pure C₂B domain binds to phospholipids, similar to the C₂A domain, we measured fluorescence resonance energy transfer (FRET) from the tryptophan residues of the protein to dansyl-labeled, negatively charged phospholipid vesicles. The fluorescence emission of the dansyl group was monitored in the presence and absence of Ca²⁺. Phospholipid binding to the C₂A domain produced strong Ca²⁺-dependent FRET as expected (Figure 4.1A). Similar Ca²⁺-dependent FRET was observed for the C₂B domain (Figure 4.1B). The specificity of the interaction was demonstrated by the observation that no FRET was induced by 2 mM Mg²⁺ (Figure 4.1B). Also, the C₂B domain carrying a Ca²⁺-binding mutation (D309N) did not exhibit Ca²⁺-dependent phospholipid binding (Figure 4.1B). Ca²⁺ titrations were done using the FRET assay and an apparent Ca²⁺ affinity of 54 μ M and a Hill coefficient of 1.3 was obtained for the C₂A domain in agreement with previous results (Nalefski *et al.*, 2001). An apparent Ca²⁺ affinity of 48 μ M and a Hill coefficient of 1.6 were measured for the C₂B domain (Figure 4.1C and D). These results showed that the C₂B domain of synaptotagmin 1 binds to negatively charged phospholipids in a Ca²⁺-dependent manner.

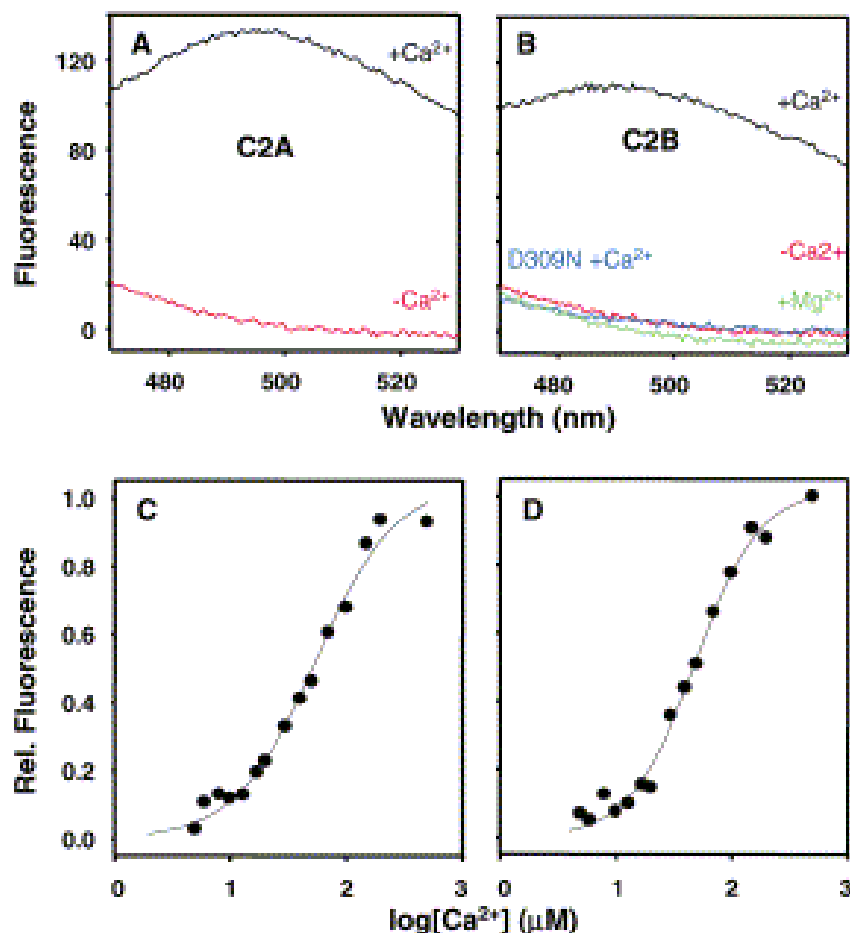


Figure 4.1 C₂B domain binds to negatively charged vesicles in a Ca²⁺-dependent manner

FRET measurements from C₂A (A) and C₂B (B) domains to negatively charged vesicles are shown in the presence of 0.5 mM EDTA (red) or 0.2 mM Ca²⁺ (black). No FRET is observed in the presence of EDTA (red), Mg²⁺ (green) or the Ca²⁺-binding mutant D309N- C₂B (blue). A spectrum acquired in the absence of protein was subtracted from each data set. Ca²⁺ dependence of lipid binding for C₂A (C) and C₂B (D) domains measured by FRET is shown. The relative change in FRET is represented as a function of Ca²⁺.

This finding immediately suggested that the C₂A and C₂B domains, which are connected by a short linker, can easily rotate and place their Ca²⁺/phospholipid binding sites in close proximity and favor a cooperative interaction with membranes. The ability of both C₂ domains to bind to membranes led to the speculation that the primary function of synaptotagmin 1 during neurotransmitter release is to bind to membranes upon Ca²⁺ influx. To establish whether the interaction of synaptotagmin 1 with membranes or with the SNARE complex is more critical, we did competition experiments as explained in Chapter 3 and showed that synaptotagmin 1 prefers to bind to membranes rather than to the SNARE complex in the presence of Ca²⁺. Next, we investigated the interaction of synaptotagmin 1 with membranes in detail.

4.2 *Introduction*

The commonly accepted idea that synaptotagmin 1 is the major Ca²⁺-sensor in neurotransmitter release and the discovery of numerous interactions of synaptotagmin 1 directed the efforts to understand the mechanism of synaptotagmin 1 action in triggering membrane fusion. Many studies summarized in Section 1.3.6 aiming to determine the physiologically relevant interaction of synaptotagmin 1 and our studies explained in Chapter 3 indicated that synaptotagmin 1 mediates membrane fusion via direct interaction with membranes upon Ca²⁺ influx. Although we cannot rule out the role of SNAREs in a Ca²⁺-dependent or Ca²⁺-independent step, it seems clear that Ca²⁺-dependent phospholipid binding is at the center of synaptotagmin 1 function. However, the mechanism of synaptotagmin 1 action is unknown.

It is puzzling that disrupting Ca^{2+} binding to the C_2B domain impairs release severely, whereas disrupting Ca^{2+} binding to the C_2A domain has only a mild effect on neurotransmitter release (Mackler *et al.*, 2002; Robinson *et al.*, 2002). On the other hand, disrupting Ca^{2+} binding to either the C_2A or C_2B domain has moderate effects on binding of synaptotagmin 1 to phospholipids because the intact C_2 domain is still able to bind Ca^{2+} /phospholipids and compensate for the disfunctional C_2 domain (Fernandez-Chacon *et al.*, 2002; Nishiki and Augustine, 2004). Hence, these observations suggest that a unique property of the C_2B domain that is related to Ca^{2+} -dependent phospholipid binding, but is not shared by the C_2A domain is key for neurotransmitter release. A potential explanation was provided by an electron microscopy study, which suggested that synaptotagmin 1 forms heptameric structures through the C_2B domain upon Ca^{2+} -dependent phospholipid binding (Wu *et al.*, 2003). However, the heptameric model of synaptotagmin 1 built based on EM images is incompatible with phospholipid binding.

We investigated the mechanism of Ca^{2+} -dependent phospholipid binding to synaptotagmin C_2 domains in detail using a variety of biophysical techniques with the aim of understanding how synaptotagmin 1 triggers neurotransmitter release. Some of the major questions we wanted to answer were: What is the binding mode of synaptotagmin 1 to lipids? Which residues interact with lipids and how deep do they insert into the membrane bilayer? Are there any differences in the lipid-binding mode of C_2A and C_2B domains? Is the depth of insertion or the lipid binding ability of C_2A or C_2B affected from the presence of a consecutive C_2 domain? Does synaptotagmin 1 form oligomeric structures on lipids or act as a monomer? And more importantly, is there a difference in the lipid binding properties of C_2A and C_2B or maybe a new Ca^{2+} -dependent activity of

synaptotagmin 1 which might explain the different effects of point mutations at homologous residues on C₂A and C₂B domains in vivo (Mackler *et al.*, 2002; Robinson *et al.*, 2002)? In the process of answering these questions, we have occasionally obtained results that are difficult to explain. However, the combination of all the data made perfect sense and unraveled a new action of synaptotagmin 1, which might be very important for understanding how membranes fuse.

We found that synaptotagmin 1 does not oligomerize upon Ca²⁺-dependent binding to phospholipid vesicles but, intriguingly, binds to two membranes simultaneously and brings them into close proximity. Interestingly, we showed that the isolated C₂B domain is sufficient to induce close membrane proximity. Mutational analysis suggested that the abundance of basic residues around the C₂B surface, which generates a highly positive electrostatic potential together with the bound Ca²⁺ ions, is essential for this activity. We suggest that the ability of the C₂B domain to bring membranes into close proximity can explain why the C₂B domain has a more critical function in vivo than the C₂A domain.

4.3 Results

4.3.1 C₂A and C₂B domains act independently of each other

4.3.1.1 NMR spectroscopy

The relative orientation of the two C₂ domains with respect to each other could dictate how they cooperate in phospholipid binding. The intramolecular interaction of the C₂A and C₂B domains has been under debate. Although there is a seven residue flexible

linker between the domains, which enable them to move independent of each other, a Ca^{2+} -dependent intramolecular interaction of the C₂A and C₂B domains has been reported in a FRET based study (Garcia *et al.*, 2000). However, it is most likely that this observation arose from misfolding of the proteins caused by the attachment of a fluorescent label to a partially buried cysteine residue.

In our lab, NMR experiments, performed by Josep Ubach, showed that there is no interaction between the C₂A and C₂B domains in the presence or absence of Ca^{2+} . ^1H , ^{15}N -HSQC spectra of the C₂A, C₂B and C₂AB domains were acquired in the absence and presence of Ca^{2+} . The HSQC spectrum of the C₂A domain overlaid with the HSQC spectrum of C₂AB in the absence of Ca^{2+} is shown in Figure 4.2A. The HSQC peaks of the C₂A domain overlap with the C₂AB peaks showing that the isolated C₂A domain has the same conformation as the C₂A within C₂AB. The absence of any shift in the HSQC peaks is a clear indication that there is no interaction of the C₂A domain with the rest of the protein. The same conclusion is reached when the HSQC spectrum of the C₂B domain is overlaid with the HSQC spectrum of the C₂AB domain (Figure 4.2B). The peaks of the C₂B domain overlap with the C₂AB peaks showing that there is no interaction of the C₂B domain with the rest of the protein. Overlay of the HSQC spectra of the C₂A, C₂B and C₂AB domains verifies this conclusion (Figure 4.2C). When the same series of experiments were repeated in the presence of Ca^{2+} (Figure 4.2D-F), similar results were obtained, showing that the C₂A and C₂B domains do not interact with each other in the presence of Ca^{2+} .

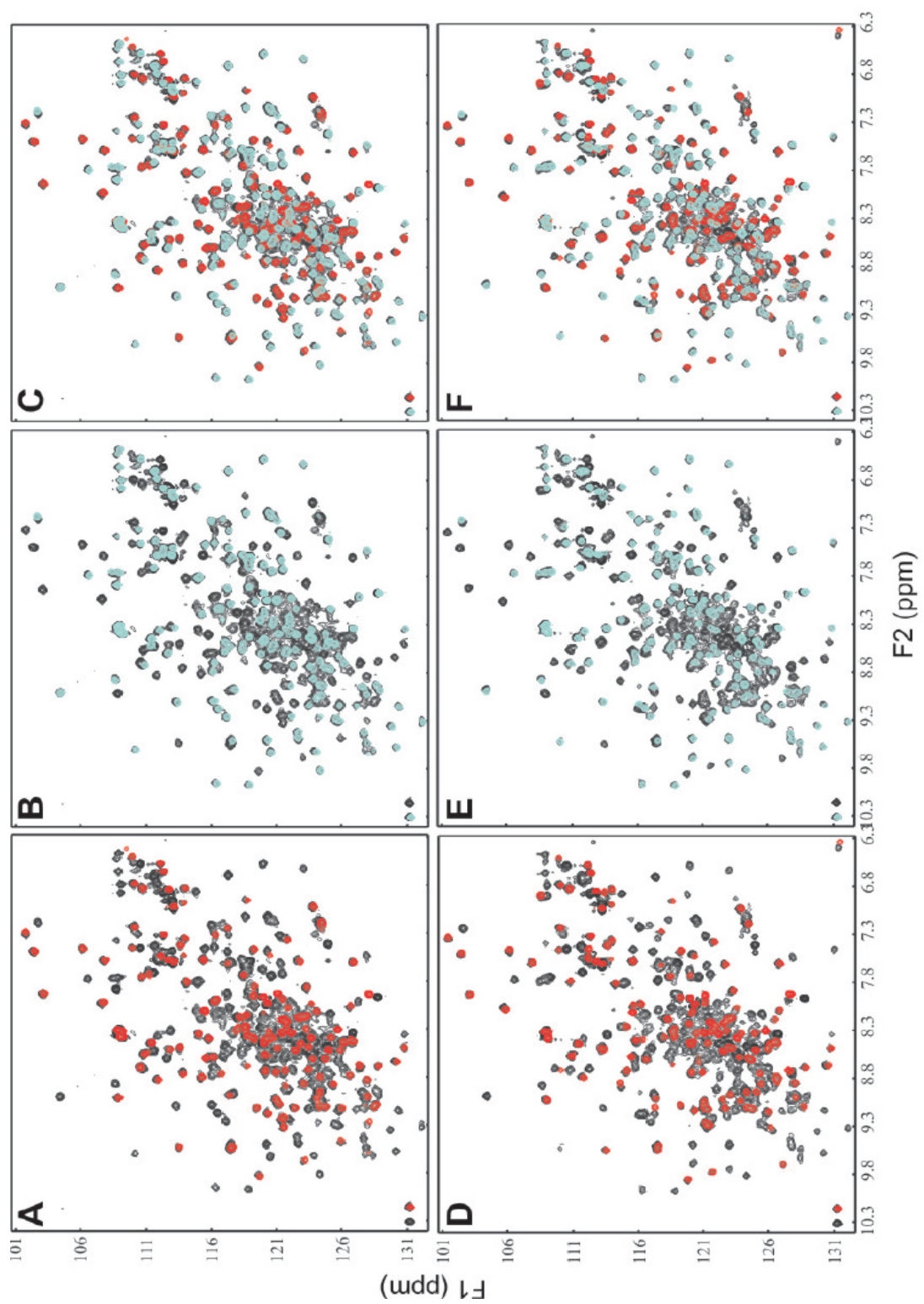


Figure 4.2 The synaptotagmin 1 C₂ domains are flexibly linked

Contour plots of ^1H - ^{15}N HSQC spectra of the C₂AB domain (black) in the absence (A-C) or presence (D-F) of 20 mM Ca^{2+} are shown. The spectra of C₂AB are superimposed with ^1H - ^{15}N HSQC spectra of the isolated C₂A domain (red) (A,D), the isolated C₂B domain (cyan) (B,E) or both (C,F).

4.3.1.2 Insertion of Ca^{2+} -binding loops into the membranes

The interaction of the C₂B domain with negatively charged membranes has been under investigation for a long time. EPR studies to determine the membrane-bound orientation of the C₂A and C₂B domains suggested that the C₂A and C₂B domains bind and insert into membranes in a similar way via their Ca^{2+} -binding loops (Frazier *et al.*, 2003; Rufener *et al.*, 2005). On the other hand, fluorescence experiments suggested that the C₂A domain activates a cryptic membrane penetration activity on the C₂B domain so that C₂B inserts into membranes only in the presence of a nearby C₂A domain (Bai *et al.*, 2002) and isolated C₂B does not penetrate membranes. Thrombin cleavage of C₂A from the C₂B domain after protein synthesis abolished the ability of the C₂B domain to penetrate lipids. These results proposed that the C₂A domain is helping the C₂B domain in a way that leads to the insertion of the Ca^{2+} -binding loops of C₂B into membranes. Such a communication between the two C₂ domains of synaptotagmin 1 was very surprising for us because our NMR experiments clearly show no interaction between C₂A and C₂B in the absence or presence of Ca^{2+} . The C₂B domain used in the experiments was treated with thrombin to cleave it from C₂AB. This protocol might cause C₂B to lose its lipid binding activity and lead to the observation of such results. We decided to investigate the validity of this hypothesis using the individually expressed C₂B domain. We used fluorescence spectroscopy to look at the depth of insertion of C₂B domain into the membranes and compared the insertion of the isolated C₂B domain with the insertion of the C₂B within C₂AB.

We made single cysteine mutations on the Ca^{2+} -binding loops 1 and 3 of the C₂A and C₂B domains. M173 (loop 1) and F234 (loop3) were mutated on both the isolated C₂A and C₂AB domains. The homologous residues, V304 (loop 1) and I367 (loop 3),

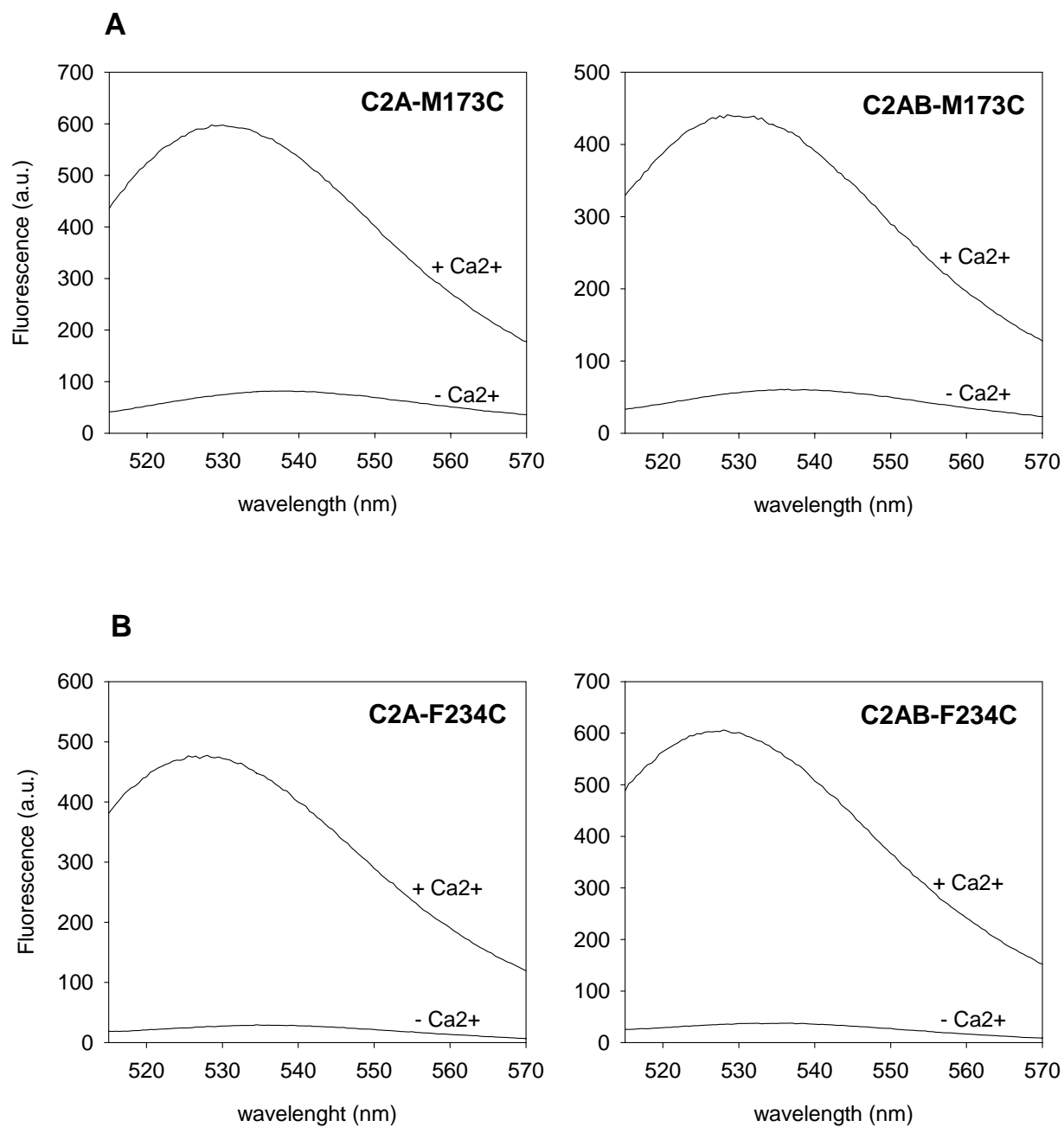
Domain	Mutation	Location	Fold increase
C2A	M173C	Loop 1	8.9
C2AB	M173C	Loop 1	8.6
C2A	F234C	Loop 3	19.1
C2AB	F234C	Loop 3	18.0
C2B	V294C	Loop 1	10.7
C2AB	V304C	Loop 1	10.9
C2B	I367C	Loop 3	6.6
C2AB	I367C	Loop 3	4.9

Table 4.1 List of single cysteine mutations on the C₂A, C₂B and C₂AB domains

The single cysteine mutations on the single and double C₂ domains are listed. The location of the mutated residue is indicated. Mutants were labeled with NBD and fluorescence emission was monitored when bound and unbound to lipids. The fold increases in the NBD signal of each mutant are listed as an indication of relative degree of insertion into the lipids.

were mutated on both the isolated C₂B and C₂AB domains (Table 1). These hydrophobic residues on the tip of the Ca²⁺-binding loops are known to insert into the membrane bilayer. The single cysteine mutants were labeled with NBD, a fluorescent dye that has enhanced fluorescence signal in hydrophobic environments. (Please, see section 4.3.2 for detailed explanation of fluorescence experiments.) The NBD fluorescence emission of the free protein was monitored and compared with the signal of the membrane-bound protein. The change in the hydrophobicity of the NBD environment upon membrane penetration causes an increase in the NBD signal indicating the degree of insertion depth. We compared the depth of insertion of the same residue within the single C₂ domains and within the C₂AB domain. If penetration of the C₂B domain does not depend on the presence of an adjacent C₂A domain, we expect to see similar degrees of increase in the NBD signal of C₂B and C₂AB. However, if the penetration of C₂B depends on the presence of an adjacent C₂A domain, the increase in the NBD signal of C₂B should be much less than that of C₂AB.

Figure 4.3 shows the signal of the NBD-labeled proteins in the presence of lipids with and without Ca²⁺. In the absence of Ca²⁺, the proteins are not bound to membranes so have a low NBD signal. Upon addition of Ca²⁺, proteins bind to lipids and the Ca²⁺-binding loops interact with lipids to yield higher NBD signal. The relative degree of insertion was determined from the fold increase in NBD fluorescence by dividing the NBD signal of the lipid-bound protein at 525 nm by the NBD signal of the isolated protein at 525 nm. The fold increase for each protein is listed in Table 1. Figure 4.3A compares the increase in NBD signal of M173C-C₂A with that of M173C-C₂AB. The fold increase in NBD signal is similar whether C₂A or C₂AB is used, showing that the



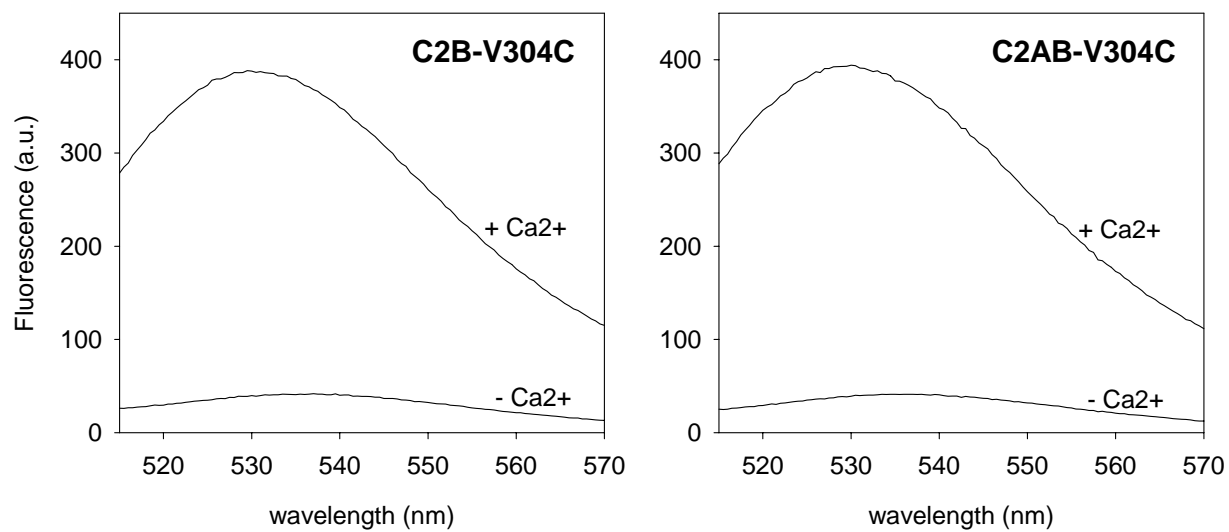
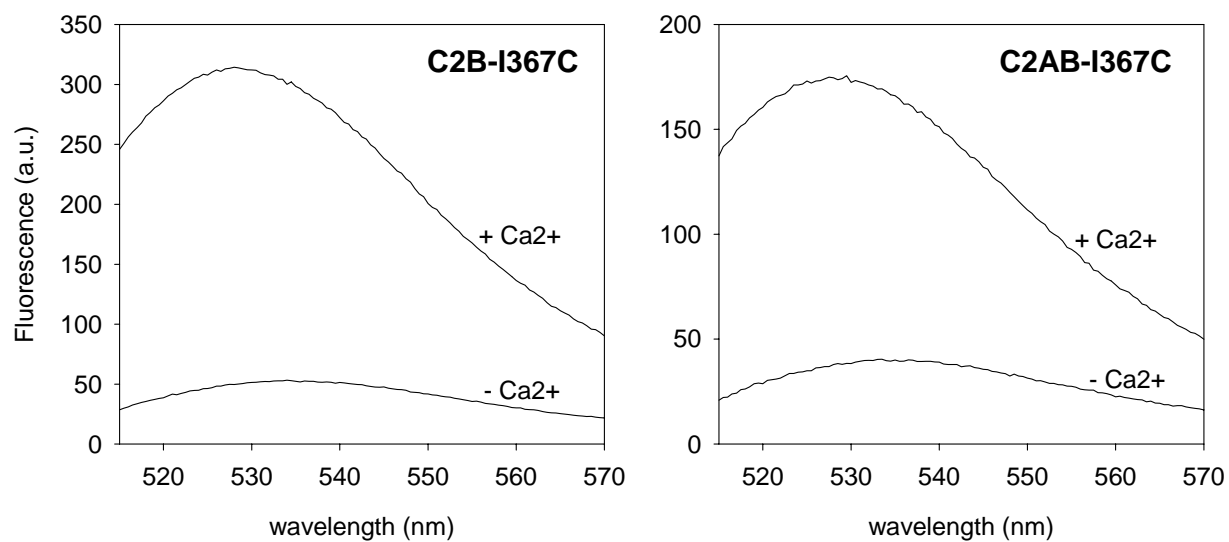
C**D**

Figure 4.3 Relative membrane insertions of the Ca^{2+} binding loops of the C_2A , C_2B and C_2AB domains

The fluorescence spectra of the NBD labeled proteins in the presence of lipids with and without Ca^{2+} are shown. The increases in the NBD fluorescence are compared when NBD is attached to the same residue in the single or double C_2 domains: (a) M173C- C_2A vs. M173C- C_2AB , (b) F234C- C_2A vs. F234C- C_2AB , (c) V304C- C_2B vs. V304C- C_2AB , (d) I367C- C_2B vs. I367C- C_2AB . The fold increases in the NBD signal upon addition of Ca^{2+} (listed in Table 1) is used to determine the relative degree of insertion. No significant difference was observed in the relative degree of insertion when NBD was attached to the single or double C_2 domains. NBD was excited with 485 nm wavelength light. The NBD fluorescence was monitored from 515 nm to 570 nm. 0.1 μM protein was mixed with 0.1mg/ml lipid vesicles in the presence of 1 mM Ca^{2+} or 1 mM EDTA. Background signal was subtracted from each spectrum.

isolated C₂A domain inserts into membranes as deeply as when a C₂B is present nearby. The same result is observed when NBD is placed on F234C in loop 3 of C₂A (Figure 4.3B). These results are in agreement with the already existing consensus in the literature that isolated C₂A inserts deeply into membranes. We repeated the same experiments by labeling the homologous residues on the Ca²⁺-binding loops of C₂B. Figure 4.3C compares the increase in the NBD signal of V304-C₂B with that of V304-C₂AB. Similar increases in the NBD signal are observed whether C₂B or C₂AB is used. When NBD is placed on I367C in loop 3 of C₂B, the same result is observed (Figure 4.3D). The fact that the fold increase in the NBD signal is similar when NBD is attached to the isolated C₂B or C₂AB domain strongly suggests that the isolated C₂B domain inserts into the lipid membranes as deeply as when an adjacent C₂A is present nearby within the C₂AB domain. We conclude that the isolated C₂B can penetrate into membrane bilayers without help from C₂A, and that the presence of C₂A does not contribute to the insertion of C₂B into lipids. These results strengthen the idea that C₂A and C₂B domains do not interact with each other and act independently even if they share a common activity such as lipid binding.

4.3.2 Lipid binding mode of synaptotagmin 1 suggests multiple sites of the C₂B domain is involved in lipid binding

Both C₂ domains of synaptotagmin 1 interact with negatively charged phospholipid membranes via their Ca²⁺-binding loops upon binding to Ca²⁺ (Davletov *et al.*, 1993; Sutton *et al.*, 1995a; Zhang *et al.*, 1998; Chapman *et al.*, 1998a). The hydrophobic residues at the tip of the loops insert into the membrane bilayer (Section

4.3.1). However, whether the C₂ domains lie parallel or perpendicular to the membrane is not known. It is possible that some side residues on the surface of the C₂ domains might be involved in the interaction of synaptotagmin 1 with membranes. An EPR study suggests that the C₂A domain of synaptotagmin 1 binds to membranes at an angle and some residues at the side of the beta sandwich come into close contact with membranes (Frazier *et al.*, 2003).

As recent studies have shown that the C₂B domain is more essential than the C₂A domain, we have done our studies with the C₂B domain but within the context of C₂AB (Mackler *et al.*, 2002; Robinson *et al.*, 2002). To determine the lipid-binding mode of synaptotagmin 1, we have made use of fluorescent probes, which we placed on the surface of the C₂B domain to look for their involvement in lipid binding. Making single cysteine mutations on the surface residues of a protein of interest and labeling the cysteines with a fluorescent dye is a method commonly used for different purposes. The fluorescent dye can then be used as a probe to monitor the binding of the protein to other molecules (FRET), to measure the accessibility of the corresponding residue to solvent (quenching) or to detect the change in the immediate surroundings of the probe (change in fluorescence signal).

We made cysteine mutations to replace the exposed residues at different positions on the surface of the C₂B domain in the context of C₂AB. The only native cysteine residue (C277) in the C₂AB domain was mutated to serine to produce mutants with a single cysteine. The ¹H, ¹⁵N HSQC spectrum of the ¹⁵N-labeled C₂AB-C277S mutant was acquired to check whether the mutation causes any problems in the folding of the protein (Figure 4.4). The HSQC spectrum is very similar to the HSQC spectrum of the wild type

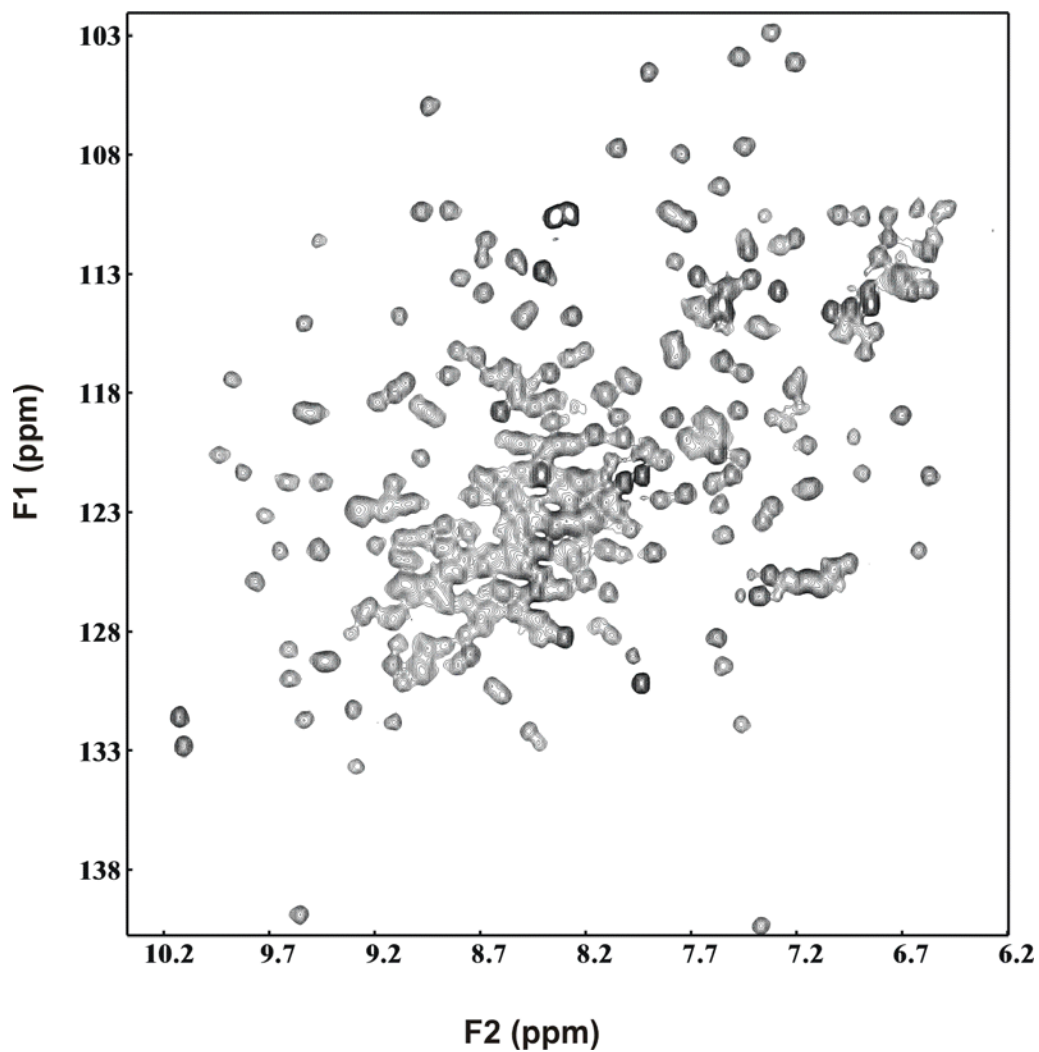


Figure 4.4 HSQC spectrum of ^{15}N -C277S-C₂AB

The HSQC spectrum of ^{15}N -C277S- C₂AB is shown. The spectrum is very similar to the HSQC spectrum of the wild type C₂AB domain and indicates that the mutation does not cause any folding problems.

C₂AB domain meaning that the mutant protein is folded and there are no conformational differences. The cysteine mutations were introduced onto the C₂AB-C277S DNA.

The single cysteine mutants were designed with the help of the 3D NMR structure of the C₂B domain and were chosen all over the surface of the C₂B domain. When possible, residues with low conservation were mutated to decrease the chance that the mutation will affect the folding and/or the function of the protein. Table 4.2 lists the single cysteine mutations on the C₂AB domain and Figure 4.5 shows the location of the residues that have been mutated to cysteine on the surface of the C₂B domain. The mutated residues are: 1) Two hydrophobic residues in loops 1 and 3 (V304 and I367), which are expected to deeply insert into membranes. 2) N333 in loop 2, which might have close proximity to membranes. 3) The C-terminal residue away from the lipid-binding region (V419). 4) Two lysine residues in the polybasic region (K326 and K327). 5) Two residues on the opposite face of the lipid-binding region (R398 and N396).

The single-cysteine mutants were expressed and purified in the same way as the wild type protein. UV light absorbance of purified proteins was measured to ensure that they are free of bacterial contaminants that absorb at 260 nm to avoid any false results. The NBD fluorescent probe was attached to the cysteine residues in a reaction shown in Figure 4.6. The reaction was done in a buffer at pH 7.5 that is optimum for such a reaction and no reducing agents such as BME or DTT were used to avoid the inhibition of the reaction.

NBD is a fluorescent dye with a high extinction coefficient ($24200 \text{ cm}^{-1}\text{M}^{-1}$) making it easy to monitor. It absorbs light at 478 nm and emits at 544 nm. The fluorescence lifetime of NBD, like most other fluorescent molecules, is sensitive to the

Mutation	Location	Fold increase
V304C	Loop 1	10.9
I367C	Loop 3	4.9
N333C	Loop 2	2.0
V419C	C-terminal	1.1
K326C	Polybasic region	1.6
K327C	Polybasic region	2.0
N396C	Opposite face of lipid binding region	1.6
R398C	Opposite face of lipid binding region	1.7

Table 4.2 List of C₂B surface residue mutations within the C₂AB domain

The single cysteine mutations on the surface of the C₂B domain within the C₂AB domain are listed. All mutants have the background C277S mutation. The mutants were labeled with NBD and fluorescence emission was monitored when bound and unbound to lipids. The fold increases in the NBD signal of each mutant are listed as an indication of the relative change of hydrophobicity in the immediate surrounding of the labeled residue.

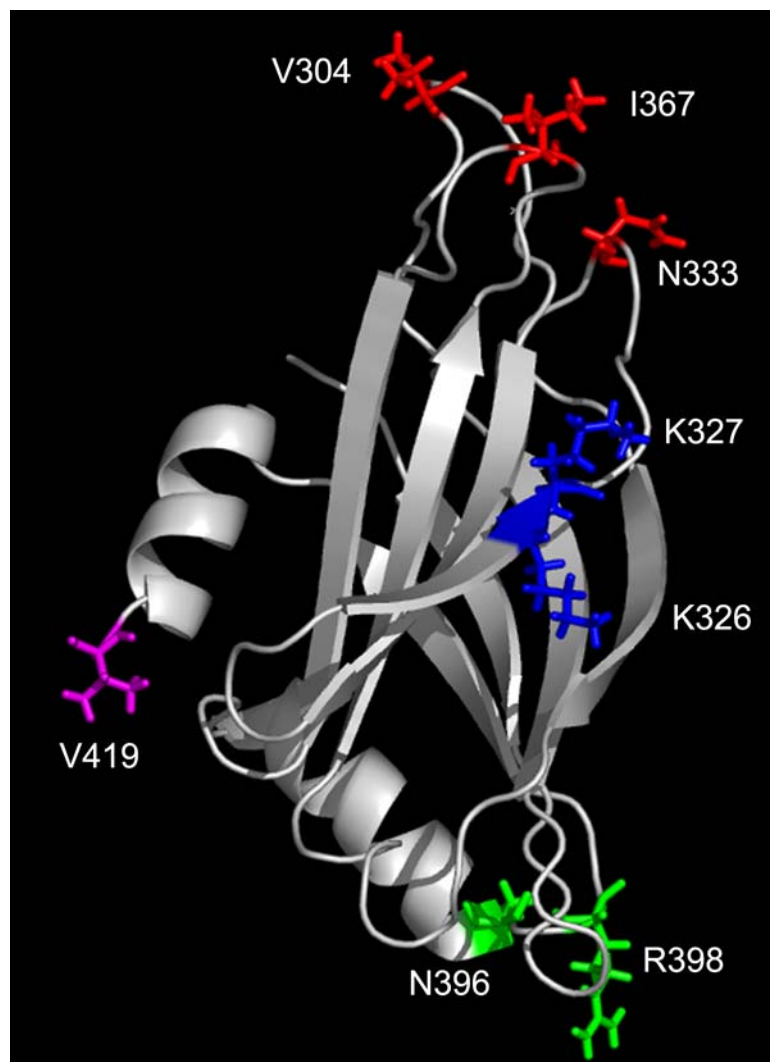


Figure 4.5 The positions of the cysteine mutations on the surface of the C₂B domain
 The locations of the C₂B surface residues that were mutated to cysteine are indicated. Residues were chosen to span the full surface of the C₂B domain in order to make a full analysis of the lipid binding mode. The Ca²⁺-binding loop mutations (V304, I367, N333) are colored in red, the polybasic region mutations (K326, K327) are colored in blue, C-terminal mutation (V419) is colored in magenta and the mutations on the opposite face of the Ca²⁺ binding loops (N396, R398) are colored in green.

A



Alkyl halide or
Haloacetamide
(X=I,Br,Cl)

Thioether

B

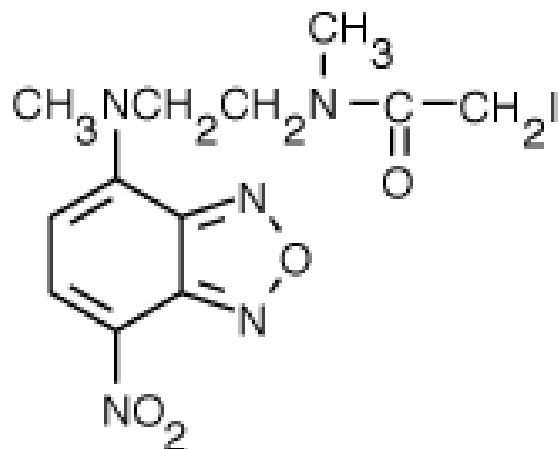
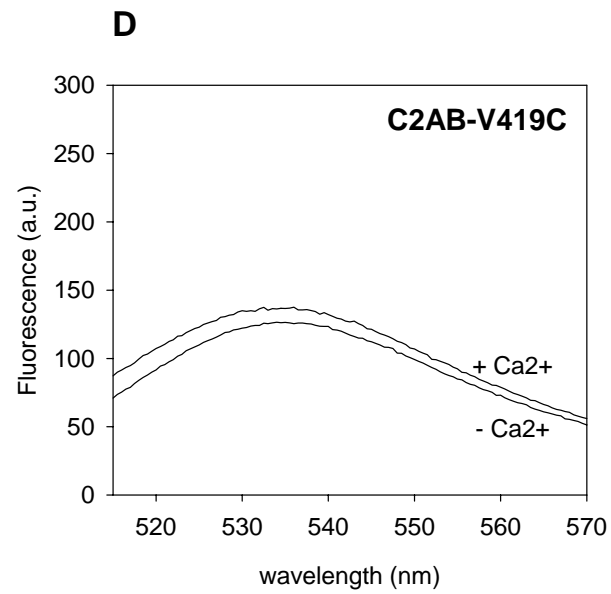
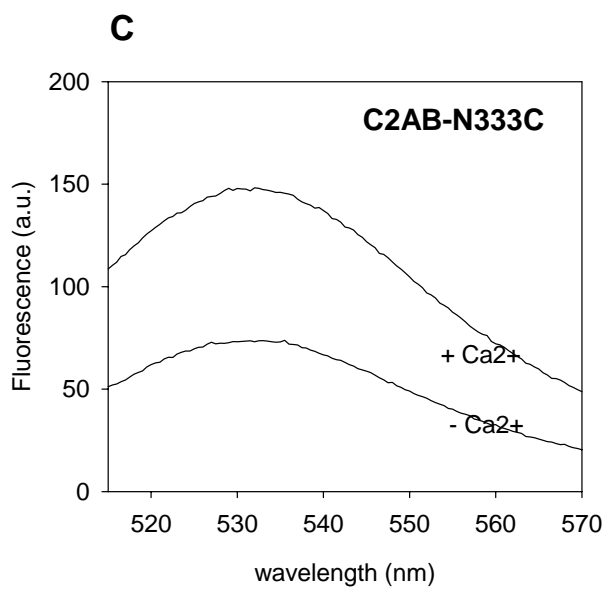
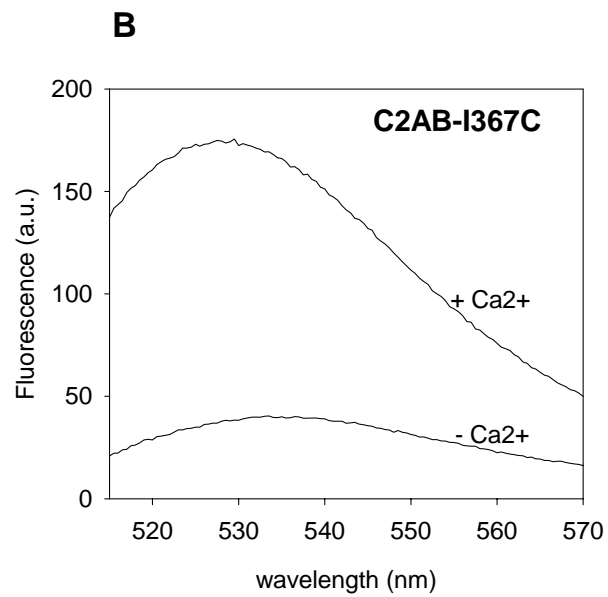
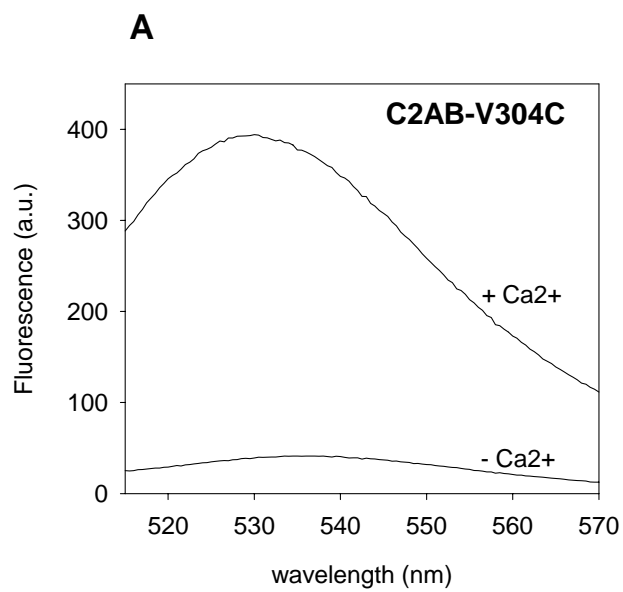


Figure 4.6 Reaction of a thiol with an alkyl halide

The general reaction of a thiol group with an alkyl halide is shown (A). Haloalkyl reagents, primarily iodoacetamides are among the most frequently used reagents for thiol modification. *N,N'*-dimethyl-*N*-(iodoacetyl)-*N'*-(7-nitrobenz-2-oxa-1,3-diazol-4-yl)ethylenediamine (NBD) is an iodoacetamide and can be attached to cysteine residues of proteins. Its structure is shown (B).

hydrophobicity of its environment. The fluorescence intensity of NBD is increased by the increasing hydrophobicity of its immediate surroundings. Thus, the signal is enhanced when NBD is involved in membrane binding or protein-protein interactions etc., whereas much lower signal will be detected when it is exposed to hydrophilic solutions.

We monitored the increase in the fluorescence intensity of the NBD probe on the single cysteine mutants upon binding of the C₂AB domain to the membranes. Figure 4.7 shows the fluorescence spectra of the C₂AB mutants mixed with phospholipid vesicles in the presence of 1 mM EDTA or 1 mM Ca²⁺. Our results are as follows: 1) The increase in the NBD signal was very large when the NBD label was attached to the residues on the Ca²⁺ binding loops 1 and 3 of C₂AB (V304C and I367C mutants), showing that these residues deeply insert into membranes as expected (A,B). 2) Moderate increase in the NBD signal was observed for the loop 2 mutant (N333C) suggesting that it is in close contact with lipids but does not insert into the lipid bilayer (C). 3) No significant increase in the NBD fluorescence signal was detected when NBD was attached to the C-terminal residue V419C showing that it does not interact with the membranes upon binding (D). 4) The polybasic region mutants (K326C and K327C) displayed an increase in the NBD signal almost as much as the loop 2 mutant N333C (E,F). The increase in the K326C mutant is slightly less than the increase in the K327C mutant as K326 is facing the inner core of the beta sheet while K327 is facing outside and is more involved in a possible intermolecular interaction. 5) The N396C and R398C mutants located on the opposite face of the lipid binding region also show a moderate increase in NBD signal upon binding to lipids (G,H). The fold increases in the NBD signal upon addition of Ca²⁺



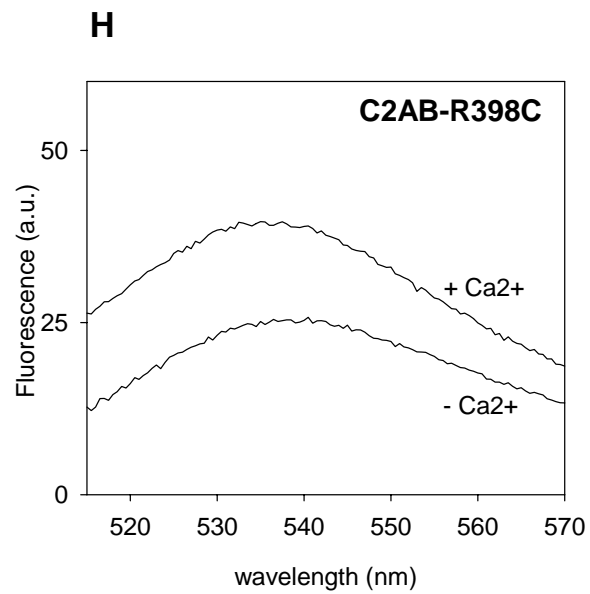
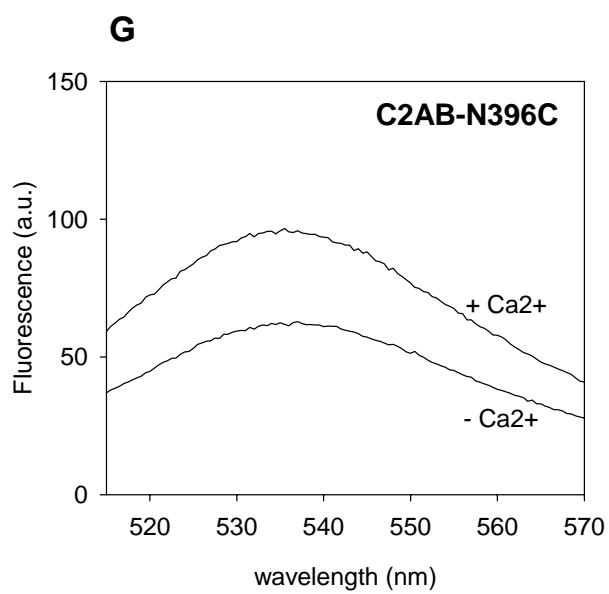
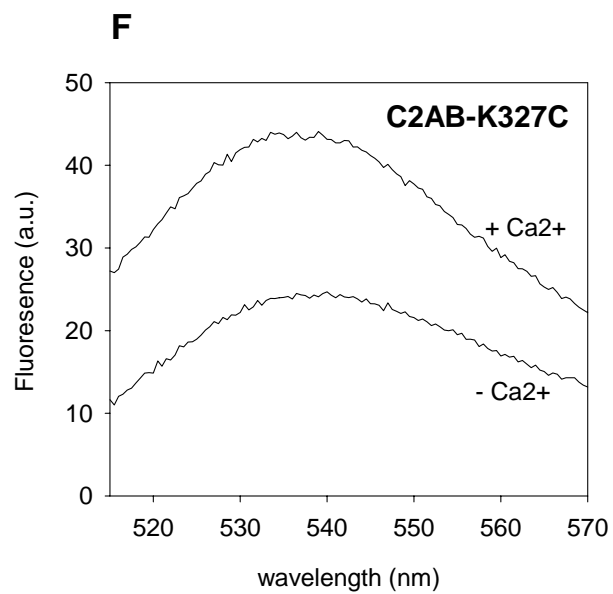
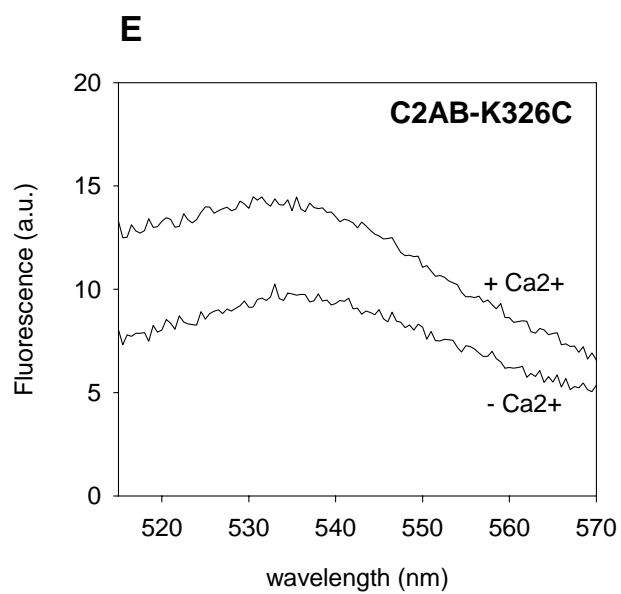


Figure 4.7 Relative NBD fluorescence increases of the C₂B surface mutants within the C₂AB domain

The fluorescence spectra of the NBD labeled proteins in the presence of lipids with and without Ca²⁺ are shown. The fold increase in the NBD signal upon addition of Ca²⁺ (listed in Table 2) is used to determine the relative change of hydrophobicity in the immediate surrounding of the labeled residue. The Ca²⁺ binding loop residues V304 (A), I367 (B) and N333 (C) have an enhanced NBD signal upon binding to lipids, whereas the negative control C-terminal residue V419 (D) has no increase in the NBD signal. Other residues around the C₂B surface (K326, K327, N396 and R398) have intermediate increases (E,F,G,H). NBD was excited with 485 nm wavelength light. The NBD fluorescence was monitored from 515 nm to 570 nm. 0.1 μM protein was mixed with 0.1 mg/ml lipid vesicles in the presence of 1 mM Ca²⁺ or 1 mM EDTA. Background signal was subtracted from each spectrum.

(listed in Table 2) are used to determine the relative change of hydrophobicity in the immediate surrounding of the labeled residue.

The results obtained from V304C, I367C, N333C and V419C mutants were expected and in agreement with the previous ideas that loops 1 and 3 deeply insert into membranes and loop 2 mediates close contacts with membranes, whereas residues away from the lipid binding site are not involved in an interaction. However, the results obtained from K326C, K327C, N396C and R398C mutants were surprising for us because we observed clear increase in the NBD signals of these mutants in spite of the fact that these residues are located away from the lipid binding region. Such a result suggests that, in the presence of Ca^{2+} , the C_2B domain of synaptotagmin 1 not only binds to lipids via the Ca^{2+} -binding loops but also is involved in another interaction, which will cause an increase in the NBD fluorescence when NBD is located at the polybasic region or the opposite face of the Ca^{2+} -binding loops. One of the following interactions may cause this effect: 1) Interaction with lipids 2) Interaction with another protein molecule. It is possible that the C_2B domain interacts with lipid membranes not only via the Ca^{2+} binding loops but also via the positively charged residues in the polybasic region and/or on the opposite face of the Ca^{2+} -binding loops. This will mean that the surface of the C_2B domain has multiple regions that can interact with lipids and can bind to more than one lipid vesicle at a time. It is noticeable that the NBD signal fold increases of the loop 2 mutant N333C (N333 does not insert into the membranes but closely interacts with the lipids) and the polybasic region mutant K327C are equal (Table 4.2). This observation might mean that K327 is interacting with lipids as closeby as N333 does. Alternatively, it is possible that, although the C_2B domain is monomeric in solution, it forms multimers

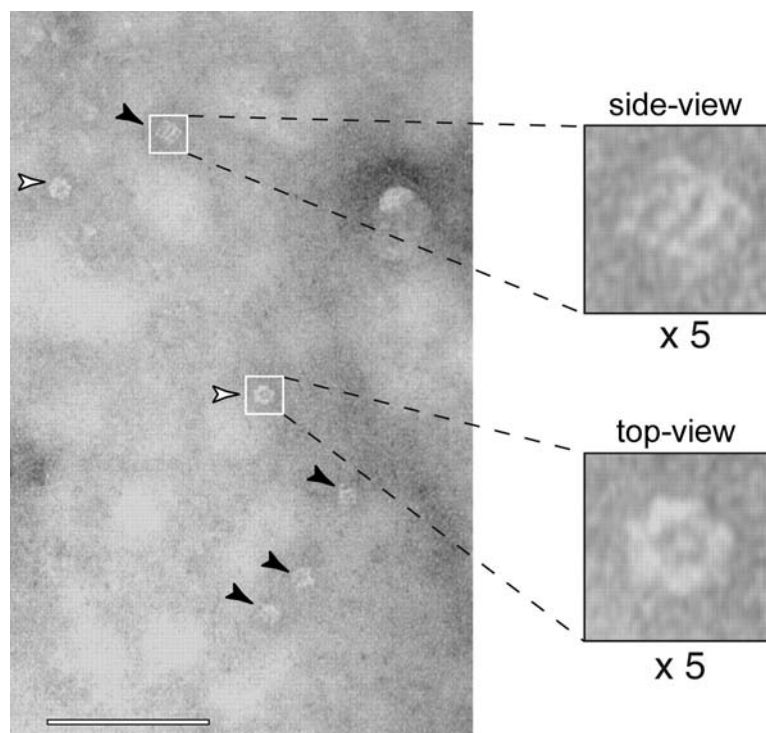
upon binding to lipids. Two C₂ domains may interact with each other via their polybasic regions and/or the opposite face of the Ca²⁺-binding loops and this interaction may enhance the NBD fluorescence.

We decided that to understand the mechanism of synaptotagmin 1 action on the lipid membranes, we need to distinguish between the two possibilities and learn whether the C₂B domain interacts with membranes via multiple regions or if it actually multimerizes upon binding to lipids. As a first set of experiments, we used different methods to look for the oligomerization of synaptotagmin 1 on the lipids. We, then, questioned whether the synaptotagmin 1 C₂B domain could bind to lipids at more than one region.

4.3.3 Synaptotagmin 1 is monomeric in solution and on membranes

Synaptotagmin 1 has been suggested to form oligomers via its C₂B domain (Chapman *et al.*, 1998b; Desai *et al.*, 2000). NMR studies in our lab have shown that well folded and purified synaptotagmin 1 is monomeric even at millimolar concentrations in solution (Ubach *et al.*, 2001). However, recent negative staining electron microscopy studies propose that although synaptotagmin 1 is monomeric in solution, it oligomerizes upon binding to negatively charged lipid monolayers in the presence of Ca²⁺ (Wu *et al.*, 2003). Low resolution single molecule reconstruction analysis of Ca²⁺ bound C₂AB on lipid monolayers revealed the formation of ring-like heptameric oligomers that are 11 nm long and 11 nm in diameter and the polybasic region of the C₂B domain was reported to be essential for this function (Figure 4.8). Oligomerization of synaptotagmin 1 suggests a very attractive model where seven synaptotagmin 1 molecules can maximize the

A



B

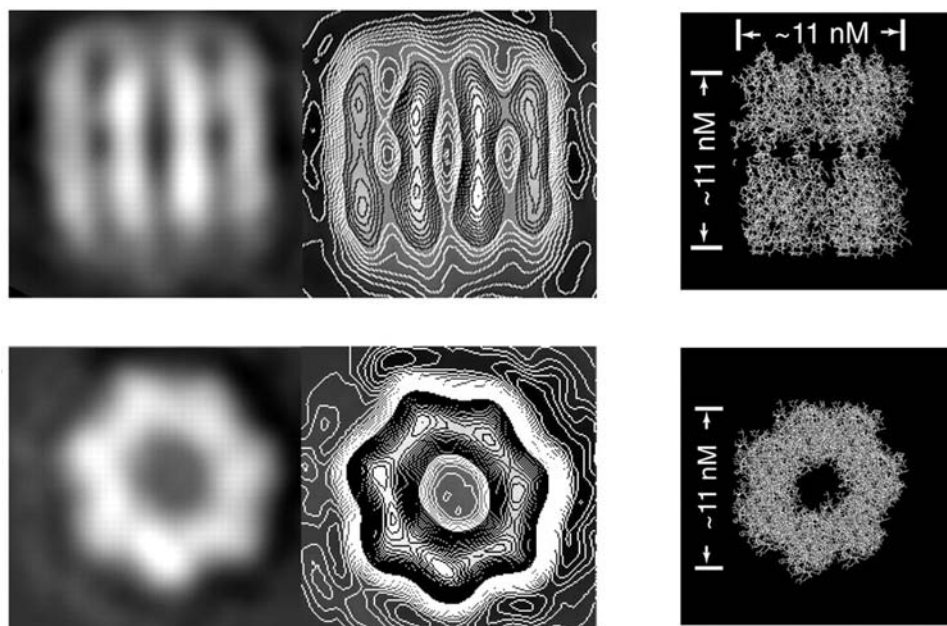


Figure 4.8 Ca^{2+} -dependent oligomerization of Synaptotagmin 1 C_2AB domain on the lipid membranes observed by negative staining EM

(A) The oligomeric structures of synaptotagmin 1 formed upon binding to lipid monolayers are shown. The oligomers can be observed in two binding modes from the side and top-views. The oligomers from the side-view are marked with filled arrowheads; the oligomers from the top-view are marked with open arrowheads. 0.1 mg/ml C_2AB domain was bound to lipid monolayers (25% PS/ 75% PC) in the presence of 50 μM to 1 mM Ca^{2+} . 1% (wt/vol) uranyl acetate was used for negative staining. (Scale bar=100 nm)

(B) Average maps of synaptotagmin 1 oligomers after single molecule reconstruction from the side and top views are shown with and without contouring (left). A single bar observed in the side views probably corresponds to a C_2AB molecule. The molecular model in which the crystal structure of C_2AB from synaptotagmin 3 (Sutton *et al.*, 1999) has been packed into a heptameric oligomer is shown from the side and top-views (right). The model was made by aligning the tandem C_2 domains along their long axis by changing the flexible linker that connects them. (Wu *et al.*, 2003)

intruding power of synaptotagmin 1 on the membranes upon Ca^{2+} binding and cause an energetic instability of the lipid membranes that may help in the fusion event. It also explains why the C₂B domain is more important than the C₂A domain for release. However, the observed EM images have some problems: 1) The ring-like oligomers are observed in both side-view and top-view suggesting two modes of binding. 2) The molecular model obtained from the crystal structure of C₂AB places the Ca^{2+} -binding loops of both C₂ domains inside the oligomer making the loops inaccessible to phospholipids. It is hard to imagine how binding to lipids can cause oligomerization if the lipid-binding region is not accessible to lipids as predicted by this oligomeric model. 3) The heptameric model seems too small to fit into the average density maps obtained from EM images.

4.3.3.1 Negative Staining Electron Microscopy

We used negative staining electron microscopy as a first method to look for the possible multimerization of synaptotagmin 1 on lipid membranes. To verify the validity of the published EM results and to find a valid explanation for the observed images, we have repeated the electron microscopy experiments and observed similar images both in the presence of phospholipid monolayers and vesicles. The ring-like oligomeric structures formed when bound to lipid vesicles are shown in Figure 4.9. Single molecule reconstitution of oligomeric structures showed that the C₂AB molecules were organized as a ring-like heptamer in agreement with the previously observed images (Wu *et al.*, 2003). In our images, the ring-like heptamers could be viewed not only in two forms but at all different angles (Figure 4.10). However, the ring-like structures did not overlap with the vesicles (Figure 4.9). Actually, we could hardly observe any vesicles, which led

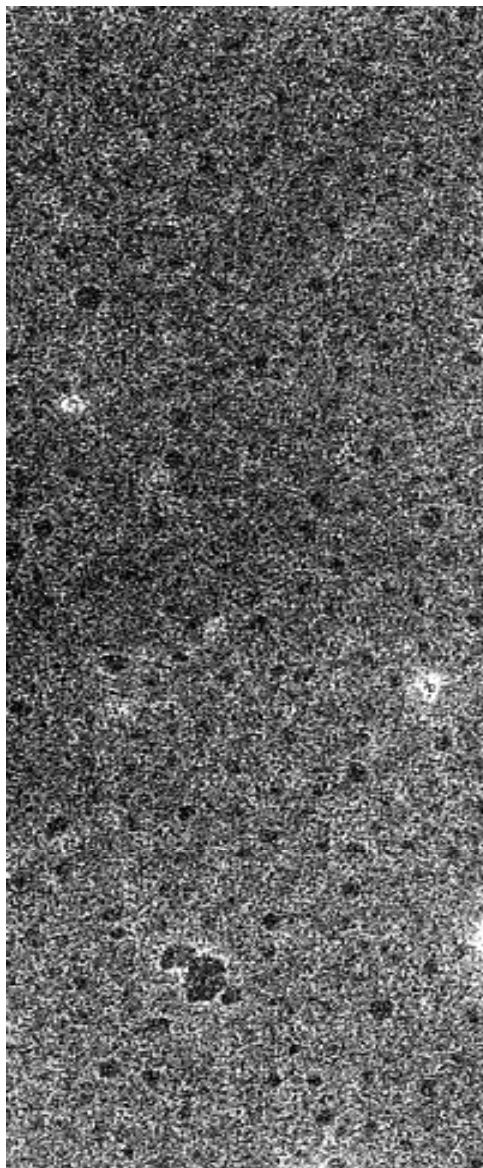


Figure 4.9 Negative staining electron microscopy images of synaptotagmin 1 bound to lipid vesicles.

The formation of ring-like oligomeric structures of synaptotagmin 1 C₂AB domain when bound to lipid vesicles is reproduced. The oligomeric structures do not overlap with the lipid vesicles. The images are reproducible but finding the oligomeric structures on the grid is very difficult. The previously published conditions were used for sample preparation (Wu *et al.*, 2003). 2 μ M C₂AB was mixed with 0.1 mg/ml lipid vesicles in the presence of 1 mM Ca²⁺. 1% (wt/vol) uranyl acetate was used for negative staining. Similar structures were observed when lipid monolayers were used instead of lipid vesicles.

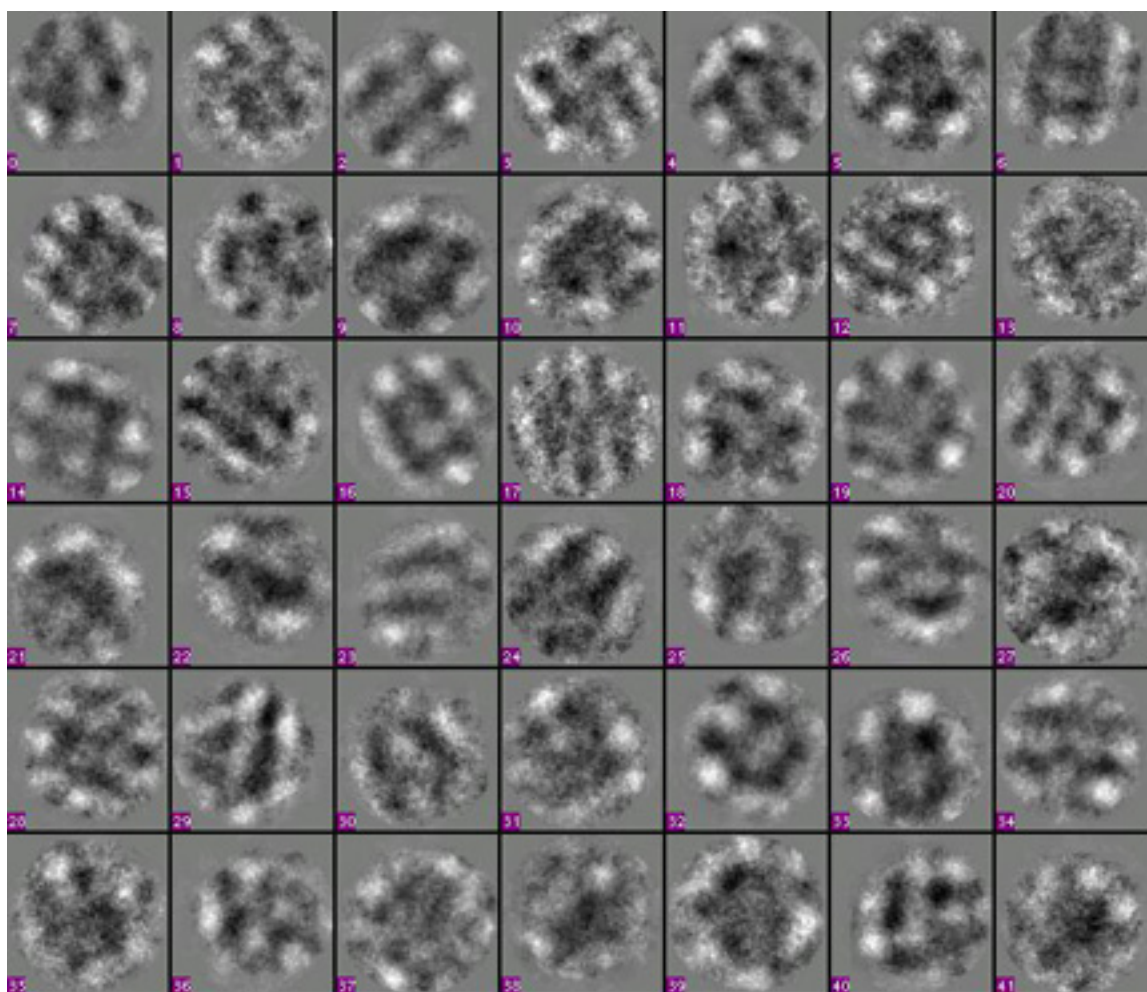


Figure 4.10 Single molecule reconstruction of synaptotagmin 1 oligomers

The two dimensional class averages of synaptotagmin 1 oligomers are shown. The single oligomeric structures were boxed out from the image and iteratively aligned. The aligned images were then classified to produce 42 class averages using the EMAN software. Heptameric ring-like structures are observed at all angles rather than only two. The group averages representing the images from the top-view reveal that the observed oligomeric structures are actually heptamers in agreement with the published structures.

us to think that vesicles might burst during negative staining. In other preparations, distorted vesicles with long, elongated, deformed arms of lipids were observed rather than round bilayers (Figure 4.11). These results suggested that harsh negative staining conditions might be breaking the lipid vesicles and forming non-native images.

The other problem was that, although the heptameric images were reproducible, it was very difficult to find them on the EM grid. For example, out of 20 photographs that were taken, only 1 would have the heptameric images. (Heptameric structures can only be seen after taking photos of the grid at random places and developing the films.) In addition, the heptamers look very similar to the published images of GroEL both from the side and top-views. Considering that GroEL is a commonly found contaminant in protein preparations expressed in bacteria, we suspected that our heptameric images are in fact GroEL and this might be the reason why finding the heptamers on the EM grid was difficult.

To compare the images of GroEL and synaptotagmin 1, we prepared GroEL samples and imaged them under identical conditions. As opposed to synaptotagmin 1 samples, working with GroEL and imaging them was much easier. The single molecule reconstruction of GroEL images was similar but not identical to that of the synaptotagmin 1 images (Figure 4.12). The slightly bigger size of GroEL images was the major difference. In addition, comparison of the number of particles per area in the synaptotagmin 1 and GroEL samples showed that heptameric structures were equally populated in both samples, which would not be observed if GroEL was the contaminant in the synaptotagmin 1 sample. We concluded that the heptameric images we observe in the synaptotagmin 1 samples were not GroEL.



Figure 4.11 Negative staining electron microscopy images of distorted lipid vesicles

The formation of distorted lipid vesicles is shown. Lipid vesicles with long, elongated arms were observed instead of the expected spherical vesicles. Such images of lipid vesicles were sometimes observed in negative staining EM preparations of synaptotagmin 1 C₂AB domain in the presence of lipid vesicles and Ca²⁺ when identical conditions as in Figure 4.8 were used. Negative staining and/or synaptotagmin 1 might cause deformation of vesicles and burst them out.

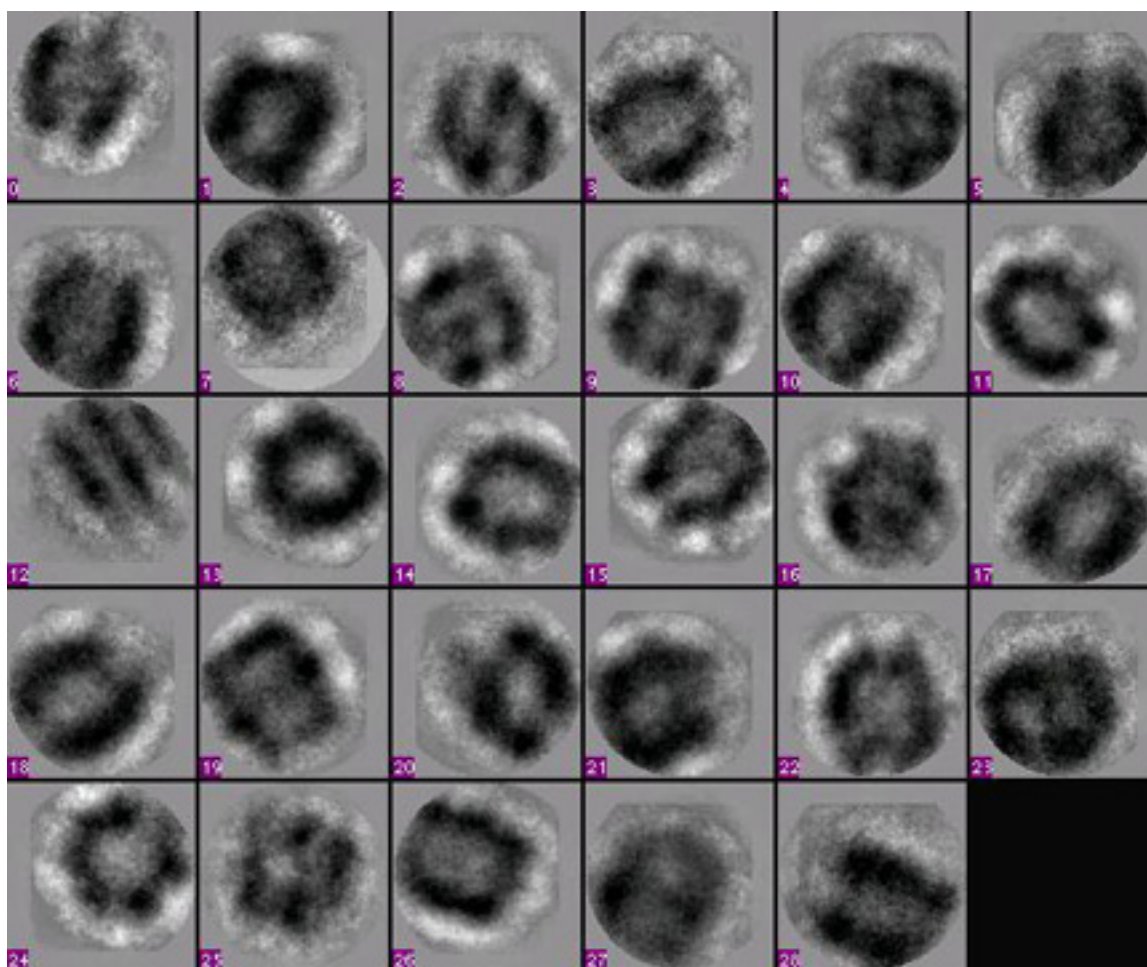


Figure 4.12 Negative staining EM images and single molecule reconstruction of GroEL

The two dimensional class averages of GroEL are shown. The single oligomeric structures were boxed out from the image and iteratively aligned. The aligned images were then classified to produce 29 class averages using the EMAN software. 3 μM GroEL was mixed with 0.1 mg/ml lipid vesicles and 1 mM Ca^{2+} . 1% (wt/vol) uranyl acetate was used for negative staining. The observed class averages look similar to synaptotagmin 1 but are not identical.

The negative staining technique used to prepare EM samples has both advantages and disadvantages: Negative staining is an easy and quick way to prepare samples. The staining dyes used to fix the sample provide good contrast to observe the particles although high resolution cannot be achieved. However, staining dyes, like uranyl acetate, produce harsh conditions for proteins and vesicles and cause formation of aggregates. Our negative staining EM experiments indicated an unusual difficulty in reproducing the heptameric images and showed that the lipid vesicles can be distorted and burst out. These results in combination with the fact that uranyl acetate may cause formation of aggregates led us to suspect that the heptameric structures in our samples might be an artifact caused by negative staining. For this reason, we felt the necessity of using different methods, which will not give us false results and will be easy enough to allow all the proper negative and positive controls, as well as many repetitions, to be performed.

4.3.3.2 Crosslinking experiments

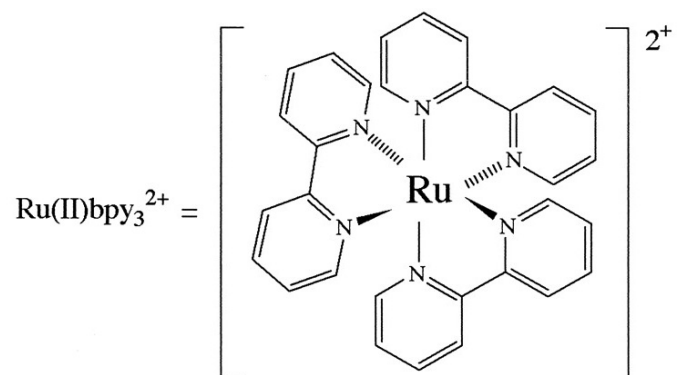
Crosslinking experiments were done to investigate the oligomerization of the synaptotagmin 1 C₂AB domain upon binding to negatively charged phospholipid membranes using different crosslinking reagents. The first set of experiments was done in the presence of glutaraldehyde, a commonly used, mild crosslinking reagent. The final glutaraldehyde concentration was varied between 0.0005% and 1%. No crosslinking of C₂AB was detected in solution or when bound to membranes even at higher glutaraldehyde concentrations. As a next step, we decided to use a strong crosslinking reagent not to miss any possible oligomerization, which might be too weak to be detected with a mild crosslinker.

Tris-bipyridylruthenium (II) is a powerful reagent that forms free radicals in ring structures upon excitation with light, and causes crosslinking especially between tyrosines (Figure 4.13A). The process involves the photolysis of tris-bipyridylruthenium(II) dication with visible light at 452 nm in the presence of the electron acceptor ammonium persulfate and the proteins of interest (Figure 4.13B). Very high efficiency of crosslinking can be obtained with irradiation times of <1 second (Fancy and Kodadek, 1999). Because of the strong reactivity, it is more likely that tris-bipyridylruthenium(II) will yield false positives rather than false negatives. There are 6 tyrosine residues in the C₂B sequence and they are located all over the surface of the C₂B domain (Figure 4.13C, tyrosines labeled in green) providing the necessary reactive groups for crosslinking by tris-bipyridylruthenium(II).

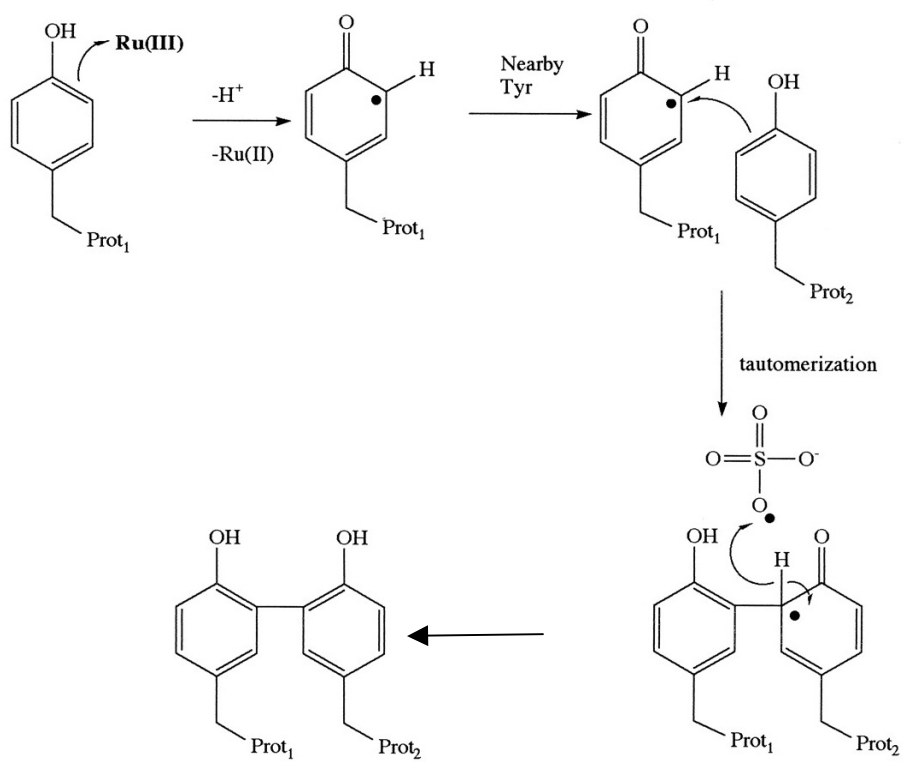
We performed crosslinking experiments using tris-bipyridylruthenium(II) as a crosslinking reagent. The C₂AB domain was in the presence and absence of Ca²⁺ and in the presence and absence of lipids (Figure 4.14A). No significant oligomerization was observed under any of these conditions. Very faint protein bands corresponding to the size of a dimer were observed in all of the conditions independent of the presence of lipids showing that the presence of lipid membranes does not cause oligomerization of C₂AB. As it is well established from NMR studies (Ubach *et al.*, 2001) that C₂AB is monomeric in solution, it is assumed that C₂AB is monomeric in all crosslinking conditions.

Poorly purified C₂B is contaminated with bacterial DNA-RNA mixtures, which bind to the polybasic region of C₂B and absorb light at the wavelength of 260 nm. The formation of the C₂B oligomers in solution was observed when unpurified C₂B was used,

A



B



C



Figure 4.13 Photo-initiated protein cross-linking reaction of tris-bipyridylruthenium(II)

A. The structure of tris-bipyridylruthenium(II).

B. The hypothetical mechanism of the reaction of tris-bipyridylruthenium(II) with tyrosines. When tris-bipyridylruthenium(II) is photolyzed in the presence of a persulfate, Ru(III) and sulfate radicals are generated. Ru(III) is a potent one-electron oxidant and would be expected to oxidize residues such as tyrosine. The resultant radical could proceed to form cross-linked products between two associated proteins mainly by this mechanism. If another tyrosine residue is nearby, then two tyrosine residues are covalently bonded. Alternatively, a nearby nucleophilic lysine or cysteine group could attack the radical to eventually cross-link.

C. The structure of the C₂B domain with tyrosine residues labeled in green is shown. There are 6 tyrosine residues in the C₂B domain sequence and they are exposed residues spanning the surface of the C₂B domain.

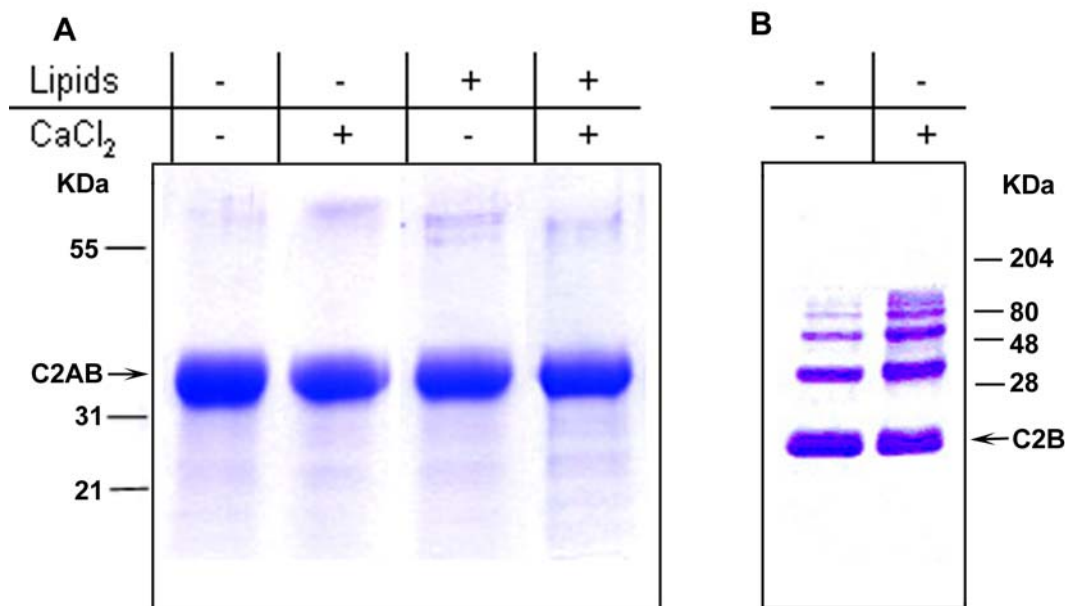


Figure 4.14 Crosslinking experiments of synaptotagmin 1 C₂AB domain using tris-bipyridylruthenium(II) as a crosslinking reagent

A. The lack of the oligomerization of synaptotagmin 1 C₂AB domain when bound or unbound to lipid membranes is shown. 5 μ M C₂AB was mixed with 1.5 mg/ml of lipid vesicles in the presence of 1 mM Ca²⁺ or 2 mM EDTA. No significant oligomerization was observed when C₂AB was bound to lipids. Very faint bands corresponding to oligomers were observed in all lanes independent of the presence of lipids or Ca²⁺ showing that binding to lipids does not trigger oligomerization of C₂AB.

B. Oligomerization of unpurified C₂B domain in the presence of Ca²⁺ or EDTA is shown. Unpurified C₂B contains bacterial contaminants bound to its polybasic region and is known to oligomerize in solution even when not bound to lipids. Bands corresponding to the size of multimeric C₂B were observed, indicating that tris-bipyridylruthenium(II) can efficiently crosslink C₂B domain when C₂B oligomers exist.

but well-purified C₂B, free of bacterial contaminants, was shown to be monomeric in solution (Ubach *et al.*, 2001). We used poorly purified C₂B as a positive control for crosslinking experiments and observed efficient crosslinking regardless of the presence of phospholipids (Figure 4.14B). This experiment proves that the C₂B domain can be efficiently crosslinked with tris-bipyridylruthenium(II). Hence, our conclusion is that well-purified C₂AB domain does not oligomerize in the presence or absence of membranes.

4.3.3.3 FRET experiments

Detecting oligomerization of a protein when bound to the phospholipid membranes is a difficult task to test with different methods. Most techniques like NMR, analytical ultracentrifugation, gel filtration etc. fail to answer this question because of the complications caused by the lipids. We utilized the idea behind the fluorescence experiments we did for determining the lipid-binding mode of synaptotagmin 1 (Section 4.3.2), and developed a series of experiments for detecting the oligomerization of synaptotagmin 1 on the lipids.

We used fluorescence resonance energy transfer (FRET) experiments to test the oligomerization of synaptotagmin 1 on the lipids. We looked for FRET between equal amounts of NBD-labeled and rhodamine-labeled C₂AB bound to membranes. We monitored the change in FRET as we increased the protein concentration and kept the lipid and Ca²⁺ concentrations constant. The protein and lipid concentrations were calculated so that at low protein concentrations no FRET would be observed for a monomeric protein as protein molecules will be too far away from each other on the surface of the lipid vesicles. On the other hand, at high protein concentrations, high

FRET will be observed because of the crowding on the vesicle membranes. However, if the protein oligomerizes, the observed FRET efficiency will be almost constant independent of the protein concentration as oligomers should form at both high and low protein concentrations and cause high FRET. Figure 4.15 schematizes the binding of NBD and Rho-labeled protein mixture on the lipid vesicles at low protein concentrations. A monomeric protein is evenly distributed on the vesicle surface resulting in low FRET (A), whereas protein oligomerization results in high FRET(B). Therefore, FRET dependence on protein concentration is different for monomeric and oligomeric proteins and this can be used to determine the quaternary structure of a protein.

Two fluorescent dyes, NBD and rhodamine, were chosen as a FRET pair. NBD absorbs light at 478 nm and emits at 540 nm, whereas rhodamine absorbs light at 540 nm and emits at 566 nm. Single cysteine mutants of C₂AB were labeled with NBD and rhodamine as described in Section 4.3.2. Equal concentrations of NBD and rhodamine-labeled C₂AB proteins were mixed with lipids in the presence of Ca²⁺. FRET between pairs was monitored by measuring the decrease in the NBD emission signal rather than the increase in rhodamine emission due to complications caused by rhodamine self-quenching. Lipid and Ca²⁺ concentrations were kept constant at 0.1 mg/ml and 1 mM, respectively, whereas protein concentration was varied between 0.02 μ M and 2 μ M. The average distance between the C₂AB molecules were calculated for each protein concentration, assuming a random distribution on the surface of the lipid vesicles. For calculations, the areas of a C₂AB molecule and a phospholipid head group were assumed as 1000 Å² and 65 Å², respectively. At a constant lipid concentration of 0.1 mg/ml, 0.1 μ M C₂AB was calculated to give an average distance of 150 Å between C₂AB molecules,

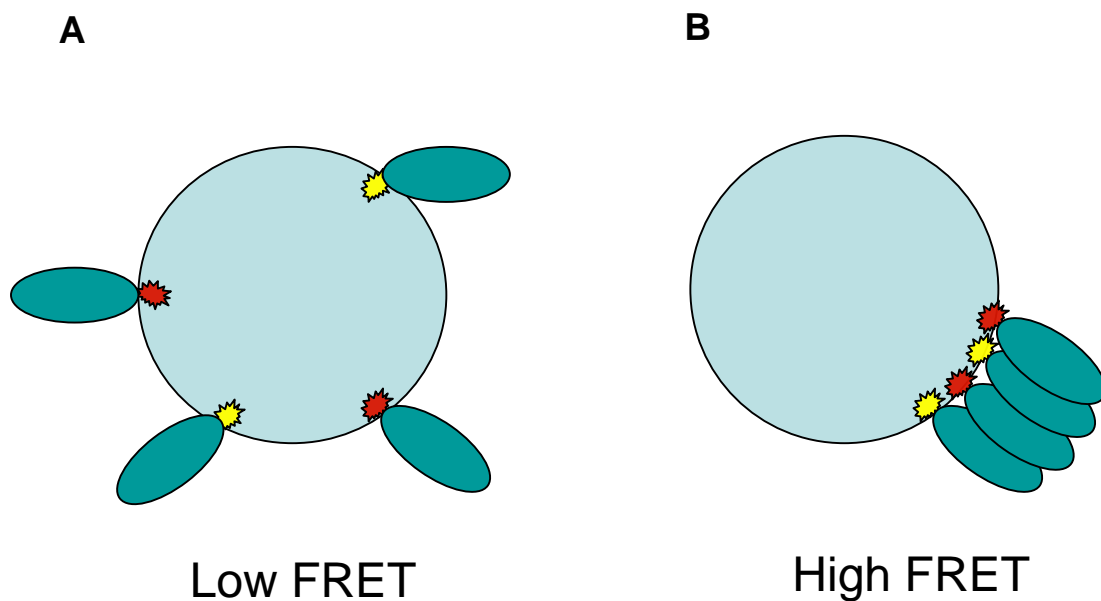


Figure 4.15 Schematic illustration of the binding of the monomeric and oligomeric proteins on the vesicle surface

Different binding modes of the monomeric and oligomeric proteins on the surface of the lipid vesicles are shown. At protein concentrations where the vesicle surface is not saturated, a monomeric protein is randomly distributed over the vesicle surface. Thus, mixing NBD and Rho-labeled protein yield very low FRET (A). When an oligomeric protein is used, protein molecules are not randomly distributed but form oligomers over the vesicle surface, which leads to the observation of high FRET even at unsaturating protein concentrations (B). Green ellipses represent a protein molecule bound to the lipid vesicle. NBD and Rho are colored in red and yellow.

whereas 1 μM C₂AB was calculated to give a shorter intermolecular distance and cover 30% of the vesicle surface. (Note that, at low protein concentrations, the actual protein concentration on the vesicle surface is much higher than in solution. Therefore, the possibility that the protein concentration is not high enough for oligomer formation is excluded.)

Three measurements were made to calculate the FRET efficiency at each protein concentration: 1) NBD-labeled C₂AB + lipids + Ca²⁺ 2) NBD-labeled C₂AB + Rho-labeled C₂AB + lipids + Ca²⁺ 3) NBD-labeled C₂AB + unlabeled C₂AB + lipids + Ca²⁺. The first measurement is the NBD-C₂AB signal enhanced upon binding to the lipids in the presence of Ca²⁺ (As explained in 4.3.2, NBD signal increases when NBD is exposed to a more hydrophobic environment. We preferred working with the mutants that have an enhanced NBD signal upon binding to lipids to increase the signal to noise ratio at low protein concentrations, where the spectrofluorometer sensitivity was low.) For the second measurement, NBD-C₂AB and Rho-C₂AB were mixed and the decrease in the NBD emission was monitored to calculate the FRET efficiency. As a control, the decrease in the NBD signal upon mixing NBD-C₂AB with unlabeled-C₂AB was also measured. At increased protein concentrations, the vesicle surface was saturated with protein and a decrease in the NBD signal was observed as the unlabeled protein competes with NBD-C₂AB to bind to lipids and excludes a portion of NBD-C₂AB leading to a decrease in the NBD signal. (The decrease in the NBD signal suggested that approximately 1 μM C₂AB can saturate the surface of 0.1 mg/ml lipids in agreement with our previous calculations.) The background signal was subtracted from each spectrum and FRET efficiency was calculated by:

$$\text{FRET efficiency} = ([F_{0wt} - F] / F_{0wt}),$$

where F_{0wt} is the fluorescence signal of NBD-labeled protein in the presence of unlabeled-protein, lipids and Ca^{2+} ; and F is the fluorescence signal of the NBD-labeled protein in the presence of the Rho labeled-protein, lipids and Ca^{2+} . We performed four sets of experiments where we used different cysteine mutants to attach the NBD and Rho probes at different positions on the C_2B surface of the C_2AB domain. This approach excludes the possibilities that the mutations may disrupt oligomerization or the two probes may, by chance, be located at the farthest points of an oligomer leading to a low FRET efficiency and avoiding the detection of the oligomer. The labeled cysteine mutant pairs we used were: 1) NBD- C_2AB -I367C and Rho- C_2AB -N333C, 2) NBD- C_2AB -V304C and Rho- C_2B -K326C, 3) NBD- C_2AB -V304C and Rho- C_2AB -V304C, and 4) NBD- C_2AB -V304C and Rho- C_2AB -V419C. The FRET efficiency vs. protein concentration graphs for the four sets of FRET pairs are shown in Figure 4.16A-D.

All results show very low FRET efficiency at low protein concentrations and a gradual increase of FRET efficiency with increasing protein concentrations. At high protein concentrations, when the vesicle surface is saturated with protein, FRET efficiency reaches a value of 0.6-0.7 and stays constant. The maximum theoretical value of 1 cannot be achieved because close contact of protein molecules is unlikely, due to the repulsion between molecules and crowding. This result is in agreement with our previous estimate that 1 μM protein saturates 0.1 mg/ml vesicles by covering only 30% of the surface.

We assumed a random distribution of monomers on the vesicle surface and estimated the expected FRET efficiency from the calculated average distances between

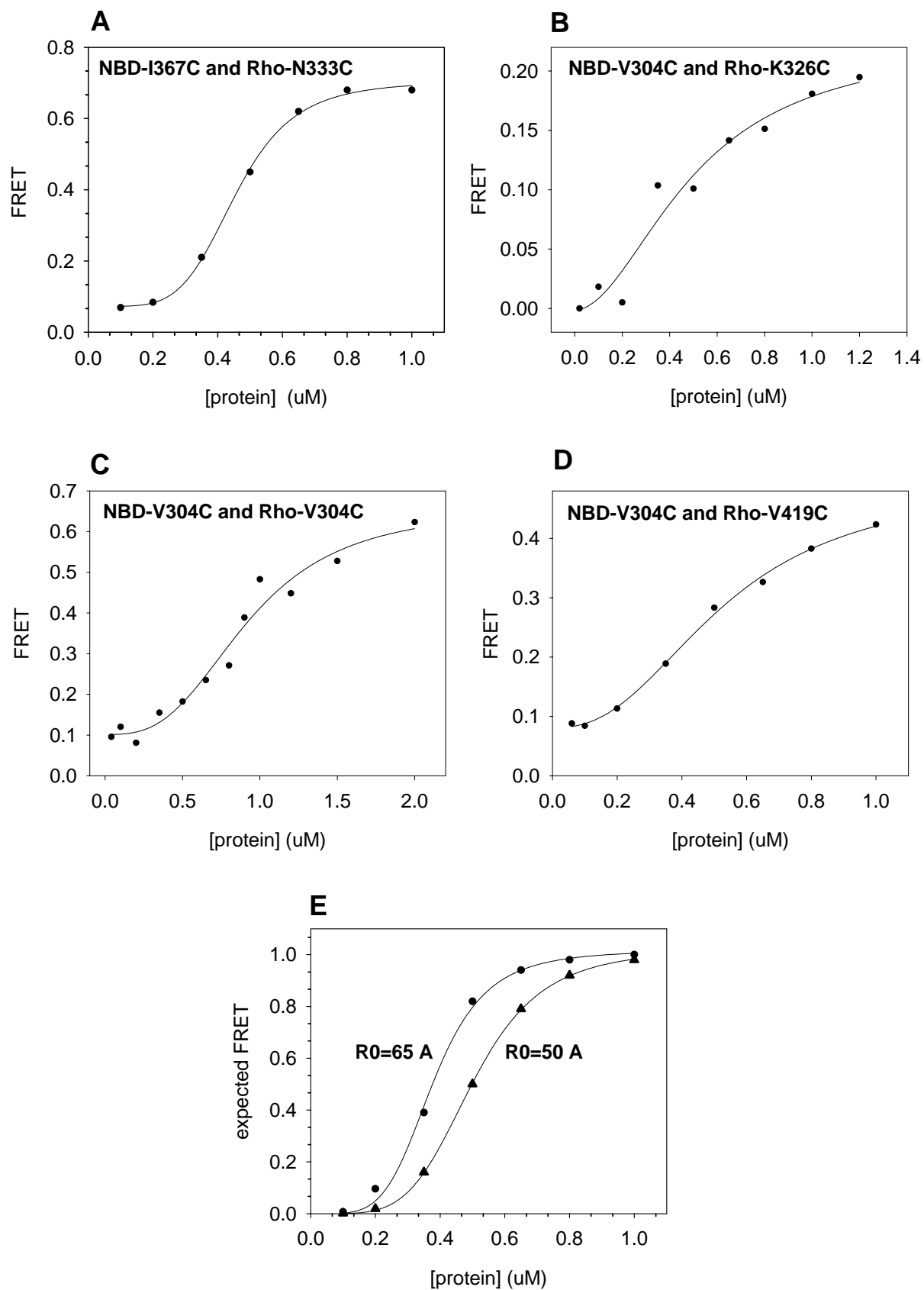


Figure 4.16 FRET efficiency between NBD-labeled and Rho-labeled C₂AB fragments upon binding to vesicles

The increase in the FRET efficiency as a function of protein concentration is shown for the NBD and Rho labeled mutant pairs NBD- C₂AB-I367C and Rho- C₂AB-N333C (A), NBD-C₂AB-V304C and Rho-C₂B-K326C (B), NBD-C₂AB-V304C and Rho-C₂AB-V304C (C) and NBD-C₂AB-V304C and Rho-C₂AB-V419C (D). The expected FRET dependence on the protein concentration for a monomeric protein randomly distributed over the surface of the lipid vesicles is shown in E for R₀ of 50 Å (triangles) and R₀ of 65 Å (circles). The expected FRET was calculated from the average distances between the molecules at given protein concentrations with the assumption that a C₂AB molecule is 1000 Å² and a phospholipid head group is 65 Å².

molecules for each protein concentration. We plotted the expected FRET efficiencies as a function of protein concentration at R_0 of 50 Å and 65 Å (Figure 4.16E). The FRET efficiency vs protein concentration plots from our experimental data nicely fit to the plot of the expected FRET efficiency of a randomly distributed monomer on the vesicle surface. These results strongly suggest that the C₂AB domain acts as a monomer and does not oligomerize upon Ca²⁺-dependent membrane binding.

We repeated experiments using half the lipid concentration (0.05 mg/ml instead of 0.1 mg/ml) and the same range of protein concentration. The idea behind this set of experiments was similar: At low lipid concentrations, a monomeric protein should reach saturated FRET efficiency at lower protein concentrations as less lipid surface is available for binding, and hence, shift the curve to the left. However, an oligomeric protein should not have an effect on the FRET efficiency curve as high FRET will be observed at both high and low lipid concentrations. Figure 4.17 shows the dependence of FRET efficiency on the protein concentration of the NBD-C₂AB-I367C / Rho-C₂AB-N333C pair measured at 0.05 mg/ml and 0.1 mg/ml vesicles. The left shift of the curve upon a two-fold decrease in lipid concentration further suggests that C₂AB is monomeric when bound to membranes.

4.3.4 Synaptotagmin 1 clusters membrane vesicles and brings membranes in close proximity

Our experiments to determine the lipid binding mode of synaptotagmin 1 suggested that upon binding to lipids, a wide area on the surface of the C₂B domain is exposed to a hydrophobic environment, which can be explained either by the

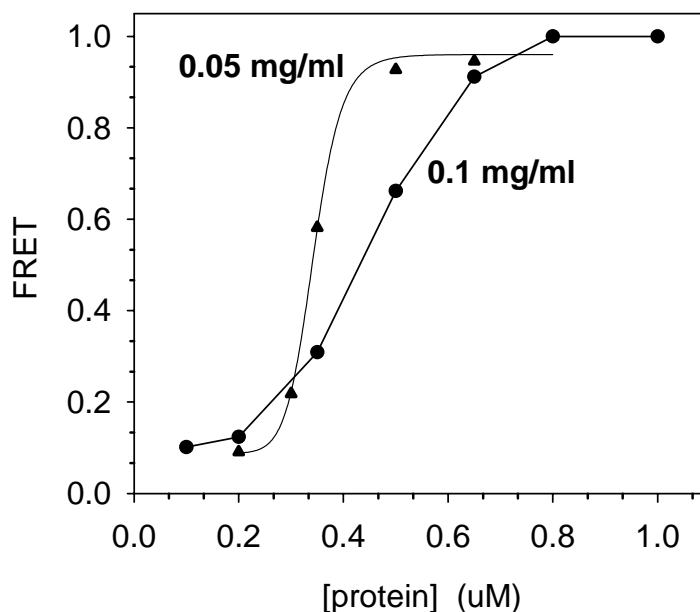


Figure 4.17 Comparison of FRET efficiency between NBD and Rho labeled proteins at different lipid concentrations

The dependence of FRET efficiency between NBD- C₂AB-I367C and Rho- C₂AB-N333C on the lipid concentration is shown. FRET efficiency at different protein concentrations was measured using constant lipid concentrations of 0.1 mg/ml or 0.05 mg/ml. Lower lipid concentration causes a left shift in the curve which is indicative of earlier saturation of the available lipid surface.

oligomerization of synaptotagmin 1 or by the interaction of synaptotagmin 1 with lipids via more than one region. To distinguish between these two possibilities, we started a series of experiments for testing synaptotagmin 1 oligomerization. Although negative staining EM experiments are in agreement with the published results and suggest oligomerization of synaptotagmin 1 on membranes, we concluded that oligomeric images might be a negative staining artifact because our crosslinking and FRET experiments clearly suggest a monomeric state for synaptotagmin 1 on lipids.

The absence of C₂AB fragment oligomerization indicated that the NBD fluorescence changes observed in multiple sites of the C₂B domain upon phospholipid binding must arise from direct contacts with the membranes. The only explanation is that synaptotagmin 1 binds to membranes not only via the Ca²⁺-binding loops but also at other sites. This observation led to the hypothesis that synaptotagmin 1 may be able to bind to two membranes simultaneously. To test this idea, we used dynamic light scattering (DLS).

4.3.4.1 Ca²⁺-dependent synaptotagmin 1 binding induces vesicle clustering

DLS is a method to measure the size of molecules by analyzing the scattered light from the sample and estimating its radius, and in turn, a molecular weight. This technique is commonly used to determine the oligomeric state of macromolecules or to check the quality of protein or liposome samples by monitoring the average molecular size and homogeneity.

The average radius of lipid vesicles was measured using DLS and was found to slightly change between 60-90 nm depending on the lipid preparation (Figure 4.18A). The vesicles are homogeneous and have the expected size. Addition of Ca²⁺, Mg²⁺ or

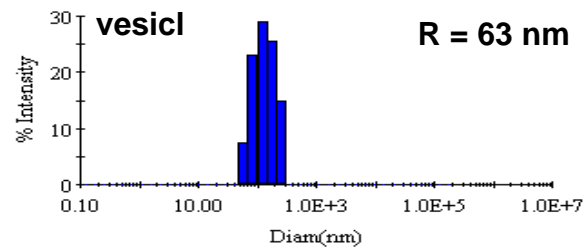
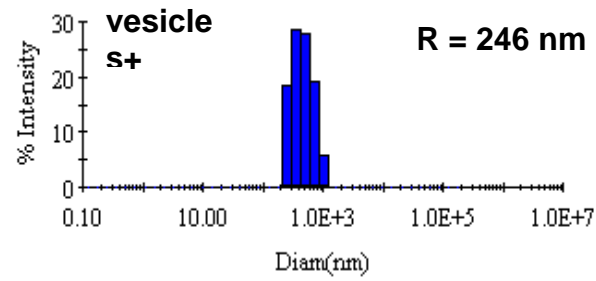
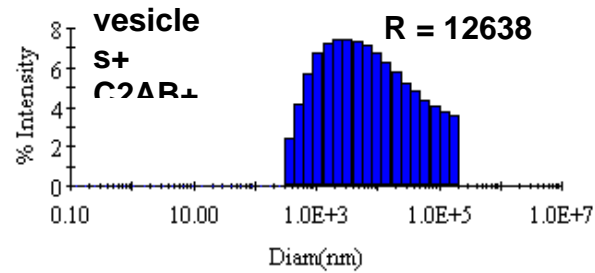
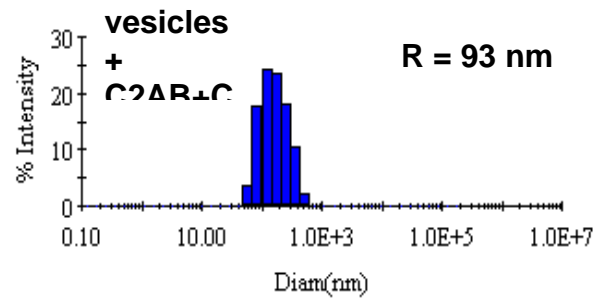
A**B****C****D**

Figure 4.18 The increase in the size of lipid vesicles upon Ca^{2+} -dependent C_2AB binding

Ca^{2+} -dependent C_2AB binding to lipids causes a dramatic increase in the size of the lipid vesicles. The results of DLS experiments are shown as intensity of scattering vs. diameter plots. The radius of the lipid vesicles is measured as 63 nm (A). The addition of Ca^{2+} and C_2AB causes an increase in the vesicle radius within minutes (B). The increase in the size of vesicles is dramatic after overnight incubation of the vesicles in the presence of Ca^{2+} and C_2AB (C). The addition of EDTA into the sample in (C) reverses the effect within minutes (D). 0.05 mg/ml lipid vesicles were incubated with 0.5 μM C_2AB and 1 mM Ca^{2+} or 2 mM EDTA.

C₂AB does not have an effect on the average vesicle size (Table 4.3.A). Importantly, the radius of the vesicles increases dramatically to >500 nm when both the C₂AB domain and Ca²⁺ are added (Figure 4.18B). The increase in size is time dependent and overnight incubation of samples results in radii of > 10000 nm (Figure 4.18C). The enhanced size of the vesicles is reversed back to 60-90 nm within minutes after the addition of EDTA, even after overnight clustering (Figure 4.18D). Intriguingly, not only the C₂AB fragment but also the C₂B domain of synaptotagmin 1 is capable of increasing the size of vesicles in the presence of Ca²⁺. However, the C₂A domain cannot cause the increase in vesicle size (Table 4.3A).

The possibility that membrane fusion causes the increase in the size of vesicles is proved wrong by our observation that the change in size can be reversed by the addition of EDTA. Therefore, we suggest that the increase in the size of the vesicles corresponds to the clustering of the vesicles without fusion upon binding of synaptotagmin 1 to the vesicles in the presence of Ca²⁺. As the isolated C₂B domain is able to cluster the vesicles, we propose that a single C₂B domain can bind to more than one vesicle at the same time.

We made use of mutagenesis to better understand the lipid-binding mode of C₂AB and the mechanism of vesicle clustering. The mutations, which are expected to disrupt vesicle clustering, were designed based on the results of lipid binding mode experiments and previous results with Ca²⁺-binding mutants. As explained before (Section 4.3.2), the NBD fluorescence results obtained from K326C, K327C, N396C and R398C mutants were surprising for us, because we observed clear increases in the NBD signals of these mutants in spite of the fact that these residues are located away from the Ca²⁺-binding

A

Protein	Ca / EDTA/Mg	Radius (nm)
-	-	60-90
-	Ca ²⁺	60-90
C2AB	Mg ²⁺	60-90
C2AB	EDTA	60-90
C2AB	Ca ²⁺	>500
C2AB	EDTA O/N	60-90
C2AB	Ca ²⁺ O/N	>10000
C2AB	Ca ²⁺ O/N + EDTA	60-90
BSA (20 uM)	Ca ²⁺	60-90
C2A +C2B	Ca ²⁺	>500
C2B	Ca ²⁺	>500
C2A	Ca ²⁺	60-90

B

Protein	Ca / EDTA/Mg	Radius (nm)
KK326/7AA C2AB	Ca ²⁺	>500
KK326/7AA C2B	Ca ²⁺	60-90
RR398/9QQ C2AB	Ca ²⁺	>500
RR398/9QQC2B	Ca ²⁺	60-90
D309N C2AB	Ca ²⁺	>500
D309N C2B	Ca ²⁺	60-90

C

Protein	Ca / EDTA/Mg	Radius (nm)
Q403K KK326/7AA C2B	Ca ²⁺	200
TQ406/408KK KK326/7AA C2B	Ca ²⁺	200

Table 4.3 List of synaptotagmin 1 proteins used in DLS experiments

A. The proteins used to determine the ability of vesicle clustering in DLS experiments are listed. C₂A, C₂B, C₂AB or BSA was mixed with lipid vesicles in the presence of Ca²⁺, Mg²⁺ or EDTA and the measured radius is listed.

B. Mutant C₂B or C₂AB domains used to understand the vesicle clustering ability of synaptotagmin 1 are listed.

C. Mutations done on the background of KK326/7AA C₂B to recover the clustering ability of C₂B domain by adding positive charges on the surface are listed. Similar concentrations were used as in Figure 4.17 unless indicated otherwise. Mg concentration was 1 mM. O/N indicates overnight incubation.

loops. We used this result as a clue to find the residues critical for binding to lipids at an additional region. We also hypothesized that positively charged residues might have more importance to bind to negatively charged lipids. Table 4.3.B shows the list of mutations and Figure 4.19 shows the location of the mutations designed on the C₂B surface of the C₂AB domain. We designed mutations in three regions on the C₂B surface: 1) The KK326/327AA double mutation is designed to neutralize the positively charged polybasic region. This mutant was reported to disrupt oligomerization of synaptotagmin 1 on the vesicles (Wu *et al.*, 2003). 2) The RR398/399QQ double mutation was designed to neutralize the positively charged residues on the C₂B surface opposite to the Ca²⁺-binding loops. 3) The D309N mutation disrupts Ca²⁺ binding to the C₂B domain and causes a dramatic decrease of neurotransmitter release *in vivo*. This mutant was designed to investigate the requirement of Ca²⁺-binding to the C₂B domain for vesicle clustering. All three mutations were made both on the C₂B and the C₂AB DNA sequences to distinguish their effect on the single and double C₂ domains. The DLS experiments showed that all three mutations behave the same way such that they all abolish the clustering of vesicles when placed on the isolated C₂B domain, but have no effect on clustering when placed on the C₂AB domain (Table 4.3.B). This suggests that all mutation sites are involved in vesicle clustering and is absolutely necessary for binding of C₂B to lipids at more than one site, but the presence of C₂A can compensate for any of the mutations.

Our expectation was to find a second region on C₂B which is able to bind lipids. The fact that both KK326/327AA and RR398/399QQ mutations abolish vesicle clustering of C₂B was surprising because they are located at distant sites on the C₂B surface. This led us to think that the overall positive charge on the C₂B domain, rather

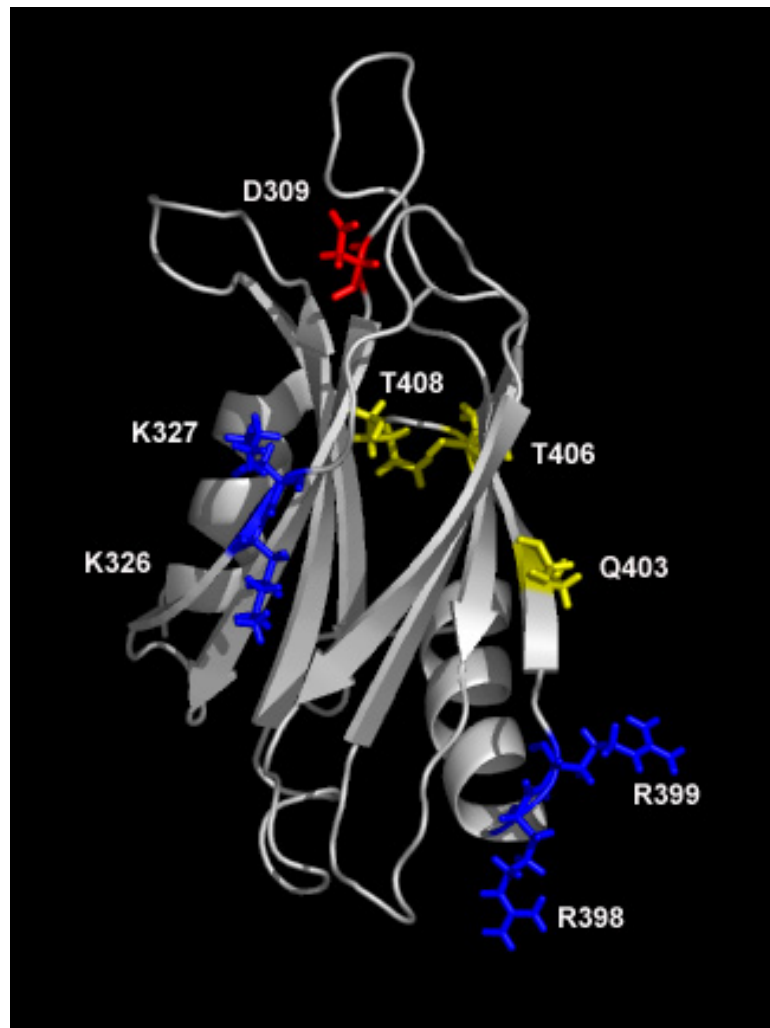


Figure 4.19 The positions of the mutations on the surface of the C₂B domain

The mutations to disrupt and to recover the vesicle clustering activity of the C₂B domain are shown. The positively charged residues that were mutated to disrupt the vesicle clustering ability of C₂B are colored in blue. The critical aspartate residue in loop 1 to coordinate the Ca²⁺ ions is colored in red. The random residues that are mutated to lysine to recover the effect of the KK326/7AA mutation are colored in yellow.

than a defined region, may cause binding to lipids at more than one site. For this reason, we designed Q403K and TQ406/408KK mutations on the KK326/327AA-C₂B background (Table 4.3.C). Our aim was to investigate whether introducing additional positive charges on the KK326/327AA-C₂B surface can rescue the vesicle clustering ability, which was abolished by the removal of positive charges. DLS experiments showed that the Q403K and TQ406/408KK mutants on the KK326/327AA-C₂B background are partially able to cluster vesicles. Although K326/K327 and Q403/T406/Q408 residues are located at opposite faces of the C₂B beta sandwich (Figure 4.19), the effect of removing the critical positive charges from one side could be partially compensated by the introduction of positive charges on the other side. This result suggests that the overall positive charge on the C₂B domain, rather than a single docking site, is important for the interaction of the C₂B domain with multiple liposomes.

The results of our mutational analysis altogether suggest the following model for the lipid-binding mode of synaptotagmin 1: Both C₂A and C₂B domains of synaptotagmin 1 have Ca²⁺-binding loops, which become positively charged upon binding to Ca²⁺ (indicated by two + signs on the top of the C₂ domains in Figure 4.20). The C₂B domain has a very positively charged polybasic region and additional positively charged residues over its surface (indicated by + signs at the bottom of the C₂B domain). However, the C₂A domain has a polybasic region including fewer positively charged residues (indicated by a single + sign at the bottom of the C₂A domain). We suggest that isolated C₂B maintains its vesicle clustering activity by the highly positive electrostatic potential on its surface created by 1) Ca²⁺ binding to the Ca²⁺ binding loops and 2) the

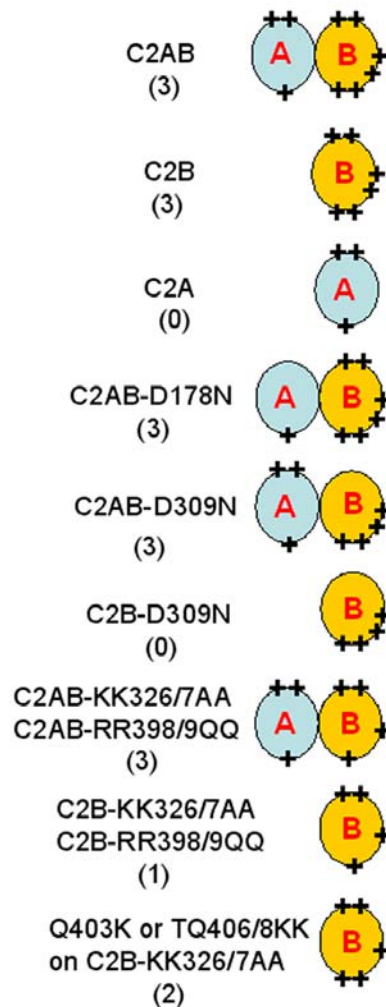


Figure 4.20 Diagrams summarizing the vesicle clustering ability of different synaptotagmin mutants

The ability of vesicle clustering for different proteins is shown. The numbers in parenthesis indicate the clustering ability on a scale measured from 0 to 3. The + signs illustrate qualitatively the amount of positive charges around the mutant proteins. The Ca^{2+} -binding sites are at the top. The C₂A and C₂B domains are represented by blue and yellow ellipses, respectively. Lipid binding is maintained by the Ca^{2+} -binding loops of both C₂ domains and by the polybasic region/positively charged residues of the C₂B domain. The presence of a high positive electrostatic potential around the protein surface is required for vesicle clustering. Introduction of additional positive charges on the surface of the clustering-deficient C₂B can partially restore vesicle clustering.

positively charged residues in the polybasic region and on the face opposite to the Ca^{2+} -binding loops. Disruption of any of these sites abolishes vesicle clustering of the isolated C_2B domain. However, mutations have no effect when made in C_2AB because the Ca^{2+} -binding loops of the C_2A domain compensate the effect of the mutations by providing an additional binding site for lipids. On the other hand, the isolated C_2A domain is unable to cluster vesicles because it lacks a high positive electrostatic potential. Also, our rescue mutants can partially reverse the effect of removing positive charges from the polybasic region by the introduction of positive charges at an unrelated region and support the hypothesis that positively charged residues are required for vesicle clustering. Figure 4.20 indicates the positive charges on the Ca^{2+} -binding loops and polybasic region of C_2 domains of synaptotagmin 1 for each mutant protein and explains the ability and inability of mutant proteins to cluster vesicles.

Clustering of negatively charged membrane vesicles in the presence of synaptotagmin 1 and Ca^{2+} is a very important finding as it suggests that upon Ca^{2+} -binding synaptotagmin 1 is able to bring lipid membranes close in space. If this is true also in vivo, this might help us to understand the mechanism of membrane fusion. In addition, the fact that C_2B can maintain vesicle clustering alone and that C_2A aids in this activity correlates with the in vivo data showing that Ca^{2+} -binding to C_2B is indispensable for neurotransmitter release whereas Ca^{2+} -binding to C_2A is not essential but helpful.

4.3.4.2 Vesicle clustering is visualized by cryo-electron microscopy

In Section 4.3.4.1, we used dynamic light scattering and discovered that upon Ca^{2+} -binding synaptotagmin 1 interacts with lipids to bring different membranes close in

space and clusters the vesicles. DLS is a biophysical method that monitors scattered light from the sample to calculate the radius of a particle. Thus, it is an indirect method to measure the size of particles. The effect of synaptotagmin 1 and Ca^{2+} on the liposomes can only be explained by the clustering of vesicles. However, we decided to use a second method to directly visualize the state of the vesicles in the sample and to corroborate our DLS results.

We used cryo-electron microscopy (EM) to visualize lipid vesicles. Cryo-EM is a microscopy technique in which the sample to be viewed is frozen in a very cold liquid refrigerant in order to preserve and protect it during observation. The freezing process must be quick enough to prevent frozen water from forming crystallized cubic ice that absorbs the electron beam and obscures the sample. Instead, the water should solidify as an amorphous solid (vitreous ice) and not have the chance to crystallize. A small volume of sample is placed on the EM grid that has holes of a desired size on a carbon layer. The EM grid is placed at the bottom of a plunger. A piece of filter paper is pressed against the sample to blot the excess buffer and the plunger is allowed to quickly drop into a vial of liquid ethane cooled by liquid nitrogen. Liquid ethane has a very high heat capacity and can freeze water quickly to form a thin vitreous ice around the sample. The vitrified ice transmits the electrons through, whereas the biological macromolecules, which are usually made of carbon, hydrogen, oxygen and nitrogen, absorb the electrons to form the contrast in the image, making the sample visible. Unfortunately, the electron absorption of biological macromolecules is not high and gives a very low signal to noise ratio for cryo-EM. The signal to noise ratio of negative staining is much higher because of the high electron absorption of heavy metal salt stains like uranyl acetate. The advantages of

using cryo-EM are: 1) There is no stain, which can distort the sample and form artifacts. 2) The sample never comes in contact with adhering surfaces. Therefore the shape that is observed is the true shape of the hydrated molecule in solution. 3) The rapid freezing technique helps to capture the native state of the molecules in the solution.

We used cryo-EM to image the negatively charged phospholipid vesicles. The conditions were optimized for preparing samples and the lipid concentration was increased to 10 mg/ml for better visualization. Figure 4.21 shows 10 mg/ml lipid vesicles in the presence of 1 mM Ca^{2+} imaged at 40000x magnification. Round and nice single vesicles are observed in the absence of the C_2AB domain. The membrane bilayer, which is known to be 6-7 nm, is clearly identified. The presence of Ca^{2+} does not cause any clustering, aggregation or fusion. Some aggregation is observed because of the high lipid concentration. Figure 4.22 shows 10 mg/ml vesicles in the presence of 40 μM C_2AB and 1 mM Ca^{2+} . Vesicle clusters composed of very high numbers of vesicles (starting from a few to hundreds) are observed. Vesicles are attached to each other at many positions. The size of the vesicle cluster can be extremely large in agreement with the high molecular size of the clusters we obtained from DLS experiments. The observed images nicely fit with what we had expected to see. The thickness of the vitreous ice in the holes of the carbon layer is estimated to be approximately 150-300 nm. This thickness is slightly larger than the radius of a vesicle. For this reason, the images we observe correspond to a thin section of a three dimensional cluster, showing the neighbors of a vesicle mostly on the sides but not on the top and bottom. The double bilayers observed in some liposomes are two vesicles inside each other formed as a result of the high lipid concentration.

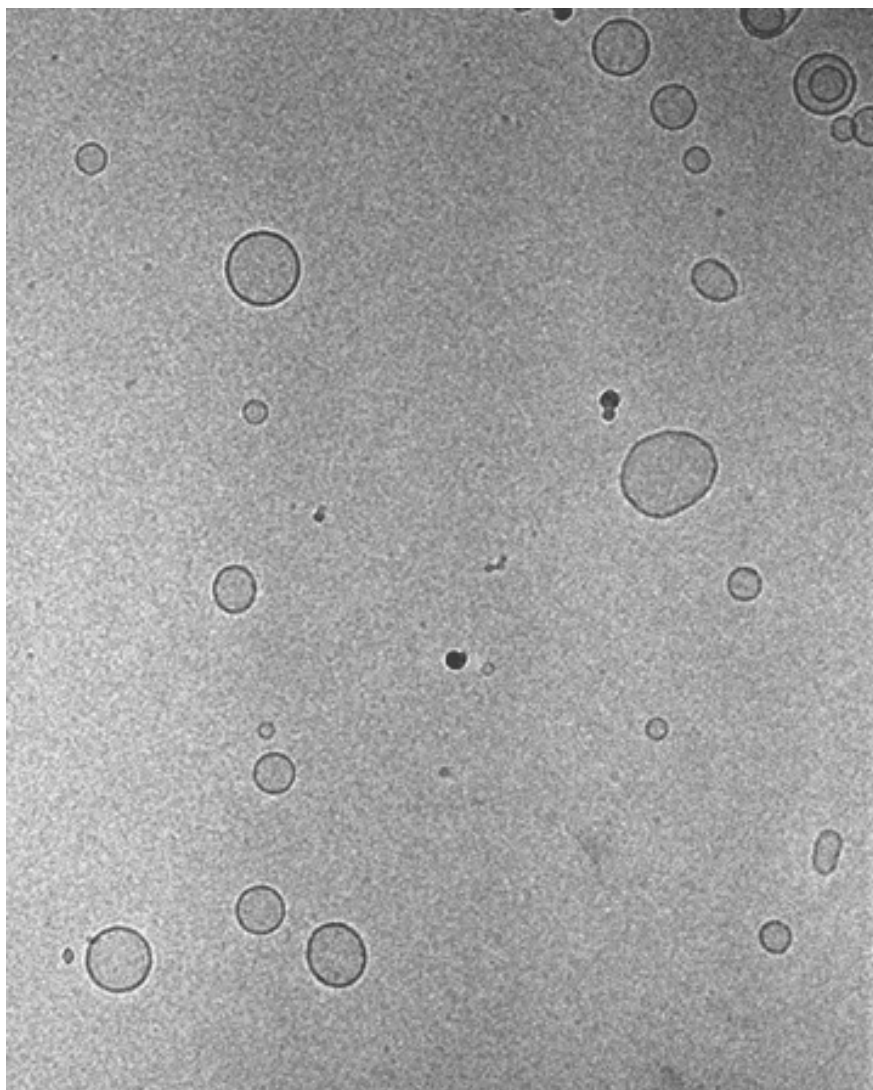


Figure 4.21 Negatively charged lipid vesicles imaged by cryo-EM

Lipid vesicles (30% PS, 70% PC) in the presence of Ca^{2+} are imaged by cryo-EM at 40000 magnification. The lipid and Ca^{2+} concentrations are 10 mg/ml and 1 mM, respectively. Isolated round-shaped vesicles with an average diameter of 50-100 nm are observed.

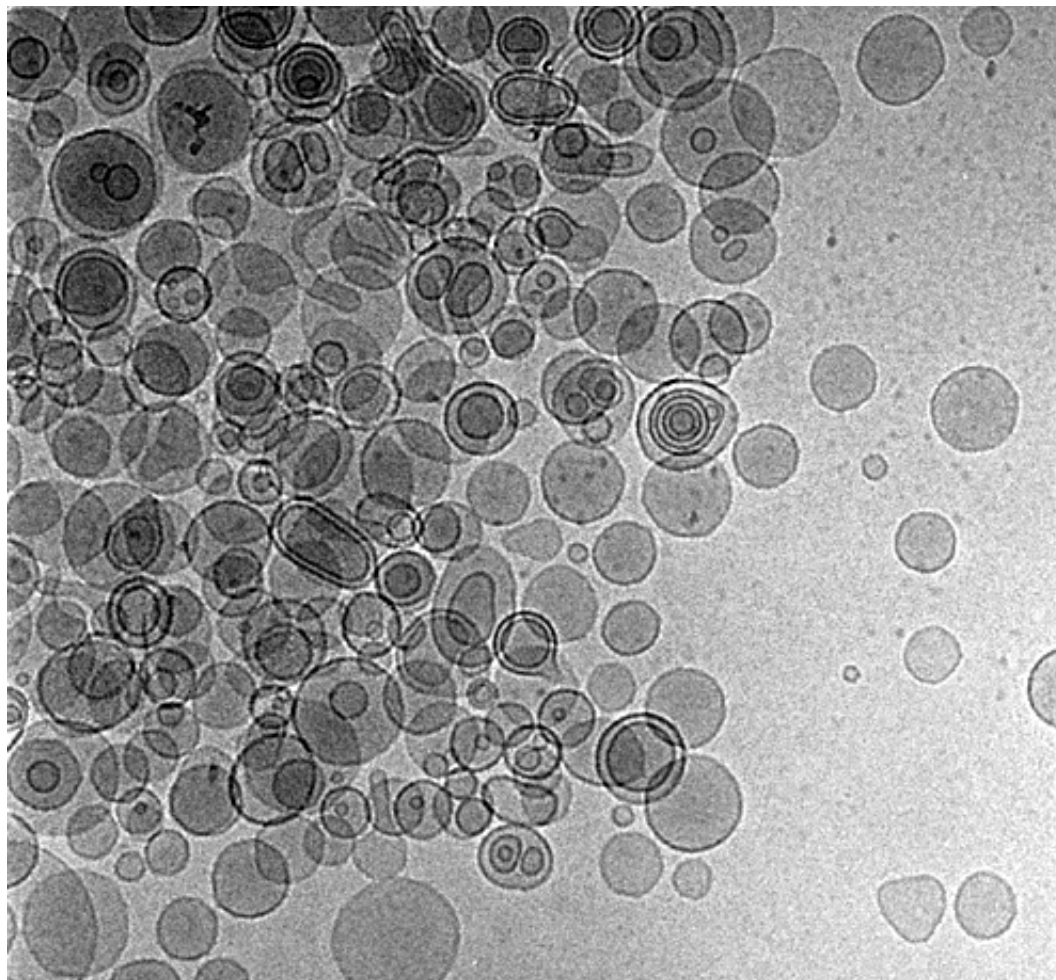


Figure 4.22 Formation of vesicle clusters in the presence of synaptotagmin 1 and Ca^{2+} imaged by cryo-EM

Lipid vesicles in the presence of Ca^{2+} and synaptotagmin 1 C_2AB domain are imaged by cryo-EM at 40000 magnification. 10 mg/ml lipids were mixed with 1 mM Ca^{2+} and 40 μM protein. The formation of vesicle clusters including high numbers of vesicles is observed.

The images of vesicles in the presence of synaptotagmin 1 clearly prove that synaptotagmin 1 has a clustering effect on the vesicles. The in vitro ability of synaptotagmin 1 to cluster vesicles can be translated to in vivo ability of bringing the synaptic vesicle membrane closer with the plasma membrane upon Ca^{2+} -binding. Although no fusion of membranes is observed in the presence of synaptotagmin 1 and Ca^{2+} in vitro, in the presence of other proteins, like SNAREs, the ability of synaptotagmin 1 to bring membranes together might be the key for membrane fusion in vivo. The two membranes, which are already placed in close proximity by the SNARE complex, might be further pulled together by synaptotagmin 1 to facilitate membrane fusion in response to Ca^{2+} influx.

4.3.4.3 Mass density of synaptotagmin 1 is visualized between the clustered vesicles

Although both DLS and cryo-EM data clearly indicate that vesicles cluster only in the presence of both Ca^{2+} and synaptotagmin 1, we have continued our EM experiments to visualize the synaptotagmin 1 protein density between the vesicle membranes. Because the dimensions of a monomeric C_2 domain are quite small (4.5 x 3 x 2.5 nm) to be seen under an electron microscope, we were unable to clearly observe the protein between the vesicles. However, many vesicle pairs appeared to come into close contact and to contain mass density between the membranes that can be attributed to the C_2AB fragment. We were concerned whether the density seen between the membranes is a defocus artifact. For this reason, we used high, moderate and low defocus values to image the same region and observed the mass density in all images. Figure 4.23 shows a small cluster visualized with moderate defocus values. The arrow indicates the protein density between the

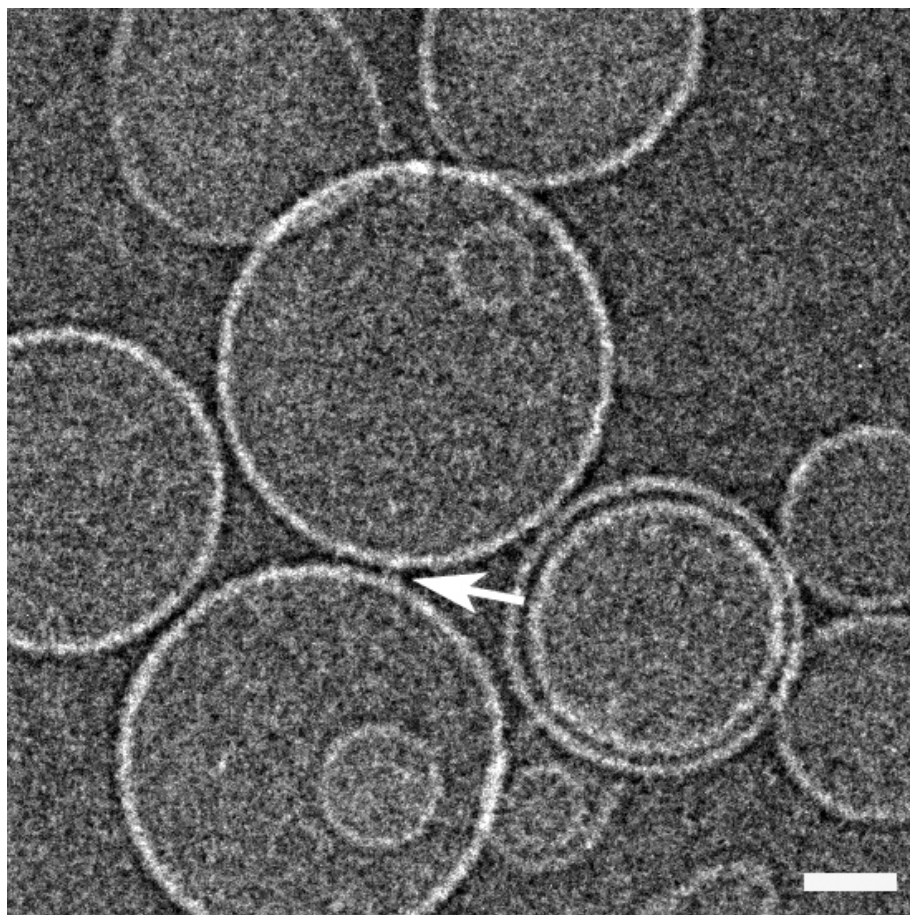


Figure 4.23 Observation of the mass density between the vesicles at moderate defocus values

Zoom-in view of a region of a vesicle cluster observed at 15,000x magnification using a moderate defocus value. The close proximity between the vesicle membranes is illustrated. Arrow indicates the appearance of mass density between the two membranes. Scale bar is 40 nm.

vesicle pair. This result convinced us that the density observed between the vesicles is not an artifact.

As no negative stains are used in cryo-EM, the only source of contrast between the particle and the background is the difference in their densities. This provides a low contrast for biomolecules and gives low signal to noise ratio. The protein density of C₂AB between the membranes became more apparent in a 3D reconstruction of a tomographic series of images that was acquired on a region that contained small clusters. Electron tomography is a method for reconstructing the 3D structure of a specimen from a series of 2D projection images taken at different tilts with a transmission electron microscope. About 100 projections, for example at each degree from projection angles – 50 to +50, are acquired from an individual object and these projections are combined to generate a 3D reconstruction of the original object. The basic steps of electron tomography include the following: 1) Specimen is prepared at a semi-thin section (250nm). 2) 2D images of a tilt series are acquired on the sample using a specialized tilting specimen stage. Software is required for automatic recording of images at different tilt angles. 3) Another software is used for image processing to align the tilt series of 2D images, reconstruct a 3D volume and visualize the model for interpretation.

Radiation damage is the main problem in electron tomography, because the recording of a single tomographic series implies taking a high number of images of the same area in the sample. Radiation damage limits the magnification used on the microscope and reduces the resolution of tomographic reconstructions. We have used 15000 magnification for imaging our vesicles. A total of 67 electron microscope pictures were taken at angles from -66 to + 66 degrees with 2 degree increments. Figure 4.24

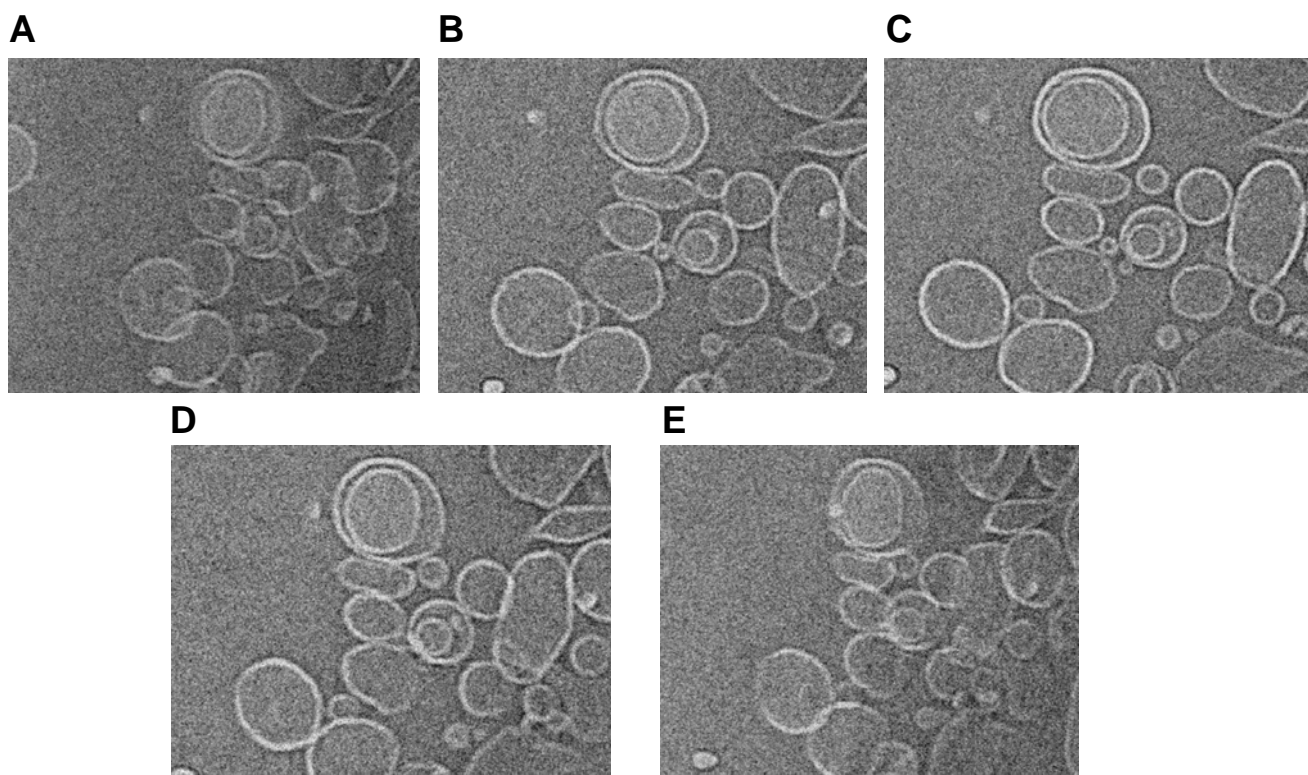


Figure 4.24 Representative images from cryo-EM tomography of lipid vesicles at different tilt angles

The tomographic tilt series of lipid vesicles in the presence of $C_{2}AB$ and Ca^{2+} was acquired from -66 to +66 degrees at 2 degree increments using 15,000x magnification. Representative images at -60(A), -30(B), 0(C), +30(D) and +60(E) degrees tilt angles are shown.

shows representative images taken at -60(A), -30(B), 0(C), +30(D) and +60(E) degree tilt angles demonstrating the relative appearance of the vesicles at different tilt angles.

We reconstructed the projection image tilt series to form a 3D structure of the vesicle pairs. By tilting the 3D reconstruction image of vesicle pairs, we revealed that there really is an observable density between the vesicles where synaptotagmin 1 is supposed to bind the vesicles and cluster them. Figure 4.25 shows the 3D reconstruction of a small cluster and arrows indicate the mass density observed between the vesicles. The 3D reconstruction of a high number of 2D images dramatically decreases the noise and enables the clear appearance of the mass density, which is attributed to synaptotagmin 1. It is likely that more than one C₂AB monomer is positioned between the vesicles.

4.3.4.4 Synaptotagmin 1 brings two membranes into close proximity

A major question that immediately comes into mind is: “What is the distance between the clustered vesicles?”. Synaptotagmin 1 brings the membranes into close proximity. However, is this distance comparable to the distance membrane fusion occurs?

To assess how close the membranes can be brought together by the C₂AB-fragment, we selected closely apposed vesicle pairs. For each vesicle pair, we visualized the 2D projection image planes of the tomographic tilt series and found the plane in which the distance between the vesicles is longest. The intermembrane distances were measured in this plane of the tomographic series, which corresponds to a parallel view of the membrane-membrane interface for each vesicle pair. The measured distances were classified in 0.5 nm bins and the number of vesicle pairs with intermembrane distances within each bin was then plotted against the intermembrane distance range corresponding to each bin. A histogram illustrating the intermembrane distances measured is shown in

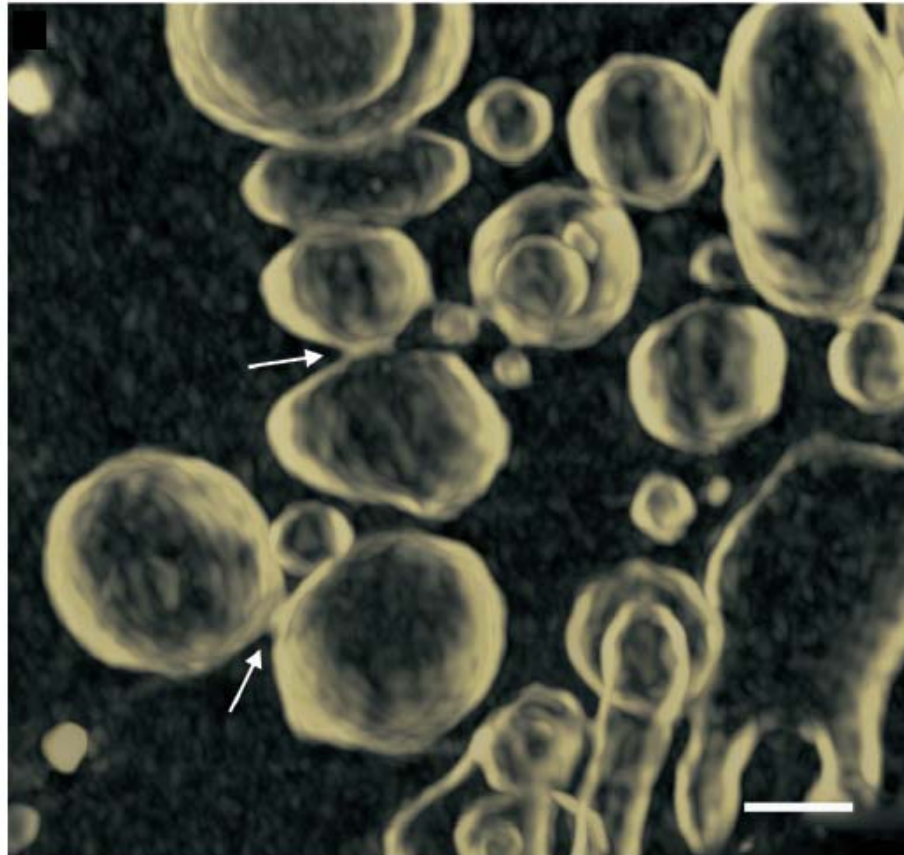


Figure 4.25 Tomographic 3D reconstruction of a vesicle cluster

The Ca^{2+} -dependent binding of synaptotagmin 1 induces vesicle clustering and close membrane-membrane proximity. The 3D reconstruction of a vesicle cluster illustrates the clear mass density between the vesicles as the signal to noise ratio is dramatically higher than the 2D projection image of the same region as shown in Figure 4.24. Arrows indicate the mass density. Scale bar is 40 nm.

Figure 4.26. The distances measured in electron micrographs can depend on the defocus of the objective lens. Nevertheless, this analysis revealed that a majority of vesicle pairs have intermembrane distances around 4-5 nm, which corresponds to the size of a single C₂-domain. Multiple vesicle pairs exhibited intermembrane distances longer than 5 nm, but it is likely that vesicle clustering is a dynamic process and that these vesicle pairs were about to or just had come into closer contact at the moment that the sample was frozen. The 4-5 nm proximity between the membranes induced by binding of synaptotagmin 1 is comparable to the distances required for membrane fusion (Chernomordik *et al.*, 1987). Hence, synaptotagmin 1 induced membrane-membrane proximity might be the key step in triggering the fast, Ca²⁺-dependent neurotransmitter release.

It is also worth noting that in these experiments, we did not observe any images that resembled the 11 nm oligomeric particles observed by negative stain EM (Wu *et al.*, 2003), and that such large particles cannot fit between the closely apposed membranes. A monomeric C₂ domain, which has the dimensions of approximately 4.5 x 3 x 2.5 nm, is able to fit into a 4-5 nm separation between the vesicles. This observation adds more support to our previous conclusion that synaptotagmin 1 does not oligomerize upon Ca²⁺-dependent binding to the lipid vesicles.

We estimate that SNARE complex formation position the two membrane surfaces within about 3 nm. This is generally considered a minimum distance for fusion between two membranes but fusion also requires the induction of membrane curvature. The 4 nm membrane-membrane approximation induced by synaptotagmin 1 binding is comparable to the distance required for membrane fusion. We think that synaptotagmin 1 may

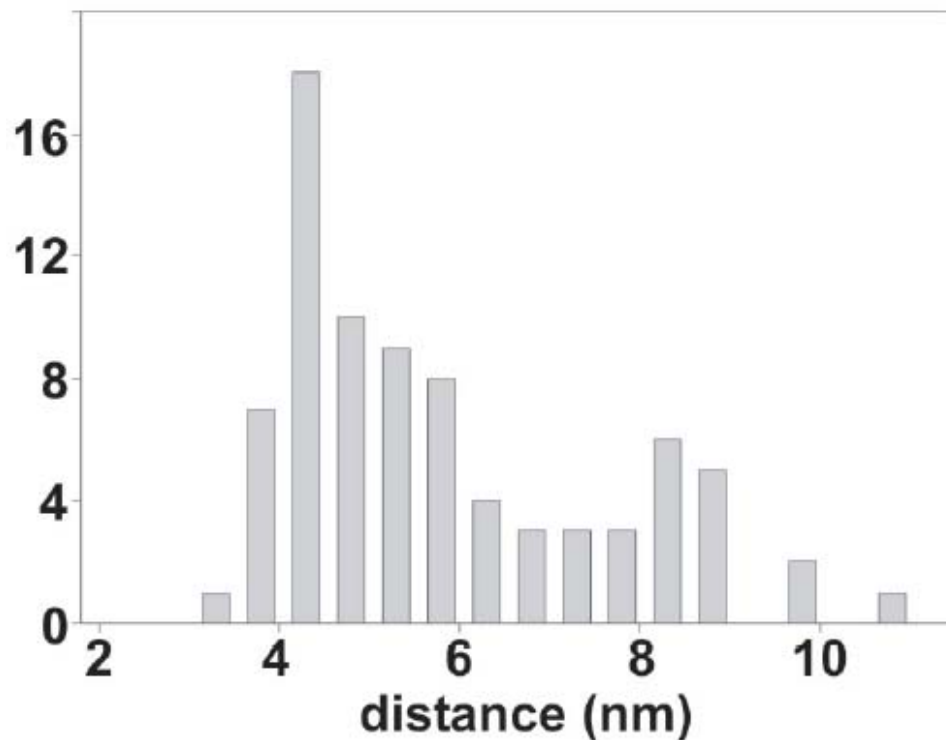


Figure 4.26 Histogram summarizing the measured distances between the vesicle clusters

A tomographic series of images acquired on a region of a sample with small vesicle clusters was used to measure the intermembrane distances. For each vesicle pair, the plane that yields the maximum distance between the two vesicle pairs was selected and the intermembrane distance was measured by counting the pixels in the EMAN software. The measurements were classified into 0.5 nm bins. The number of vesicle pairs with intermembrane distances within each bin was plotted against the intermembrane distance range of each bin.

accelerate membrane fusion by bending the membranes via the highly positive electrostatic potential of the C₂B domain.

4.4 Discussion

The Ca²⁺ sensor in fast neurotransmitter release is now widely believed to be synaptotagmin 1. Ca²⁺-dependent phospholipid binding was known to be essential for the role of synaptotagmin 1 but how this activity helps to trigger neurotransmitter release was unclear. The observation that Ca²⁺-binding to the C₂B domain is much more critical for release than Ca²⁺-binding to the C₂A domain is puzzling as it suggests that although both C₂ domains of synaptotagmin 1 cooperate to bind phospholipids, they somehow have asymmetric functions in neurotransmitter release. The results described in Chapter 4 uncover an unexpected property of synaptotagmin 1 and explain the puzzling *in vivo* data in the literature. This property of synaptotagmin 1, which is described as the ability to bring two membranes into close proximity, arises from the Ca²⁺-dependent phospholipid binding activity but is primarily driven by the C₂B domain. Induction of close membrane-membrane proximity is reminiscent of the role of the SNARE complex in fusion. SNARE complex formation is strongly believed to overcome the repulsion between the headgroups of the vesicle membrane and plasma membranes and pull them together. Our results indicate that synaptotagmin 1 may cooperate with the SNAREs to bring the membranes together as an essential step for fast neurotransmitter release.

The idea that the major consequence of SNARE complex assembly is to bring the synaptic vesicle and plasma membranes together arose from biophysical studies, which show that C-terminal membrane proximal sequences of synaptobrevin and syntaxin are

aligned in a parallel fashion (Hanson *et al.*, 1997; Lin *et al.*, 1997). In vitro fusion experiments performed using reconstituted SNARE proteins suggested that SNAREs may constitute the minimal machinery for membrane fusion (Weber *et al.*, 1998). However, the relevance of these results is under debate (Hu *et al.*, 2002; Kweon *et al.*, 2003). In spite of the unclear role of SNAREs in membrane fusion, there is consensus on the idea that the ability of SNAREs to bring membranes together is essential for their function. It is also believed that SNARE function must be coupled to the Ca^{2+} sensor, since the defect in release arising from cleavage of SNAP25 by botulinum neurotoxin A can be compensated by increased Ca^{2+} levels (Schiavo *et al.*, 2000). Also, the Ca^{2+} -dependence of secretion in chromaffin cells is altered by a mutation that hinders SNARE complex assembly (Sorensen *et al.*, 2002; Chen *et al.*, 2005b). The nature of this coupling is not understood. The finding that synaptotagmin 1 enhances the rate of liposome fusion induced by reconstituted SNAREs in the presence of Ca^{2+} (Tucker *et al.*, 2004) suggests that SNAREs and synaptotagmin 1 cooperate in membrane fusion, but the mechanism of this cooperation is not known.

Our observation that synaptotagmin 1 induces vesicle clustering in the presence of Ca^{2+} leads to a clear explanation for this result. It has been observed that no clustering of reconstituted vesicles occurs in the absence of synaptotagmin 1 (Chen *et al.*, 2005a). Also, the rate of clustering in the presence of synaptotagmin 1 is much faster than the rate of fusion. Therefore, we think that synaptotagmin 1-induced vesicle clustering facilitates the formation of SNARE complexes, and thus, enhances the rate of membrane fusion. This proposal is supported by the preliminary reconstitution experiments showing that the isolated C₂B domain, which is capable of clustering vesicles, is also able to enhance

fusion, whereas the isolated C₂A domain, which is unable to cluster vesicles, is also unable to enhance fusion. Although the results of our fusion experiments performed using the C₂B domain is in contradiction with previous results (Tucker *et al.*, 2004), the difference in the results most likely arises from the method of preparation of C₂B, which requires very thorough purification to remove polyacidic contaminants.

Although the above explanation might help to understand *in vitro* fusion, the docking role of synaptotagmin 1/Ca²⁺ is unlikely to be relevant *in vivo* because synaptotagmin 1 is not expected to induce clustering of synaptic vesicles *in vivo* and the vesicles are already docked to the plasma membrane before Ca²⁺ influx. Also, our observation that the mutation disrupting the Ca²⁺ binding to the C₂B domain does not abolish the clustering ability of the C₂AB domain contradicts with the severe effect of similar mutations on neurotransmitter release *in vivo* (Mackler *et al.*, 2002; Nishiki *et al.*, 2004). Hence, the ability of synaptotagmin 1/ Ca²⁺ to cluster vesicles and to enhance SNARE mediated liposome fusion probably does not reflect the actual mechanism of synaptotagmin 1 action in triggering neurotransmitter release. As a result, what is important about our results is not the vesicle clustering but the observed close membrane-membrane proximity induced by synaptotagmin 1 upon Ca²⁺ binding.

Synaptotagmin 1 is tethered to the vesicles by its transmembrane region. The assumption that binding of Ca²⁺ triggers binding of the C₂ domains to the plasma membrane led to the notion in the literature that synaptotagmin 1 can bring the synaptic vesicles close to the plasma membrane. However, there is a 60-residue flexible linker between the C₂ domains and the transmembrane region. Such a binding would bring the membranes only within 15-20 nm distance, which is probably longer than the distance

between the docked vesicles and the plasma membrane before the Ca^{2+} influx. In contrast, the 4-5 nm distance induced by the simultaneous Ca^{2+} -dependent binding of synaptotagmin 1 to two membranes is comparable to those required for membrane fusion (Chernomordik *et al.*, 1987). Our observation that synaptotagmin 1, the Ca^{2+} sensor that acts at the last step of release, induces such close intermembrane proximity strongly suggests that this ability should be related to its mechanism of action. The observation that this ability is linked to the Ca^{2+} -dependent membrane binding activity and is primarily driven by the C₂B domain correlates well with the previous *in vivo* results suggesting that a unique property of the C₂B domain that is related to phospholipid binding but is not shared by the C₂A domain should be critical for synaptotagmin 1 action.

The fact that neurotransmitter release requires not only a close distance between the membranes but also actual membrane fusion raises an immediate question: How can the properties of synaptotagmin 1 uncovered in our studies help to trigger release? To bring insight to this question and propose a model for the mechanism of synaptotagmin 1 to trigger membrane fusion, we have made use of the geometrical constraints and the electrostatic potentials of the SNAREs and the C₂ domains based on their known 3D structures. The model in Figure 4.27A was built to scale. The membranes are about 6 nm thick and the C₂A and C₂B domains are approximately 4.5 nm in length. The SNARE complex is fully assembled and the short linkers that connect to the transmembrane regions of syntaxin and synaptobrevin are assumed to be in a random conformation. This arrangement would position the membranes within ca. 3 nm.

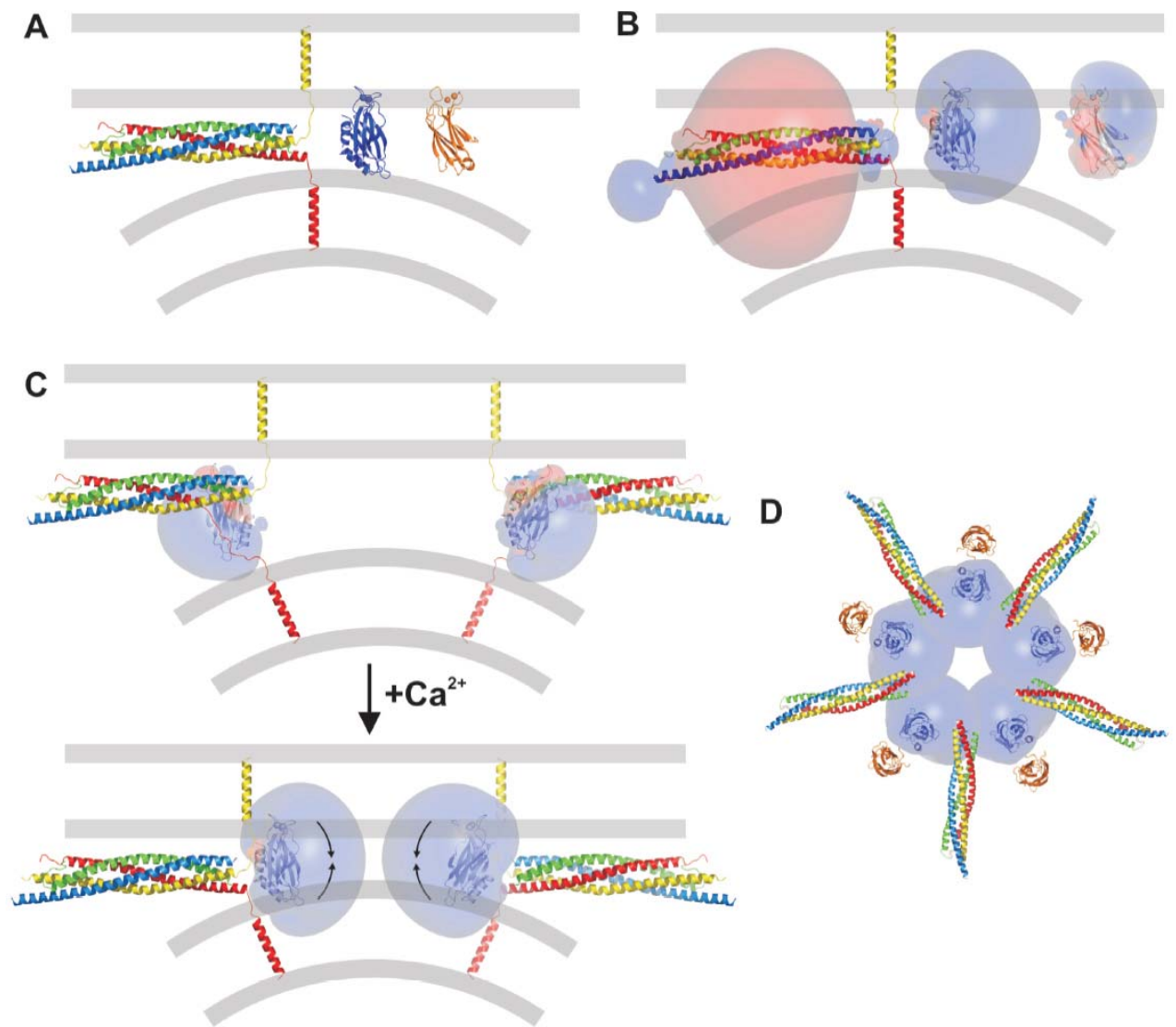


Figure 4.27 Hypothetical model of synaptotagmin action in neurotransmitter release

(A) The known 3D structures of the SNARE complex and the synaptotagmin1 C₂ domains (PDB accession numbers 1SFC, 1BYN and 1K5W) are shown in scale with the plasma and vesicle membranes. The SNARE complex is shown attached to the predicted transmembrane helices via linkers in random conformation. The ribbon diagrams of the Ca²⁺-bound C₂A and C₂B domains are shown as bound to one and two membranes, respectively (syntaxin: yellow, synaptobrevin: red, SNAP25: cyan and green, C₂A: orange, C₂B: blue, phospholipid headgroups: light gray).

(B) Same as (A) but the electrostatic isopotential contours are shown around the structures (blue, 2 k_BT/e; red, -2 k_BT/e). The electrostatic potentials are calculated with GRASP.

(C) Hypothetical arrangement of the C₂B and SNARE proteins before (top) and after (bottom) Ca²⁺ influx. Electrostatic isopotential contours of the Ca²⁺-free (top) and Ca²⁺-bound (bottom) C₂ domains are shown. Upon Ca²⁺ binding, C₂ domains dissociate from the SNARE complex and bind to membranes. The pulling forces induced by the high electrostatic potential of the C₂B domain to bend the membranes are represented by black arrows. The C₂A domain is omitted for simplicity.

(D) Hypothetical arrangement of synaptotagmin and SNARE proteins as a ring. The formation of the fusion pore is facilitated by this arrangement. The number of SNARE and synaptotagmin proteins is arbitrarily set to five. All models are drawn to scale with membrane thickness as approximately 6 nm and the length of a C₂ domain as approximately 4.5 nm.

However, for membrane fusion initiation, the membranes should bend and have curvatures. The electrostatic potential of each structure calculated by the GRASP program (Nicholls *et al.*, 1991) is shown in Figure 4.27B. The SNARE complex has a highly negative electrostatic potential that should cause strong repulsion with the phospholipid headgroups at close distances. On the other hand, the electrostatic potential of the Ca^{2+} -bound C_2A domain has both positive and negative sides that favors binding to a single membrane, whereas the Ca^{2+} -bound C_2B domain has a highly positive electrostatic potential around its surface that facilitates simultaneous binding to two membranes. The direct interactions between the positively charged sites of the C_2B surface and the negatively charged phospholipid headgroups could initiate local membrane bending and induce or accelerate membrane fusion. In fact, our fluorescence data to determine the lipid-binding mode of synaptotagmin 1 (Section 4.3.2) is inconsistent with a single orientation of the C_2B domain between two planes, suggesting that C_2B domain locally bends the membranes to maximize interactions with its basic surface residues. Due to the resolution limit of cryo-EM, we were unable to visualize such local membrane bending. However, the observations that polybasic peptides strongly bend membrane surfaces (Hartmann and Galla, 1978) and that electrostatic potentials induce fusion of closely apposed membranes (Chernomordik *et al.*, 1987) support this possibility.

Figure 4.27C,D shows a model of Ca^{2+} -triggered neurotransmitter release. This model is proposed based on previous observations and the following points of view.

- 1) In an orientation as in Figure 4.27A where the SNARE complex is fully assembled, the synaptotagmin 1 C_2 domains can barely fit between the membranes and

would be in close contact with membranes. With the consideration that, in the absence of Ca^{2+} , the C_2 domains do not bind to membranes and their Ca^{2+} -binding site is yet negatively charged and should have electrostatic repulsion with membranes, our model predicts that the SNARE complex is only partially assembled before the Ca^{2+} influx and membranes are farther away from each other, which allows space for the incoming C_2 domains (Figure 4.27C, top panel).

2) Synaptotagmin 1 binds to the syntaxin/SNAP25 heterodimers with high affinity in the absence of Ca^{2+} through the C_2B domain (Rickman *et al.*, 2004). This interaction will localize synaptotagmin 1 at the active site so that it will be ready to quickly trigger fusion upon the arrival of Ca^{2+} . Moreover, this interaction facilitates the coupling of synaptotagmin 1 and the SNARE complex. Hence, our model predicts that synaptotagmin 1 interacts with the SNARE complex in the absence of Ca^{2+} .

3) Our experiments explained in Chapter 3 suggest that Ca^{2+} -dependent binding of synaptotagmin 1 to phospholipids is incompatible with the SNARE binding (Arac *et al.*, 2003). Hence, the interaction of synaptotagmin 1 with the SNARE complex is disrupted in the presence of Ca^{2+} as synaptotagmin 1 interacts with the lipids and brings membranes together by the multivalent binding of the C_2B domain to membranes. In this step, the SNARE complex is fully assembled (Figure 4.27C, bottom panel).

4) As it is the general assumption that the release machinery is arranged in a ring-like structure and promote the formation of the fusion pore, several molecules of synaptotagmin 1 and SNAREs are suggested to arrange in a ring-like fashion (Figure 4.27D).

Our model suggests that simultaneous interaction of the C₂B domain with both membranes and the highly electrostatic potential generated by the multiple C₂ domains arranged in a ring contribute to create local curvatures and bending in the membranes and may accelerate membrane fusion. The C₂A domain assists the C₂B domain by binding to one membrane and helping to dictate the apparent Ca²⁺ affinity of synaptotagmin 1 for Ca²⁺/phospholipids. A study reports that mutations in the polybasic region of the C₂B domain decrease the affinity of synaptotagmin 1 for lipids in vitro (Li *et al.*, 2005) and the Ca²⁺ sensitivity of neurotransmitter release in vivo (Borden *et al.*, 2005; Li *et al.*, 2005). Our model is supported by these findings. However, to test the validity of the model, more mutants that modify the electrostatic properties of the C₂B domain should be produced and the effect of mutations on the biochemistry and function of the protein should be compared.

We think that additional proteins are needed to mediate the ring organization of the synaptotagmin 1 and SNARE proteins because orienting several C₂B domains with their positive electrostatic potentials pointing to the center of a ring is highly unfavorable. Thus, synaptotagmin 1 will not be able to trigger neurotransmitter release in the absence of such ancillary factors. Considering that the rates of in vitro membrane fusion are much slower (minutes to hours) than the in vivo rates of release (<0.5 ms), the roles of other proteins such as Munc18-1 and Munc13s should be essential for fast neurotransmitter release. Understanding the roles of these proteins and determining the supramolecular structure of the release machinery is the next step to understand the mechanism of neurotransmitter release.

4.5 *Materials and Methods*

4.5.1 Expression and Purification of proteins

All proteins were expressed and purified as explained in Chapter 2.

4.5.2 Preparation of lipid vesicles

Negatively charged lipid vesicles composed of 30% PS and 70% PC were used in all experiments except for the dansyl labeled liposomes containing 10% dansyl-PE, 25% PS and 65% PC. Synthetic 1,2-dioleoyl-*sn*-glycero-3-[phospho-L-serine] (PS) and 1-palmitoyl-2-oleoyl-*sn*-Glycero-3-phosphocholine (PC) were obtained from Avanti Polar Lipids. Lipids, dissolved in chloroform, were mixed in a glass tube and chloroform was evaporated under a stream of N₂ gas until lipids are completely dry. Required amount of a solution of 40 mM Hepes (pH 7.5) and 100 mM NaCl was added on the lipids to give a final concentration of 1-15 mg/ml lipids depending on the type of experiment. The lipid solution was vortexed for 5 minutes to resuspend the lipids. The lipids were hydrated by freezing and thawing in liquid N₂ for 2-3 times. A mini extruder purchased from Avanti Polar Lipids was used to homogenize the lipids. The mini extruder is a system of two plunges with a filter in between. We used filters with pores of 0.08 µm diameter to produce small liposomes with radius in the range of 60-90 nm as measured by DLS. The lipid solution is passed through the filter 10-20 times to form liposomes of homogeneous size. The liposomes were stored at 4°C and used within 1-2 days.

4.5.3 Labeling proteins with fluorescent dyes

Most fluorescent probes are thiol-reactive reagents that react with the thiol groups on the proteins. To label our proteins, we first mutated the single intrinsic cysteine residue (C277) in the C₂B domain to serine. This mutant was used to introduce the cysteine mutations at specific sites and create single cysteine mutants.

The proteins were buffer exchanged into 40 mM Hepes, 100 mM NaCl, 0.3 mM TCEP. The pH was adjusted to 7.5 as the efficiency of labeling is highest at near physiological pH. Extensive buffer exchange was pursued to remove any DTT or BME, which might inhibit the labeling reaction. TCEP, a reducing agent without any thiol groups, was used to avoid oxidation of the proteins. The buffers were deoxygenated to carry out the reaction under an inert atmosphere and prevent formation of disulfides. The fluorescent dye was dissolved in DMSO to make a 5 mM stock solution immediately prior to use as haloalkyl derivatives are not stable in solution. All samples containing the fluorescent probe were wrapped in aluminum foil to protect from light at all times. 0.5 to 1 ml of approximately 50-100 μ M protein was mixed with the fluorescent dye to give 10-20 moles of reagent for each mole of protein. The proteins were incubated at room temperature for 6 hrs. 10 mM DTT was added to consume the excess thiol-reactive reagent and stop the reaction. The labeled proteins were dialyzed overnight to remove the excess dye. Percent labeling was calculated by measuring the final concentrations of protein and fluorescent dye in the sample. The extinction coefficients for NBD, Rho, C₂A, C₂B and C₂AB are 25000, 87000, 15000, 18300 and 32900 $\text{cm}^{-1} \text{M}^{-1}$, respectively. The percent labeling of the proteins were variable especially depending on the location of the mutated residue as more exposed residues are easier to label. The labeled proteins were aliquoted and stored at -80°C.

4.5.4 Fluorescence experiments

Fluorescence measurements were done using a Perkin Elmer LS50B luminescence spectrometer. NBD was excited at 485 nm and NBD emission was monitored between 515 nm and 570 nm wavelength. 0.1 μ M protein was mixed with 0.1 mg/ml lipids in the presence of 1 mM EDTA or 1 mM Ca^{2+} . At these protein and lipid concentrations, the protein fully binds to lipids but does not saturate the lipid surface. For FRET experiments, FRET between NBD and rhodamine was measured by monitoring the decrease in NBD signal. Increasing concentrations of NBD-labeled protein (0.1, 0.2, 0.35, 0.5, 0.8, 1, 1.2, 2 μ M) was mixed with equivalent molar amount of rhodamine-labeled protein. Background signal was measured by monitoring the lipids and subtracted from each measurement. Maximum slit widths (15 and 20 nm) were used for low protein concentrations and varied accordingly at different protein concentrations. Expected FRET efficiency was calculated from the average distances between the molecules by the formula:

$$\text{FRET efficiency} = R_0^6 / (r^6 + R_0^6)$$

where r is the average distance between the molecules and R_0 is the Förster distance of the FRET pair. Average distances were calculated from the protein concentrations by the assumption that the protein molecules will be randomly distributed over the surface of the vesicle. The area of a phospholipid molecule and a C_2AB molecule was assumed to be 65 \AA^2 and 1000 \AA^2 , respectively. FRET efficiency was calculated for Förster distances of 50 \AA and 65 \AA as Förster distance for NBD-Rho FRET pair is known to be 40-70 \AA .

Extreme care was taken for handling samples and making measurements as fluorescent signal of a solution might change by time, by the order the protein, Ca^{2+} and lipids are mixed and by the small differences in pipeting. The experiments were repeated at least twice and most experiments were repeated using different protein preparations to avoid any false conclusions, which might be caused by poor labeling of the protein or insufficient removal of excess dye from the sample as these have a direct effect on the observed fluorescence signal.

The FRET experiments, in which the energy transfer between the tryptophans and the dansyl labeled lipid vesicles, were performed by exciting the tryptophans at 285 nm and observing the dansyl emission at 500 nm wavelength. The phospholipid vesicles contained 10% dansyl-PE, 25% PS and 65% PC. 0.022 mg/ml lipids were mixed with 1 μM protein in the presence of 1 mM EDTA or varying amounts of Ca^{2+} .

4.5.5 Crosslinking Experiments

Crosslinking reactions with tris-bipyridylruthenium(II) were carried out in a total volume of 60 μl in a buffer of 40 mM Tris (pH7.5), 100 mM NaCl and 0.125 mM $\text{Ru}(\text{bpy})_3\text{Cl}_2$ (Aldrich). Protein samples were extensively dialyzed to remove easily oxidized components such as BME or DTT. Instead, TCEP was used to protect the protein from oxidation. The protein (5 μM) was mixed with the lipid vesicles (concentrations changing from 0.1 to 2.5 mg/ml) in the presence of EDTA (2 mM) or Ca^{2+} (1-2 mM) and the solution was placed in an eppendorf tube positioned parallel to the beam of light at a distance of 50 cm from a 150-W xenon arc lamp (Oriel, Stamford, CT). 2.5 mM final concentration ammonium persulfate (APS) was added to the sample just

before irradiation. Light was filtered through 10 cm of distilled water and a 380-to-2500 nm cut-on filter (Oriel 49470). Timed shutters of a single lens reflex camera were used to adjust the exposure time of the sample to the light. The samples were irradiated for 0.5 seconds. Immediately after irradiation, the samples were quenched by the addition of 10 mM DTT. 20 μ l of sample was mixed with 10 μ l of gel loading buffer (0.2 M Tris, 8% SDS, 2.88 M BME, 40% glycerol, 0.4 % xylene cyanol and 0.4% bromophenol blue). The samples were heated to 95°C for 5 minute and loaded on 4-20% polyacrylamide gel (Biorad). The gels were stained by Coomassie blue staining.

Crosslinking experiments with glutaraldehyde were carried out in a total volume of 500 μ l in a buffer of 20 mM Hepes (pH 7.5) and 100 mM NaCl. Protein (3 μ M) was incubated with lipid vesicles (0.1 mg/ml) in the presence of EDTA or Ca^{2+} for 2 hrs and then with different concentrations (0.0005-1%) of crosslinking reagent for 30 min. The reaction was quenched with the addition of 25 μ l of 1 M glycine. The samples were loaded on 4-20% polyacrylamide gel and stained with Coomassie blue stain.

4.5.6 Negative staining electron microscopy

C_2AB (or GroEL) was mixed with lipid vesicles and Ca^{2+} in a buffer containing 50 mM Tris (pH 7.4) 100 mM NaCl and 1 mM DTT. The final concentrations were 2 μ M C_2AB , 3 μ M GroEL, 0.1 mg/ml lipid vesicles and 1 mM Ca^{2+} . 4 μ l of the sample was placed on an electron microscopy grid and excess solution was absorbed using a Whatman paper. The sample was negative stained with 1% (wt/vol) uranyl acetate two times. The excess stain was absorbed and the grid was fully dried. For experiments where C_2AB was bound to lipid monolayers, the samples were prepared as reported before (Wu

et al., 2003). 15 μ l protein droplet was placed on a Teflon well and bulged out. The surface of the droplet was then coated with 0.5-1 μ l of lipid mixture in chloroform:methanol (3:1 vol:vol) to form a lipid monolayer on the droplet surface. Samples were incubated at 4°C overnight. Lipid monolayers at the air-water interface were picked up with hydrophobic carbon-coated grids. After washing with the incubation buffer, the grids were blotted and negatively stained with a uranyl acetate solution. Same structures were observed when lipid monolayers were used instead of lipid vesicles.

The negatively stained samples were examined and photographed in a JEOL 1200 EX transmission electron microscope under the accelerating voltage of 120 kV at 40000x magnification. Minimum dose system (MDS mode) was used to minimize the irradiation damage to the sample. The negatives were scanned at 2.5 Å/pixel. Images of the individual C₂AB oligomers were then boxed in 80x80 pixels and the particles were aligned and centered using EMAN software. The aligned particles were classified into groups and the average density maps of each group were created to proceed with single particle reconstruction. A total of 853 single images were used for C₂AB reconstruction.

4.5.7 Cryo electron microscopy

Cryo-electron microscopy requires samples approximately 10-fold concentrated than negative staining because the sample is in a 3D volume rather than fixed in 2D and also tends to get attached to the carbon support rather than staying within the thin ice hole. 1-10 mg/ml lipid vesicles were mixed with 1 mM Ca²⁺ in the presence or absence of 10-40 μ M C₂AB.

Samples were rapidly frozen on Quantifoil holey grids (Quantifoil Micro Tools GMBH) in liquid ethane using a Vibrobot Automated vitrification device (FEI, Eindhoven). Images were recorded on a Gatan 4k x 4k CCD camera using a JEM2010F electron microscope with 200 kV accelerating voltage. Sample temperature was kept at -175°C using a Gatan cryoholder. Cryo-EM images were visualized at 40,000x magnification. Single axis tomographic imaging was performed at 15,000x magnification. The tilt series were acquired between -66 and $+66$ degrees at 2 degree increments with a total dose of less than $100 \text{ electrons}/\text{\AA}^2$. Focal series images were also taken at 15,000x magnification at a low dose condition with a total dose of less than $16 \text{ electrons}/\text{\AA}^2$. The tilt series images were aligned by cross-correlation with successive images using EMAN software (Ludtke *et al.*, 2001). 3D structures were reconstructed using IMOD software (Kremer *et al.*, 1996). The 3D reconstruction was visualized with UCSF's Chimera software (Pettersen *et al.*, 2004).

For each vesicle pair, the vesicles were monitored and the 2D image plane, in which the vesicle pair is observed directly from the top, was chosen for distance measurements. The distance measurements were done using the EMAN software by counting pixels. The vesicle pairs, which are more than 15 nm to each other, were disregarded as they are not clustered. 40 vesicle pairs, for which vesicles are in less than 16 nm of each other, were found and the distance between them were measured twice. The distances were grouped into 0.5 nm bins. A histogram showing the number of vesicle pairs for each intermembrane distance was plotted.

4.5.8 Dynamic Light Scattering

Dynamic light scattering experiments were done in a Protein Solutions DynaPro and Temperature Controlled Microsampler at 20°C. Very low lipid concentrations had to be used as high concentrations causes too much scattering and saturates the detector. Final concentrations were 0.05 mg/ml lipid vesicles, 0.5 μ M protein (unless indicated otherwise), 1 mM Ca^{2+} and 1 mM EDTA. This lipid to protein ratio saturates the surface of the lipids with almost no excess protein left in solution. Each measurement was done as an average of 20 data points. The samples were prepared in a total volume of 20 μ l and immediately placed in the cuvette for measurement. The experiments were repeated at different incubation times at room temperature. Similar results were observed. However, the size of the vesicle clusters was observed to increase by time being approximately 500 nm after a few minutes, 1000 nm after 10 minutes and > 10000 after O/N incubation.

4.5.9 NMR Spectroscopy

NMR spectra were acquired on a Varian INOVA500 NMR spectrometer at 27 °C in 50 mM MES (pH6.3), 0.15 M NaCl, and 2 mM DTT, with samples containing 0.1 mM C₂B-KK326/7AA and 1 mM EDTA or 20 mM Ca^{2+} . ¹H-¹⁵N HSQC spectra were acquired using a sensitivity-enhanced pulse sequence (Zhang *et al.*, 1994b) with total acquisition times of 1-2 h.

CHAPTER 5

THREE-DIMENSIONAL STRUCTURE OF THE rSLY1 N- TERMINAL DOMAIN: A CONFORMATIONAL CHANGE INDUCED BY BINDING TO SYNTAXIN 5

5.1 *Introduction*

Intracellular membrane fusion is crucial for normal functioning of the cell and occurs in compartments such as endoplasmic reticulum, Golgi, endosomes, vacuoles and synaptic vesicles. Several important families of conserved proteins including soluble NSF-attachment protein receptors (SNAREs) (Sollner *et al.*, 1993b) and Sec1/Munc18-like (SM) proteins (Hata *et al.*, 1993; Garcia *et al.*, 1994) regulate this process. The involvement of the same protein families in most types of intracellular traffic suggests a common mechanism for membrane fusion at different cellular compartments. However, the differences in the properties and interactions of these proteins suggest that they might be acting via distinct mechanisms.

5.1.1 A SNARE protein: Syntaxin

SNAREs share a 70-residue homologous sequence, called the SNARE motif, within their N-terminal cytoplasmic domains and are anchored to the membranes via their C-terminal transmembrane regions (Jahn *et al.*, 1999). Four SNARE motifs, from opposing membranes, form a highly stable coiled coil bundle, known as the SNARE

complex, and bring the two membranes close in space (Hanson *et al.*, 1997;Nichols *et al.*, 1997;Weber *et al.*, 1998;Sutton *et al.*, 1998).

Syntaxin is one of the SNARE proteins and has a C-terminal transmembrane region that is anchored to the plasma membrane. The cytoplasmic region of syntaxin contains the SNARE motif and also an N-terminal regulatory domain, called the H_{abc} domain, which forms a three-helix bundle (Fernandez *et al.*, 1998;Munson *et al.*, 2000;Dulubova *et al.*, 2001b;Yamaguchi *et al.*, 2002;Dulubova *et al.*, 2002). The H_{abc} domain of neuronal syntaxin 1 can fold back onto the SNARE motif to form a closed conformation and prevent SNARE complex formation (Nicholson *et al.*, 1998;Dulubova *et al.*, 1999). This property suggests a mechanism for the regulation of membrane fusion via the availability of syntaxin SNARE motif in the brain. However, other syntaxins are not regulated in the same way (Dulubova *et al.*, 2001b;Dulubova *et al.*, 2002).

5.1.2 SM Proteins

Sec1/Munc18 (SM) proteins are 600-700 residue cytosolic proteins with homology throughout their entire sequence (Rizo and Sudhof, 2002;Toonen and Verhage, 2003;Gallwitz and Jahn, 2003). X-ray crystallography studies of different members of the SM protein family show that SM proteins have three domains arranged in an arch shape which forms a central cavity of 15 Å (Figure 5.1A) (Misura *et al.*, 2000;Bracher *et al.*, 2000;Bracher and Weissenhorn, 2002). In addition, NMR studies indicate that the N-terminal domain is an autonomously folded domain (Dulubova *et al.*, 2003). Electrophysiological analysis of mammalian synapses showed the absolute requirement of munc18-1 for neurotransmitter release while mutations in SM proteins completely

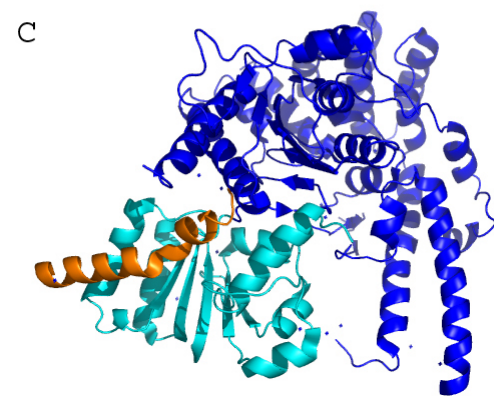
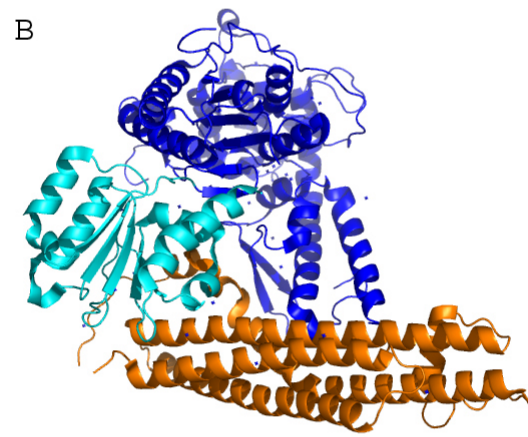
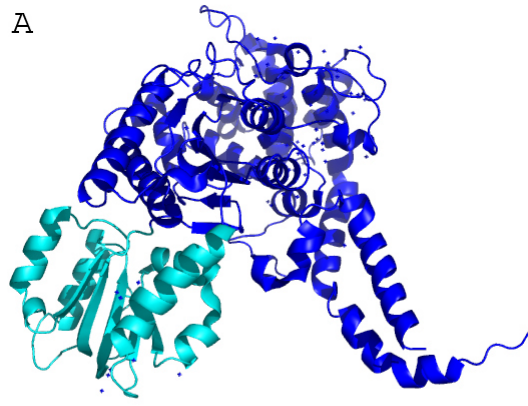


Figure 5.1 Three dimensional structures of SM proteins demonstrate the different modes of SM protein/syntaxin interactions

Ribbon diagrams of the crystal structures of (A) the isolated squid Munc18-1 (PDB accession number 1EPU), (B) the neuronal Munc18-1 in complex with the closed conformation of syntaxin 1a (PDB accession number 1DN1) and (C) the yeast Sly1p in complex with the N-terminal peptide of yeast syntaxin Sed5p (PDB accession number 1MQS) are shown. The N-terminal domains of SM proteins are colored in cyan and the other domains of SM proteins are colored in blue. Syntaxin 1a or Sed5p peptide are colored in orange. Syntaxin 1a in the closed conformation binds to the cavity of the neuronal Munc18-1 (B), whereas the N-terminal Sed5p peptide binds to the N-terminal domain of Sly1p at an opposite region (C). PYMOL (DeLano Scientific, San Carlos, CA; <http://pymol.sourceforge.net/>) was used to prepare the diagrams.

block membrane fusion in other systems (Ossig *et al.*, 1991; Hosono *et al.*, 1992; Schekman, 1992; Harrison *et al.*, 1994; Verhage *et al.*, 2000). These observations indicate that SM proteins are essential for membrane fusion but the exact function of SM proteins is unclear. Although over-expression and microinjection experiments (Wu *et al.*, 1998; Dresbach *et al.*, 1998) suggested an inhibitory role to neuronal Munc18-1 for binding to syntaxin 1a and avoiding SNARE complex formation (Misura *et al.*, 2000), genetic and biochemical data postulate a positive function (Wu *et al.*, 1999) such as a role in vesicle docking (Voets *et al.*, 2001) or core complex assembly (Dulubova *et al.*, 1999; Misura *et al.*, 2000; Sato *et al.*, 2000; Bryant and James, 2001).

5.1.3 Interactions of SM Proteins with Syntaxins

In spite of many SNARE isoforms in vertebrates and yeast, SM proteins have only seven isoforms in vertebrates (Munc18-1, 18-2, 18c, Sly1, Vps45, Vps33a, and Vps33b) and four isoforms in yeast (Sec1p, Sly1p, Vps45p, and Vps33p) (reviewed in (Rizo *et al.*, 2002). Sec1/Munc18 isoforms control exocytosis, Sly1 acts in the Golgi and endoplasmic reticulum (ER), Vps45 is involved in the trans-Golgi network (TGN) and endosomal transport processes, and Vps33 is active at the vacuole and lysosome (Jahn *et al.*, 1999; Chen and Scheller, 2001).

The action of SM proteins in membrane fusion appear to be related to their interaction with syntaxins. SM proteins interact with syntaxins via their N-terminal domains. However, these interactions exhibit an intriguing diversity as the mode of SM protein and syntaxin binding have been observed to be in at least three different ways. The difference lies in both the required conformation and region of the syntaxins, and also in the syntaxin binding region of the SM proteins. Neuronal munc18/syntaxin 1a

interaction requires the presence of most of the cytoplasmic region of syntaxin 1a in a closed conformation where the SNARE motif folds onto the N-terminal H_{abc} domain (Dulubova *et al.*, 1999). The crystal structure of the nMunc18/syntaxin1a complex demonstrates that munc18 binds to closed syntaxin 1 through its central cavity (Misura *et al.*, 2000) (Figure 5.1B). On the other hand, some SM proteins (e.g., yeast Sec1p and Vps33p) directly or indirectly interact with syntaxins only when participating in a functional trans-SNARE complex (Carr *et al.*, 1999b); (Rizo *et al.*, 2002). In contrast, yeast and mammalian Sly1 and Vps45s bind tightly to a short N-terminal peptide motif of their cognate syntaxins (Yamaguchi *et al.*, 2002;Dulubova *et al.*, 2002), Sed5/Syntaxin5 in the Golgi, Ufe1/Syntaxin18 in the ER, Tlg2/syntaxin 16 in the TGN and early endosomes. Also, NMR studies of the syntaxin5 peptide/rat Sly1 interaction and the crystal structure of yeast Sly1p in complex with a short N-terminal Sed5p peptide illustrate that the syntaxin peptides interact with the N-terminal domain of Sly1 on the opposite side of the nMunc18/syntaxin-1-binding site (Bracher *et al.*, 2002;Dulubova *et al.*, 2003) (Figure 5.1C).

The most common mode of syntaxin/SM protein interaction is the type that is observed in the ER, Golgi, TGN and early endosomes. As opposed to the nMunc18/syntaxin 1 interaction in the brain, for which a closed syntaxin conformation is needed, this widespread mode of binding requires only a short N-terminal peptide of syntaxin and thus is compatible with SNARE complex formation. The observation that abrogation of Sly1/syntaxin5 binding results in complete block in ER to Golgi transport and disruption of the Golgi structure demonstrates the functional importance of the Sly1/syntaxin5 interaction (Yamaguchi *et al.*, 2002;Williams *et al.*, 2004).

The crystal structures of isolated squid Munc18-1 (Bracher *et al.*, 2000) and rat munc18-1 bound to syntaxin 1 (Misura *et al.*, 2000) (Figure 5.1) show that syntaxin 1 binding does not cause major conformational changes in the neuronal Munc18-1 structure that might regulate its function. The structure of yeast Sly1p bound to the Sed5p N-terminal peptide (Bracher *et al.*, 2002) also shows similarity to other structures but there is no high resolution structure of the isolated Sly1p to conclude about the absence of a conformational change upon syntaxin binding. As the syntaxin binding mechanisms of munc18s are very different from those of Sly1s and Vps45s, a question that arises is whether syntaxin5/Sed5 binding causes a conformational change in Sly1.

We used three dimensional NMR experiments to observe the structural changes in the rat Sly1 N-terminal domain upon binding of a syntaxin5 N-terminal peptide and solved the NMR structure of the isolated rat Sly1 N-terminal domain. Comparison of the NMR structure of the isolated rat Sly1 with the crystal structure of the peptide-bound yeast Sly1 indicates a conformational switch mediated by a two-residue shift in the register of β sheets upon peptide binding. The change in the register of the last β strand with the rest of the β sheet makes the peptide binding region available for interaction while it is changing the length of the loop between the N-terminal domain and domain 2, which might alter the position of the N-terminal domain with respect to the rest of the protein. In addition, a multiple sequence alignment indicates that the conformational change is conserved in all Sly1 homologues but is not in other SM proteins, and shows a difference in the binding modes of Sly1s and Vps45s to syntaxins, suggesting a possible explanation for the functional distinctions of these homologues.

5.2 Results

5.2.1 Secondary structure determination of isolated and peptide bound rSly1N

We produced the N-terminal domain of rat Sly1 (residues 2-147) (rSly1N) as a ^{15}N -labeled recombinant protein and examined it in the presence and absence of syntaxin5 peptide (residues 1-33) (Syx5(1-33)) using NMR spectroscopy. ^1H , ^{15}N HSQC spectra of ^{15}N -rSly1N with and without unlabeled syntaxin5 peptide were recorded previously (Dulubova *et al.*, 2003) (Figure 5.2). The addition of syntaxin 5 peptide was observed to dramatically change the HSQC spectrum of ^{15}N -rSly1N (Dulubova *et al.*, 2003). Crosspeaks corresponding to residues V135, T136, Q137 and V138 underwent a severe change in their ^1H and ^{15}N chemical shift values upon peptide binding. Severe broadening of the resonances was observed for the rSly1N/Syx5 complex due to slow exchange between the free and bound protein. However, we were able to obtain most of the backbone assignments of the free and peptide-bound ^{15}N , ^{13}C -labeled rSly1N using triple resonance experiments. (All the NMR experiments and backbone assignments performed in the presence of Syx5 peptide were done by Irina Dulubova.)

The secondary structure elements of the free and peptide-bound rSly1N were determined by the difference between the observed C_α and C_β chemical shifts and the chemical shifts expected from a random coil conformation (Wishart and Sykes, 1994). The secondary structures of free and peptide-bound Sly1 showed that syntaxin5 peptide did not induce large changes in the secondary structure of the N-terminal domain of Sly1. However, residues involved in β strand 5, which was clearly defined in the free Sly1, had C_α and C_β chemical shift values different than β sheet in the peptide-bound Sly1 (Dulubova *et al.*, 2003) (Figure 5.3). Interestingly, these are the same residues which

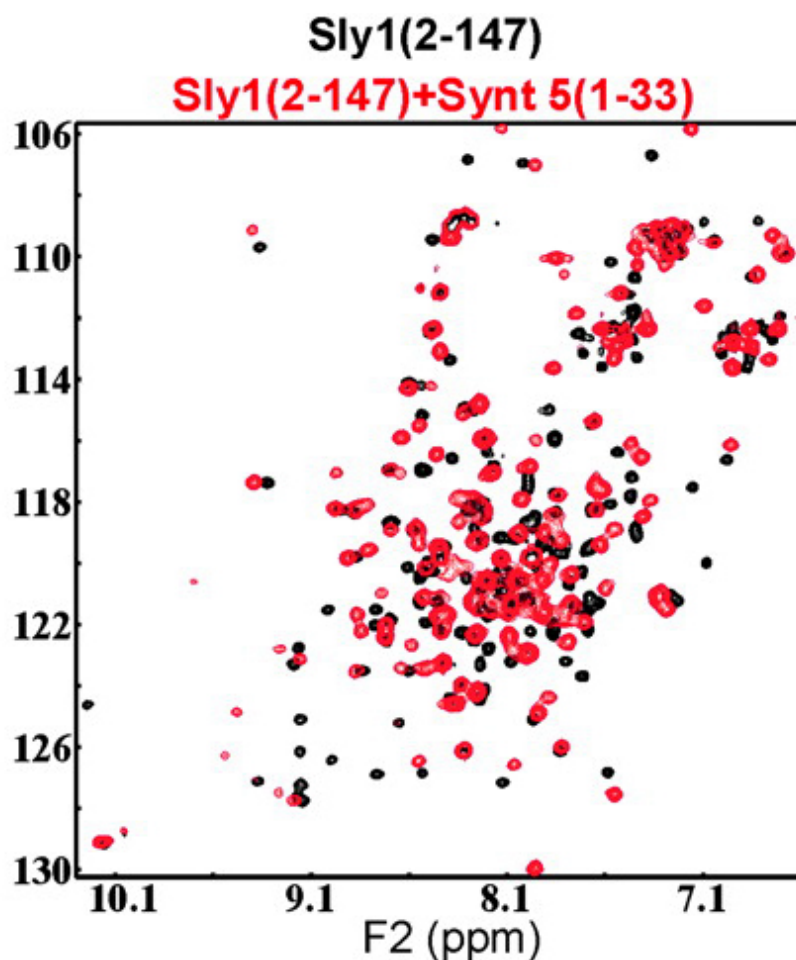


Figure 5.2 The N-terminal domain of rSly1 binds to the N-terminal Syntaxin 5 peptide.

Superposition of the $^1\text{H},^{15}\text{N}$ HSQC spectra of ^{15}N -labeled rSly1N (residues 2-147, 65 μM) in the absence (black) and presence (red) of unlabeled syntaxin 5 peptide (residues 1-33, 200 μM) are shown. Addition of Syx5 peptide to the sample causes changes in many crosspeaks of the HSQC spectrum. Severe broadening was observed for the rSly1N/Syx5 complex due to slow exchange rates.

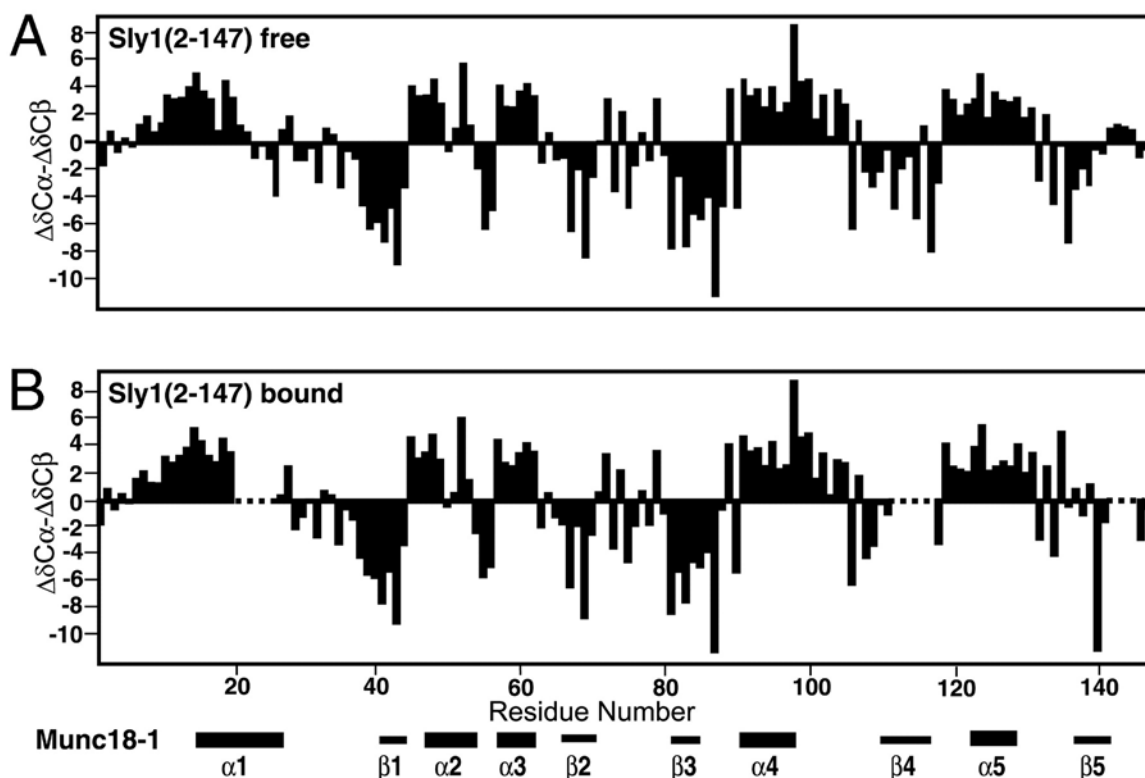


Figure 5.3 The secondary structure elements of the isolated and Syx5 peptide bound N-terminal domain of rSly1.

The differences between the observed C_{α} and C_{β} chemical shifts of rSly1N from the chemical shift values expected from a random coil conformation are plotted as a function of residue number in a graph for (A) isolated rSly1N and (B) rSly1N in complex with Syx5 N-terminal peptide. Five regions with positive chemical shift differences correspond to α -helices and five regions with negative chemical shift differences correspond to β -sheets. The region between helix 5 and strand 5 shows different chemical shifts. The residues 21-26, 112-114 and 143-146 of the rSly1N/Syx5 complex could not be assigned due to broadening. The secondary structure of the corresponding residues in Munc18-1 is shown at the bottom.

have severe chemical shift changes in the HSQC spectrum and are in the peptide binding region.

5.2.2 Peptide-induced chemical shift changes in rSly1N

To explore the possibility that binding of Syx5(1-33) peptide causes a conformational change in Sly1, we acquired three dimensional ^1H - ^{15}N nuclear Overhauser effect spectroscopy (NOESY)-HSQC spectra of ^{15}N -labeled rSly1N in the presence and absence of unlabeled Syx5(133). We obtained the backbone NOE patterns and compared them to those predicted from the crystal structure of the yeast Sly1p/Sed5p peptide complex using the sequence homology between rat Sly1 and yeast Sly1p. Generally, the NOE patterns observed for both the rSly1N and rSly1N/Syx5(1-33) complex were as expected from the crystal structure. Although there were no unforeseen NOE patterns for the rSly1N/Syx5(1-33) complex, numerous unexpected NOEs were observed for the isolated rSly1N between two C-terminal β strands (strand 4 and 5). Figure 5.4 shows the long range and sequential NOEs of representative residues in strand 4 and 5 both in peptide-free and peptide-bound rSly1N. For example, in peptide-free rSly1N, Y109 NH/T136 H_α , L111 NH/V138 H_α and A139 NH/L111 NH NOEs were unexpectedly observed, whereas several expected NOEs, e.g. L111 NH/K140 H_α and A139 NH/Y109 NH, were missing (Figure 5.4A). In contrast, expected interstrand NOEs were observed for the rSly1N/Syx(1-33) complex, indicating the similarity to the crystal structure of Sly1p/ Sed5p complex (Figure 5.4B).

The striking difference in the NOE patterns of Q137 NH in free and peptide-bound rSly1N is also noticeable. The homologous residue of Q137 in yeast Sly1p is

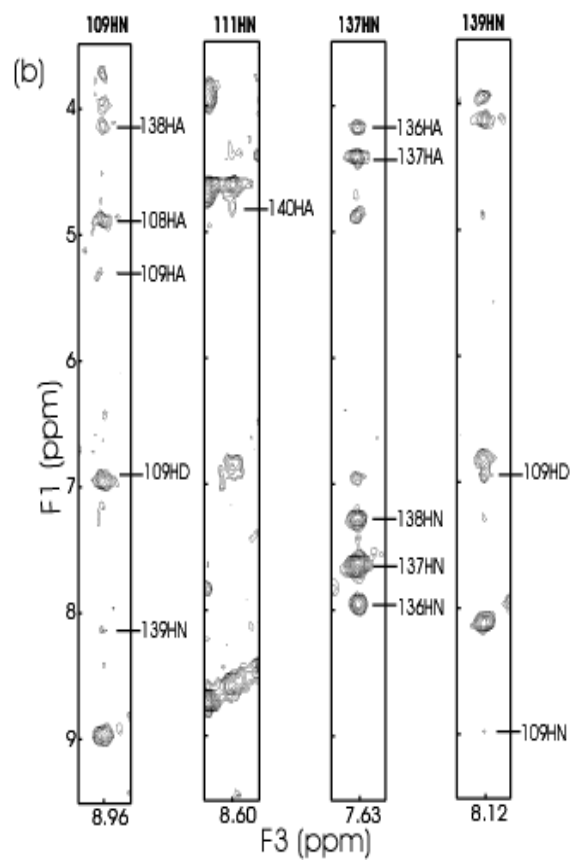
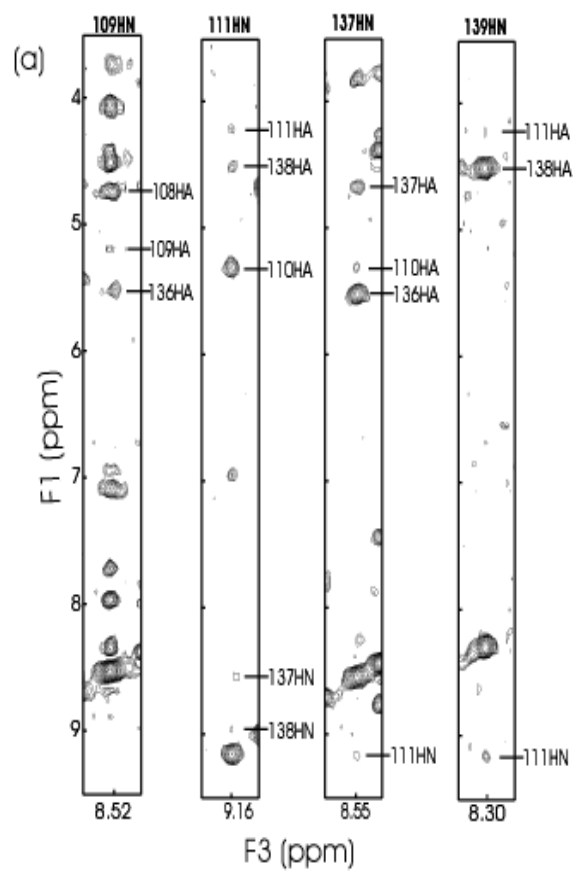


Figure 5.4 Binding of Syntaxin 5 peptide induces changes in the NOE patterns of rSly1N.

Contour plots of selected F3/F1 strips from 3D ^1H - ^{15}N NOESY-HSQC spectra are shown for (A) the isolated ^{15}N -labeled rSly1N and (B) the ^{15}N -labeled rSly1N bound to unlabeled Syx5(1-33). The amide group corresponding to each stripe is shown above. The assignments for selected cross-peaks are labeled. The differences in the NOE patterns reflect the conformational changes in the rSly1N structure induced by Syx5(1-33) peptide binding.

involved in a short 3_{10} helix that precedes strand 5 in the crystal structure of Sly1p/ Sed5p complex. In the rSly1N/Syx5(1-33) complex, Q137 NH exhibits strong NOEs with T136 NH and V138 NH which is an indication of a helical structure, in agreement with the crystal structure (Figure 5.4B). However, the NOE pattern of Q137 in the free rSly1N is characteristic of a β strand and has interstrand NOEs with L111 NH and Y110 H $_{\alpha}$ (Figure 5.4A).

The conclusion we have reached from these observations is that the structure of rSly1N/Syx5(1-33) complex is analogous to the crystal structure of the yeast Sly1p/Sed5p complex. The similarity of these structures was also shown in a previous study where numerous intermolecular NOEs between hydrophobic residues of rSly1N and a key phenylalanine residue (F10) in the Syx5(1-33) peptide was observed (Dulubova *et al.*, 2003). However, the NOE patterns of isolated rSly1 clearly indicate that the register between strands 4 and 5 is shifted by two residues in the absence of peptide and causes a helix-to-strand structural change in the sequence preceding strand 5.

As the structural change is observed at the C-terminal β strands of the protein, we questioned the possibility that the different conformation of rSly1N in the absence of peptide might be an artifact induced by the early truncation of the domain at the C-terminus. However, the HSQC spectrum of an rSly1 fragment (2-154), which has seven additional residues at the C-terminus, is identical to the HSQC spectrum of rSly1N with only a few extra cross-peaks that correspond to the additional unstructured C-terminal residues. This observation indicates that the conformational change observed in the isolated rSly1N is not a result of early truncation of the domain.

5.2.3 Three dimensional structure of the isolated rSly1N

To better visualize and understand the conformational change induced by Syx5(1-33) peptide binding to rSly1N, we used multidimensional heteronuclear NMR experiments to determine the three dimensional structure of the isolated rSly1N in solution. The final structures were obtained using a total of 2493 experimental restraints which included 738 long-range NOEs. Backbone superpositions of the 20 structures with the lowest energies show that the structure is well defined through most of the domain, with a 0.72 rms deviation. Only the loop between helix 1 and strand 1 (loop 1) is poorly defined. The lack of structural definition in loop 1 correlates with the observation that the NMR data corresponding to this region exhibits sharp resonances and fast amide proton exchange rates, which are indicative of flexibility. The average rms deviation of backbone residues decreases to 0.42 when this loop is excluded from the calculations and is 0.37 for backbone secondary structure. The ribbon diagram of a representative structure is shown in Figure 5.5B and the structural statistics are summarized in Table 1. The quality of the structure is also illustrated by low deviations from the idealized covalent geometry and good Ramachandran map statistics (Table 1).

The N-terminal domain of rat Sly1 contains a parallel five-stranded β -sheet with a 2-1-3-4-5 topology (Figure 5.5.A). It starts with an α -helix followed by a long loop, then goes into the five stranded β -sheet. Each strand is followed by either an α -helix or by a loop. After β -strand 5, the structure is terminated at the end of the loop that connects domain 1 to domain 2.

5.2.4 Peptide induced conformational changes in rSly1N

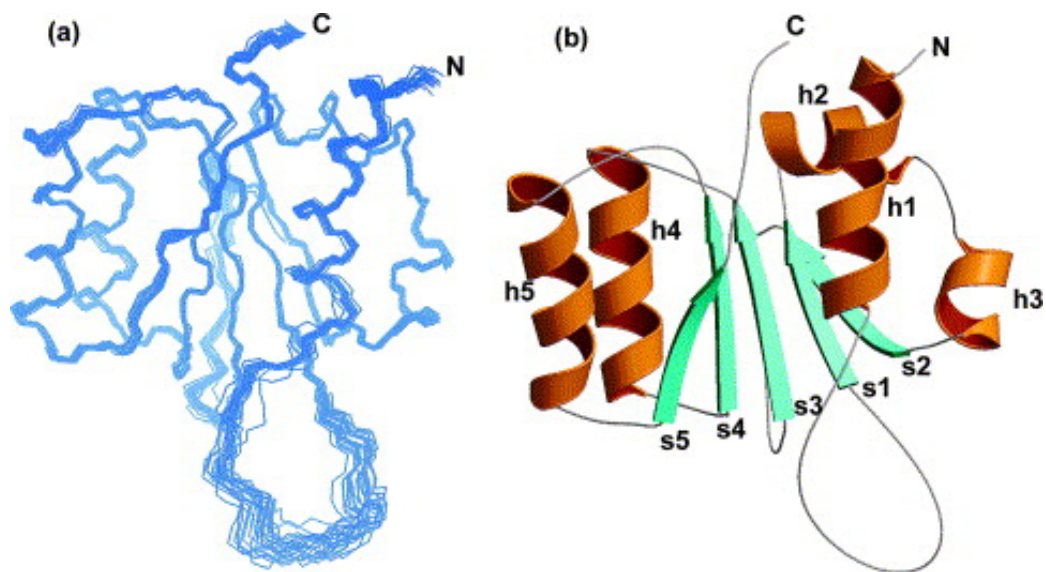


Figure 5.5 Three-dimensional NMR structure of the N-terminal domain of rat Sly1
 (A) Backbone representations of the 20 structures with the lowest energies are superimposed.
 (B) A ribbon diagram of the lowest energy structure is shown. B-strands are colored in cyan and alpha helices are colored in orange. The strands are labeled s1-s5 and helices are labeled h1-h5. The N and C termini of the protein are labeled as N and C. Insight II (MSI, San Diego, CA) and MOLSCRIPT (Kraulis, 1991) were used to prepare the diagrams.

Table 1. Structural statistics for the 20 structures of the N-terminal domain of ratSly1 with the lowest energies¹.

Average rms deviations from experimental restraints (2493 total)

NOE distance restraints (Å)		
All	2133	0.0118 ± 0.0009
Intraresidue	451	0.0147 ± 0.0027
Sequential (i-j = 1)	485	0.0068 ± 0.0014
Short range (i-j = 2-4)	459	0.0112 ± 0.0008
Long range (i-j > 4)	738	0.0126 ± 0.0006
Hydrogen bonds (Å)	132	0.0107 ± 0.0018
Dihedral angles (deg)	228	0.107 ± 0.016

Average rms deviations from idealized covalent geometry

Bonds (Å)	0.0019 ± 0.00007
Angles (deg)	0.380 ± 0.005
Impropers (deg)	0.24 ± 0.01

Ramachandran plot statistics²

Residues in most favored regions	83.7%
Residues in additionally allowed regions	16.3%
Residues in generously allowed regions	0.0%
Residues in nonallowed regions	0.0%

Average rms deviations of atomic coordinates (Å)

<u>structure</u>	<u>Among 20 structures</u>	<u>To average</u>
Backbone residues 8-147	0.72	0.49
Heavy atoms residues 8-147	1.36	0.92
Backbone residues without the flexible loop ³	0.42	0.29
Heavy atoms residues without the flexible loop ³	1.16	0.80

¹ All 20 structures have NOE energies below 30.3 kcal/mol. There were no NOE violations larger than 0.2 Å or dihedral angle violations larger than 2°.

² Calculated using the program PROCHECK (Laskowski *et al.*, 1993).

³ Residues 8-23, 38-147.

Due to the strong resonance broadening in the NMR spectra of the rSly1N/Syx5(1-33) complex, the three dimensional atomic structure of the peptide-bound rSly1N could not be determined. Because the binding mode and structure of the yeast Sly1p/Sed5p complex is analogous to that of rSly1N/Syx5(1-33), we compared the crystal structure of the Sly1p/Sed5p complex to the NMR structure of the isolated rSly1N to reveal the conformational change induced by Syx5 peptide binding to rSly1N.

We used the DALI program to superimpose the rSly1N and the N terminal domain of the yeast Sly1p/Sed5p complex structures and obtained an rms deviation of 2.9 Å for 130 equivalent C α atoms. The superimposition in Figure 5.6A shows that the core regions of both structures are very similar. However, there are differences in two regions: 1) The N-terminal helix1 and loop1, 2) The peptide binding region composed of helix 5-loop-strand 5. The N terminal loop1 in the rat Sly1 structure is longer in yeast Sly1 and involves an additional short α -helix. This structural difference might be caused by the low sequence homology at the N terminus. It is also possible that an alternative conformation is induced because of the high crystal contacts this region is involved in, as such a flexible loop would not be observable in the crystal structure if it was not involved in crystal contacts. The second difference between the two structures is in the helix 5-loop-strand 5 region where the cognate syntaxins bind. Hence this structural difference between the rSly1N and Sly1p/Sed5p structures reflect the conformational change required for binding of Syntaxin 5 to rSly1N and probably for binding of Sed5p to Sly1p.

The crystal structure of the yeast Sly1p/Sed5p complex shows that Sed5p binds at a groove formed by helix 5 and strand 5 (Bracher *et al.*, 2002;Dulubova *et al.*, 2003). Multiple hydrogen bonds and hydrophobic contacts are involved in the interactions,

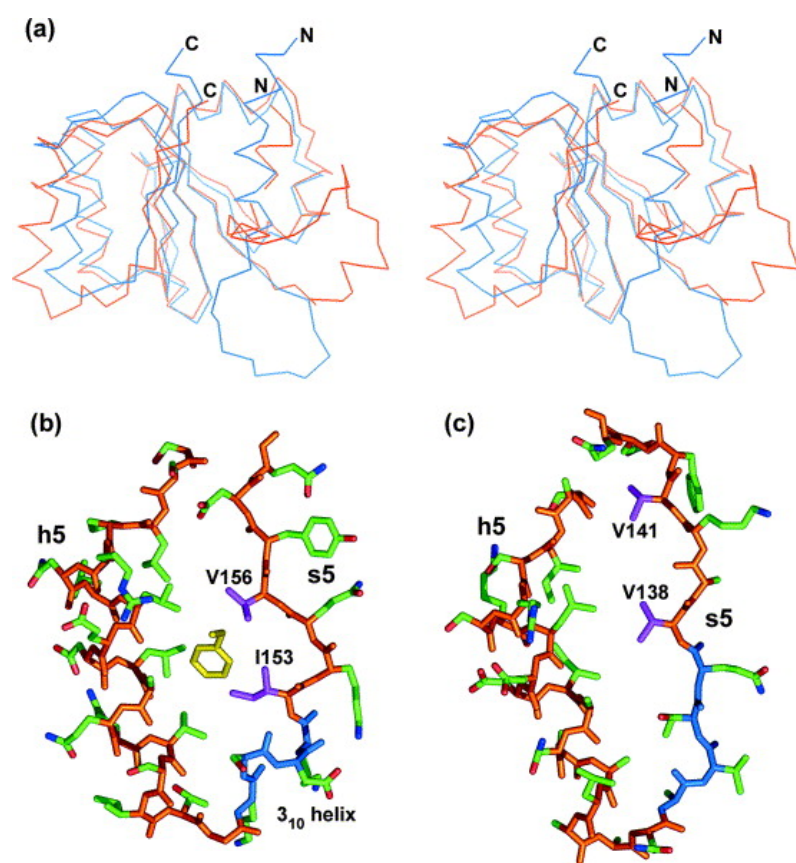


Figure 5.6 Conformational change of rSly1N structure upon binding to syntaxin 5

(A) Stereo trace superposition of the NMR structure of the isolated rSly1N (blue) and the crystal structure of the N-terminal domain of yeast Sly1p bound to Sed5p peptide (orange, PDB accession number 1MQS). The peptide is not shown for simplicity. N and C termini are labeled as N and C. The helix5-strand 5 regions of (B) the Sly1p/Sed5p complex and (C) the isolated rSly1N are shown as stick models. The side chain of F10 from Sed5p peptide is shown in yellow in the Sly1p/Sed5p complex structure in (B). Backbone atoms of the sequence that forms the 3_{10} helix in the complex and part of the strand 5 in isolated rSly1N are colored blue. All other backbone atoms are colored orange. Side chain atoms are colored in green for carbons, blue for nitrogens and red for oxygens except for two hydrophobic side chains from strand 5 of Sly1p, which forms the hydrophobic pocket for F10 of Sed5p, and the homologous side chains in rSly1N, which are colored magenta. Helix 5 and strand 5 are labeled. The orientations of all diagrams are similar to the structure in Figure 5.5. Insight II (MSI, San Diego, CA) and PYMOL (DeLano Scientific, San Carlos, CA; <http://pymol.sourceforge.net/>) were used to prepare the diagrams.

which are mostly between the residues in the Sly1p groove and a key phenylalanine residue (F10) in the Sed5p peptide (Figure 5.6B). The superposition in Figure 5.6A illustrates the requirement for a larger separation between helix 5 and strand 5 for the accommodation of the Sed5p peptide in the Sly1p/Sed5p structure. The peptide binding groove of yeast Sly1p/Sed5p and rSly1N structures are shown by stick models in Figure 5.6B and C and by surface representations in Figure 5.7A and B. The F10 side chain of the Sed5p peptide, which is conserved in syntaxin 5, inserts into the cavity surrounded by hydrophobic residues of strand 5 and helix 5 of Sly1p (Figure 5.6B). The occlusion of the cavity with the peptide prevents the close packing of hydrophobic residues in strand 5 and helix 5 against each other. The surface representation of the Sly1p/Sed5p complex (peptide is not shown for simplicity) in Figure 5.7A shows the peptide binding groove and the lack of tight hydrophobic packing.

In contrast, in the isolated rSly1N structure, the groove in the peptide binding region is smaller, helix 5 and strand 5 are less separated, and the hydrophobic packing is tighter so that there is no cavity in the peptide binding region to accommodate syntaxin 5 (Figure 5.6C and 5.7B). This difference in the protein conformation is made possible by the fact that the sequence between helix 5 and strand 5, which separates the two secondary structure elements, is shorter in the isolated rSly1N structure than it is in the yeast Sly1p/Sed5p complex structure. The comparison of the two structures shows that, in the isolated rSly1N, helix 5 is followed by a short loop region after which β -sheet 5 starts. However, in the peptide-bound yeast Sly1, helix 5 is followed by a short loop and a short 3_{10} helix, then by strand 5 (Figure 5.6B and C). The first two residues of strand 5 in the isolated rSly1N structure (T136 and Q137) are involved in the formation of the 3_{10}

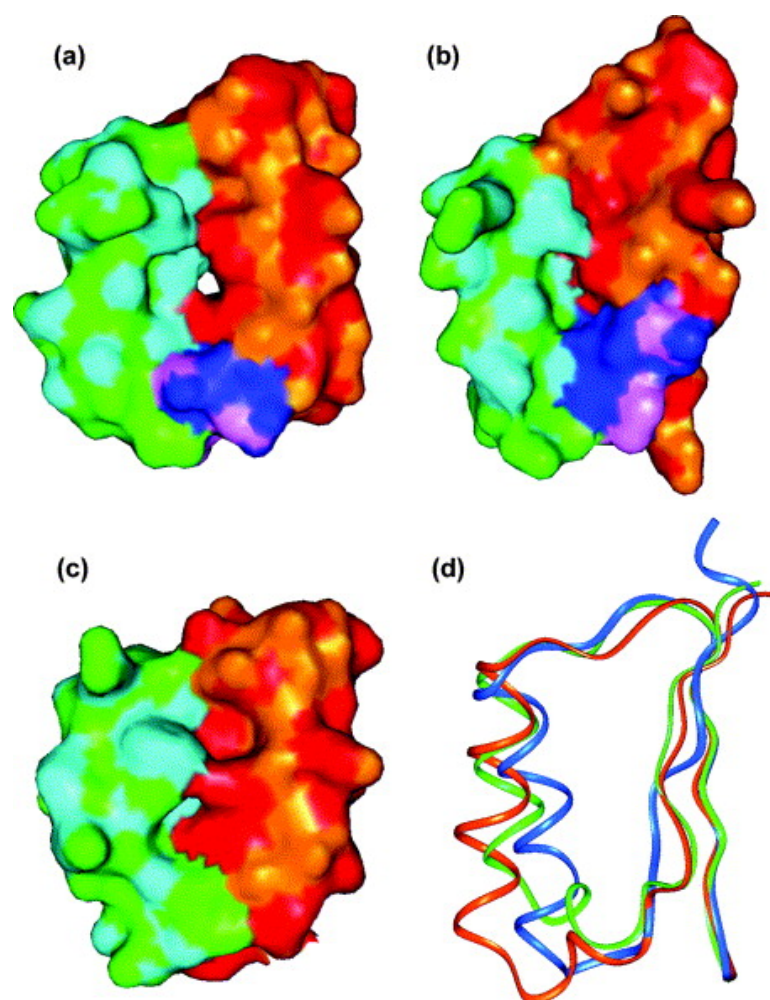


Figure 5.7 Peptide-binding induced changes in the hydrophobic packing between helix 5 and strand 5

Partial surface representations of strand 4, helix 5 and strand 5 regions are shown for (A) Sly1p in complex with the Sed5p peptide (PDB accession number 1MQS), (B) Isolated rSly1N and (C) the N terminal domain of isolated squid munc18-1 (PDB accession number 1EPU). The peptide in (A) is not shown for simplicity. Different secondary structure elements and the different hydrophobic packing elements are highlighted by color coding the side chain carbons (scc) and other atoms (oa) of strand 4 and 5 (scc: red, oa: orange), helix 5 (scc: cyan, oa: green) and the sequence forming the 3_{10} helix in complex structure and part of strand 5 in isolated rSly1N (scc: violet, oa: blue). (D) The ribbon diagrams corresponding to the strand 4-helix 5-strand 5 regions are superimposed for rSly1N (blue), the N-terminal domain of isolated squid munc18-1 (green) and the N-terminal domain of Sly1p in complex with Sed5p peptide (orange). The superimposition was performed using the backbone atoms of strand 4. Insight II (MSI, San Diego, CA) and PYMOL (DeLano Scientific, San Carlos, CA; <http://pymol.sourceforge.net/>) were used to prepare the diagrams.

helix in the Sly1p/Sed5p structure (D151 and K152). The upward movement of residues that form the 3_{10} helix to form strand 5 is illustrated in Figure 5.8A and B, where the backbone of the sequence that forms the 3_{10} helix is colored in blue. It is also noticeable that the first two residues following strand 5 in the isolated rSly1N are forming the last two residues of strand 5 in the peptide-bound yeast Sly1p.

This conformational change upon peptide binding is caused by a two-residue shift in the register of the C-terminal strand 5 with respect to strand 4. However, the formation of a β -bulge in the N terminus of strand 5 upon peptide binding increases the shift in the β -sheet registry from two to three residues (Figure 5.8A, star represents bulge). The presence of another bulge in the C terminus of strand 5 in the peptide-free structure brings the registry difference back to two residues (Figure 5.8B). Strand 5 in both structures contains bulge regions and deviations from the usual geometry and hydrogen bonding pattern of a parallel β sheet. This property might make such a conformational switch easier to occur by peptide binding as such a change will require high energy to break the interactions between strand 5 and 4. The hydrogen bonding of the peptide residues 5-7 with strand 5 to form a short antiparallel β sheet might also weaken the interactions of strand 5 with strand 4 and contribute to the reorganization of the β sheet structure upon peptide binding.

Two hydrophobic residues in strand 5 (V153, V156 in yeast, I138, V141 in rat), which are involved in the binding to F10 residue in the peptide, are displaced ca. 7 Å toward the top of the domain in the absence of peptide as a result of two-residue shift in β strand registry (Figure 5.6B and C). These residues are not properly located for the formation of the hydrophobic pocket required for peptide binding. Thus, peptide binding

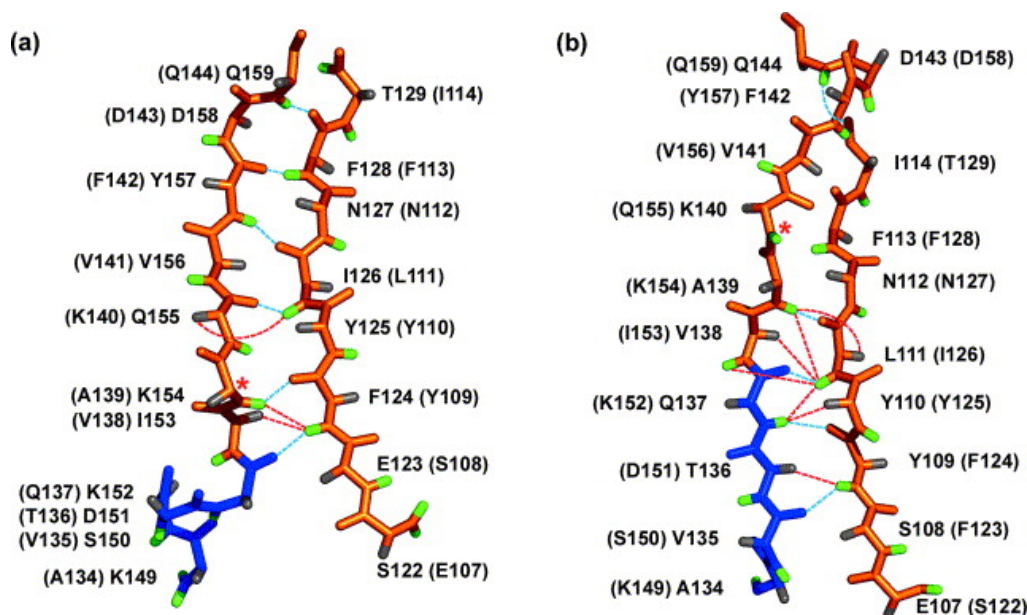


Figure 5.8 The register of strand 5 shifts with respect to strand 4 upon binding of Syntaxin 5 to rSly1N.

Backbone of strands 4 and 5 of (A) the N-terminal domain of Sly1p bound to Sed5p peptide (PDB accession number 1MQS) and (B) the isolated rSly1N are shown as stick models. HN and H_α atoms are colored green and gray, respectively. The residues (A) forming the 3₁₀ helix in the complex structure and (B) the corresponding homologous residues in the isolated rSly1N are colored blue. Other atoms are colored orange. Each residue of Sly1p in (A) is labeled by the residue name and the homologous residue of rSly1N in parenthesis. Each residue of rSly1N in (B) is labeled by the residue name and the homologous residue of Sly1p in parenthesis. Blue broken lines indicate hydrogen bonds. Red broken lines illustrate the interstrand NOEs observed in the 3D NOESY-HSQC strips of Figure 5.4. The similarity between the structures of rSly1N/Syx5 and Sly1p/Sed5p complexes allows the illustration of the NOEs from Figure 1 corresponding to the rSly1N/Syx5(1-33) complex on the structure of the Sly1p/Sed5p complex in (A).

can occur only when these two residues slide down to establish the required interactions and allow the formation of the 3_{10} helix and opening of the groove between helix 5 and strand 5.

Another consequence of the conformational change induced by peptide binding is the change in the length of the loop that connects domain 1 to domain 2. The two residue shift in the register of strands 4 and 5 results in the emergence of two additional residues at the C terminus of the N terminal domain of the isolated rSly1N. The change in the length of the loop between two domains induced by syntaxin binding is expected to cause a substantial alteration in the relative orientation of the two domains affecting the size of the cavity and the overall shape of the molecule.

5.2.5 Syx5-induced conformational changes are conserved in the Sly1 family

The observation that Syx5 peptide binding causes a conformational change in rSly1N raised the question whether this conformational change is common in other SM proteins. The four SM proteins in yeast (Sec1p, Sly1p, Vps45p and Vps33p) and their mammalian homologues (munc18-1, munc18-2, munc18-3, Sly1, Vps45, Vps33a and Vps33b) interact with syntaxins in distinct modes. Only the Sly1 and Vps45 families interact with short N-terminal peptides of syntaxins whereas munc18s require the H_{abc} domain and SNARE motif of syntaxin to fold into a closed conformation for binding. Also, the syntaxin binding surface of Sly1/Vps45s is opposite to that of munc18s. Thus, the conformational change observed in Sly1 is expected not to occur in munc18s, Sec1 and Vps33s. Comparison of the crystal structures of the isolated squid munc18 and the rat munc18 bound to syntaxin 1 indicate great similarity between their N-terminal domains

with 1 Å rms deviation. The superimposition of the structures in Figure 5.7D shows that the separation between helix 5 and strand 5 in the squid munc18 (green) is larger than in the isolated rSly1N (blue) but smaller than in the Sly1p/Sed5p complex (orange). Strand 5 and helix 5 of squid Sly1 are tightly packed against each other due to the bulkier hydrophobic residues at the interface. Importantly, the register of strand 5 with respect to strand 4 in isolated squid munc18 is the same as the register of the rat munc18/syntaxin 1 complex and the Sly1p/Sed5p complex, but not the isolated rSly1N. Thus, the munc18 N-terminal domain is unlikely to experience a conformational change similar to rSly1N.

We performed a multiple sequence alignment of the SM proteins to look for a possible conservation of the rSly1N conformational change. The alignment was done by Jimin Pei in Nick Grishin's laboratory using T-coffee (Notredame *et al.*, 2000b) followed by manual adjustment. Part of the sequence alignment corresponding to helix 5 and strand 5 of the N-terminal domain is shown in Figure 5.9. The sequences can be classified into four families corresponding to four SM proteins in yeast (Figure 5.10). The evolutionary tree shows that these four protein families diverged early in evolution. This observation suggest that, in spite of the common function of SM proteins, this function was probably specialized early in evolution and that such a specialization is conserved from yeast to mammals. The sequence alignment pointed out an intriguing difference in the linker sequence connecting helix 5 to strand 5. This linker sequence is three to four residues longer in the Sly1 family than in all other SM proteins, including Vps45 homologues, which have a similar mode of syntaxin binding to Sly1. Hence, the length of this linker is a distinctive feature of the Sly1 family proteins and is likely to be the key for the conformational change of rSly1. The sequence alignment suggests that the

		helix 5	3 ₁₀	strand 5
Sec1p/Munc18-1				
6981602	Rn	PDALFNEILVK----	SRAAKV	IKTILTEINI
479373	Dm	PEELFNDLCK----	SCAAGK	IKTLKEINI
7511537	Ce	SDQLFSTLSK----	SAAARF	IKTLKEINI
12659318	At	SKELVGHILKKD---	SSVLPR	IGALREMNL
7493457	Sp	KEPLINKLRT----	SRIASK	IRTQVAYL
6320368	Sc	TNPIFQFFQSK---	RYIAQN	LESEKPIEL
Sly1				
2143972	Rn	SRSKLEDIANAALANAVTQ	VAKV	FDQYL
2209280	Dm	TRSKIENLAAAALHAGCVAN	IHRV	VDQYV
7503307	Ce	ARPRLESLASAAVHGGAVSQ	VQKV	VDQYL
4406820	At	PRKFLEELASGTLKSGSVEKV	SKVH	DQYL
7493437	Sp	SRALLEQFAELASKTNTSHM	IHQV	VDQYL
6320395	Sc	PRNLLEDLAQQVSITGKSDK	IKQV	VDQYL
Vps45				
2047326	Rn	SKSDVKSLAE----	ADEQEV	VAEVQEFYG
7299206	Dm	PRIDIKYLAE----	CDESESV	REVKELYA
7497389	Ce	NKYDVKRLAE----	ADKNETV	REVQEVFL
2921406	At	KDTQIHILAD----	SDEQEV	VQQVQEYYA
1175476	Sp	PKSFLERLAE----	SDDFEAV	KSIQEFFL
6321343	Sc	SKSOLERLAE----	SDDLEAV	TKVEEIFQ
Vps33				
12621146	Rn	SLICEQRILKD----	LGVLGS	FIYREEYSL
5052344	Dm	SCLCVSQLEV----	SGVLGS	FGNIEELAW
41019531	Ce	WFFVRESILKTRA-	EGKYWER	LESVKEIPL
13898891	At	SVACEKILEQ-----	EKVHNL	LVTVKEFPL
11359292	Sp	NILFETVLQE-----	EGVFGEL	LVTEWPL
6323428	Sc	IESQLKELSN----	EYTLYP	WDLLPFPQI

Figure 5.9 Multiple sequence alignment of the helix 5-strand 5 region of SM proteins

The four families of the sequence alignment correspond to the four SM protein families in yeast (Sec1p, Sly1p, Vps45p and Vps33p). Each family in the alignment is shown by six sequences from different species. The sequences are identified by their NCBI gene identification number (gi). The abbreviations of the species names are indicated. The gi number corresponding to rat Sly1 is underlined. Residues that have at least 80% conservation within all of the proteins in the alignment are highlighted in red, those within the Sly1p and Vps45p homologues are in blue, and those within either Sly1p or Vps45p homologues are in green. The secondary structure elements are indicated on top of the alignment. Species name abbreviations are: Rn, *Rattus norvegicus*; Dm, *Drosophila melanogaster*; Ce, *Caenorhabditis elegans*; At, *Arabidopsis thaliana*; Sp, *Schizosaccharomyces pombe*; Sc, *Saccharomyces cerevisiae*.

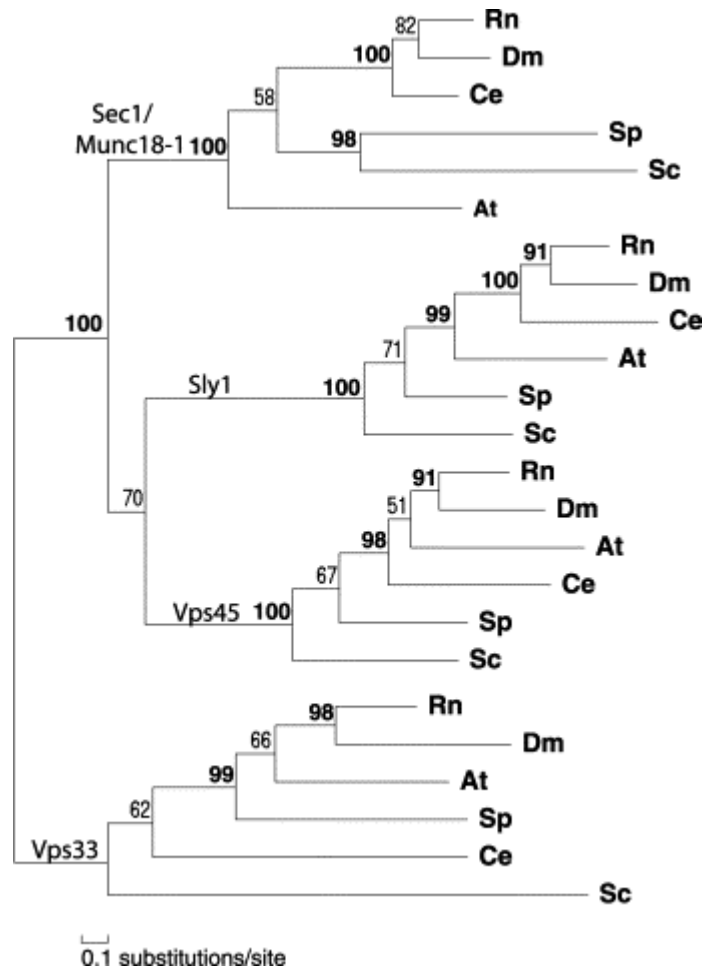


Figure 5.10 An evolutionary tree of SM proteins

Same sequences as in the sequence alignment in Figure 5.9 were used to build the tree. The Vps33p family is separated from the other tree families. The local bootstrap supporting values are indicated at each branch point. Supporting values over 90 are highlighted in bold. The abbreviations for species names are the same as in Figure 5.9.

conformational change induced by peptide binding to rSly1N is conserved among Sly1 family members from yeast to mammals, but does not occur in other SM proteins.

5.3 Discussion

The discovery that SNARE and SM protein families are conserved in most types of intracellular membrane traffic led to the idea that a conserved core machinery controls all fusion events. It was assumed that these proteins have conserved functions and perform them by similar mechanisms. Thus, the interaction of neuronal munc18-1 with the closed conformation of syntaxin 1 resulting in the inhibition of core complex formation was thought as a general mechanism to regulate membrane fusion. However, the discovery that yeast Sec1p binds to assembled SNARE complexes rather than the closed conformation of a syntaxin Sso1p (Carr *et al.*, 1999a), and that yeast vacuolar syntaxin Vam3p has a constitutively open conformation (Dulubova *et al.*, 2001a) indicated the diversity in the modes of interactions of SM proteins with syntaxins and the fundamental differences in their mechanism to mediate or regulate fusion in different compartments and in different species. The diverse mechanism of SM protein/syntaxin interaction was clarified by the finding that Sly1 and Vps45, the SM proteins involved in the ER, Golgi, TGN and endosomes, bind to a short N-terminal peptide of their cognate syntaxins. This result also suggested that most internal membrane compartments have a unified mechanism of fusion, which is different than neurotransmitter release. Our study shows that Syx5 peptide binding causes a striking conformational change in rSly1N, which involves a two-residue shift in the registry of the C-terminal β -strand. The prediction from sequence comparisons suggests that this conformational change is

conserved only in the Sly1 family. Our results uncover a new level of divergence in the SM protein/syntaxin coupling and distinguish the Sly1 and Vps45 families. The four families of SM proteins have distinctions between their functions and mechanism of actions. Our sequence analysis estimate that these differences emerged early in evolution.

During the early evolution, distinct intracellular membrane compartments emerged to give rise to eukaryotic cells. The evolution of the membrane resident proteins that confer a particular identity to the compartments and mediate specific fusion of the compartments is probably the result of or the reason for the evolution of distinct compartments. Subtle mutations that change the interactions of the membrane fusion components or drastic changes that change the nature of the interactions might have contributed to the specific differentiation of the membrane compartments. The different regulatory requirements of membrane traffic in distinct compartments probably resulted in drastic changes in the modes of interactions within the fusion machinery. Detailed characterization of membrane fusion in different compartments is needed to evaluate whether these possibilities are correct.

The critical role of the rSly1p/syntaxin 5 interaction was shown by the observation that abrogation of the rSly1/syntaxin 5 interaction causes complete disruption of the Golgi complex (Yamaguchi *et al.*, 2002) and the inhibition of ER-to-Golgi transport (Williams *et al.*, 2004) in mammalian cells. In contrast, yeast strains bearing single mutation to disrupt Sly1p and Sed5p interaction was fully functional. However, it was unclear whether these mutations can abolish binding completely (Peng and Gallwitz, 2004). Thus, it is possible that residual Sed5p/Sly1p interaction results in the lack of functional defects. The biological importance of the conformational change in rSly1

induced by binding of syntaxin 5 should be explored to understand its mechanistic effect in fusion.

The conformational change, which is conserved only in the Sly1 family proteins, may impose a kinetic barrier for syntaxin binding and select only the cognate sequences to bind. Another possible explanation for the role of the conformational change in Sly1 family proteins is that the two residue shift in the register of the β strand may be important for the activation of Sly1 by increasing/decreasing the length of the loop between domain 1 and 2, thus changing the relative orientation of these domains with respect to each other. The overall shape of the molecule may be altered by this conformational change and modify the accessibility of the arch cavity which is thought to be critical for SM protein function.

The conformational change of rSly1 upon binding to syntaxin 5, independent of its biological importance, constitutes an example of protein structure flexibility. The shift of β strands with respect to each other is reminiscent of the structural rearrangement for the ARF1 GTPase activation (Goldberg, 1998). GTP binding to ARF1 shifts the register of strand 2 and 3 with respect to the rest of the β -sheet and exposes the myristoylated N-terminus, thus coupling the GTP-GDP conformational switch to membrane binding. Both rSly1 and ARF1 undergo conformational changes that result from the ability of β strands to pack against each other via alternative sequences. This ability is also reported in other protein conformational changes such as β -strand swaps or insertions. Some examples are activation/deactivation of serpins (Ye and Goldsmith, 2001), binding of the spindle checkpoint protein Mad2 to its downstream and upstream targets (Luo *et al.*, 2004) and Ca^{2+} binding to the active zone protein Piccolo (Garcia *et al.*, 2004). The increasing

number of observations of promiscuity in β -strand to β -strand interactions suggests that this can be a general mechanism of conformational switches in proteins.

5.4 Materials and Methods

5.4.1 Protein expression and Purification

The construct for the expression of rat Sly1 N-terminal domain (residues (2-147) was prepared in a pGEX-KG vector. Uniformly ^{15}N - or ^{15}N , ^{13}C -labeled recombinant GST-fusion proteins were expressed in *Escherichia coli* BL21 cells (Novagen) in minimal media supplemented with $^{15}\text{NH}_4\text{Cl}$ and with or without [$^{13}\text{C}_6$]glucose (CIL, Andover, MA) as the sole nitrogen and carbon sources. GST-fusion proteins were affinity purified on glutathion sepharose beads (Amersham Pharmacia). The recombinant protein was cleaved with thrombin (Sigma) and further purified by gel filtration in 40 mM Tris (pH 8.1), 150 mM NaCl, 1 mM DTT. The synthetic peptide corresponding to the N-terminal fragment of syntaxin 5 (residues 1-33) was purchased from the Center for Biomedical Inventions (University of Texas Southwestern Medical Center).

5.4.2 NMR Spectroscopy

All NMR experiments were acquired at 27°C on Varian Inova500 or Inova600 spectrophotometers. The rat Sly1 N-terminal domain (residues 2-147) was dissolved in buffer containing 20 mM MES (pH 5.7), 200 mM KCl and 1 mM DTT. The samples were concentrated up to 1.2 mM protein concentration. Initial 3D ^1H - ^{15}N -NOESY-HSQC experiments were performed with samples of ^{15}N -labeled rSly1N in the presence and absence of 2 mM Syx5(1-33) peptide. A ^{15}N -labeled sample and a ^{15}N , ^{13}C -labeled sample

of the isolated rSly1N was used to acquire the pulse-field gradient enhanced NMR experiments to be used for structure determination (Kay *et al.*, 1993; Kay, 1993; Kay *et al.*, 1994; Muhandiram and Kay, 1994). These experiments includes 3D ^1H - ^{15}N total correlated spectroscopy (TOCSY)-HSQC, HNCO, HNCACB, CBCA(CO)NH, (H)C(CO)NH-TOCSY, H(C)(CO)NH-TOCSY and HCCH-TOCSY spectra for resonance assignments, and 2D NOESY, 3D ^1H - ^{15}N -NOESY-HSQC and 3D ^1H - ^{13}C NOESY-HSQC experiments (100 ms mixing time) to measure NOEs for structure determination. A ^1H - ^{13}C HSQC spectrum acquired on a 10% ^{13}C -labeled sample (1 mM) was used to obtain stereospecific assignments of Val and Leu methyl groups. Intensities of exchange cross-peaks with water resonance in the 3D ^1H - ^{15}N -TOCSY-HSQC spectrum was used to determine the protection of the amide groups from the solvent. All data were processed with the NmrPipe (Delaglio *et al.*, 1995) program and analyzed with NMRview (Johnson *et al.*, 1994).

5.4.3 Structure Calculations

5.4.3.1 Backbone Assignments

The ^1H - ^{15}N HSQC spectrum provides cross-peaks for each directly bonded proton-nitrogen pair of atoms in a protein, mostly including the backbone amide groups from each non-proline residue and side chains of asparagines, glutamines, arginines and tryptophans. The cross-peaks on the HSQC spectrum were picked and the chemical shift values of amide nitrogen (N) and amide proton (NH) of each residue were organized into a table. The chemical shifts of carbonyl carbon (C) were obtained from the HNCO spectrum and added to the table.

The backbone assignments were obtained by using three-dimensional (3D) HNCACB and CBCA(CO)NH experiments. The HNCACB experiment correlates the amide H(i) and N(i) frequencies with both the intraresidues C_α(i) and the sequential C_α(i-1) due to the similar sizes of the one bond J_{NC_α} coupling constant (11 Hz) and the two bond J_{NC_α} coupling constant (-7 Hz), whereas the CBCA(CO)NH experiment provides only interresidue connectivity due to the correlation of the amide H(i) and N(i) frequencies with the C_α(i-1) via the carbonyl resonance. Sequential HN/HN nuclear Overhauser effect (NOE) connectivities were used to confirm the assignments and resolve ambiguities.

The secondary structure elements of the rSly1N were elucidated by the comparison of the C_α and C_β chemical shifts of all residues with the chemical shifts characteristic of random coil (Wishart *et al.*, 1994). The difference values obtained by the equation :

$$\Delta C_{\alpha} - \Delta C_{\beta} = (C_{\alpha} - C_{\alpha\text{random}}) - (C_{\beta} - C_{\beta\text{random}})$$

were plotted for each residue. The regions with positive value represent α -helices and the regions with negative values represent β -strands.

5.4.3.2 Side Chain Assignments

In addition to the already mentioned HNCO, HNCACB and CBCA(CO)NH experiments, we used (TOCSY)-HSQC, (H)C(CO)NH-TOCSY, H(C)(CO)NH-TOCSY and HCCH-TOCSY spectra for resonance assignments, and 2D NOESY, 3D ¹H-¹⁵N-NOESY-HSQC and 3D ¹H-¹³C NOESY-HSQC experiments to measure NOEs. ¹H-¹⁵N (TOCSY)-HSQC yields intraresidue ¹⁵N-NH connectivity with the aliphatic protons of the same residue. (H)C(CO)NH-TOCSY correlates aliphatic carbons of one residue with

the ^{15}N -NH of the following residue whereas H(C)(CO)NH-TOCSY correlates aliphatic protons of one residue with the ^{15}N -NH of the following residue. Correlations between the aliphatic protons with the intraresidue aliphatic carbon and protons are obtained from HCCH-TOCSY experiment. The side chain assignments obtained from these triple resonance experiments were confirmed by the 3D ^1H - ^{15}N -NOESY-HSQC and 3D ^1H - ^{13}C NOESY-HSQC experiments.

Stereospecific assignments of Val and Leu methyl groups were obtained from constant time ^1H - ^{13}C HSQC spectrum of a 10% ^{13}C -labeled sample (1 mM concentration). NH_2 groups in Asn and Gln were assigned using ^1H , ^{15}N -NOESY-HSQC spectrum. The aromatic side-chain assignments were obtained from 2D homonuclear DQF-COSY, NOESY and TOCSY experiments acquired with a ^{15}N -labeled sample in D_2O as solvent, in combination with 3D ^1H , ^{15}N -NOESY-HSQC and ^1H - ^{13}C -NOESY-HSQC spectra.

5.4.3.3 NOE Assignments and Structure Calculation

Nuclear Overhauser effects for structure determination were measured from 2D NOESY, and 3D ^1H - ^{15}N -NOESY-HSQC and 3D ^1H - ^{13}C NOESY-HSQC experiments. NOE crosspeaks were manually picked and their intensities were classified as strong, medium, weak and very weak corresponding to restraints of 1.8-2.8 Å, 1.8-3.5 Å, 1.8-5.0 Å and 1.8-6.0 Å, respectively, with appropriate pseudoatom corrections. The NOEs from the methyl groups were classified using different restraints as they have higher intensities than other NOEs. A partial model of the structure based on homology was generated by the 3djigsaw program (www.bmm.icnet.uk/~3djigsaw) and was used for NOE assignments. For regions where the model is not well defined, unique long range NOEs were found to determine the overall conformation.

Phi and psi torsion angle restraints were obtained by the analysis of HN, ^{15}N , $^{13}\text{C}_\alpha$, ^{13}CO and $^{13}\text{C}_\beta$ chemical shifts using the program TALOS (Cornilescu *et al.*, 1999). The dihedral angles were restrained to maximum 22.5° or 1.5 times the standard deviation observed in the TALOS database matches. Protection of amide protons from the solvent was measured from the intensities of exchange cross-peaks with the water resonance in ^1H - ^{15}N -NOESY-HSQC and ^1H - ^{15}N -TOCSY-HSQC experiments. The hydrogen bonds were restrained by setting the H/O distance restraints to 1.3-2.5 Å and N/O distance restraints to 2.3-3.5 Å. Initial calculations and the refinement of the rSly1N structures were done by torsion angle simulated annealing with CNS (Brunger *et al.*, 1998). A total of 2133 restraints were used to calculate structures. 20 structures with the lowest NOE energy were selected out of 1400 calculated structures.

The structures have been deposited in the Protein Data Bank with the accession code 1Y9J.

5.4.4 Sequence Analysis

The homologues of SM proteins were searched by PSI-BLAST (Altschul *et al.*, 1997). Syntaxin binding protein 1 from *Rattus Norvegicus* (NCBI gene identification number 6981602) was used to start the query and PSI-BLAST iterations were performed to converge on the nr database (May 2001, 686,213 sequences, 216,043,563 total letters) with e-value cutoff 0.001. The resulting homologues were grouped by single-linkage clustering (1 bit per site threshold, about 50% identity) as implemented in the SEALS package (Walker and Koonin, 1997). Subsequent PSI-BLAST iterations were performed using the representative sequences from each group as new queries. After two rounds of

extensive searches, about 100 SM proteins were identified. T-Coffee was (Notredame *et al.*, 2000a) used to align the sequences and the alignment was adjusted manually. Representative sequences from six selected species were used to build a maximum-likelihood tree using the MOLPHY package (version 2.3). For tree building, only the positions with gap fraction less than 20% were selected. The local estimates of bootstrap percentages were obtained by the REL method (Hasegawa *et al.*, 1991), as implemented in the ProtML program of MOLPHY.

REFERENCES

1. Altschul SF, Madden TL, Schaffer AA, Zhang J, Zhang Z, Miller W, and Lipman DJ (1997) Gapped BLAST and PSI-BLAST: a new generation of protein database search programs. *Nucleic Acids Res*, **25**, 3389-3402.
2. Antonin W, Fasshauer D, Becker S, Jahn R, and Schneider TR (2002) Crystal structure of the endosomal SNARE complex reveals common structural principles of all SNAREs. *Nat Struct Biol*, **9**, 107-111.
3. Arac D, Murphy T, and Rizo J (2003) Facile detection of protein-protein interactions by one-dimensional NMR spectroscopy. *Biochemistry*, **42**, 2774-2780.
4. Aravamudan B, Fergestad T, Davis WS, Rodesch CK, and Broadie K (1999) Drosophila UNC-13 is essential for synaptic transmission. *Nat Neurosci*, **2**, 965-971.
5. Augustin I, Rosenmund C, Sudhof TC, and Brose N (1999) Munc13-1 is essential for fusion competence of glutamatergic synaptic vesicles. *Nature*, **400**, 457-461.
6. Bai J, Earles CA, Lewis JL, and Chapman ER (2000) Membrane-embedded synaptotagmin penetrates cis or trans target membranes and clusters via a novel mechanism. *J Biol Chem*, **275**, 25427-25435.
7. Bai J, Wang CT, Richards DA, Jackson MB, and Chapman ER (2004) Fusion Pore Dynamics Are Regulated by Synaptotagmin-t-SNARE Interactions. *Neuron*, **41**, 929-942.
8. Bai J, Wang P, and Chapman ER (2002) C2A activates a cryptic Ca(2+)-triggered membrane penetration activity within the C2B domain of synaptotagmin I. *Proc Natl Acad Sci U S A*, **99**, 1665-1670.
9. Banerjee A, Kowalchyk JA, DasGupta BR, and Martin TF (1996) SNAP-25 is required for a late postdocking step in Ca²⁺-dependent exocytosis. *J Biol Chem*, **271**, 20227-20230.
10. Barrett EF and Stevens CF (1972) The kinetics of transmitter release at the frog neuromuscular junction. *J Physiol*, **227**, 691-708.
11. Bennett MK, Calakos N, and Scheller RH (1992) Syntaxin: a synaptic protein implicated in docking of synaptic vesicles at presynaptic active zones. *Science*, **257**, 255-259.
12. Bennett MK and Scheller RH (1994) A molecular description of synaptic vesicle membrane trafficking. *Annu Rev Biochem*, **63**, 63-100.

13. Bennett MR (1999) The concept of a calcium sensor in transmitter release. *Prog Neurobiol*, **59**, 243-277.
14. Bentz J (2000) Minimal aggregate size and minimal fusion unit for the first fusion pore of influenza hemagglutinin-mediated membrane fusion. *Biophys J*, **78**, 227-245.
15. Betz A, Okamoto M, Benseler F, and Brose N (1997) Direct interaction of the rat unc-13 homologue Munc13-1 with the N terminus of syntaxin. *J Biol Chem*, **272**, 2520-2526.
16. Betz WJ and Bewick GS (1992) Optical analysis of synaptic vesicle recycling at the frog neuromuscular junction. *Science*, **255**, 200-203.
17. Blasi J, Chapman ER, Link E, Binz T, Yamasaki S, De Camilli P, Sudhof TC, Niemann H, and Jahn R (1993a) Botulinum neurotoxin A selectively cleaves the synaptic protein SNAP-25. *Nature*, **365**, 160-163.
18. Blasi J, Chapman ER, Yamasaki S, Binz T, Niemann H, and Jahn R (1993b) Botulinum neurotoxin C1 blocks neurotransmitter release by means of cleaving HPC-1/syntaxin. *EMBO J*, **12**, 4821-4828.
19. Bollmann JH, Sakmann B, and Borst JG (2000) Calcium sensitivity of glutamate release in a calyx-type terminal. *Science*, **289**, 953-957.
20. Bommert K, Charlton MP, DeBello WM, Chin GJ, Betz H, and Augustine GJ (1993) Inhibition of neurotransmitter release by C2-domain peptides implicates synaptotagmin in exocytosis. *Nature*, **363**, 163-165.
21. Borden CR, Stevens CF, Sullivan JM, and Zhu Y (2005) Synaptotagmin mutants Y311N and K326/327A alter the calcium dependence of neurotransmission. *Mol Cell Neurosci*, **29**, 462-470.
22. Bracher A, Perrakis A, Dresbach T, Betz H, and Weissenhorn W (2000) The X-ray crystal structure of neuronal Sec1 from squid sheds new light on the role of this protein in exocytosis. *Structure Fold Des*, **8**, 685-694.
23. Bracher A and Weissenhorn W (2002) Structural basis for the Golgi membrane recruitment of Sly1p by Sed5p. *EMBO J*, **21**, 6114-6124.
24. Broadie K, Prokop A, Bellen HJ, O'Kane CJ, Schulze KL, and Sweeney ST (1995) Syntaxin and synaptobrevin function downstream of vesicle docking in *Drosophila*. *Neuron*, **15**, 663-673.
25. Brose N, Hofmann K, Hata Y, and Sudhof TC (1995) Mammalian homologues of *Caenorhabditis elegans* unc-13 gene define novel family of C2-domain proteins. *J Biol Chem*, **270**, 25273-25280.

26. Brose N, Petrenko AG, Sudhof TC, and Jahn R (1992b) Synaptotagmin: a calcium sensor on the synaptic vesicle surface. *Science*, **256**, 1021-1025.
27. Brose N, Petrenko AG, Sudhof TC, and Jahn R (1992a) Synaptotagmin: a calcium sensor on the synaptic vesicle surface. *Science*, **256**, 1021-1025.
28. Brunger AT, Adams PD, Clore GM, DeLano WL, Gros P, Grosse-Kunstleve RW, Jiang JS, Kuszewski J, Nilges M, Pannu NS, Read RJ, Rice LM, Simonson T, and Warren GL (1998) Crystallography & NMR system: A new software suite for macromolecular structure determination. *Acta Crystallogr D Biol Crystallogr*, **54** (Pt 5), 905-921.
29. Bryant NJ and James DE (2001) Vps45p stabilizes the syntaxin homologue Tlg2p and positively regulates SNARE complex formation. *EMBO J*, **20**, 3380-3388.
30. Butz S, Fernandez-Chacon R, Schmitz F, Jahn R, and Sudhof TC (1999) The subcellular localizations of atypical synaptotagmins III and VI. Synaptotagmin III is enriched in synapses and synaptic plasma membranes but not in synaptic vesicles. *J Biol Chem*, **274**, 18290-18296.
31. Carr CM, Grote E, Munson M, Hughson FM, and Novick PJ (1999b) Sec1p binds to SNARE complexes and concentrates at sites of secretion. *J Cell Biol*, **146**, 333-344.
32. Carr CM, Grote E, Munson M, Hughson FM, and Novick PJ (1999a) Sec1p binds to SNARE complexes and concentrates at sites of secretion. *J Cell Biol*, **146**, 333-344.
33. Chapman ER, An S, Edwardson JM, and Jahn R (1996) A novel function for the second C2 domain of synaptotagmin. Ca²⁺-triggered dimerization. *J Biol Chem*, **271**, 5844-5849.
34. Chapman ER and Davis AF (1998a) Direct interaction of a Ca²⁺-binding loop of synaptotagmin with lipid bilayers. *J Biol Chem*, **273**, 13995-14001.
35. Chapman ER, Desai RC, Davis AF, and Tornehl CK (1998b) Delineation of the oligomerization, AP-2 binding, and synprint binding region of the C2B domain of synaptotagmin. *J Biol Chem*, **273**, 32966-32972.
36. Chapman ER, Hanson PI, An S, and Jahn R (1995) Ca²⁺ regulates the interaction between synaptotagmin and syntaxin 1. *J Biol Chem*, **270**, 23667-23671.
37. Chen X, Arac D, Want TM, and Gilpin C (2005a) An evaluation of SNARE-mediated lipid mixing. *in press*.
38. Chen X, Tang J, Sudhof TC, and Rizo J (2005b) Are neuronal SNARE proteins Ca²⁺ sensors? *J Mol Biol*, **347**, 145-158.

39. Chen X, Tomchick DR, Kovrigin E, Arac D, Machius M, Sudhof TC, and Rizo J (2002) Three-dimensional structure of the complexin/SNARE complex. *Neuron*, **33**, 397-409.
40. Chen YA and Scheller RH (2001) SNARE-mediated membrane fusion. *Nat Rev Mol Cell Biol*, **2**, 98-106.
41. Chernomordik L (1996) Non-bilayer lipids and biological fusion intermediates. *Chem Phys Lipids*, **81**, 203-213.
42. Chernomordik LV, Melikyan GB, and Chizmadzhev YA (1987) Biomembrane fusion: a new concept derived from model studies using two interacting planar lipid bilayers. *Biochim Biophys Acta*, **906**, 309-352.
43. Chieriegatti E, Witkin JW, and Baldini G (2002) SNAP-25 and synaptotagmin 1 function in Ca²⁺-dependent reversible docking of granules to the plasma membrane. *Traffic*, **3**, 496-511.
44. Cornilescu G, Delaglio F, and Bax A (1999) Protein backbone angle restraints from searching a database for chemical shift and sequence homology. *J Biomol NMR*, **13**, 289-302.
45. Dai H, Shin OH, Machius M, Tomchick DR, Sudhof TC, and Rizo J (2004) Structural basis for the evolutionary inactivation of Ca²⁺ binding to synaptotagmin 4. *Nat Struct Mol Biol*, **11**, 844-849.
46. Davis AF, Bai J, Fasshauer D, Wolowick MJ, Lewis JL, and Chapman ER (1999) Kinetics of synaptotagmin responses to Ca²⁺ and assembly with the core SNARE complex onto membranes. *Neuron*, **24**, 363-376.
47. Davletov BA and Sudhof TC (1993) A single C2 domain from synaptotagmin I is sufficient for high affinity Ca²⁺/phospholipid binding. *J Biol Chem*, **268**, 26386-26390.
48. Delaglio F, Grzesiek S, Vuister GW, Zhu G, Pfeifer J, and Bax A (1995) Nmrpipe - A Multidimensional Spectral Processing System Based on Unix Pipes. *Journal of Biomolecular Nmr*, **6**, 277-293.
49. Desai RC, Vyas B, Earles CA, Littleton JT, Kowalchuck JA, Martin TF, and Chapman ER (2000) The C2B domain of synaptotagmin is a Ca(2+)-sensing module essential for exocytosis. *J Cell Biol*, **150**, 1125-1136.
50. Deveraux QL and Reed JC (1999) IAP family proteins--suppressors of apoptosis. *Genes Dev*, **13**, 239-252.
51. DiAntonio A and Schwarz TL (1994) The effect on synaptic physiology of synaptotagmin mutations in *Drosophila*. *Neuron*, **12**, 909-920.

52. Dobrunz LE and Garner CC (2002) Priming plasticity. *Nature*, **415**, 277-278.
53. Dodge FA, Jr. and Rahamimoff R (1967) Co-operative action a calcium ions in transmitter release at the neuromuscular junction. *J Physiol*, **193**, 419-432.
54. Dresbach T, Burns ME, O'Connor V, DeBello WM, Betz H, and Augustine GJ (1998) A neuronal Sec1 homolog regulates neurotransmitter release at the squid giant synapse. *J Neurosci*, **18**, 2923-2932.
55. Du C, Fang M, Li Y, Li L, and Wang X (2000) Smac, a mitochondrial protein that promotes cytochrome c-dependent caspase activation by eliminating IAP inhibition. *Cell*, **102**, 33-42.
56. Dulubova I, Sugita S, Hill S, Hosaka M, Fernandez I, Sudhof TC, and Rizo J (1999) A conformational switch in syntaxin during exocytosis: role of munc18. *EMBO J*, **18**, 4372-4382.
57. Dulubova I, Yamaguchi T, Arac D, Li H, Huryeva I, Min SW, Rizo J, and Sudhof TC (2003) Convergence and divergence in the mechanism of SNARE binding by Sec1/Munc18-like proteins. *Proc Natl Acad Sci U S A*, **100**, 32-37.
58. Dulubova I, Yamaguchi T, Gao Y, Min SW, Huryeva I, Sudhof TC, and Rizo J (2002) How Tlg2p/Syntaxin 16 "Snares" Vps45. *EMBO J*.
59. Dulubova I, Yamaguchi T, Wang Y, Sudhof TC, and Rizo J (2001b) Vam3p structure reveals conserved and divergent properties of syntaxins. *Nat Struct Biol*, **8**, 258-264.
60. Dulubova I, Yamaguchi T, Wang Y, Sudhof TC, and Rizo J (2001a) Vam3p structure reveals conserved and divergent properties of syntaxins. *Nat Struct Biol*, **8**, 258-264.
61. Earles CA, Bai J, Wang P, and Chapman ER (2001) The tandem C2 domains of synaptotagmin contain redundant Ca²⁺ binding sites that cooperate to engage t-SNAREs and trigger exocytosis. *J Cell Biol*, **154**, 1117-1123.
62. Fancy DA and Kodadek T (1999) Chemistry for the analysis of protein-protein interactions: rapid and efficient cross-linking triggered by long wavelength light. *Proc Natl Acad Sci U S A*, **96**, 6020-6024.
63. Fasshauer D, Bruns D, Shen B, Jahn R, and Brunger AT (1997a) A structural change occurs upon binding of syntaxin to SNAP-25. *J Biol Chem*, **272**, 4582-4590.
64. Fasshauer D, Eliason WK, Brunger AT, and Jahn R (1998) Identification of a minimal core of the synaptic SNARE complex sufficient for reversible assembly and disassembly. *Biochemistry*, **37**, 10354-10362.

65. Fasshauer D, Otto H, Eliason WK, Jahn R, and Brunger AT (1997b) Structural changes are associated with soluble N-ethylmaleimide-sensitive fusion protein attachment protein receptor complex formation. *J Biol Chem*, **272**, 28036-28041.
66. Fernandez I, Arac D, Ubach J, Gerber SH, Shin O, Gao Y, Anderson RG, Sudhof TC, and Rizo J (2001) Three-dimensional structure of the synaptotagmin 1 c(2)b-domain. Synaptotagmin 1 as a phospholipid binding machine. *Neuron*, **32**, 1057-1069.
67. Fernandez I, Ubach J, Dulubova I, Zhang X, Sudhof TC, and Rizo J (1998) Three-dimensional structure of an evolutionarily conserved N-terminal domain of syntaxin 1A. *Cell*, **94**, 841-849.
68. Fernandez-Chacon R, Konigstorfer A, Gerber SH, Garcia J, Matos MF, Stevens CF, Brose N, Rizo J, Rosenmund C, and Sudhof TC (2001) Synaptotagmin I functions as a calcium regulator of release probability. *Nature*, **410**, 41-49.
69. Fernandez-Chacon R, Shin OH, Konigstorfer A, Matos MF, Meyer AC, Garcia J, Gerber SH, Rizo J, Sudhof TC, and Rosenmund C (2002) Structure/function analysis of Ca²⁺ binding to the C2A domain of synaptotagmin 1. *J Neurosci*, **22**, 8438-8446.
70. Ferro-Novick S and Jahn R (1994) Vesicle fusion from yeast to man. *Nature*, **370**, 191-193.
71. Frazier AA, Roller CR, Havelka JJ, Hinderliter A, and Cafiso DS (2003) Membrane-bound orientation and position of the synaptotagmin I C2A domain by site-directed spin labeling. *Biochemistry*, **42**, 96-105.
72. Fukuda M, Aruga J, Niinobe M, Aimoto S, and Mikoshiba K (1994) Inositol-1,3,4,5-tetrakisphosphate binding to C2B domain of IP4BP/synaptotagmin II. *J Biol Chem*, **269**, 29206-29211.
73. Fukuda M and Mikoshiba K (2000) Calcium-dependent and -independent hetero-oligomerization in the synaptotagmin family. *J Biochem (Tokyo)*, **128**, 637-645.
74. Gallwitz D and Jahn R (2003) The riddle of the Sec1/Munc-18 proteins - new twists added to their interactions with SNAREs. *Trends Biochem Sci*, **28**, 113-116.
75. Garcia EP, Gatti E, Butler M, Burton J, and De Camilli P (1994) A rat brain Sec1 homologue related to Rop and UNC18 interacts with syntaxin. *Proc Natl Acad Sci U S A*, **91**, 2003-2007.
76. Garcia EP, McPherson PS, Chilcote TJ, Takei K, and De Camilli P (1995) rbSec1A and B colocalize with syntaxin 1 and SNAP-25 throughout the axon, but are not in a stable complex with syntaxin. *J Cell Biol*, **129**, 105-120.

77. Garcia J, Gerber SH, Sugita S, Sudhof TC, and Rizo J (2004) A conformational switch in the Piccolo C2A domain regulated by alternative splicing. *Nat Struct Mol Biol*, **11**, 45-53.
78. Garcia RA, Forde CE, and Godwin HA (2000) Calcium triggers an intramolecular association of the C2 domains in synaptotagmin. *Proc Natl Acad Sci U S A*, **97**, 5883-5888.
79. Gavin AC, Bosche M, Krause R, Grandi P, Marzioch M, Bauer A, Schultz J, Rick JM, Michon AM, Cruciat CM, Remor M, Hofert C, Schelder M, Brajenovic M, Ruffner H, Merino A, Klein K, Hudak M, Dickson D, Rudi T, Gnau V, Bauch A, Bastuck S, Huhse B, Leutwein C, Heurtier MA, Copley RR, Edelmann A, Querfurth E, Rybin V, Drewes G, Raida M, Bouwmeester T, Bork P, Seraphin B, Kuster B, Neubauer G, and Superti-Furga G (2002) Functional organization of the yeast proteome by systematic analysis of protein complexes. *Nature*, **415**, 141-147.
80. Geppert M, Goda Y, Hammer RE, Li C, Rosahl TW, Stevens CF, and Sudhof TC (1994) Synaptotagmin I: a major Ca²⁺ sensor for transmitter release at a central synapse. *Cell*, **79**, 717-727.
81. Gerber SH, Rizo J, and Sudhof TC (2002) Role of electrostatic and hydrophobic interactions in ca(2+)-dependent phospholipid binding by the c(2)a-domain from synaptotagmin I. *Diabetes*, **51 Suppl 1**, S12-S18.
82. Gerona RR, Larsen EC, Kowalchuk JA, and Martin TF (2000) The C terminus of SNAP25 is essential for Ca(2+)-dependent binding of synaptotagmin to SNARE complexes. *J Biol Chem*, **275**, 6328-6336.
83. Goldberg J (1998) Structural basis for activation of ARF GTPase: mechanisms of guanine nucleotide exchange and GTP-myristoyl switching. *Cell*, **95**, 237-248.
84. Gronenborn AM and Clore GM (1993) Identification of the contact surface of a streptococcal protein G domain complexed with a human Fc fragment. *J Mol Biol*, **233**, 331-335.
85. Grote E, Carr CM, and Novick PJ (2000) Ordering the final events in yeast exocytosis. *J Cell Biol*, **151**, 439-452.
86. Hanson PI, Roth R, Morisaki H, Jahn R, and Heuser JE (1997) Structure and conformational changes in NSF and its membrane receptor complexes visualized by quick-freeze/deep-etch electron microscopy. *Cell*, **90**, 523-535.
87. Harrison SD, Broadie K, van de GJ, and Rubin GM (1994) Mutations in the Drosophila Rop gene suggest a function in general secretion and synaptic transmission. *Neuron*, **13**, 555-566.

88. Hartmann W and Galla HJ (1978) Binding of polylysine to charged bilayer membranes: molecular organization of a lipid-peptide complex. *Biochim Biophys Acta*, **509**, 474-490.
89. Hasegawa M, Kishino H, and Saitou N (1991) On the maximum likelihood method in molecular phylogenetics. *J Mol Evol*, **32**, 443-445.
90. Hata Y, Slaughter CA, and Sudhof TC (1993) Synaptic vesicle fusion complex contains unc-18 homologue bound to syntaxin. *Nature*, **366**, 347-351.
91. Hayashi T, McMahon H, Yamasaki S, Binz T, Hata Y, Sudhof TC, and Niemann H (1994) Synaptic vesicle membrane fusion complex: action of clostridial neurotoxins on assembly. *EMBO J*, **13**, 5051-5061.
92. Hayashi T, Yamasaki S, Nauenburg S, Binz T, and Niemann H (1995) Disassembly of the reconstituted synaptic vesicle membrane fusion complex in vitro. *EMBO J*, **14**, 2317-2325.
93. Helm CA and Israelachvili JN (1993) Forces between phospholipid bilayers and relationship to membrane fusion. *Methods Enzymol*, **220**, 130-143.
94. Hess DT, Slater TM, Wilson MC, and Skene JH (1992) The 25 kDa synaptosomal-associated protein SNAP-25 is the major methionine-rich polypeptide in rapid axonal transport and a major substrate for palmitoylation in adult CNS. *J Neurosci*, **12**, 4634-4641.
95. Ho Y, Gruhler A, Heilbut A, Bader GD, Moore L, Adams SL, Millar A, Taylor P, Bennett K, Boutilier K, Yang L, Wolting C, Donaldson I, Schandorff S, Shewnarane J, Vo M, Taggart J, Goudreau M, Muskata B, Alfarano C, Dewar D, Lin Z, Michalickova K, Willems AR, Sassi H, Nielsen PA, Rasmussen KJ, Andersen JR, Johansen LE, Hansen LH, Jespersen H, Podtelejnikov A, Nielsen E, Crawford J, Poulsen V, Sorensen BD, Matthiesen J, Hendrickson RC, Gleeson F, Pawson T, Moran MF, Durocher D, Mann M, Hogue CW, Figeys D, and Tyers M (2002) Systematic identification of protein complexes in *Saccharomyces cerevisiae* by mass spectrometry. *Nature*, **415**, 180-183.
96. HODGKIN AL (1964) THE IONIC BASIS OF NERVOUS CONDUCTION. *Science*, **145**, 1148-1154.
97. Hosono R, Hekimi S, Kamiya Y, Sassa T, Murakami S, Nishiwaki K, Miwa J, Taketo A, and Kodaira KI (1992) The unc-18 gene encodes a novel protein affecting the kinetics of acetylcholine metabolism in the nematode *Caenorhabditis elegans*. *J Neurochem*, **58**, 1517-1525.
98. Hu K, Carroll J, Fedorovich S, Rickman C, Sukhodub A, and Davletov B (2002) Vesicular restriction of synaptobrevin suggests a role for calcium in membrane fusion. *Nature*, **415**, 646-650.

99. HUXLEY AF (1964) EXCITATION AND CONDUCTION IN NERVE: QUANTITATIVE ANALYSIS. *Science*, **145**, 1154-1159.
100. Ikura M, Clore GM, Gronenborn AM, Zhu G, Klee CB, and Bax A (1992) Solution structure of a calmodulin-target peptide complex by multidimensional NMR. *Science*, **256**, 632-638.
101. Ishizuka T, Saisu H, Odani S, and Abe T (1995) Synaphin: a protein associated with the docking/fusion complex in presynaptic terminals. *Biochem Biophys Res Commun*, **213**, 1107-1114.
102. Ito T, Chiba T, Ozawa R, Yoshida M, Hattori M, and Sakaki Y (2001) A comprehensive two-hybrid analysis to explore the yeast protein interactome. *Proc Natl Acad Sci U S A*, **98**, 4569-4574.
103. Jahn R, Lang T, and Sudhof TC (2003) Membrane fusion. *Cell*, **112**, 519-533.
104. Jahn R and Sudhof TC (1999) Membrane fusion and exocytosis. *Annu Rev Biochem*, **68**, 863-911.
105. Jessell TM and Kandel ER (1993) Synaptic transmission: a bidirectional and self-modifiable form of cell-cell communication. *Cell*, **72 Suppl**, 1-30.
106. Johnson BA and Blevins RA (1994) Nmr View - A Computer-Program for the Visualization and Analysis of Nmr Data. *Journal of Biomolecular Nmr*, **4**, 603-614.
107. Katz B and Miledi R (1968) The role of calcium in neuromuscular facilitation. *J Physiol*, **195**, 481-492.
108. Kay LE (1993) Pulsed-Field Gradient-Enhanced 3-Dimensional Nmr Experiment for Correlating C-13-Alpha-Beta, C-13', and H-1-Alpha Chemical-Shifts in Uniformly C-13-Labeled Proteins Dissolved in H2O. *Journal of the American Chemical Society*, **115**, 2055-2057.
109. Kay LE, Xu GY, Singer AU, Muhandiram DR, and Formankay JD (1993) A Gradient-Enhanced Hcch Tocsy Experiment for Recording Side-Chain H-1 and C-13 Correlations in H2O Samples of Proteins. *Journal of Magnetic Resonance Series B*, **101**, 333-337.
110. Kay LE, Xu GY, and Yamazaki T (1994) Enhanced-Sensitivity Triple-Resonance Spectroscopy with Minimal H2O Saturation. *Journal of Magnetic Resonance Series A*, **109**, 129-133.
111. Kee Y and Scheller RH (1996) Localization of synaptotagmin-binding domains on syntaxin. *J Neurosci*, **16**, 1975-1981.

112. Kikkawa U, Kishimoto A, and Nishizuka Y (1989) The protein kinase C family: heterogeneity and its implications. *Annu Rev Biochem*, **58**, 31-44.
113. Kipp RA, Case MA, Wist AD, Cresson CM, Carrell M, Griner E, Wiita A, Albinia PA, Chai J, Shi Y, Semmelhack MF, and McLendon GL (2002) Molecular targeting of inhibitor of apoptosis proteins based on small molecule mimics of natural binding partners. *Biochemistry*, **41**, 7344-7349.
114. Koushika SP, Richmond JE, Hadwiger G, Weimer RM, Jorgensen EM, and Nonet ML (2001) A post-docking role for active zone protein Rim. *Nat Neurosci*, **4**, 997-1005.
115. Kraulis PJ (1991) Molscript - A Program to Produce Both Detailed and Schematic Plots of Protein Structures. *Journal of Applied Crystallography*, **24**, 946-950.
116. Kremer JR, Mastronarde DN, and McIntosh JR (1996) Computer visualization of three-dimensional image data using IMOD. *J Struct Biol*, **116**, 71-76.
117. Kweon DH, Kim CS, and Shin YK (2003) Regulation of neuronal SNARE assembly by the membrane. *Nat Struct Biol*, **10**, 440-447.
118. Laskowski RA, Macarthur MW, Moss DS, and Thornton JM (1993) Procheck - A Program to Check the Stereochemical Quality of Protein Structures. *Journal of Applied Crystallography*, **26**, 283-291.
119. Leveque C, Boudier JA, Takahashi M, and Seagar M (2000) Calcium-dependent dissociation of synaptotagmin from synaptic SNARE complexes. *J Neurochem*, **74**, 367-374.
120. Li C, Ullrich B, Zhang JZ, Anderson RG, Brose N, and Sudhof TC (1995) Ca(2+)-dependent and -independent activities of neural and non-neural synaptotagmins. *Nature*, **375**, 594-599.
121. Li L, Shin OH, Rhee SH, Arac D, Rizo J, Sudhof TC, and Rosenmund C (2005) Phosphatidylinositolphosphates are co-activators of Ca²⁺-binding by synaptotagmin 1: Functional asymmetry of synaptotagmin 1 C₂-domains. *submitted*.
122. Lin RC and Scheller RH (1997) Structural organization of the synaptic exocytosis core complex. *Neuron*, **19**, 1087-1094.
123. Link E, Edelmann L, Chou JH, Binz T, Yamasaki S, Eisel U, Baumert M, Sudhof TC, Niemann H, and Jahn R (1992) Tetanus toxin action: inhibition of neurotransmitter release linked to synaptobrevin proteolysis. *Biochem Biophys Res Commun*, **189**, 1017-1023.
124. Littleton JT, Bai J, Vyas B, Desai R, Baltus AE, Garment MB, Carlson SD, Ganetzky B, and Chapman ER (2001) synaptotagmin mutants reveal essential

- functions for the C2B domain in Ca²⁺-triggered fusion and recycling of synaptic vesicles in vivo. *J Neurosci*, **21**, 1421-1433.
125. Littleton JT, Stern M, Perin M, and Bellen HJ (1994) Calcium dependence of neurotransmitter release and rate of spontaneous vesicle fusions are altered in *Drosophila* synaptotagmin mutants. *Proc Natl Acad Sci U S A*, **91**, 10888-10892.
 126. Littleton JT, Stern M, Schulze K, Perin M, and Bellen HJ (1993) Mutational analysis of *Drosophila* synaptotagmin demonstrates its essential role in Ca(2+)-activated neurotransmitter release. *Cell*, **74**, 1125-1134.
 127. Liu Z, Sun C, Olejniczak ET, Meadows RP, Betz SF, Oost T, Herrmann J, Wu JC, and Fesik SW (2000) Structural basis for binding of Smac/DIABLO to the XIAP BIR3 domain. *Nature*, **408**, 1004-1008.
 128. Llinas R, Sugimori M, and Silver RB (1995) The concept of calcium concentration microdomains in synaptic transmission. *Neuropharmacology*, **34**, 1443-1451.
 129. Llinas R, Sugimori M, and Silver RB (1992) Microdomains of high calcium concentration in a presynaptic terminal. *Science*, **256**, 677-679.
 130. Ludtke SJ, Jakana J, Song JL, Chuang DT, and Chiu W (2001) A 11.5 Å single particle reconstruction of GroEL using EMAN. *J Mol Biol*, **314**, 253-262.
 131. Luo X, Tang Z, Xia G, Wassmann K, Matsumoto T, Rizo J, and Yu H (2004) The Mad2 spindle checkpoint protein has two distinct natively folded states. *Nat Struct Mol Biol*.
 132. Mackler JM, Drummond JA, Loewen CA, Robinson IM, and Reist NE (2002) The C(2)B Ca(2+)-binding motif of synaptotagmin is required for synaptic transmission in vivo. *Nature*, **418**, 340-344.
 133. Margittai M, Fasshauer D, Pabst S, Jahn R, and Langen R (2001) Homo- and heterooligomeric SNARE complexes studied by site-directed spin labeling. *J Biol Chem*, **276**, 13169-13177.
 134. Maruyama IN and Brenner S (1991) A phorbol ester/diacylglycerol-binding protein encoded by the unc-13 gene of *Caenorhabditis elegans*. *Proc Natl Acad Sci U S A*, **88**, 5729-5733.
 135. Matos MF, Rizo J, and Sudhof TC (2000) The relation of protein binding to function: what is the significance of munc18 and synaptotagmin binding to syntaxin 1, and where are the corresponding binding sites? *Eur J Cell Biol*, **79**, 377-382.

136. Matthew WD, Tsavaler L, and Reichardt LF (1981) Identification of a synaptic vesicle-specific membrane protein with a wide distribution in neuronal and neurosecretory tissue. *J Cell Biol*, **91**, 257-269.
137. McMahon HT, Missler M, Li C, and Sudhof TC (1995) Complexins: cytosolic proteins that regulate SNAP receptor function. *Cell*, **83**, 111-119.
138. McNew JA, Parlati F, Fukuda R, Johnston RJ, Paz K, Paumet F, Sollner TH, and Rothman JE (2000) Compartmental specificity of cellular membrane fusion encoded in SNARE proteins. *Nature*, **407**, 153-159.
139. Miledi R (1973) Transmitter release induced by injection of calcium ions into nerve terminals. *Proc R Soc Lond B Biol Sci*, **183**, 421-425.
140. Misura KM, Gonzalez LC, Jr., May AP, Scheller RH, and Weis WI (2001) Crystal structure and biophysical properties of a complex between the N-terminal SNARE region of SNAP25 and syntaxin 1a. *J Biol Chem*, **276**, 41301-41309.
141. Misura KM, Scheller RH, and Weis WI (2000) Three-dimensional structure of the neuronal-Sec1-syntaxin 1a complex. *Nature*, **404**, 355-362.
142. Muhandiram DR and Kay LE (1994) Gradient-Enhanced Triple-Resonance 3-Dimensional Nmr Experiments with Improved Sensitivity. *Journal of Magnetic Resonance Series B*, **103**, 203-216.
143. Munson M, Chen X, Cocina AE, Schultz SM, and Hughson FM (2000) Interactions within the yeast t-SNARE Sso1p that control SNARE complex assembly. *Nat Struct Biol*, **7**, 894-902.
144. Nalefski EA, McDonagh T, Somers W, Seehra J, Falke JJ, and Clark JD (1998) Independent folding and ligand specificity of the C2 calcium-dependent lipid binding domain of cytosolic phospholipase A2. *J Biol Chem*, **273**, 1365-1372.
145. Nalefski EA, Wisner MA, Chen JZ, Sprang SR, Fukuda M, Mikoshiba K, and Falke JJ (2001) C2 domains from different Ca²⁺ signaling pathways display functional and mechanistic diversity. *Biochemistry*, **40**, 3089-3100.
146. Nicholls A, Sharp KA, and Honig B (1991) Protein folding and association: insights from the interfacial and thermodynamic properties of hydrocarbons. *Proteins*, **11**, 281-296.
147. Nichols BJ, Ungermann C, Pelham HR, Wickner WT, and Haas A (1997) Homotypic vacuolar fusion mediated by t- and v-SNAREs. *Nature*, **387**, 199-202.
148. Nicholson KL, Munson M, Miller RB, Filip TJ, Fairman R, and Hughson FM (1998) Regulation of SNARE complex assembly by an N-terminal domain of the t-SNARE Sso1p. *Nat Struct Biol*, **5**, 793-802.

149. Nishiki T and Augustine GJ (2004) Dual roles of the C2B domain of synaptotagmin I in synchronizing Ca²⁺-dependent neurotransmitter release. *J Neurosci*, **24**, 8542-8550.
150. Nonet ML, Grundahl K, Meyer BJ, and Rand JB (1993) Synaptic function is impaired but not eliminated in *C. elegans* mutants lacking synaptotagmin. *Cell*, **73**, 1291-1305.
151. Notredame C, Higgins DG, and Heringa J (2000b) T-Coffee: A novel method for fast and accurate multiple sequence alignment. *J Mol Biol*, **302**, 205-217.
152. Notredame C, Higgins DG, and Heringa J (2000a) T-Coffee: A novel method for fast and accurate multiple sequence alignment. *J Mol Biol*, **302**, 205-217.
153. Osborne SL, Herreros J, Bastiaens PI, and Schiavo G (1999) Calcium-dependent oligomerization of synaptotagmins I and II. Synaptotagmins I and II are localized on the same synaptic vesicle and heterodimerize in the presence of calcium. *J Biol Chem*, **274**, 59-66.
154. Ossig R, Dascher C, Trepte HH, Schmitt HD, and Gallwitz D (1991) The yeast SLY gene products, suppressors of defects in the essential GTP-binding Ypt1 protein, may act in endoplasmic reticulum-to-Golgi transport. *Mol Cell Biol*, **11**, 2980-2993.
155. Pabst S, Margittai M, Vainius D, Langen R, Jahn R, and Fasshauer D (2002) Rapid and selective binding to the synaptic SNARE complex suggests a modulatory role of complexins in neuroexocytosis. *J Biol Chem*, **277**, 7838-7848.
156. Parlati F, Varlamov O, Paz K, McNew JA, Hurtado D, Sollner TH, and Rothman JE (2002) Distinct SNARE complexes mediating membrane fusion in Golgi transport based on combinatorial specificity. *Proc Natl Acad Sci U S A*, **99**, 5424-5429.
157. Paumet F, Brugger B, Parlati F, McNew JA, Sollner TH, and Rothman JE (2001) A t-SNARE of the endocytic pathway must be activated for fusion. *J Cell Biol*, **155**, 961-968.
158. Pelham HR (1999) SNAREs and the secretory pathway-lessons from yeast. *Exp Cell Res*, **247**, 1-8.
159. Peng R and Gallwitz D (2004) Multiple SNARE interactions of an SM protein: Sed5p/Sly1p binding is dispensable for transport. *EMBO J*, **23**, 3939-3949.
160. Pereira-Leal JB and Seabra MC (2001) Evolution of the Rab family of small GTP-binding proteins. *J Mol Biol*, **313**, 889-901.
161. Perin MS, Brose N, Jahn R, and Sudhof TC (1991a) Domain structure of synaptotagmin (p65). *J Biol Chem*, **266**, 623-629.

162. Perin MS, Fried VA, Mignery GA, Jahn R, and Sudhof TC (1990) Phospholipid binding by a synaptic vesicle protein homologous to the regulatory region of protein kinase C. *Nature*, **345**, 260-263.
163. Perin MS, Johnston PA, Ozcelik T, Jahn R, Francke U, and Sudhof TC (1991b) Structural and functional conservation of synaptotagmin (p65) in *Drosophila* and humans. *J Biol Chem*, **266**, 615-622.
164. Pettersen EF, Goddard TD, Huang CC, Couch GS, Greenblatt DM, Meng EC, and Ferrin TE (2004) UCSF Chimera--a visualization system for exploratory research and analysis. *J Comput Chem*, **25**, 1605-1612.
165. Phizicky EM and Fields S (1995) Protein-protein interactions: methods for detection and analysis. *Microbiol Rev*, **59**, 94-123.
166. Poirier MA, Hao JC, Malkus PN, Chan C, Moore MF, King DS, and Bennett MK (1998a) Protease resistance of syntaxin.SNAP-25.VAMP complexes. Implications for assembly and structure. *J Biol Chem*, **273**, 11370-11377.
167. Poirier MA, Xiao W, Macosko JC, Chan C, Shin YK, and Bennett MK (1998b) The synaptic SNARE complex is a parallel four-stranded helical bundle. *Nat Struct Biol*, **5**, 765-769.
168. Reim K, Mansour M, Varoqueaux F, McMahon HT, Sudhof TC, Brose N, and Rosenmund C (2001) Complexins regulate a late step in Ca²⁺-dependent neurotransmitter release. *Cell*, **104**, 71-81.
169. Rhee JS, Li L, Shin OH, Rizo J, Sudhof TC, and Rosenmund C (2005) Augmenting neurotransmitter release by enhancing the Ca²⁺-sensitivity of synaptotagmin 1. *in press*.
170. Richmond JE, Davis WS, and Jorgensen EM (1999) UNC-13 is required for synaptic vesicle fusion in *C. elegans*. *Nat Neurosci*, **2**, 959-964.
171. Richmond JE, Weimer RM, and Jorgensen EM (2001) An open form of syntaxin bypasses the requirement for UNC-13 in vesicle priming. *Nature*, **412**, 338-341.
172. Rickman C, Archer DA, Meunier FA, Craxton M, Fukuda M, Burgoyne RD, and Davletov B (2004) Synaptotagmin Interaction with the Syntaxin/SNAP-25 Dimer Is Mediated by an Evolutionarily Conserved Motif and Is Sensitive to Inositol Hexakisphosphate. *J Biol Chem*, **279**, 12574-12579.
173. Rickman C and Davletov B (2003) Mechanism of calcium-independent synaptotagmin binding to target SNAREs. *J Biol Chem*, **278**, 5501-5504.
174. Rizo J and Sudhof TC (2002) Snares and munc18 in synaptic vesicle fusion. *Nat Rev Neurosci*, **3**, 641-653.

175. Rizo J and Sudhof TC (1998a) C2-domains, structure and function of a universal Ca^{2+} -binding domain. *J Biol Chem*, **273**, 15879-15882.
176. Rizo J and Sudhof TC (1998b) Mechanics of membrane fusion. *Nat Struct Biol*, **5**, 839-842.
177. Robinson IM, Ranjan R, and Schwarz TL (2002) Synaptotagmins I and IV promote transmitter release independently of Ca^{2+} binding in the C(2)A domain. *Nature*, **418**, 336-340.
178. Rosenmund C, Sigler A, Augustin I, Reim K, Brose N, and Rhee JS (2002) Differential control of vesicle priming and short-term plasticity by Munc13 isoforms. *Neuron*, **33**, 411-424.
179. Rothman JE (1994) Mechanisms of intracellular protein transport. *Nature*, **372**, 55-63.
180. Rufener E, Frazier AA, Wieser CM, Hinderliter A, and Cafiso DS (2005) Membrane-bound orientation and position of the synaptotagmin C2B domain determined by site-directed spin labeling. *Biochemistry*, **44**, 18-28.
181. Ryan TA, Reuter H, Wendland B, Schweizer FE, Tsien RW, and Smith SJ (1993) The kinetics of synaptic vesicle recycling measured at single presynaptic boutons. *Neuron*, **11**, 713-724.
182. Sabatini BL and Regehr WG (1999) Timing of synaptic transmission. *Annu Rev Physiol*, **61**, 521-542.
183. Sassa T, Harada S, Ogawa H, Rand JB, Maruyama IN, and Hosono R (1999) Regulation of the UNC-18-Caenorhabditis elegans syntaxin complex by UNC-13. *J Neurosci*, **19**, 4772-4777.
184. Sato TK, Rehling P, Peterson MR, and Emr SD (2000) Class C Vps protein complex regulates vacuolar SNARE pairing and is required for vesicle docking/fusion. *Mol Cell*, **6**, 661-671.
185. Schekman R (1992) Genetic and biochemical analysis of vesicular traffic in yeast. *Curr Opin Cell Biol*, **4**, 587-592.
186. Schiavo G, Benfenati F, Poulain B, Rossetto O, Polverino dL, DasGupta BR, and Montecucco C (1992) Tetanus and botulinum-B neurotoxins block neurotransmitter release by proteolytic cleavage of synaptobrevin. *Nature*, **359**, 832-835.
187. Schiavo G, Gu QM, Prestwich GD, Sollner TH, and Rothman JE (1996) Calcium-dependent switching of the specificity of phosphoinositide binding to synaptotagmin. *Proc Natl Acad Sci U S A*, **93**, 13327-13332.

188. Schiavo G, Matteoli M, and Montecucco C (2000) Neurotoxins affecting neuroexocytosis. *Physiol Rev*, **80**, 717-766.
189. Schiavo G, Stenbeck G, Rothman JE, and Sollner TH (1997) Binding of the synaptic vesicle v-SNARE, synaptotagmin, to the plasma membrane t-SNARE, SNAP-25, can explain docked vesicles at neurotoxin-treated synapses. *Proc Natl Acad Sci U S A*, **94**, 997-1001.
190. Schluter OM, Schmitz F, Jahn R, Rosenmund C, and Sudhof TC (2004) A complete genetic analysis of neuronal Rab3 function. *J Neurosci*, **24**, 6629-6637.
191. Schneggenburger R and Neher E (2000) Intracellular calcium dependence of transmitter release rates at a fast central synapse. *Nature*, **406**, 889-893.
192. Schoch S, Castillo PE, Jo T, Mukherjee K, Geppert M, Wang Y, Schmitz F, Malenka RC, and Sudhof TC (2002) RIM1alpha forms a protein scaffold for regulating neurotransmitter release at the active zone. *Nature*, **415**, 321-326.
193. Schoch S, Deak F, Konigstorfer A, Mozhayeva M, Sara Y, Sudhof TC, and Kavalali ET (2001) SNARE function analyzed in synaptobrevin/VAMP knockout mice. *Science*, **294**, 1117-1122.
194. Schulze KL, Broadie K, Perin MS, and Bellen HJ (1995) Genetic and electrophysiological studies of *Drosophila* syntaxin-1A demonstrate its role in nonneuronal secretion and neurotransmission. *Cell*, **80**, 311-320.
195. Shao X, Davletov BA, Sutton RB, Sudhof TC, and Rizo J (1996) Bipartite Ca²⁺-binding motif in C2 domains of synaptotagmin and protein kinase C. *Science*, **273**, 248-251.
196. Shao X, Fernandez I, Sudhof TC, and Rizo J (1998) Solution structures of the Ca²⁺-free and Ca²⁺-bound C2A domain of synaptotagmin I: does Ca²⁺ induce a conformational change? *Biochemistry*, **37**, 16106-16115.
197. Shao X, Li C, Fernandez I, Zhang X, Sudhof TC, and Rizo J (1997) Synaptotagmin-syntaxin interaction: the C2 domain as a Ca²⁺-dependent electrostatic switch. *Neuron*, **18**, 133-142.
198. Sheng ZH, Yokoyama CT, and Catterall WA (1997) Interaction of the synprint site of N-type Ca²⁺ channels with the C2B domain of synaptotagmin I. *Proc Natl Acad Sci U S A*, **94**, 5405-5410.
199. Shin OH, Rhee JS, Tang J, Sugita S, Rosenmund C, and Sudhof TC (2003) Sr²⁺ binding to the Ca²⁺ binding site of the synaptotagmin 1 C2B domain triggers fast exocytosis without stimulating SNARE interactions. *Neuron*, **37**, 99-108.
200. Shin OH, Rizo J, and Sudhof TC (2002) Synaptotagmin function in dense core vesicle exocytosis studied in cracked PC12 cells. *Nat Neurosci*, **5**, 649-656.

201. Siegel DP (1993) Energetics of intermediates in membrane fusion: comparison of stalk and inverted micellar intermediate mechanisms. *Biophys J*, **65**, 2124-2140.
202. Sollner T, Bennett MK, Whiteheart SW, Scheller RH, and Rothman JE (1993a) A protein assembly-disassembly pathway in vitro that may correspond to sequential steps of synaptic vesicle docking, activation, and fusion. *Cell*, **75**, 409-418.
203. Sollner T, Whiteheart SW, Brunner M, Erdjument-Bromage H, Geromanos S, Tempst P, and Rothman JE (1993b) SNAP receptors implicated in vesicle targeting and fusion. *Nature*, **362**, 318-324.
204. Sorensen JB, Matti U, Wei SH, Nehring RB, Voets T, Ashery U, Binz T, Neher E, and Rettig J (2002) The SNARE protein SNAP-25 is linked to fast calcium triggering of exocytosis. *Proc Natl Acad Sci U S A*, **99**, 1627-1632.
205. Sudhof TC (1995) The synaptic vesicle cycle: a cascade of protein-protein interactions. *Nature*, **375**, 645-653.
206. Sudhof TC (2004) The synaptic vesicle cycle. *Annu Rev Neurosci*, **27**, 509-547.
207. Sudhof TC, De Camilli P, Niemann H, and Jahn R (1993) Membrane fusion machinery: insights from synaptic proteins. *Cell*, **75**, 1-4.
208. Sugita S, Han W, Butz S, Liu X, Fernandez-Chacon R, Lao Y, and Sudhof TC (2001) Synaptotagmin VII as a plasma membrane Ca(2+) sensor in exocytosis. *Neuron*, **30**, 459-473.
209. Sugita S, Hata Y, and Sudhof TC (1996) Distinct Ca(2+)-dependent properties of the first and second C2-domains of synaptotagmin I. *J Biol Chem*, **271**, 1262-1265.
210. Sugita S and Sudhof TC (2000) Specificity of Ca²⁺-dependent protein interactions mediated by the C2A domains of synaptotagmins. *Biochemistry*, **39**, 2940-2949.
211. Sutton RB, Davletov BA, Berghuis AM, Sudhof TC, and Sprang SR (1995a) Structure of the first C2 domain of synaptotagmin I: a novel Ca²⁺/phospholipid-binding fold. *Cell*, **80**, 929-938.
212. Sutton RB, Davletov BA, Berghuis AM, Sudhof TC, and Sprang SR (1995b) Structure of the first C2 domain of synaptotagmin I: a novel Ca²⁺/phospholipid-binding fold. *Cell*, **80**, 929-938.
213. Sutton RB, Ernst JA, and Brunger AT (1999) Crystal structure of the cytosolic C2A-C2B domains of synaptotagmin III. Implications for Ca(2+)-independent snare complex interaction. *J Cell Biol*, **147**, 589-598.

214. Sutton RB, Fasshauer D, Jahn R, and Brunger AT (1998) Crystal structure of a SNARE complex involved in synaptic exocytosis at 2.4 Å resolution. *Nature*, **395**, 347-353.
215. Takahashi S, Yamamoto H, Matsuda Z, Ogawa M, Yagyu K, Taniguchi T, Miyata T, Kaba H, Higuchi T, Okutani F, and . (1995) Identification of two highly homologous presynaptic proteins distinctly localized at the dendritic and somatic synapses. *FEBS Lett*, **368**, 455-460.
216. Terrian DM and White MK (1997) Phylogenetic analysis of membrane trafficking proteins: a family reunion and secondary structure predictions. *Eur J Cell Biol*, **73**, 198-204.
217. Thomas DM, Ferguson GD, Herschman HR, and Elferink LA (1999) Functional and biochemical analysis of the C2 domains of synaptotagmin IV. *Mol Biol Cell*, **10**, 2285-2295.
218. Tokumaru H, Umayahara K, Pellegrini LL, Ishizuka T, Saisu H, Betz H, Augustine GJ, and Abe T (2001) SNARE complex oligomerization by synaphin/complexin is essential for synaptic vesicle exocytosis. *Cell*, **104**, 421-432.
219. Toonen RF and Verhage M (2003) Vesicle trafficking: pleasure and pain from SM genes. *Trends Cell Biol*, **13**, 177-186.
220. Tsien RY (1998) The green fluorescent protein. *Annu Rev Biochem*, **67**, 509-544.
221. Tucker WC and Chapman ER (2002) Role of synaptotagmin in Ca²⁺-triggered exocytosis. *Biochem J*, **366**, 1-13.
222. Tucker WC, Weber T, and Chapman ER (2004) Reconstitution of Ca²⁺-Regulated Membrane Fusion by Synaptotagmin and SNAREs. *Science*.
223. Ubach J, Lao Y, Fernandez I, Arac D, Sudhof TC, and Rizo J (2001) The C2B domain of synaptotagmin I is a Ca²⁺-binding module. *Biochemistry*, **40**, 5854-5860.
224. Ubach J, Zhang X, Shao X, Sudhof TC, and Rizo J (1998) Ca²⁺ binding to synaptotagmin: how many Ca²⁺ ions bind to the tip of a C2-domain? *EMBO J*, **17**, 3921-3930.
225. Uellner R, Zvelebil MJ, Hopkins J, Jones J, MacDougall LK, Morgan BP, Podack E, Waterfield MD, and Griffiths GM (1997) Perforin is activated by a proteolytic cleavage during biosynthesis which reveals a phospholipid-binding C2 domain. *EMBO J*, **16**, 7287-7296.
226. Uetz P, Giot L, Cagney G, Mansfield TA, Judson RS, Knight JR, Lockshon D, Narayan V, Srinivasan M, Pochart P, Qureshi-Emili A, Li Y, Godwin B, Conover

- D, Kalbfleisch T, Vijayadamodar G, Yang M, Johnston M, Fields S, and Rothberg JM (2000) A comprehensive analysis of protein-protein interactions in *Saccharomyces cerevisiae*. *Nature*, **403**, 623-627.
227. Ullrich B, Li C, Zhang JZ, McMahon H, Anderson RG, Geppert M, and Sudhof TC (1994) Functional properties of multiple synaptotagmins in brain. *Neuron*, **13**, 1281-1291.
 228. Verdaguer N, Corbalan-Garcia S, Ochoa WF, Fita I, and Gomez-Fernandez JC (1999) Ca(2+) bridges the C2 membrane-binding domain of protein kinase Calpha directly to phosphatidylserine. *EMBO J*, **18**, 6329-6338.
 229. Verhage M, Maia AS, Plomp JJ, Brussaard AB, Heeroma JH, Vermeer H, Toonen RF, Hammer RE, van den Berg TK, Missler M, Geuze HJ, and Sudhof TC (2000) Synaptic assembly of the brain in the absence of neurotransmitter secretion. *Science*, **287**, 864-869.
 230. Voets T, Toonen RF, Brian EC, de Wit H, Moser T, Rettig J, Sudhof TC, Neher E, and Verhage M (2001) Munc18-1 promotes large dense-core vesicle docking. *Neuron*, **31**, 581-591.
 231. von MC, Krause R, Snel B, Cornell M, Oliver SG, Fields S, and Bork P (2002) Comparative assessment of large-scale data sets of protein-protein interactions. *Nature*, **417**, 399-403.
 232. Walker DR and Koonin EV (1997) SEALS: a system for easy analysis of lots of sequences. *Proc Int Conf Intell Syst Mol Biol*, **5**, 333-339.
 233. Wang L, Seeley ES, Wickner W, and Merz AJ (2002) Vacuole fusion at a ring of vertex docking sites leaves membrane fragments within the organelle. *Cell*, **108**, 357-369.
 234. Washbourne P, Thompson PM, Carta M, Costa ET, Mathews JR, Lopez-Bendito G, Molnar Z, Becher MW, Valenzuela CF, Partridge LD, and Wilson MC (2002) Genetic ablation of the t-SNARE SNAP-25 distinguishes mechanisms of neuroexocytosis. *Nat Neurosci*, **5**, 19-26.
 235. Weber T, Zemelman BV, McNew JA, Westermann B, Gmachl M, Parlati F, Sollner TH, and Rothman JE (1998) SNAREpins: minimal machinery for membrane fusion. *Cell*, **92**, 759-772.
 236. Weimbs T, Low SH, Chapin SJ, Mostov KE, Bucher P, and Hofmann K (1997) A conserved domain is present in different families of vesicular fusion proteins: a new superfamily. *Proc Natl Acad Sci U S A*, **94**, 3046-3051.
 237. Weimbs T, Mostov K, Low SH, and Hofmann K (1998) A model for structural similarity between different SNARE complexes based on sequence relationships. *Trends Cell Biol*, **8**, 260-262.

238. White JM (1992) Membrane fusion. *Science*, **258**, 917-924.
239. Williams AL, Ehm S, Jacobson NC, Xu D, and Hay JC (2004) rsly1 binding to syntaxin 5 is required for endoplasmic reticulum-to-Golgi transport but does not promote SNARE motif accessibility. *Mol Biol Cell*, **15**, 162-175.
240. Wishart DS and Sykes BD (1994) The ¹³C chemical-shift index: a simple method for the identification of protein secondary structure using ¹³C chemical-shift data. *J Biomol NMR*, **4**, 171-180.
241. Wu G, Chai J, Suber TL, Wu JW, Du C, Wang X, and Shi Y (2000) Structural basis of IAP recognition by Smac/DIABLO. *Nature*, **408**, 1008-1012.
242. Wu MN, Fergestad T, Lloyd TE, He Y, Broadie K, and Bellen HJ (1999) Syntaxin 1A interacts with multiple exocytic proteins to regulate neurotransmitter release in vivo. *Neuron*, **23**, 593-605.
243. Wu MN, Littleton JT, Bhat MA, Prokop A, and Bellen HJ (1998) ROP, the *Drosophila* Sec1 homolog, interacts with syntaxin and regulates neurotransmitter release in a dosage-dependent manner. *EMBO J*, **17**, 127-139.
244. Wu Y, He Y, Bai J, Ji SR, Tucker WC, Chapman ER, and Sui SF (2003) Visualization of synaptotagmin I oligomers assembled onto lipid monolayers. *Proc Natl Acad Sci U S A*, **100**, 2082-2087.
245. Xiao W, Poirier MA, Bennett MK, and Shin YK (2001) The neuronal t-SNARE complex is a parallel four-helix bundle. *Nat Struct Biol*, **8**, 308-311.
246. Yamaguchi T, Dulubova I, Min SW, Chen X, Rizo J, and Sudhof TC (2002) Sly1 binds to Golgi and ER syntaxins via a conserved N-terminal peptide motif. *Dev Cell*, **2**, 295-305.
247. Yang B, Steegmaier M, Gonzalez LC, Jr., and Scheller RH (2000) nSec1 binds a closed conformation of syntaxin1A. *J Cell Biol*, **148**, 247-252.
248. Ye S and Goldsmith EJ (2001) Serpins and other covalent protease inhibitors. *Curr Opin Struct Biol*, **11**, 740-745.
249. Yoshida A, Oho C, Omori A, Kuwahara R, Ito T, and Takahashi M (1992) HPC-1 is associated with synaptotagmin and omega-conotoxin receptor. *J Biol Chem*, **267**, 24925-24928.
250. Zhang JZ, Davletov BA, Sudhof TC, and Anderson RG (1994a) Synaptotagmin I is a high affinity receptor for clathrin AP-2: implications for membrane recycling. *Cell*, **78**, 751-760.
251. Zhang O, Kay LE, Olivier JP, and Forman-Kay JD (1994b) Backbone ¹H and ¹⁵N resonance assignments of the N-terminal SH3 domain of drk in folded and

- unfolded states using enhanced-sensitivity pulsed field gradient NMR techniques. *J Biomol NMR*, **4**, 845-858.
252. Zhang X, Kim-Miller MJ, Fukuda M, Kowalchuk JA, and Martin TF (2002) Ca^{2+} -dependent synaptotagmin binding to SNAP-25 is essential for Ca^{2+} -triggered exocytosis. *Neuron*, **34**, 599-611.
253. Zhang X, Rizo J, and Sudhof TC (1998) Mechanism of phospholipid binding by the C2A-domain of synaptotagmin I. *Biochemistry*, **37**, 12395-12403.
254. Zuiderweg ER (2002) Mapping protein-protein interactions in solution by NMR spectroscopy. *Biochemistry*, **41**, 1-7.

VITAE

Demet Araç-Özkan was born in Izmir, Turkey on May 12, 1977, the daughter of Inci Araç and Burhan Araç. She has a brother and a sister. After completing her work at Izmir Science High School in 1995, she entered Bilkent University in Ankara, Turkey. She received the degree of Bachelor of Science with a major in Molecular Biology and Genetics from Bilkent University in June, 1999. She entered the Biochemistry Department of the University of California, Riverside as a Ph.D. student in September, 1999. One year later, she entered the Graduate School of Biomedical Sciences at the University of Texas Southwestern Medical Center at Dallas. In May 2001, she joined the laboratory of Dr. Rizo-Rey. She was awarded the degree of Doctor of Philosophy in November 2005 from the Molecular Biophysics Graduate Program. She married Engin Özkan in 2001.

Permanent Address: 6342 Shady Brook Ln Apt 2164
Dallas, TX, 75206